

AD-A285 088

SC71024.FR



Copy No. 5

SC71024.FR

THERMAL DISSOCIATION OF HALOGEN AZIDES

FINAL TECHNICAL REPORT
FOR PERIOD APRIL 15, 1990 THROUGH JUNE 30, 1994

CONTRACT NO. F49620-90-C-0025

AEOSR-TR- 94 0552

Prepared for:

Maj. Glen Perram
Air Force Office of Scientific Research
Directorate of Chemical and Atmospheric Sciences
Bolling AFB, DC 20332

Prepared by:

D. Benard
Rockwell International Science Center
Thousand Oaks, CA 91360

DTIC
SELECTED
SEP 23 1994
S B

SEPTEMBER 1994

94-30996



DISTRIBUTION STATEMENT A
Approved for public release
Distribution Unlimited

UNCLASSIFIED



Rockwell International
Science Center

94 8

2

19 AUG 1994

REPORT DOCUMENTATION PAGE

Form Approved
OMB No. 0704-0188

Public reporting burden for this collection of information is estimated to average 1 hour per response, including the time for reviewing instructions, searching existing data sources, gathering and maintaining the data needed, and completing and reviewing the collection of information. Send comments regarding this burden estimate or any other aspect of this collection of information, including suggestions for reducing this burden, to Washington Headquarters Services, Directorate for Information Operations and Reports, 1215 Jefferson Davis Highway, Suite 1204, Arlington, VA, 22202-4302, and to the Office of Management and Budget, Paperwork Reduction Project (0704-0188), Washington, DC 20503

1. AGENCY USE ONLY (Leave Blank)	2. REPORT DATE September 1994	3. REPORT TYPE AND DATES COVERED Final 04-15-90 through 06-30-94	
4. TITLE AND SUBTITLE THERMAL DISSOCIATION OF HALOGEN AZIDES		5. FUNDING NUMBERS FC9620-94-C-0025	
4. AUTHOR(S) D.J. Benard		7. PERFORMING ORGANIZATION REPORT NUMBER SC71024.FR	
7. PERFORMING ORGANIZATION NAME(S) AND ADDRESS(ES) Rockwell International Science Center P.O. Box 1085 Thousand Oaks, CA 91358		9. SPONSORING / MONITORING AGENCY REPORT NUMBER AEOSR-TR- 94 0512	
9. SPONSORING / MONITORING AGENCY NAME(S) AND ADDRESS(ES) AOSR/NC (Bldg. 410) Directorate of Chemical and Atmospheric Sciences Bolling AFB, DC 20332 <i>Dr. Boman</i>		11. SUPPLEMENTARY NOTES	
12a. DISTRIBUTING/AVAILABILITY STATEMENT Approved for public release: distribution unlimited.		12b. DISTRIBUTION CODE	
13. ABSTRACT (Maximum 200 Words) Both FN3 and CIN3 were dissociated in the presence of a variety of donor molecules, either by pulsed CO2 laser excitation (using SF6 as a sensitizer) or by thermal excitation in a chemically driven shock tube. The donors were selected to support energy transfer from the metastable NF(a) and NCl(a) products of the azide dissociation reactions, and optical diagnostics were employed to study energy transfer rates, optical gain and lasing at visible wavelengths. Production of NCl(a) was shown to be inefficient, however, both gain and lasing were achieved in two systems driven by NF(a). Lasing at 471 nm on the BiF(A-X) transition was obtained by transient heating of FN3/Bi(CH3)3 gas mixtures, however, power extraction was highly inefficient due to the low gain provided by this emitter and the short duration of the shock tube experiment. Much higher gain coefficients were obtained by CO2 laser heating of FN3/B2H6/SF6 gas mixtures, which produced intense BH(A-X) chemiluminescence and lasing at 433 nm in a low volume cavity with a threshold gain of 2.5 %/cm. An improved BH donor was synthesized by reacting B2H6 with NH3 in a heated capillary oven and optical absorption diagnostics were developed for the dark BH(X) and BH(a) states. The rate coefficients for excitation of the BH(a) and BH(A) states by NF(a) were determined to be > 8E-10 and ~ 3E-11 cm3/s, respectively, and the principal difficulties were due to rapid scavenging of the BH emitters by reaction with the SF6 sensitizers (in the CO2 laser triggered experiment) and thermal dissociation of the tetraazidoborane donor into non-productive diazidoborane monomers (in the shock tube reactor). Other concepts that were also investigated included excitation schemes for production of NF(b), IF(B) and NS(B).			
14. SUBJECT TERMS Halogen azides, nitrogen halides, bismuth fluoride, boron hydride, chemical lasers, kinetics, radiation, dissociation, reaction, quenching, energy transfer, pooling, donor molecules, metastables, scaling, gain, inversion, saturation		15. NUMBER OF PAGES at final	
17. SECURITY CLASSIFICATION OF REPORT Unclassified		16. PRICE CODE	
12. SECURITY CLASSIFICATION OF THIS PAGE Unclassified	19. SECURITY CLASSIFICATION OF ABSTRACT Unclassified	20. LIMITATION OF ABSTRACT	



Table of Contents

	Page
Introduction	1
Objectives	1
Methodology.....	2
Candidates.....	3
Progress Summaries	3
Production of Halogen Azides.....	3
Production and Decay of NCl(a ¹ Δ)	3
Alternate Emitters.....	8
Kinetics and Scaling	9
Bismuth Fluoride	10
Boron Hydride.....	10
Gain and Lasing	11
Bismuth Fluoride	11
Boron Hydride.....	11
Physical Sciences Subcontract.....	12
Conclusions and Recommendations	13
References	16
Publications	17

Accession For	
NTIS GRA&I	<input checked="" type="checkbox"/>
DTIC TAB	<input type="checkbox"/>
Unannounced	<input type="checkbox"/>
Justification	
By _____	
Distribution/_____	
Availability Codes	
Dist	Avail and/or Special
A-1	

DTIC QUALITY ASSURED 3



Introduction

Objectives

The principal goal of this work was to develop new short wavelength chemical lasers that are suitable for ballistic missile negation and target identification/discrimination applications. These lasers are based on energy transfer and pooling from the metastable species $\text{NF}(a^1\Delta)$ and $\text{NCl}(a^1\Delta)$, which are both analogues of $\text{O}_2(a^1\Delta)$. Under a prior AFWL/AFRPL contract¹, large ($3 \times 10^{16} / \text{cm}^3$) densities of $\text{NF}(a^1\Delta)$ were efficiently generated by rapid dissociation of the energetic fluorine azide (FN_3) molecule, and the rate of $\text{NF}(a^1\Delta)$ self-annihilation was measured as $10^{-12} \text{ cm}^3/\text{s}$. In parallel with these efforts, Herbelin² used an alternate source of $\text{NF}(a^1\Delta)$ to demonstrate the feasibility of a blue-green laser based on energy transfer and pooling in BiF , and the kinetics/scaling issues for this concept were investigated at Science Center (under the same contract) using FN_3 to generate the metastables. Also, similar production of $\text{NCl}(a^1\Delta)$ by dissociation of ClN_3 was demonstrated under an IR&D program at Science Center; but the yield was not determined quantitatively, since the radiative rate for the $\text{NCl}(a-X)$ transition (required to measure the metastable concentration) was in doubt. Several issues were addressed under the present contract including:

1. Optimizing the production of FN_3 and ClN_3 .
2. Determining the yield of $\text{NCl}(a^1\Delta)$ from dissociation of ClN_3 , the $\text{NCl}(a^1\Delta)$ self-annihilation rate, and the A-coefficient of the $\text{NCl}(a-X)$ transition.
3. Performing a survey of potential visible wavelength emitters that are excited by $\text{NF}(a^1\Delta)$, $\text{NCl}(a^1\Delta)$, or a combination of these metastables, to identify an alternative to the NF/BiF concept.
4. Demonstration of optical gain and lasing in the NF/BiF system under conditions that simulate a high energy laser device.
5. Development of the most suitable alternative to BiF through kinetic investigation and scaling studies as well as gain and lasing demonstrations.

Significant progress was achieved in each of these areas, and several conclusions were obtained in relation to each of the topics. Important results are summarized in a following section



of this report and readers are referred to the publication record for full technical details. For completeness, the publication section includes two papers on $\text{NF}(a^1\Delta)$ and $\text{NCl}(a^1\Delta)$ generation and a third paper on BiF scaling resulting from prior work, as well as a current paper on scaling the NF/IF system, which was pursued under a parallel subcontract with Physical Sciences. The results of these prior and parallel efforts are also included in the progress summary.

Methodology

The FN_3 was generated on-line by reacting HN_3 with F_2 following the method of Haller³. The HN_3 was obtained by the thermally activated batch reaction of NaN_3 with excess stearic acid. The ClN_3 was generated by batch reaction of dry NaN_3 with Cl_2 , by on-line reaction of moist NaN_3 with Cl_2 , and by the dry on-line reaction of HN_3 with ClF . The yield of azide product and its purity were assessed by visible/ultraviolet and infrared absorption spectroscopy as well as mass spectroscopy. In practice, HN_3 was storable indefinitely, ClN_3 decayed significantly over the period of a day, and FN_3 decomposed in ~15 minutes at ambient temperature. The halogen azide decay rates were strongly influenced by relatively minor temperature changes.

Two reactors were used to study the generation and decay of the metastable and emitting species. In the first reactor, halogen azides (in He diluent) were mixed on-the-fly with SF_6 and various donor molecules before exposure to a pulsed CO_2 laser beam. The laser photons were absorbed by the SF_6 resulting in high vibrational temperatures⁴ which dissociated the parent azide and donor molecules on the μs time scale. Energy transfer from the metastable products to the donor (emitter) fragments was then studied by time resolved, spectrally resolved, and absolutely calibrated emission/absorption spectroscopy, as well as by pulsed and cw laser induced fluorescence techniques. Application of a pulsed electric discharge to FN_3 did not yield a significant quantity of $\text{NF}(a^1\Delta)$.

The second reactor was a novel tabletop scale shock tube, driven by an electrically triggered $\text{H}_2\text{-F}_2$ explosion. The reagents FN_3 and TMB (trimethylbismuth) were dissociated behind the reflected shock to yield $\text{NF}(a^1\Delta)$ and BiF . The principal diagnostics used with this reactor were piezoelectric transducers and time/wavelength resolved emission spectroscopy, both with and without an optical cavity. Both reactors produced comparable (torr level) concentrations of $\text{NF}(a^1\Delta)$; however, the appearance of the metastables in the CO_2 laser driven reactor was immediate, whereas in the shock tube an avalanche of $\text{NF}(a^1\Delta)$ was obtained after a characteristic 50 μs induction period following passage of the reflected shock wave. The mechanism of dissociation of the azide in the shock tube is suitable for high energy laser applications, and the



operation of this reactor also provides a transient simulation of the compression and expansion phenomena that occur in a supersonic laser nozzle. Use of a CO₂ laser to trigger reaction chemistry, on the other hand, is largely a convenient research tool for use in the laboratory. Further details regarding these techniques are contained in the publications section.

Candidates

The principal reaction systems of interest were: NF/NCI/I₂ for production of NF(b-X) emission at 528 nm, NF/I₂/F for production of IF(B-X) emission at 500-700 nm, NF/TMB for production of BiF(A-X) emission at 425-475 nm, and NF/B₂H₆ for production of BH(A-X) emission at 433 nm, although other (less successful) candidate schemes were also investigated. The corresponding energy level diagrams, A-coefficients and key reaction steps for these four primary laser concepts are presented in Figs. 1 through 4.

Progress Summaries

Production of Halogen Azides

1. Fluorine azide is most easily produced by reacting 10% F₂ in He with 5% HN₃ in He at 350 torr total pressure and ambient temperature. Approximately 3% FN₃ in He is generated when the F₂ flow is adjusted to half the HN₃ flow. The principal byproduct is solid NH₄F. The reactor volume (~ 200 cm³) was filled with 0.25 inch dia. stainless steel balls to mix the gases at a net flow rate of ~ 3.5 scc/s.
2. Chlorine azide is produced similarly to FN₃ upon replacing the F₂ by ClF at the same dilution in He, but with the ClF flow matched to the HN₃ flow. The yield of ClN₃ is about half the yield of FN₃, and gas phase byproducts are negligible. This source of ClN₃ is cleaner than the wet reaction of ClN₃ with NaN₃, and produces higher concentrations/flow rates of the azide than the dry reaction of Cl₂ with NaN₃.

Production and Decay of NCl(a¹Δ₁)

1. The radiative rate of the NCl(a-X) transition is ~ 0.9/s.
2. The yield of NCl(a¹Δ) from dissociation of ClN₃ is ~ 10%. This result occurs because a singlet-triplet crossing near the peak of the potential energy barrier allows dissociation of the parent molecule into ground state fragments.

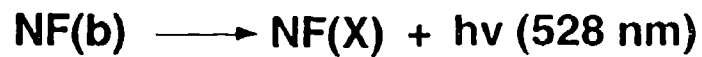
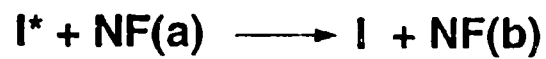
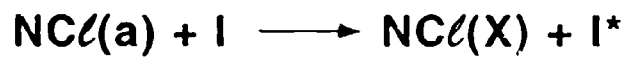
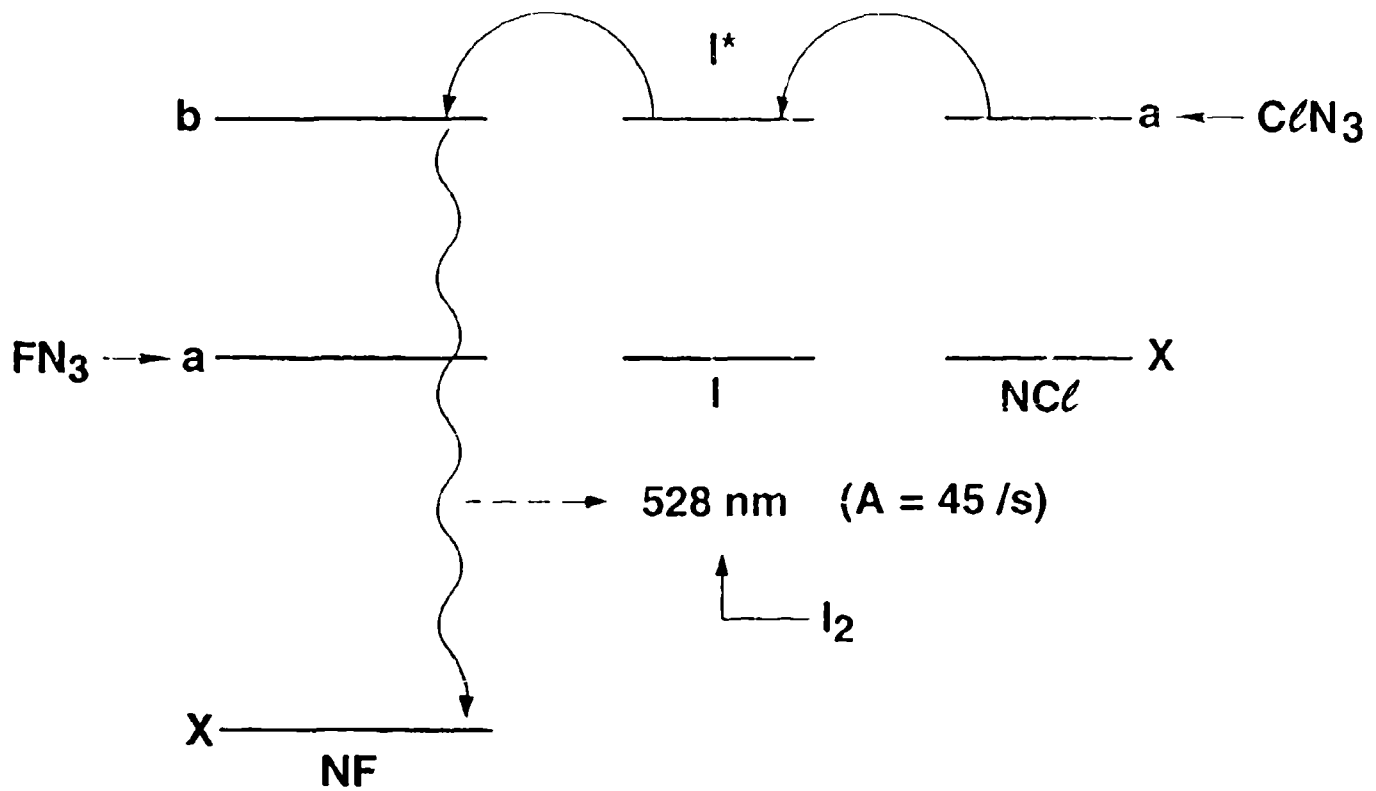


Fig. 1 Energy levels and key pumping reactions in the NF / NCℓ / I₂ system.

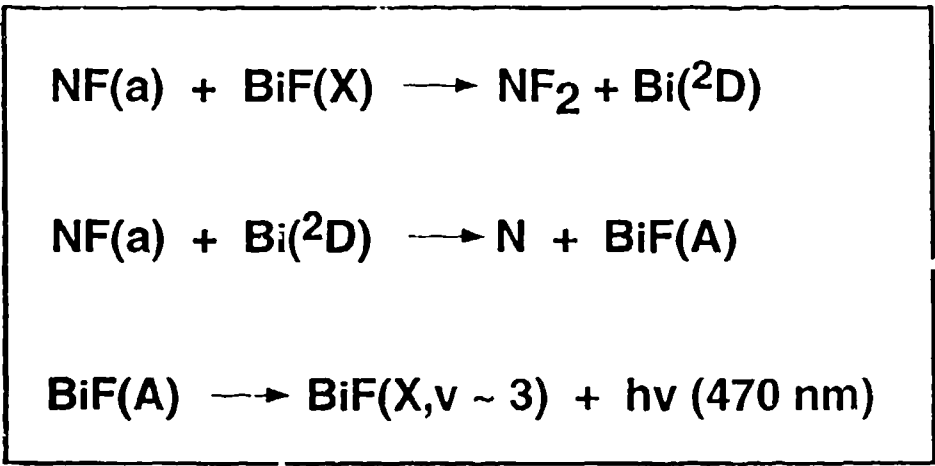
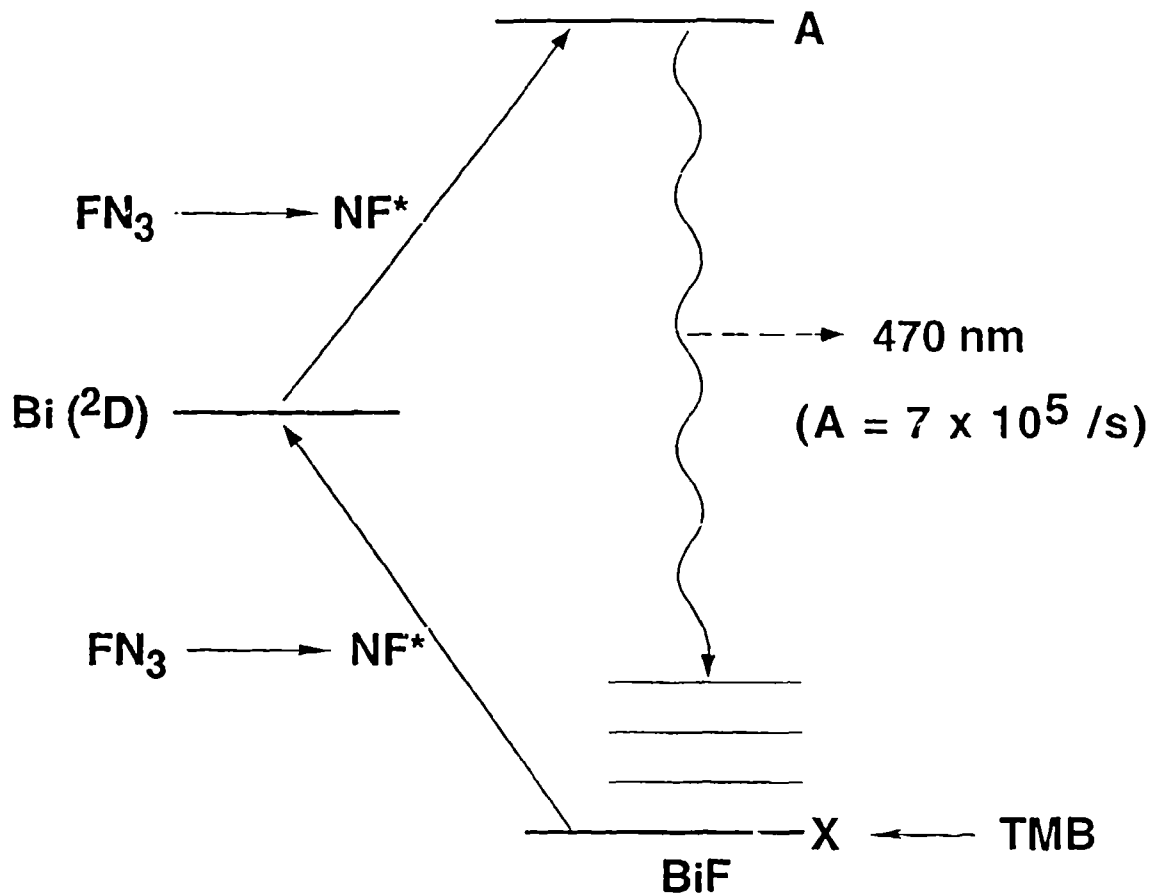


Fig. 3 Energy levels and key pumping reactions in the NF / TMB system.

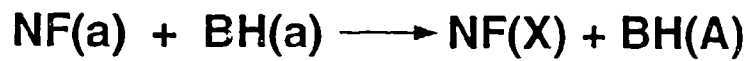
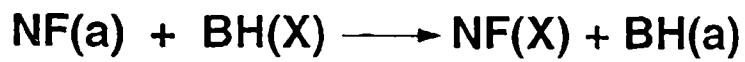
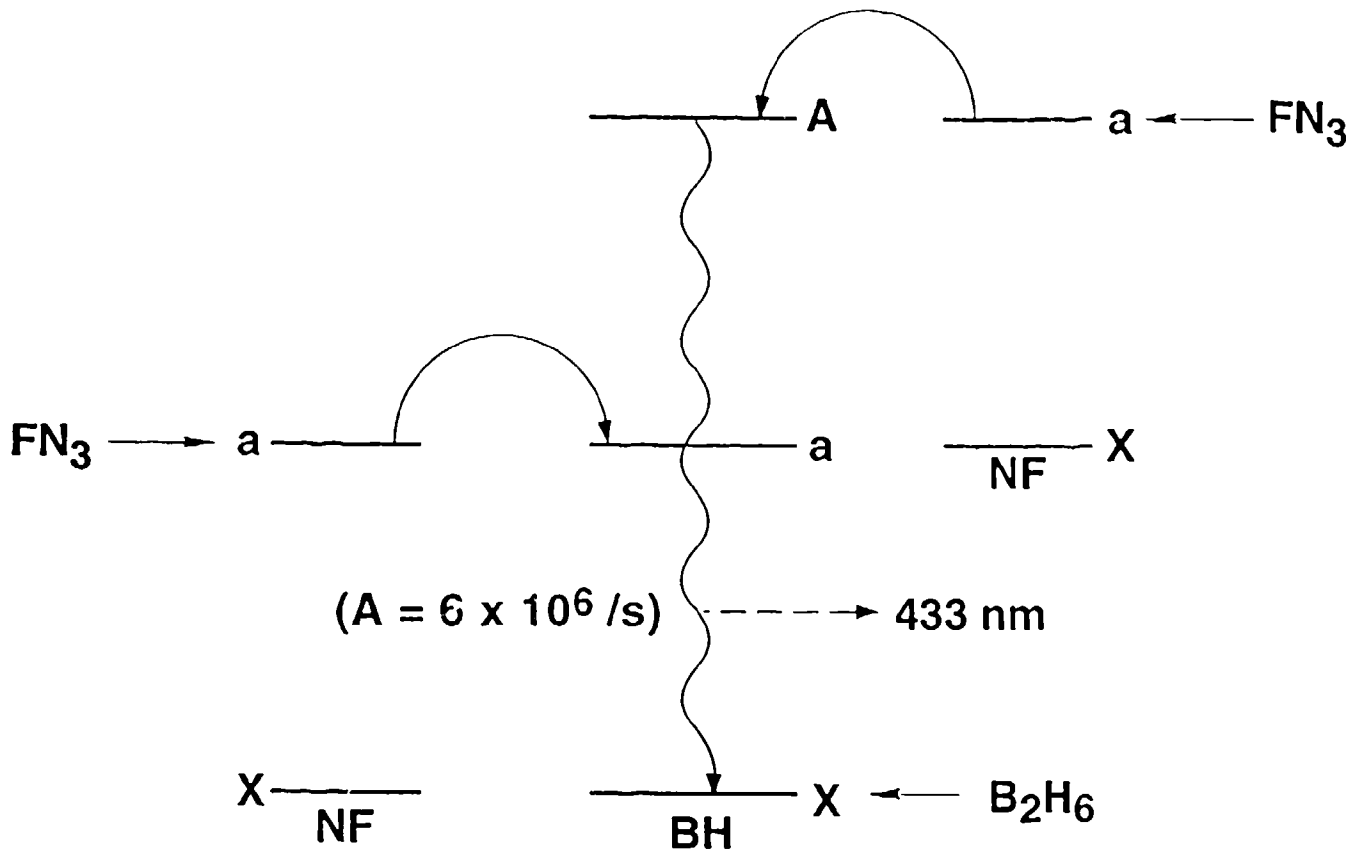


Fig. 4 Energy levels and key pumping reactions in the NF / B₂H₆ system.



3. The rate of NCl ($a^1\Delta$) self-annihilation is $\sim 3 \times 10^{-11}$ cm³/s.
4. The barrier to dissociation of CIN₃ is ~ 0.7 eV, compared to ~ 0.5 eV in FN₃.

Alternate Emitters

1. Production of NF(b) was studied in the FN₃/CIN₃/I₂ system. Dissociation of the I₂, and the I-atom catalyzed energy pooling transfer processes, were both found to be rapid and efficient, consistent with the results of prior investigations. Also, quenching of I* and NF(b) was insignificant in comparison to the rates of the equilibrium reactions. The low stimulated emission cross section of the NF(b-X) transition, however, is inconsistent with successful development of the concept for high energy laser applications. The principal benefit of this work was to extract the unknown radiative rate of the NCl(a-X) transition by modeling, which enabled subsequent determination of the NCl($a^1\Delta$) yield and the corresponding self-annihilation rate. The results obtained demonstrate that systems driven by NCl($a^1\Delta$) will be of much lower overall efficiency than systems driven by NF($a^1\Delta$), given equal kinetics in the transfer and lasing reactions.
2. Production of IF(B) was studied in the FN₃/CIN₃/CF₃I system. Large concentrations of IF(X) were achieved, but the global rate of IF(B) generation was very slow. The probable cause of this difficulty is a mismatch between the energy of NCl($a^1\Delta$) and the state splitting in IF, resulting in pumping of the B state above the predissociation limit. This result does not, however, carry negative implications for other NF/IF laser concepts that do not involve NCl, or for concepts involving NCl where a molecule (such as O₂) mediates the transfer to IF. The low efficiency of NCl($a^1\Delta$) production from CIN₃ remains as a significant problem, nonetheless.
3. Excitation of FN₃/CIN₃/Sb(CH₃)₃ gas mixtures by a CO₂ laser, in the presence of SF₆ sensitizer, yielded no measurable Sb-atom chemiluminescence.
4. Similar excitation of FN₃/CIN₃/Bi(CH₃)₃ gas mixtures yielded no enhancement of the BiF emission and no new emissions of comparable intensity.
5. Excitation of FN₃/S₂Cl₂/SF₆ gas mixtures by the pulsed CO₂ laser yielded NS(B-X) chemiluminescence⁵. Cold trap experiments showed that small levels of H₂O impurity (in the azide flow) react with the S₂Cl₂ to yield the HS precursor of the NS molecule, and the



pumping reaction is thought to be $\text{NF}(a^1\Delta) + \text{HS} \rightarrow \text{HF} + \text{NS(B)}$. An NS(B) excitation rate coefficient of $1.5 \times 10^{-11} \text{ cm}^3/\text{s}$ was measured based on this mode¹; however, curve crossings⁶ between the emitting singlet state and the dark triplet states in NS make this concept poorly suited to the laser application.

6. Comparison of the known spectroscopies⁷ of NO, NS and NSe suggested that the replacement of Se for S may eliminate the problematical singlet-triplet crossings encountered above. Excitation of gas mixtures containing FN_3 , SF_6 and $(\text{CH}_3)_2\text{Se}_2$ produced measurable NSe(B-X) emission⁸, but this concept was not scalable due to the rapid quenching⁹ induced by the organic byproducts of the donor molecule. Attempts to synthesize H_2Se_2 as a superior donor were only partially successful. Sodium diselenide (Na_2Se_2) was first synthesized in diglyme solvent, using the method of Boudjouk¹⁰. The H_2Se_2 was then obtained (in solution) upon reaction of Na_2Se_2 with stearic acid. In diglyme, it was possible to entrain H_2Se_2 from the solution phase by bubbling with a stream of He, and NSe emission was subsequently generated by adding FN_3/SF_6 prior to CO_2 laser excitation. Due to the vapor pressure of diglyme and the attraction between the solvent and solute, however, organics were carried over to the reactor as evidenced by production of intense CN emission and concurrent quenching of $\text{NF}(a^1\Delta)$. Since the CN potential curves and radiative rates are not suited to the laser application⁷, the work was repeated using a chemically similar but much lower vapor pressure (tetraglyme) solvent. In this case the CN emission was eliminated, but it was not possible to disengage the H_2Se_2 donor from the solvent before the unstable molecule decomposed to H_2Se and Se metal.
7. Attempts were made to generate HPCl_2 , a potential PCl donor, by passage of PCl_3 over heated NaBH_4 pellets. Upon mixing the reaction products with FN_3/SF_6 , and exciting the gas stream by a CO_2 laser, intense BH(A-X) emission⁷ was obtained instead of the expected PCl chemiluminescence¹¹. Subsequent investigation proved this result to be caused by accidental generation of B_2H_6 rather than HPCl_2 . Evaluation of the known spectroscopy, radiative rates and potential excitation mechanisms suggested that the BH(A-X) transition at 433 nm was well-suited to the laser application.

Kinetics and Scaling

The remainder of the work done under contract focused on the NF/BiF and NF/BH concepts. In each case an initial study was performed to determine the mechanism of excitation, the key kinetic rate coefficients, the feasibility of inversion, and scalability to emitter concentrations



that would generate useful gain coefficients as well as permit efficient extraction of energy stored as metastable $\text{NF}(a^1\Delta)$ in competition with the self-annihilation reaction.

Bismuth Fluoride

1. Both TMB and BiH_3 were found to be efficient sources of BiF under selected conditions. It was not possible, however, to generate or store BiH_3 at a concentration that was large enough for the laser application. Use of TMB on the other hand was problematical with respect to both the slow rate of dissociation and rapid quenching of $\text{NF}(a^1\Delta)$. Consequently, under optimal conditions only very small gain coefficients were anticipated. No other efficient BiF donors, with suitable vapor pressure, were identified.
2. The measured time profiles of $\text{Bi}(^2D)$, $\text{BiF}(A)$ and $\text{NF}(a^1\Delta)$ were consistent with a mechanism of excitation involving the reaction $\text{Bi}(^2D) + \text{NF}(a^1\Delta) \rightarrow \text{BiF}(A) + \text{N}$ at a limiting rate of $\sim 4 \times 10^{-11} \text{ cm}^3/\text{s}$.
3. Under low metastable density conditions, using trace concentrations of TMB donor, the yield of $\text{BiF}(A-X)$ photons exceeded the number of donor molecules in the reaction zone, and the intensity of the emission was consistent with the previously measured pump rate. This finding shows that ground state BiF is recycled by $\text{NF}(a^1\Delta)$, and a population inversion should develop at high metastable concentration.
4. Under optimized conditions, using CO_2 laser excitation, $\text{BiF}(A)$ state concentrations scaled to $\sim 10^{14}/\text{cm}^3$ with a pulse width of a few μs .

Boron Hydride

1. The mechanism of excitation of the $\text{BH}(A)$ state by $\text{NF}(a^1\Delta)$ was determined to be resonant energy transfer and pooling through the intermediate (dark) $a^3\Pi$ state based on ab initio calculations of the corresponding energy levels by Michels.
2. An optical absorption diagnostic was developed for the ground and intermediate states of BH , which used a pulsed molecular resonance discharge lamp. The measured yield of BH radicals from B_2H_6 precursor was determined to be $\sim 10^{-3}$.
3. The rate constants for sequential excitation of the $a^3\Pi$ and $A^1\Pi$ states of BH were determined to be $\sim 3 \times 10^{-11} \text{ cm}^3/\text{s}$ and $> 8 \times 10^{-10} \text{ cm}^3/\text{s}$, respectively. These findings



demonstrate that inversion of the A-X transition at 433 nm is feasible for metastable NF concentrations of $\sim 10^{16}/\text{cm}^3$ or higher.

4. Addition of boron precursors to FN_3 occurred without significant pre-reaction, and quenching of $\text{NF}(a^1\Delta)$ by the donor byproducts was minimal. These results, in combination with the large stimulated emission cross section, suggested that exceptionally high gain coefficients are achievable in this system.
5. Reactions between B_2H_6 and a variety of gaseous reagents in a discharge flow system failed to improve the yield of BH radicals. Reaction of B_2H_6 with HN_3 in a heated capillary oven generated tetraazidodiborane. This unstable molecule was a superior source of BH radicals (branching ratio $\geq 14\%$) but rapid removal of BH by vibrationally excited SF_6 (in the CO_2 laser triggered experiment) reduced the concentration yield to $\sim 2\%$. In the shock tube reactor, however, this donor was no better than B_2H_6 since the molecule dissociated into diazidoborane during the metastable induction period. Upon further fragmentation, diazidoborane forms non-productive ($\text{HNBN}_3 + \text{N}_2$) molecules in preference to the desired ($\text{BH} + 3 \text{N}_2$) products.

Gain and Lasing

Both the NF/BiF and NF/BH schemes were evaluated in CO_2 laser driven reactors for optical gain, and positive results were obtained in each case. Since the optical characteristics of these two systems are disparate, different gain measurement techniques were used in each case. Subsequent successful lasing experiments were also performed, using the shock tube reactor to provide a long (50 cm) optical path for the low gain BiF system, and using the CO_2 laser triggered reactor (which provided a 1 cm amplification zone) for the high gain BH system.

Bismuth Fluoride

1. A cavity ringdown experiment demonstrated an optical gain coefficient of $\sim 3 \times 10^{-4}/\text{cm}$ on a selected BiF (A-X, $v' = 1$ to $v'' = 4$) transition near 471 nm.
2. Unsaturated lasing was achieved in the shock tube reactor at 471 nm under conditions that approximated the CO_2 laser driven experiment. Saturated lasing was not achieved due to a low gain-time product, hence power extraction was highly inefficient. The circulating intracavity power, however, was in excess of 100 mW.



3. A TMB precombustion scheme was identified that will allow higher BiF concentrations to be achieved, as the reaction byproducts will be weaker quenchers of $\text{NF}(a^1\Delta)$. If successful, this approach will increase the gain coefficient sufficiently to saturate the laser and thereby increase power output significantly. The concept is explained in detail in a proposal to AFOSR which has been recently awarded¹². Modifications to the shock tube reactor to enable donor precombustion have been completed, but testing and optimization remain to be done.

Boron Hydride

1. Resonance radiation from an electrical discharge lamp was amplified by the NF/BH chemistry. The measured gain was up to 10% /cm with a pulse width of $\sim 2 \mu\text{s}$.
2. Lasing at 433 nm was achieved in an optical cavity with a threshold gain of 2.5 %/cm and a 1 cm gain length. The design of the reactor and optical resonator limited the active volume to less than 2 cubic millimeters. Consequently, only a very small fraction of the $\sim 1 \text{ cm}^3$ reaction zone contributed to stimulated emission.
3. Photographs of the laser output beam were captured and incorporated into a 20-minute video presentation that was recorded in VHS format. A copy of the presentation has been forwarded to the project officer.

Physical Sciences Subcontract

The systems $\text{FN}_3/\text{SF}_6/\text{I}_2$ and $\text{FN}_3/\text{SF}_6/\text{CF}_3\text{I}$ were evaluated for IF(B) production in the CO_2 laser triggered reactor. This concept, originally due to Davis, involves transfer from $\text{NF}(a^1\Delta)$ to vibrationally excited IF molecules to produce the emitting species. The goal of this work was to investigate the system at high $\text{NF}(a^1\Delta)$ concentration, and compare the results with the prior (low density) work at PSI, to gain an understanding of the critical scaling relationships. Potential difficulties include thermal dissociation and reaction of the IF(B) state with $\text{NF}(a)$ or related byproducts and change of pumping mechanism at high metastable concentration. The reactor conditions were modified (lower pressure) to optimize the yield of F-atoms from multiphoton dissociation⁴ of the SF_6 , with the following results:

1. Excitation of IF(B-X) chemiluminescence was optimized at 25 torr total pressure. Dependence on SF_6 concentration suggested a trade-off between F-atom production (favored by lower SF_6) and $\text{NF}(a^1\Delta)$ production (favored by higher SF_6).



2. No differences between CF_3I and I_2 were measurable, suggesting the $\text{IF}(\text{X})$ vibrational ladder was thermalized, since these donors have significantly different nascent product distributions.
3. The vibrational temperatures, F-atom and $\text{NF}(\text{a}^1\Delta)$ concentrations were found to be 1200 to 2000 K, $2 \times 10^{14}/\text{cm}^3$ and $3 \times 10^{15}/\text{cm}^3$, respectively, by spectroscopic analysis, titration experiments and absolute photometry.
4. The kinetic lifetime of the $\text{IF}(\text{B})$ state was measured as $\sim 2 \mu\text{s}$, independent of the FN_3 concentration. This result demonstrates that $\text{IF}(\text{B})$ is not thermally dissociated at a high rate and the rate of deleterious reaction between $\text{NF}(\text{a}^1\Delta)$ and $\text{IF}(\text{B})$ is too slow to significantly limit scaling of this emitter.
5. Based on the $\sim 2.5 \times 10^{-12} \text{ cm}^3/\text{s}$ rate for $\text{NF}(\text{a}^1\Delta)$ pumping of $\text{IF}(\text{X}, \nu'' \geq 10)$ to the B state, measured by Davis¹³, a non-thermal vibrational distribution exists in the IF ground state (under scaled-up conditions) that is fed by means other than the $\text{F} + \text{I}_2$ reaction. A likely candidate for this process is E-V transfer from $\text{NF}(\text{a}^1\Delta)$.

Conclusions and Recommendations

Three concepts have been identified and found worthy of further development as visible wavelength chemical lasers. Each starts with synthesis of FN_3 from stable reactants, followed by rapid dissociation of the azide to efficiently yield high concentrations of $\text{NF}(\text{a}^1\Delta)$. Although the rate coefficients for radiation (A) and excitation (k) by $\text{NF}(\text{a}^1\Delta)$ vary in these candidate systems, the required metastable concentrations for inversion (A/k) are approximately the same in each case. Each concept also requires fast initiation, and energy transfer from the metastable to the emitter at a high rate, to extract power before significant losses occur due to self-annihilation of the metastable energy store. The emitters (BiF , BH and IF) are capable of supporting lasing at 471, 433 and 625 nm, respectively. The remaining operational characteristics of these lasers depend principally on the efficiency and scalability of the donors or precursors used, since in each case, the emitting molecules are radicals which cannot be transported and, therefore, must be obtained by in situ decomposition of a parent molecule. Consequently, further improvements are most likely to result from theoretical identification, synthesis, and testing of new donor species. Fully satisfactory donors that have adequate vapor pressure, and are capable of rapid/efficient dissociation to form the desired emitters, without liberation of byproducts that significantly quench $\text{NF}(\text{a}^1\Delta)$, are yet to



be found. Since the difficulties imposed by poor donor performance are not correctable by hardware design, large-scale demonstrations are premature until this barrier has been eliminated. All future work should therefore be focused on improving the donor chemistry.

The NF/BiF system is the best known of the three laser concepts and, despite its low gain, must be considered the primary candidate since neither the BH nor IF systems have demonstrated lasing in the shock tube reactor, which simulates a high energy laser device on a transient basis. Precombustion of TMB to yield BiH₃, and byproducts that are slower quenchers of NF(a¹Δ), appears to be the best short-term approach for this concept. Work in this direction using the established facilities will be done under a new BMDO funded AFOSR contract. A parallel approach with considerable merit, however, is to use a computational chemist to define an improved donor molecule through ab initio calculations, and a synthetic chemist to develop a preparation of the species and supply gram sized quantities for testing in the CO₂ laser triggered or shock tube reactors.

In the long run, improvements in the area of donor chemistry are most likely to occur in the BH system, since organics that induce rapid quenching are not required for donor volatility as in the BiF system. The short wavelength, inherently high gain, lack of dependence on vibrational relaxation to sustain inversion, and absence of solid reaction products all favor this laser concept, once a practical high-yield donor has been identified. A suitable BH donor molecule for the shock tube experiment will be characterized by a high positive heat of formation and a barrier to dissociation that approximates FN₃.

Ab initio calculations by Bartlett¹⁴ suggest that BC₂ ring structures (borirenes) may be useful in this application. A photolytic synthesis based on ring closure of boron-acetylide precursors has recently been developed for tri-mesityl borirene.¹⁵ Additional theoretical work is therefore required to determine which functional group (R) will best stabilize an H(BC₂)R₂ ring system against self-annihilation, and facilitate dissociation into HB + RCCR fragments. Once the optimized donor has been identified, work must then turn to development of an effective synthesis and characterization of the physical properties prior to testing in a laboratory scale laser reactor.

An alternative approach is to modify the TADB donor to increase its thermodynamic stability against cleavage into non-productive DAB monomers. The related molecule (CH₃)₂BH₂B(N₃)₂ is similar to TADB in that azide-azide annihilation can still lead to desirable BH + N₂ products via a thermoneutral dissociation reaction. The hydrogen bridge bonds in this donor, however, are strengthened in relation to TADB by replacing one pair of azide radicals



(which act as electron withdrawing groups) by a pair of methyl radicals (which act as electron donors) to increase the charge density in the center of the molecule. Based on the heats of dissociation of B_2H_6 and TADB, this donor should be at least as stable as FN_3 , and therefore useful as a BH source in the shock tube reactor. Synthesis of the dimethyl-diazo-diborane donor would most likely proceed by first generating dimethyl-diborane, which can then be thermally reacted with HN_3 (on-the-fly) to replace the terminal H-atoms with azide groups.

In any case, further effort on the NF/BH laser should concentrate on either developing a superior donor or replacing SF_6 by a more inert sensitizer¹⁶ such as SiF_4 (in the CO_2 laser triggered experiment) to eliminate the rapid removal of BH radicals. Either of these approaches, if successful will significantly enhance the photon energy available from a lab-scale laser demonstration experiment.

The IF system is the least well studied of the three candidates, at high $NF(a^1\Delta)$ concentration, although the initial results are favorable. The reactions for producing IF are well-known, and large IF densities are obtainable.¹⁷ On the other hand, the lower pumping rate coefficient in this system is likely to be problematical with respect to donor scaling for efficient power extraction, and the dependence on vibrational distributions will be critical. High yields of $IF(X, v'' \geq 10)$ are needed to pump the laser transition, but the terminal $IF(X, v'' \sim 5)$ states must be depopulated to generate gain. Therefore, an inverted vibrational distribution is required in the $IF(X)$ state. The shallow well depth of the $IF(B)$ state, however, requires a vibrational distribution that is thermalized at relatively low temperatures to control losses due to predissociation. Such disparate vibrational distributions can only be maintained under conditions where vibrational relaxation and equilibration are insignificant. Sustaining a population inversion during power extraction, however, requires a rapid V-T process. Therefore, defining a suitable environment in which both of these seemingly contradictory goals can be met will be a significant challenge.

Once efficient power extraction has been demonstrated in one of these concepts, large scale (blow-down) demonstrations can be pursued with confidence. These experiments, which enable realistic testing of nozzles and resonators, are nonetheless economical since large steady state vacuum facilities are not required, removal of waste heat from the hardware is not an issue, the quantity of hazardous reagents is limited, and work may proceed using current low flow rate FN_3 generators with storage of the azide gas in refrigerated surge tanks. Development of high flow rate FN_3 generators can therefore be postponed until all of the cavity performance issues for this concept have been resolved. A starting point for the development of advanced FN_3 generators is the literature¹⁸ on the direct reaction of F_2 with NaN_3 .



References

1. AFRPL Contract F4611-86-C-0072.
2. J.M. Herbelin and R.A. Klingberg, *Int. J. Chem. Kinetics*, **16** (1984) 849.
3. J.F. Haller, Ph.D. Dissertation, Cornell University (1942).
4. C.R. Quick and C. Wittig, *Chem. Phys. Lett.* **48** (1977) 420.
5. A. Ongstead, USAF Academy (private communication).
6. K. Raghuvver and N.A. Narasimham, *J. Astrophys. Astr.* **3** (1982) 13.
7. B. Rosen, *Spectroscopic Data Relative to Diatomic Molecules* (Pergammon, 1970).
8. G. Pannetier, P. Goudmand, O. Dessaux and I. Aràiti, *Cong. des Soc. Savantes* (Nice, 1965), Vol. 1. pg. 117.
9. K.Y. Du and D.W. Setser, *J. Phys. Chem.* **94** (1990) 2425.
10. D.P. Thompson and P. Boudjouk, *J. Org. Chem.* **53** (1988) 2109.
11. J.A. Coxon and M.A. Wickramaaratchi, *J. Molec. Spectrosc.* **68** (1977) 372.
12. AFOSR Contract F49620-94-C-0025.
13. S.J. Davis, Physical Sciences, Inc. (private communication).
14. I. Cernusak, S. Beck and R.J. Bartlett, *J. Phys. Chem.* **96** (1992) 10284.
15. J.J. Eisch, B. Shafii and A.L. Rheingold, *J. Am. Chem. Soc.* **109** (1987) 2526.
16. K.J. Olszyna, E. Grunwald, P.M. Keehn and S.P. Anderson, *Tetrahedron Lett.* **19** (1977) 1609.
17. C.A. Helms, L. Hanko, K. Healy, G. Hager and G. Perram, *J. Appl. Phys.* **66** (1989) 6093.
18. H.W. Roesky, O. Glemser and D. Bormann, *Chem. Ber.* **99** (1966) 1589.



Publications

The following section contains ten manuscripts that were generated as a result of this contract or related (preceding or parallel) efforts. The first two papers principally relate to production of the metastable species, $\text{NF}(a^1\Delta)$ and $\text{NCl}(a^1\Delta)$, by dissociation of halogen azides. The third paper presents a study of $\text{NF}(b)$ and $\text{IF}(B)$ excitation by these energy carriers. The fourth paper is focused on the mechanism, kinetics and scaling of the NF/BiF system. Measurement of optical gain and demonstration of lasing in BiF are related in the fifth and sixth papers, respectively. The seventh, eighth and ninth papers present the development of the NF/BH concept in a parallel manner, and the last paper addresses the NF/IF scaling study. These papers should be read in the order presented for maximum understanding of the technical results.

"Production of $\text{NF}(a^1\Delta)$ by Dissociation of Fluorine Azide", *J. Phys. Chem.* **93** (1989) 4790.

"Production of $\text{NCl}(a)$ by Thermal Decomposition of ClN_3 ", *J. Phys. Chem.* **94** (1990) 7507.

"Investigation of Two Potential Visible Wavelength Chemical Laser Schemes Based on Thermal Dissociation of Chlorine Azide", *Lasers* **91**, pg. 188.

"Chemical Pumping of Potential Visible Laser Transitions in Bismuth Monofluoride by Thermal Dissociation of Fluorine Azide", *SPIE* **1225** (1990) 543.

"Chemical Generation of Optical Gain at 411 nm", *J. Appl. Phys.* **69** (1991) 2805.

"Threshold Oscillation of an $\text{NF}(a^1\Delta)$ / BiF Visible Wavelength Chemical Laser", *J. Appl. Phys.* **74** (1993) 2900.

"Energy Transfer from Metastable NF to Boron Hydride", in press, *J. Phys. Chem.* (1994).

"A Chemically-Pumped Visible-Wavelength Laser with High Optical Gain", *Appl. Phys. Letters*, in press (1994).

"Investigation of the $\text{BH}(a^3\Pi)$ State in the Presence of Metastable $\text{NF}(a^1\Delta)$ ", submitted to *J. Phys. Chem.* (1994).

"Production of $\text{IF}[B^3\Pi(0^+)]$ in the Presence of High $\text{NF}(a^1\Delta)$ Densities", Report to PSI (1994).

Production of $\text{NF}(a^1\Delta)$ by Dissociation of Fluorine Azide

D. J. Benard,* B. K. Winker, T. A. Seder, and R. H. Cohn

Rockwell International Science Center, Thousand Oaks, California 91360 (Received: November 8, 1988;
In Final Form: February 14, 1989)

The reactions of vibrationally excited HF or DF molecules with FN_3 were found to dissociate the azide, but not to yield metastable NF fragments. Thermal dissociation of FN_3 , on the other hand, yielded metastable $\text{NF}(a^1\Delta)$ with near-unit efficiency. Concentrations of $\text{NF}(a^1\Delta)$ approaching $3 \times 10^{16}/\text{cm}^3$ were obtained at temperatures near 1000 K, and the decay of $\text{NF}(a^1\Delta)$ was found to be dominated by self-annihilation. The activation energy for production of $\text{NF}(a^1\Delta)$ by thermal dissociation of FN_3 was found to agree with ab initio calculations by Michels.

Introduction

Fluorine azide (FN_3) was first synthesized in 1942 by Haller, upon gas-phase reaction of HN_3 with F_2 . In preliminary studies, Haller found that FN_3 reacted by fracture of the azide group which he attributed to a weak central bond. Haller also found that FN_3 was highly explosive when condensed and the gaseous material was slowly but efficiently converted to N_2F_2 and N_2 upon mild heating.¹ Later, Gipstein and Haller² obtained an ultraviolet absorption spectrum of FN_3 , while Pankratov et al.³ demonstrated that FN_3 could be obtained by the reaction of F_2 with NaN_3 . Also, Milligan and Jacox⁴ obtained the infrared absorption spectrum of FN_3 in an Ar matrix. More recently, we studied the ArF laser photolysis of FN_3 and determined the heat of formation as 125–135 kcal/mol, sufficient to allow the molecule to dissociate to electronically excited NF radicals by an exothermic reaction.⁵ Moreover, analysis of the direct products in this experiment

suggested that FN_3 had a singlet ground state; therefore, upon dissociation, only metastable $\text{NF}(a^1\Delta, b^1\Sigma)$ should be formed if spin is conserved. Similar results were obtained for ClN_3 and BrN_3 by Coombe et al.⁶ and Coombe and Lam,⁷ respectively. On the basis of these findings, we began an investigation of FN_3 dissociation in hopes of developing an efficient and chemically clean (scalable) source of singlet NF. Since Hartford⁸ had demonstrated analogous production of $\text{ND}(a^1\Delta)$ upon CO_2 laser multiphoton dissociation of DN_3 , we decided to concentrate on methods to add thermal or vibrational energy to the FN_3 ground state. In parallel with our study, Michels⁹ performed ab initio calculations of the FN_3 potential energy surfaces which yielded vibrational frequencies in good agreement with infrared absorption data^{4,10} and which demonstrated a 0.5–0.7-eV barrier to dissociation of the electronic ground state by central bond rupture. A substantially larger

(1) Haller, J. F. Ph.D. Thesis, Cornell University, Ithaca, NY, 1942.
(2) Gipstein, E.; Haller, J. F. *Appl. Spectrosc.* 1976, 20, 417.
(3) Pankratov, A. V.; Sokolov, O. M.; Savenkova, N. I. *Zh. Neorg. Khim.* 1964, 9, 2030.
(4) Milligan, D. E.; Jacox, M. R. *J. Chem. Phys.* 1964, 40, 2461.
(5) Patel, D.; Pritt, A. T.; Benard, D. J. *J. Phys. Chem.* 1986, 90, 1981.

(6) Coombe, R. D.; Patel, D.; Pritt, A. T.; Wodarczyk, F. J. *J. Chem. Phys.* 1981, 75, 2177.
(7) Coombe, R. D.; Lam, C. H. T. *J. Chem. Phys.* 1983, 79, 3746.
(8) Hartford, A. *Chem. Phys. Lett.* 1978, 57, 352.
(9) Michels, H. H. United Technologies Research Center, Hartford, CT, private communication.
(10) Gholivand, K.; Schatte, G.; Willner, H. *Inorg. Chem.* 1987, 26, 2137.

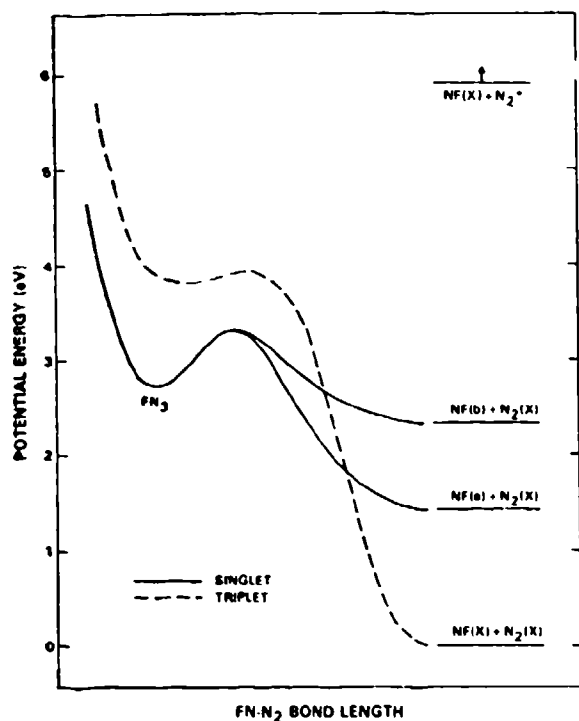


Figure 1. Illustrative potential energy curves of FN_3 . The excited states of N_2 lie at and above the energy level indicated by $\text{NF}(X) + \text{N}_2^*$.

barrier to dissociation of FN_3 was found for rupture of the $\text{F}-\text{N}_2$ bond. These results implied that FN_3 could possibly be dissociated to yield $\text{NF}(a^1\Delta, b^1\Sigma)$ by vibrational energy transfer from molecules such as HF/DF or even by rapid pyrolysis at modest temperatures. Also, in parallel with our work, Gholivand et al.¹⁰ developed a batch method for the preparation of distilled samples of FN_3 . These authors investigated the vapor pressure curve, the infrared and visible/ultraviolet absorption spectrum, and the mass spectrometric signatures of the molecule.

The dissociation physics of FN_3 can be understood by examination of the potential energy surfaces that correlate to the various electronic states of N_2 and NF at infinite separation, as shown in Figure 1. The triplet surface derived from $\text{NF}(X^3\Sigma)$ and $\text{N}_2(X^1\Sigma)$ is strongly repulsive, because as the N_2 and NF molecules are brought together, some of the triplet character originally associated with NF becomes associated with N_2 in which the triplet states are highly excited.¹¹ The singlet states derived from $\text{NF}(a^1\Delta, b^1\Sigma)$ and $\text{N}_2(X^1\Sigma)$ are less repulsive but are nonetheless still influenced by other higher lying states. The interaction of the excited triplet states of N_2 with $\text{NF}(X^3\Sigma)$ yields higher lying singlet states that are strongly bound due to spin cancellation. These states repel the lower singlet states derived from $\text{NF}(a^1\Delta, b^1\Sigma)$ and $\text{N}_2(X^1\Sigma)$, resulting in a potential well that forms the singlet ground state of the FN_3 molecule. The repulsive triplet state, arising from $\text{NF}(X^3\Sigma)$ and $\text{N}_2(X^1\Sigma)$, must pass above the minimum of this well for FN_3 to be a stable molecule, since otherwise the bound FN_3 molecules would spontaneously dissociate following radiative decay. Michels⁹ has calculated that the triplet state actually crosses the lowest singlet state of FN_3 on the outside of the dissociation barrier and that the singlet-triplet splittings inside the barrier lie in the range 1–2 eV. Addition of energy to the FN_3 molecule can therefore result in dissociation to NF and N_2 by either of two mechanisms. Transfer of thermal or vibrational energy to the FN_3 ground state, sufficient to surmount the barrier, should lead to dissociation on the singlet surface, yielding $\text{NF}(a^1\Delta, b^1\Sigma)$ and $\text{N}_2(X^1\Sigma)$ as products. On the other hand, transfer of larger amounts of vibrational or even electronic energy to the ground state of FN_3 could access the triplet state of FN_3 ,

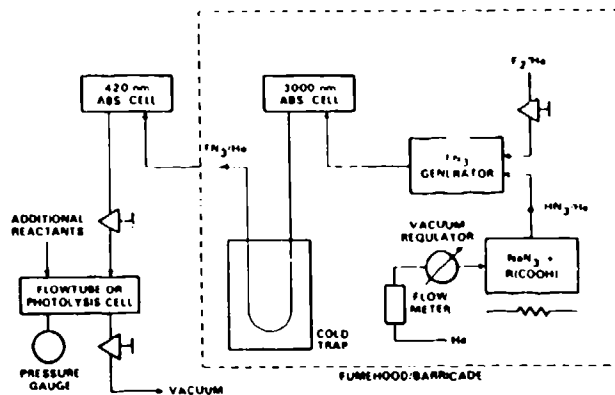


Figure 2. Schematic of gas flow system used to generate and study dissociation of FN_3 .

which dissociates to $\text{NF}(X^3\Sigma)$ and $\text{N}_2(X^1\Sigma)$ instead. To investigate these phenomena, we have studied the production of $\text{NF}(a^1\Delta, b^1\Sigma)$ from FN_3 molecules that were suddenly exposed to either a high-temperature inert buffer gas environment or vibrationally excited molecules such as HF/DF , which have harmonic spacings that approximate the barrier to dissociation.

Experimental Section

A gas flow system, shown schematically in Figure 2, was developed as a continuous or "on-line" source of FN_3 molecules. The lasers and optical diagnostics used to induce and monitor the FN_3 dissociation have been omitted from this figure for the sake of clarity. FN_3 was produced following the method of Haller,¹ with some refinements, by titrating HN_3 diluted in He with a similarly diluted flow of F_2 at 35 °C. HN_3 was obtained by electrically heating a mixture of NaN_3 and a large (20/1) excess of stearic acid to approximately 100–110 °C.¹² The end point of the titration was determined by monitoring the residual HN_3 concentration in absorption at 3000 nm.¹³ To maintain an optimum yield of FN_3 , the temperature of the NaN_3 /stearic acid mix was programmed so that the HN_3 evolution was constant, since excess F_2 slowly reacts¹ with FN_3 to yield NF_3 and N_2 . The FN_3/He stream was purified of residual HN_3 and byproduct HF by passage through a cold trap^{10,14} at -100 °C, and the FN_3 concentration was monitored in absorption at 420 nm, using the extinction coefficient data of Gholivand et al.¹⁰ The entire apparatus, except the 420-nm absorption cell, was barricaded inside a fume hood for the protection of the experimenter. Typical concentrations of FN_3 were 7 Torr in 350 Torr of He at a net flow rate of 3 cm^3 (STP)/s, which (within the accuracy of our measurements) corresponds to converting approximately 50–100% of HN_3 into FN_3 . Mass spectrometric analysis revealed that initial N_2F_2 formation was less than 10% of FN_3 , and roughly 50% of FN_3 decayed to N_2F_2 over a period of about 1 h when stored at a temperature of 14 °C and at a net pressure of 150 Torr in a Teflon-lined cylinder. The mass spectrometer was calibrated by monitoring the mass 61 (FN_3) and mass 66 (N_2F_2) peaks before and after passing the FN_3 flow through a heated section of tubing which induced complete conversion to N_2F_2 . The FN_3/He stream was reduced in pressure and carried to the various experiments by stainless steel and Teflon tubing, which typically delivered FN_3 to the reactor in less than 60 s from generation. Further details regarding the production and measurement of FN_3 are contained in a previous publication.¹⁵

Three experiments were performed in which FN_3 was reacted to form $\text{NF}(a, b)$. In the first experiment, the FN_3/He flow was

(12) Krakow, B.; Lord, R. C.; Neeley, G. O. *J. Mol. Spectrosc.* 1968, 27, 148.

(13) Dows, D. A.; Pimentel, J. C. *J. Chem. Phys.* 1955, 23, 1258.

(14) Weast, R. C. *Handbook of Chemistry and Physics*, 60th ed.; CRC Press: Boca Raton, FL, 1980.

(15) Benard, D. J.; Cohn, R. H. "Model Studies of CBES Decomposition"; Technical Report 87-071; Air Force Astronautics Laboratory: Edwards AFB, CA, Feb 1988.

(11) Rosen, B. *Spectroscopic Data Relative to Diatomic Molecules*; Pergamon Press: New York, 1970.

admitted to a chemiluminescence flow-tube reactor along with a variable flow of D_2 and a fixed flow of dilute F_2 in He that was passed through a microwave discharge¹⁶ to generate approximately 50 mTorr of F atoms.¹⁷ The flow tube was operated at a plug flow velocity of 10^3 cm/s and at a net pressure of 1–2 Torr. The concentration of FN_3 in the flow tube was approximately 5–10 mTorr, and the D_2 flow was adjusted in the range 0–50 mTorr, with the balance of the gases as He. The D_2 and FN_3 flows were admitted to the reactor through coaxial injectors whose position was variable with respect to a fixed (1-in. diameter) sapphire window on the side of the flow tube. The F atoms were admitted to the outer annulus of the flow tube well upstream of the mixing region, and the interior of the flow tube was Teflon coated to minimize wall recombination. Additional details¹⁷ regarding the flow tube reactor are contained in a prior publication. Previous studies using this reactor and the Cl_2 titration method^{17–18} have demonstrated negligible loss of F atoms enroute to the mixing region. The injectors were staged so that the D_2 was admitted to the reacting flow approximately 2 cm upstream of the FN_3 inlet. The resulting chemiluminescence was monitored by an optical multichannel analyzer (OMA) through the observation port.

In the second experiment, the FN_3/He gas mixture was admitted to a slowly flowing stainless steel photolysis cell, along with a variable concentration of HF or DF and a variable concentration of SF_6 . The cell was then optically pumped through a sapphire window by a pulsed HF or DF electrical discharge laser, and the resulting chemiluminescence was monitored at right angles to the laser beam through a sapphire window by a temporally gated OMA and a filtered Si photodiode that was interfaced to a digital signal averager. The concentration of FN_3 in these experiments was also followed on a time-resolved basis by absorption of 210-nm radiation,^{5,10} from a D_2 lamp that was propagated through the cell coaxial with and internal to the HF/DF laser beam. Overtone emission¹¹ from vibrationally excited HF or DF was also monitored with 1- μ s temporal resolution by a liquid nitrogen cooled intrinsic Ge detector filtered to a narrow band around 1300 nm. Typical cell conditions were 100–150-Torr total pressure, of which 1–2 Torr was FN_3 , 1–10 Torr of either HF or DF, and 0–50 Torr of SF_6 , with the balance as He. The HF/DF laser was constructed following references in the literature¹⁹ by suitable modification of an excimer laser. The maximum obtainable pulse energy was 350 mJ with a submicrosecond pulse width. The reactants in the laser (H_2 or D_2 and SF_6) were typically adjusted, however, to yield 10–20- μ s-long pulses of 20–40-mJ energy that were focused to a uniform 0.3×0.5 cm² spot inside the photolysis cell as measured by exposure of thermal image paper. Based on measurements of the laser energy that was transmitted through the cell (2-cm active length), only a small fraction (<5%) of the incident radiation was absorbed. Spectral and temporal analysis of the HF laser revealed simultaneous operation on the $2 \rightarrow 1$ and $i \rightarrow 0$ transitions over most of the laser pulse, with the majority of the pulse energy concentrated in the P(6) and P(7) rotational lines.²⁰ The DF laser was used in preference to the HF laser when $NF(a-X)$ measurements were critical, because HF($\Delta v=3$) overtone emission, typically present at early times, spectrally overlapped the $NF(a-X)$ band.¹¹

In the third experiment, approximately 5 J of multimode untuned 10.6- μ m radiation from a carbon dioxide TEA laser (300-ns pulse width) was focused to a 1-cm-diameter spot inside a second photolysis cell that was equipped with NaCl windows at Brewster's angle for passage of the laser beam and orthogonal quartz windows for viewing of the chemiluminescence. The cell contained approximately 0.1 Torr of FN_3 , 5 Torr of SF_6 , 0–1 Torr of H_2 , and 5 Torr of Ar used to purge the NaCl windows, with the balance He to a total pressure of 25 Torr. Apertures were placed in the

side arms of the reactor for passage of the laser beam and Ar purge flows, which were set to limit the absorption of the laser radiation to the center of the photolysis cell. The resulting chemiluminescence emissions were analyzed by the gated OMA and filtered Si photodiode/signal averager. The same experiment was repeated in a redesigned cell using a line-focused 500-mJ CO_2 laser to optically side-pump a 0.25-cm length of a 0.25×7.5 cm² jet of reactive gas contained inside a velocity-matched Ar shield flow. In the active portion of this reactor, the partial pressures were approximately 1.5 Torr of FN_3 , 15 Torr of SF_6 , and balance He to a total pressure of 150 Torr.

In both laser experiments, trace quantities (<2% of initial FN_3) of $Bi(CH_3)_3$ were admitted to the reactors by injecting a small flow of He that was bubbled through the liquid, which was stored in a trap that was cooled to $-63.5^\circ C$ by a chloroform slush bath. The gas pressures in all of the reactors were monitored by electronic manometers, and the concentrations of $Bi(CH_3)_3$ in the reactors were inferred from the vapor pressure curve provided by the manufacturer. Absolute concentrations of $NF(a)$ and $NF(b)$ were calculated from the Si photodiode signals by using the known A coefficients for the $a \rightarrow X$ and $b \rightarrow X$ emission bands at 874 and 528 nm, respectively.^{21,22} Calibration factors were determined for the photodiode/filter combinations using a standard lamp whose spectral output is traceable to the National Bureau of Standards. The major uncertainty in these measurements was estimation of the emitting volume which was defined by the exciting laser beam and other apertures in the optical detection system. The accumulated error in the absolute $NF(a,b)$ concentrations is estimated to be in the range 25–50%.

Results

Flow Tube Chemiluminescence. Flow tube experiments were conducted with the cold trap (used to purify the FN_3/He flow) at ambient temperature, since the presence of HF byproduct impurities was not critical to the results or their interpretation. In the absence of D_2 addition, no visible emission resulted from the reaction of F atoms with FN_3 . Upon addition of D_2 , however, a bright diffuse rose-colored flame appeared and extended 10–20 cm downstream of the mixing region. Spectral scans with the OMA revealed that the major emitters were $N_2(B)$ and $NF(a,b)$.¹¹ The N_2 emissions were expected following production of $NF(a)$, since D atoms (obtained from the $F + D_2$ reaction) are known to initiate a chain with $NF(a)$ that leads to formation of $N_2(B)$.²³ To quantify the yield of $NF(a)$, the D_2 flow was stopped and the F_2 flow that was titrated with HN_3 (for generation of FN_3) was also turned off, so that HN_3 was admitted to the flow tube in place of FN_3 . The reaction of HN_3 with excess F atoms is known to produce $NF(a)$ with near-unit efficiency²⁴ as well as a much smaller yield of $NF(b)$ due to energy pooling between $NF(a)$ and vibrationally excited HF from the $F + HN_3$ reaction.²⁵ The green $NF(b-X)$ emission was readily visible, while the near-infrared $NF(a-X)$ emission was monitored by the OMA. The HN_3 is completely reacted, the $NF(a)$ reaches its peak concentration, and the $NF(b-X)$ emission is totally contained within the field of view in this experiment. Turning on the F_2 flow to the FN_3 generator progressively diminished the $NF(b-X)$ emission, which was extinguished entirely when the F_2 was adjusted to either maximize the yield of FN_3 (measured at 420 nm) or just eliminate the residual HN_3 (measured at 3000 nm), as expected. With the F_2 flow turned off again, D_2 was then added to the flow tube until the $NF(a-X)$ emission was attenuated significantly ($\sim 4\times$) due to competition between the $F + D_2$ and $F + HN_3$ reactions. The F_2 flow to the FN_3 generator was then reestablished to optimally

(16) Fehsenfeld, F. C.; Evenson, K. M.; Broida, H. P. *Rev. Sci. Instrum.* **1965**, *36*, 294.

(17) Chowdhury, M. A.; Pritt, A. T.; Patel, D.; Benard, D. J. *J. Chem. Phys.* **1986**, *84*, 6687.

(18) Ganguli, P. S.; Kaufmann, M. *Chem. Phys. Lett.* **1974**, *25*, 221.

(19) Pummer, H.; Kompa, K. L. *Appl. Phys. Lett.* **1972**, *20*, 356.

(20) Deutsch, T. F. *Appl. Phys. Lett.* **1967**, *10*, 234.

(21) Malins, R. J.; Setser, D. W. *J. Phys. Chem.* **1981**, *85*, 1342.

(22) Tennyson, P. H.; Fontijn, A.; Clyne, M. A. *Chem. Phys.* **1981**, *62*, 171.

(23) Cheah, C. T.; Clyne, M. A. A.; Whitefield, P. D. *J. Photochem.* **1981**, *15*, 21.

(24) Hadbas, J.; Wategaonkar, S.; Setser, D. W. *J. Phys. Chem.* **1987**, *91*, 451.

(25) Pritt, A. T.; Patel, D.; Coombe, R. D. *Int. J. Chem. Kinet.* **1984**, *16*, 977.

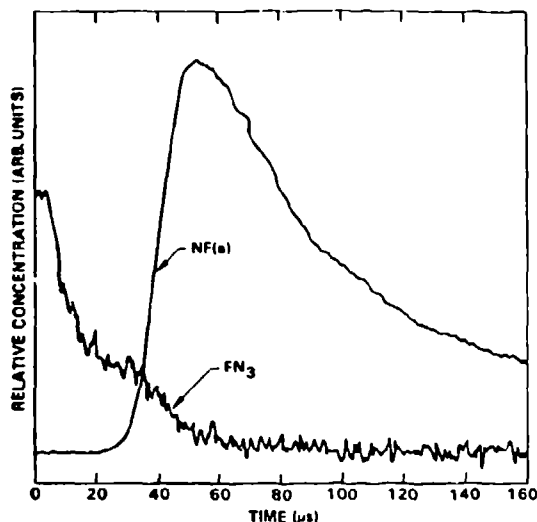


Figure 3. Comparison of typical NF(a) and FN₃ time profiles following pulsed DF laser excitation of FN₃/DF gas mixture.

convert HN₃ to FN₃. This procedure restored the NF(a-X) emission to near its original intensity (F + HN₃ reaction). Since at most one FN₃ molecule is formed from each HN₃ molecule (upon titration with F₂) and since HN₃ is an efficient precursor of NF(a), these results show that FN₃ is also an efficient precursor of NF(a). The mechanism of reaction, however, cannot be determined from the flow tube experiment, since there is no temporal resolution and D₂ addition both heats the bath gas and generates vibrationally excited DF molecules. These data, nonetheless, provided the initial motivation for the more definitive experiments that followed.

HF/DF Laser Photolysis. Since the infrared absorption bands^{4,10} of FN₃ do not match the HF/DF laser wavelengths,²⁰ HF/DF was added to FN₃ in the photolysis cell to act as a sensitizer. Laser excitation of the FN₃/sensitizer gas mixture also resulted in rose-colored chemiluminescence. The principal emitters, as in the flow tube, were NF(a,b) and N₂(b). Overtone emission from the HF/DF was also present. Careful titration of HN₃ with F₂ (to generate FN₃), use of the cold trap to remove residual HN₃ (and byproduct HF), and freeze-thaw-pumping of the HF/DF sensitizer before use (to remove H₂/D₂ generated by passivation of the cylinder walls) were almost completely effective in eliminating the N₂ emissions. When these procedures were not followed, the laser pulse occasionally initiated a deflagration of all gas inside the photolysis cell. By avoiding this condition and using apertures to limit the field of view of the detector, we were able to confirm that the HF/DF overtone and the NF emissions were confined to the volume of gas that was optically pumped by the laser.

The time profile of the HF/DF emissions closely followed the laser pulse in most experiments, while the appearance of NF(a) due to DF laser excitation was delayed, as shown in Figure 3. (The laser was fired at $t = 0$.) The peak concentration of NF(a) increased with increasing HF/DF concentration and moved forward in time. With lower HF/DF concentrations, a significant gap in time opened up between the decay of the HF/DF emissions and the appearance of NF(a) during which there was no significant emission. Figure 4a shows a similar time profile of the 874-nm emission collected with HF in place of DF as the sensitizer and by use of the HF laser for excitation. In this experiment, the detector responded to both the HF($\Delta v=3$) and the NF(a-X) emissions; however, an emission spectrum collected with the OMA temporally gated to the early portion of the time profile demonstrated that the initial (0–25 μs) decay is due solely to HF emission. This result is expected in view of the absence of any NF(a) emission during the similar time period in Figure 3. Figure 3 also demonstrates that the corresponding decay of the FN₃ concentration occurred in two stages. The first stage of FN₃ decay was coincident with the decay of the HF/DF emission, while the second

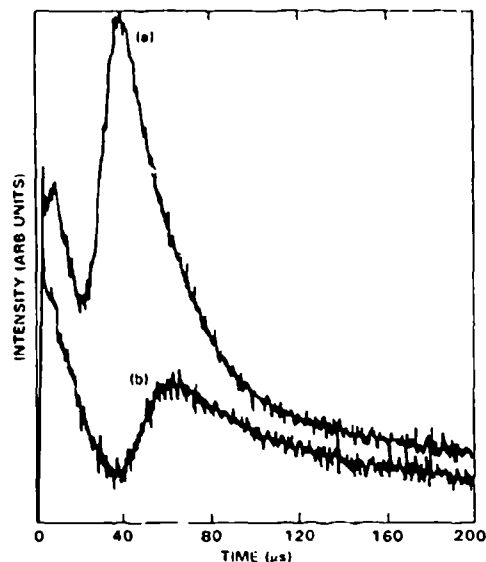


Figure 4. Time profile of 874-nm emission intensity following pulsed HF laser excitation of FN₃/HF gas mixture (a) and effect of adding 10 Torr of SF₆ to the gas mixture (b).

stage was coincident with the delayed appearance of NF(a). The fraction of FN₃ consumed in the initial decay increased with increasing HF/DF concentration, but the amplitude of the net decay remained constant, suggesting that all the FN₃ was consumed in each case. These observations suggest that vibrationally excited HF/DF dissociates FN₃, but does not yield NF(a), and that a second mechanism is responsible for the subsequent decay of FN₃ which liberates NF(a). The largest peak NF(a) concentration was $9.7 \times 10^{15}/\text{cm}^3$, obtained with 9 Torr of DF and 2 Torr of initial FN₃, approximately 50 μs after initiation of a 20-mJ, 10-μs laser pulse. The peak NF(b) concentrations were nominally 2 orders of magnitude smaller than the corresponding NF(a) yields.

By use of low HF concentrations (1 Torr) and relatively short (1–2 μs) laser pulses, it was possible to observe the free decay of the HF($\Delta v=3$) emission. The approximate decay time of the HF(ν) signal was diminished from 20 μs (in the absence of FN₃) to about 10 μs when 1 Torr of FN₃ was added. Therefore, the rate of FN₃ quenching of HF(ν), which sets an upper limit on the rate of FN₃ dissociation by HF(ν), is shown to approximate the V–T rate for HF self-quenching²⁶ or about $3 \times 10^{-12} \text{ cm}^3/\text{s}$. The decays of NF(a) following its peak were also too fast to be explained by quenching due to He, HF, or N₂ resulting from FN₃ decomposition.²⁷ Setser²⁸ recently reported that NF(a) is subject to second-order decay (self-annihilation) at a rate of $2.2 \times 10^{-12} \text{ cm}^3/\text{s}$, based on low-density flow tube experiments at NF(a) concentrations of $10^{17-18} \text{ cm}^{-3}$. We therefore fit our decay curves to second-order kinetics and obtained an average rate constant of $3 \times 10^{-12} \text{ cm}^3/\text{s}$, in good agreement with Setser's finding. Since our data were collected at NF(a) concentrations that were typically 3 orders of magnitude larger than in the Setser study, the second-order nature of the quenching is apparent.

Addition of 50 Torr of SF₆ to the photolysis cell eliminated the appearance of NF(a) completely. As shown in Figure 4b, intermediate levels of SF₆ addition reduced the peak NF(a) concentration significantly and delayed the onset of NF(a) production relative to no SF₆ addition (Figure 4a) but had little effect on the subsequent rate of NF(a) decay. This behavior is incompatible with quenching by SF₆ as an explanation for the reduction of the peak NF(a) signal, since quenching would also advance the peak

(26) Hancock, J. K.; Green, W. H. *J. Chem. Phys.* 1972, 56, 2474.

(27) Koffend, J. B.; Gardner, C. E.; Heidner, R. F. "Kinetics of the H₂-NF₃ System"; Technical Report 85-55; Aerospace Corporation: El Segundo, CA, Sept 1985.

(28) Quinones, E.; Habdas, J.; Setser, D. W. *J. Phys. Chem.* 1987, 91, 5155.

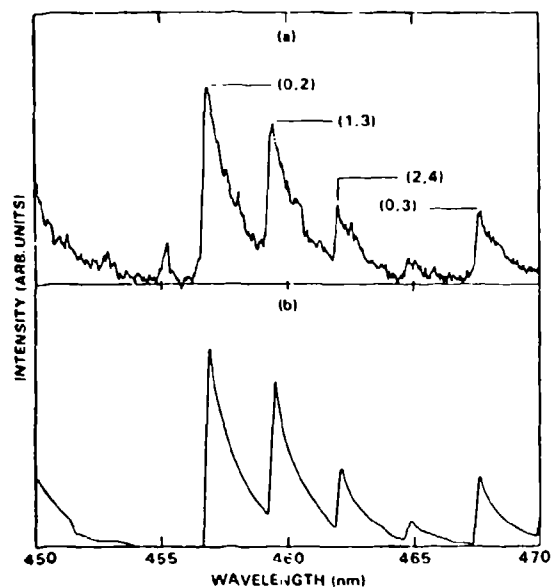


Figure 5. Comparison of (a) measured and (b) calculated BiF(A-X) emission spectra.

NF(a) concentration in time and increase the rate of NF(a) decay in proportion to the amplitude reduction, which is not observed. The result is not surprising, since SF₆ is expected to be a slow quencher of NF(a). The heat capacity²⁹ of SF₆, however, is substantially larger than He. Addition of SF₆ therefore tends to reduce the rise in temperature of the bath gas due to reactive heating, which in turn slows the rate of thermal dissociation of the FN₃. Consequently, the observations noted above are consistent with delayed production of NF(a) by thermal dissociation of FN₃, which begins to occur when the temperature of the bath gas had increased sufficiently due to heat released in the preceding reactions.

The gas temperature was measured spectroscopically by trace addition of Bi(CH₃)₃ which resulted in intense BiF(A-X) emission^{11,30} that tracked the NF(a) time profile. A high-resolution (0.2-nm fwhm) spectrum of the $\Delta v = 2$ and $0 \rightarrow 3$ transitions was recorded by using the OMA with a 40- μ s gate initiated at the peak of the NF(a)/BiF(A) time profile. The recorded spectrum was normalized on a relative basis by assuming that the instrument response was a smooth (linear) function of wavelength over the limited range between the $0 \rightarrow 2$ and $0 \rightarrow 3$ transitions. The slope of the instrument response function was then adjusted so that the normalized $0 \rightarrow 2$ and $0 \rightarrow 3$ intensities were in accord with the ratio of the corresponding Franck-Condon factors.³¹ The vibrational and rotational temperatures were then obtained from the relative intensities and widths of the $0 \rightarrow 2$, $1 \rightarrow 3$, $2 \rightarrow 4$, and $3 \rightarrow 5$ bands, by comparison to a series of temperature-dependent synthetically calculated BiF(A-X) emission spectra that were adjusted for instrument resolution. The calculations were performed and provided to us by Koffend and Herbelin.³² The normalized and synthetic spectra were shown in Figure 5, a and b, respectively, which demonstrate a good fit to $T = 950 \pm 50$ K for both the rotational and vibrational temperatures.

CO₂ Laser Pyrolysis. The preceding experiments provided mechanistic information on the dissociation of FN₃ but were not optimal for determining the NF(a) branching ratio, since only a fraction of the FN₃ was dissociated thermally and the second-order decay of NF(a) occurred on a time scale that was competitive with the dissociation reaction. To overcome these difficulties, as well as to verify the thermal dissociation mechanism, a CO₂

laser-induced temperature jump experiment was performed to trigger the thermal dissociation reaction directly. The incident laser radiation was absorbed by SF₆, resulting in both generation of F atoms by multiphoton processes and heating of the bath gas by V-T quenching. At the high concentrations of SF₆ used (5 Torr), thermalizing SF₆-SF₆ collisions limit the F atom yield³³ to approximately 100 mTorr; consequently, the major effect of the laser excitation was to induce a rapid jump in gas temperature. Recall that in the flow tube experiment no visible emission resulted from admitting FN₃ to a similar environment of F atoms. Direct absorption of the incident laser radiation by FN₃ does not occur in this experiment,^{4,10} therefore, appearance of NF(a) demonstrates thermal dissociation of the FN₃. Because of the higher temperatures that can be achieved by CO₂ laser pumping in relatively short times, NF(a) is expected to reach its peak concentration much more rapidly than in the HF/DF laser experiments, where the heating is due to relatively slow quenching reactions. The FN₃ concentration in these experiments was also lower than in the HF/DF experiments, since the cell design required lower pressures to promote uniform mixing. Visual observation of the NF(b-X) emission demonstrated that the Ar window purges tended to sweep the FN₃ out of the laser beam when the photolysis cell was operated at pressures greater than 25 Torr. At these lower FN₃ concentrations, less NF(a) is formed, and consequently the second-order decay of NF(a) is slower. Therefore, the peak NF(a) concentration in this experiment is much closer to the nascent yield of NF(a) produced by the dissociation of FN₃ than in the HF/DF experiments.

Excitation of the SF₆/FN₃/buffer gas mixture by the CO₂ laser generated both NF(a) and NF(b) rapidly, with no significant N₂ emission,¹¹ and the peak yield of NF(a) corresponded to 70% of the FN₃ molecules that were initially within the active volume of the CO₂ laser beam. As in prior experiments, the yield of NF(b) was typically 1% or less of the NF(a) concentration. The NF(a) signal peaked in approximately 2 μ s, consistent with the bandwidth limitation of the high-gain preamplifier that was used to couple the filtered Si photodiode to the signal averager. The majority of the FN₃ was therefore converted to NF(a) on a submicrosecond time scale. A fit of the NF(a) decay (150- μ s half-life) to second-order kinetics also yielded a rate constant of 3×10^{12} cm³/s, in good agreement with both Setser's data²⁸ and the HF/DF laser experiments, where the peak NF(a) concentrations were a factor of 2-5 higher. Addition of H₂ to the gas mixture produced N₂(B) and enhanced the yield of NF(b) by the same mechanisms^{23,25} that occurred in the flow tube, while addition of trace Bi(CH₃)₃ yielded an intense BiF(A-X) signal that followed the NF(a) time profile after an induction period of approximately 10 μ s.

Since FN₃ is not consumed to heat the buffer gas in these experiments, it is more efficiently utilized to generate NF(a). Consequently, the attainable NF(a) concentrations are limited primarily by the initial FN₃ concentration, provided the dissociation reaction remains fast compared to the second-order annihilation of NF(a). To achieve the highest possible NF(a) concentrations, we therefore performed similar experiments in the redesigned high-pressure reactor which yielded peak NF(a) concentrations as large as 3×10^{16} /cm³. The time for FN₃ consumption (10% \rightarrow 90%) in this reactor was approximately 2 μ s as revealed by absorption measurements at 210 nm; the temperature at the peak of the NF(a) time profile (coincident with 90% FN₃ consumption) was found to be approximately 1150 K by spectroscopic analysis with trace addition of Bi(CH₃)₃, and the NF(a) decayed to 50% of its peak concentration in about 5 μ s. A detailed study of the performance of this reactor is in progress, and the results will be forthcoming in a future publication.

Discussion

While NF(a) production by thermal dissociation of FN₃ is clearly indicated by the above experiments, the source of the reactive heat to raise the gas temperature in the HF/DF laser

(29) Chase, M. W.; et al. *JANAF Thermochemical Tables*, 3rd ed.; *J. Phys. Chem. Ref. Data* 1985, 14, (Suppl. No. 1).

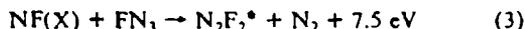
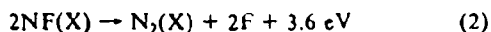
(30) Herbelin, J. M.; Klingberg, R. A. *Int. J. Chem. Kinet.* 1984, 16, 849.

(31) Jones, W. E.; McLean, T. D. *J. Mol. Spectrosc.* 1981, 90, 481.

(32) Koffend, J. B.; Herbelin, J. M. The Aerospace Corporation, El Segundo, CA, private communication.

(33) Quick, C. K.; Witting, C. *Chem. Phys. Lett.* 1977, 48, 420.

experiments is uncertain. Since the decay of the vibrationally excited HF/DF molecules can be separated in time from the appearance of the NF(a), it follows that reactive heating of the bath gas is controlled by the decay of metastable intermediates, at least for low HF/DF concentrations. Also, since interaction of FN₃ with vibrationally excited HF/DF dissociates the molecule, but does not yield NF(a), it is likely that NF(X) is produced instead. A potential mechanism for NF(X) generation is V → E energy transfer from vibrationally excited HF/DF molecules to FN₃, yielding the triplet state which then dissociates. Wilkins has performed a series of NEST calculations³⁴ that model the optical pumping of HF molecules under our experimental conditions (without FN₃). These calculations show peak $v = 1$ and $v = 2$ mole fractions of roughly 10% and 1%, respectively. Based on Michel's placement of the triplet state⁹ in FN₃, only the energy levels of HF at or above $v = 2$ could dissociate FN₃ by this mechanism. If dissociation of FN₃ upon collisions with HF($v=2$) occurs at a rate of 3×10^{-11} cm/s, then the apparent rate of quenching of HF(v) by FN₃ would be 3×10^{-12} cm³/s (the HF ladder is equilibrated by rapid V-V collisions), and the initial decay of the FN₃ should occur on the 10-μs time scale, consistent with the data. The following reactions are therefore capable of heating²⁹ the bath gas:



The estimated rate of quenching of vibrationally excited HF by FN₃ shows that reaction 1, induced by vibrationally excited HF/DF, is probably the rate-limiting step, as might be expected since spin is not conserved. When NF(X) is produced slowly at ambient temperature by thermal dissociation of FN₃ and subsequent quenching of the NF(a), reaction 3 is expected to dominate over reaction 2 because of the linear vs quadratic dependence on NF(X) concentration. This result is consistent with Haller's observation¹ that N₂F₂ is formed efficiently by slow thermal decomposition of FN₃. In the HF/DF laser-driven experiments, however, the NF(X) and FN₃ concentrations may be comparable which would allow reactions 2 and 3 to compete with each other. Energy released by any of these reactions can be tied up in vibrational excitation of the products, which then heat the bath gas upon V-T quenching after a time delay. Moreover, spin conservation in reaction 3 implies that electronically excited triplet N₂F₂* is formed in preference to the singlet ground state. Ab initio calculations of the N₂F₂ potential surfaces performed by Brenner³⁵ have indicated that the lowest triplet (metastable) state lies at 4.5 eV, within easy reach of the heat released^{5,29} in reaction 3. Therefore, slow electronic quenching may also be a factor in the heating of the bath gas prior to thermal dissociation of FN₃. In any case, since vibrationally excited HF/DF initiates and controls the (first) decomposition of FN₃ (which reactively heats the bath gas), increasing the HF/DF concentration is expected to accelerate the NF(a) time profile, as observed. Thermodynamic estimates^{5,29} also show that decomposing approximately two-thirds of the initial FN₃ yields the observed gas temperatures at the peak of the NF(a) time profile, in good agreement with the FN₃ absorption data in Figure 3.

To achieve the highest NF(a) concentrations in the HF/DF experiments, thermal dissociation of FN₃ must be induced as rapidly as possible to minimize the effect of the second-order decay. Since even 1 mJ of incident radiation saturates the HF/DF molecules that are exposed to the laser beam, increased laser energy has little effect. Larger HF/DF concentrations and longer laser pulses are useful, however, because only about 10% of the HF/DF rotational distribution is directly pumped by the laser, and these factors increase the number of molecules that interact with the laser beam as well as promote faster and more complete

rotational redistribution during the laser pulse.³⁶ At 10 Torr of HF concentration, a maximum temperature rise of 100 °C due to laser absorption is estimated based on the NEST calculations,³⁴ adjusted for quenching of HF(v) by FN₃. This temperature rise is insufficient to drive the thermal dissociation of FN₃ by itself; however, it can have a significant effect in combination with reactions 1-3 due to the exponential dependence of the dissociation rate on temperature. Finally, since thermal dissociation of FN₃ (to yield NF(a)) and the subsequent self-quenching of NF(a) are both exothermic processes, the dissociation reaction is expected to drive to completion once it is thermally initiated, in line with our experimental observation.

Regardless of the mechanisms that heat the bath gas, the critical factors that control the NF(a) time profile are the temperature, the frequency of collisions between FN₃ and the bath gas, the activation energy for dissociation, and the second-order decay process. Since Setser's data²⁸ and both of our laser experiments show good agreement, the second-order decay rate of $k_q = 3 \times 10^{-12}$ cm³/s is confirmed. As an aside we also confirm Setser's finding that too little NF(b) is produced to account for the second-order decay rate by energy pooling of two NF(a) molecules to yield NF(X) and NF(b). On the other hand, the reaction to form a N₂ molecule and two F atoms could possibly account for the observed decay kinetics. The activation energy and collision frequency can be estimated from the value of k_q and the HF/DF data as follows.

Once a FN₃ molecule is sufficiently energized to overcome the activation barrier, dissociation will occur on the time scale of a vibrational period or 10⁻¹³ s, while the time between collisions is longer than 10⁻¹⁰ s at 150 Torr. Substantially (10³ times) longer lifetimes for the activated FN₃ molecules are unlikely because of the simple structure which allows the molecule to be treated as a pseudodiatomic as discussed in the Introduction. Consequently, collisions with the buffer gas are not effective in restabilizing the activated FN₃ molecules, and the conversion of FN₃ to NF(a) is rate-limited by the production of the activated FN₃ molecules. In this (low-pressure) limit, the rate of appearance of the dissociation products is proportional to the concentration of collision partners.³⁷ The rate equation for NF(a) at the peak of its time profile can therefore be written as

$$d[\text{NF(a)}]/dt = k_a[\text{C}][\text{FN}_3] - k_q[\text{NF(a)}]^2 = 0 \quad (4)$$

where [C] is the concentration of collision partners (bath gas) and k_a is the apparent dissociation rate constant. Since the activation energy (E_a) is large compared to kT , the FN₃ molecule must accumulate sufficient energy to dissociate as a result of several collisions and since typically one vibrational quantum of energy (E_v) is either added to or subtracted from the azide in each of these events, the energy necessary to dissociate the molecule is acquired in random-walk fashion. Statistics also favors collisions that relax FN₃ over those that increase its internal energy. Consequently, the number of collisions required to induce dissociation is $(\bar{e}_a/E_v)^2 \exp(\bar{e}_a/kT)$. The collision frequency is given by the product of the cross section (σ_c) and the thermal velocity term $(8\pi RT/M)^{1/2}$ where M is the reduced mass of the colliding pair. The dissociation rate can therefore be written as

$$k_a = \sigma_c(8\pi RT^*/M)^{1/2}(E_v/E_a)^2 \exp(-E_a/RT^*) \quad (5)$$

where T^* is the temperature at the peak of the NF(a) time profile. Solving eq 4 and 5 to eliminate k_a yields

$$\sigma_c(8\pi RT^*/M)^{1/2}(E_v/E_a)^2 \exp(-E_a/RT^*) = k_q \frac{[\text{NF(a)}]^2}{[\text{FN}_3][\text{C}]} \quad (6)$$

The right-hand side of eq 6 can be evaluated from the HF/DF data (Figure 3) as 8.5×10^{-15} cm³/s, assuming $[\text{NF(a)}] \sim 10^{16}$ /cm³, $[\text{FN}_3] \sim 7 \times 10^{15}$ /cm³, and $[\text{C}] \sim 5 \times 10^{18}$ cm³, at $T^* = 950$ K. Since the NF(a) yield drops very rapidly with

(34) Kwok, M. A.; Wilkins, R. L. *Appl. Opt.* 1983, 22, 2721.

(35) Brenner, N. University of Louisiana, Baton Rouge, LA, private communication.

(36) Gurev, V. I.; Vasilev, G. K.; Batovskii, O. M. *JETP Lett.* 1976, 23, 230.

(37) Weston, R. E.; Schwartz, H. A. *Chemical Kinetics*; Prentice-Hall: Englewood Cliffs, NJ, 1972; Section 5.2.

temperature, it is not practical to solve eq 6 for σ_c and E_a by collecting additional emission data at a significantly lower temperature. On the other hand, the slow decay of FN_3 at ambient temperature (T_0) is described by the similar relation

$$\sigma_c(8\pi RT_0/M)^{1/2}(E_c/E_a)^2 \exp(-E_a/RT_0) = 1/\tau[C_3] = k_0 \quad (7)$$

where $T_0 = 287$ K, $[C_0] \times 5 \times 10^{18}/\text{cm}^3$, and the decay time (τ) is approximately 4×10^3 s, which yields $k_0 = 5 \times 10^{-23}$ cm^3/s . Taking $M \sim 4$, since He is the predominant collision partner in each case, and setting $E_c = 503$ cm^{-1} (the lowest vibrational frequency⁴ of FN_3) then allows simultaneous solution of eq 6 and 7 to yield $E_a = 0.63$ eV and $\sigma_c = 34$ \AA^2 .

The potential errors in the preceding analysis include quenching of NF(a) by FN_3 and NF(X) , catalytic dissociation of FN_3 on the walls of the holding tank, and errors in the measurement of T^* . Since the NF(a) branching ratio approaches unity and since NF(X) would be scavenged by reactions 2 and 3, it is unlikely that NF(X) achieves a concentration that is comparable to NF(a) . Also, since FN_3 is not a radical species, it is not likely to quench NF(a) as rapidly as NF(a) . Gholivand et al. found that the infrared absorption spectrum of gaseous FN_3 and thin films of condensed FN_3 were nearly identical, which demonstrates negligible intramolecular interaction.¹⁰ Consequently, the Teflon-lined walls of the holding tank are not likely to catalyze FN_3 decomposition. Each of these potential errors results in an underestimation of both σ_c and E_a . Since E_a is determined from a logarithmic ratio of the decay rates, relatively large errors are required to change its value significantly. Such errors would also tend to increase σ_c to physically unrealistic values, since σ_c is already close to the gas kinetic limit. The value of E_a , however, scales much more directly with the value of T^* (which is accurate to about $\pm 5\%$). The measured value of E_a therefore supports Michel's calculation of the barrier height.⁹ The value of σ_c we obtained is also in good agreement with a calculated hard-sphere collision cross section of 38 \AA^2 based on bond lengths³⁸ and van der Waals radii.³⁹ The agreement between our data and the above estimate should be considered as fortuitous, however, since the effects of long-range $T \rightarrow R$ collisions and steric factors have not been included in the analysis.

A computer code was assembled to numerically integrate the differential rate equations for the gas temperature and the $\text{FN}_3/\text{NF(a)}$ concentrations in the side-pumped reactor which achieved the highest NF(a) concentrations. The optical pumping by the CO_2 laser was treated as a heat input, and the only reactions were thermal dissociation of FN_3 to yield NF(a) with unity branching ratio and NF(a) self-annihilation to form $\text{N}_2 + 2\text{F}$.

(38) Radmacher, P.; Bittner, A. J.; Schatte, G.; Willner, H. *Chem. Ber.* **1988**, *121*, 555.

(39) Maitland, G. C.; Rigby, M.; Smith, E. B.; Wakeman, W. A. *Inter-nuclear Forces*; Clarendon Press: Oxford, 1981.

By use of the kinetic rates discussed above and available thermodynamic data,^{5,11,29} good agreement ($\pm 10\%$) was obtained between the model and the data for the simultaneous $\text{FN}_3/\text{NF(a)}$ time profiles and the peak temperature/ NF(a) concentration with only modest ($\pm 25\%$) variation of the rate parameters. These results confirm our basic understanding of the kinetics of generation and decay of NF(a) upon rapid thermal dissociation of FN_3 .

It is also interesting to compare the production of NF(a) by thermal dissociation of FN_3 to the $\text{F} + \text{HN}_3$ reaction,^{24,25} which proceeds by first generating N_3 radicals (HF abstraction) and then passing through an FN_3 intermediate ($\text{F} + \text{N}_3$ reaction) to generate NF(a) . It therefore follows that efficient production of NF(a) in the $\text{F} + \text{HN}_3$ reaction tends to imply efficient production of NF(a) upon thermal dissociation of FN_3 , as observed. The thermal dissociation reaction, however, is much easier to scale to large NF(a) concentrations, since it does not involve reactive intermediates (N_3) which tend to self-annihilate.⁴⁰ The very large concentrations of NF(a) that have been obtained ($\sim 10^3$ of the $\text{F} + \text{HN}_3$ reaction²⁵) reflect this difference and the slow quenching²⁸ of NF(a) by the reaction byproducts (N_2). The attainable yields appear to be limited only by the self-annihilation reaction which is inherent to any scheme for generation of NF(a) .

In summary, thermal dissociation of FN_3 is a process with an activation energy of approximately 0.6 eV, which yields metastable NF(a) with near-unit efficiency. Large ($> 10^{16}/\text{cm}^3$) concentrations of NF(a) can be generated by this reaction; however, the gas temperature must be increased rapidly, so that the NF(a) concentration builds up on time scale that is shorter than the second-order decay, which occurs at a rate of approximately 3×10^{-12} cm^3/s . A significant application for this new source of NF(a) is the development of advanced short-wavelength chemical transfer lasers that are analogous to the oxygen-iodine system.⁴¹ With greater than $10^{16}/\text{cm}^3$ concentrations of NF(a) and transfer rates⁴² approaching 10^{-10} cm^3/s , it will be possible to obtain partial inversions on molecules such as BiF which have radiative lifetimes⁴³ on the order of 1 μs .

Acknowledgment. This research was supported in part by a contract from the Air Force Weapons Laboratory and the Air Force Astronautics Laboratory.

Registry No. FN_3 , 14986-60-8.

(40) Piper, L. G.; Krech, R. H.; Taylor, R. L. *J. Chem. Phys.* **1979**, *71*, 2099.

(41) McDermott, W. E.; Pchelkin, N. R.; Benard, D. J.; Bousek, R. R. *Appl. Phys. Lett.* **1978**, *32*, 469.

(42) Herbelin, J. M. Electronic Energy Transfer Between NF(a) and BiF(X) . *Proc. Int. Conf. Lasers* **1986**.

(43) Heidner, R. F.; Helvajian, H.; Hollaway, J. S.; Koffend, J. B. "BiF(A) Radiative Lifetimes and Rate Coefficients for V-T Transfer and Electronic Quenching"; Technical Report 87-19; Aerospace Corporation; El Segundo, CA, April 1987.

Reprinted from *The Journal of Physical Chemistry*, 1990, 94.
Copyright © 1990 by the American Chemical Society and reprinted by permission of the copyright owner.

Production of NCl(a) by Thermal Decomposition of ClN₃

D. J. Benard,* M. A. Chowdhury, B. K. Winker, T. A. Seder,

Rockwell International Science Center, Thousand Oaks, California 91360

and H. H. Michels

*United Technologies Research Center, E. Hartford, Connecticut 06108 (Received: December 21, 1989;
In Final Form: May 8, 1990)*

Thermal decomposition of ClN₃ by pulsed CO₂ laser pyrolysis has been investigated by using SF₆ as a sensitizer. The electronically excited decomposition products, NCl(a) and NCl(b), were monitored by absolute time-resolved emission spectroscopy while ClN₃ was followed by ultraviolet absorption. The results indicate a higher barrier to dissociation of ClN₃ than FN₃, consistent with *ab initio* calculations, and an NCl(a) yield of order unity, based on a nominal 0.7/s radiative rate for the NCl(a-X) transition. Studies of simultaneous dissociation of FN₃ and ClN₃ have also revealed that NCl(a), when coproduced with NF(a), upconverts the latter species to NF(b) efficiently (in the presence of trace I₂) and cooperatively pumps the IF(B) state (upon addition of CF₃I) by an energy pooling mechanism that does not involve NF(b) as an intermediate. These results indicate a potential for development of chemical lasers that operate on either the NF(b→X) or IF(B→X) transitions at visible wavelength.

Introduction

Production of electronically excited metastable species via direct chemical reaction is central to the development of short-wavelength chemical lasers such as the near-infrared O₂-I system. Here the reaction of Cl₂ gas with base-saturated H₂O₂ generates the 1.0-eV metastable species O₂(a¹Δ) which subsequently pumps the I* lasing species by resonant energy transfer.^{1,2} In the continued

pursuit of this type of laser, which is operable at visible wavelengths, generation of large concentrations of metastable NF(a¹Δ) has recently been demonstrated³ by fast thermal dissociation of gaseous FN₃. Also reaction with and energy transfer from NF(a) to Bi has been shown to result in intense visible BiF(A→X) radiation^{1,4} between 430 and 470 nm. Since NF(a) stores 1.4 eV of electronic energy,¹ the excitation of the BiF(A) state at 2.8 eV requires at least two collisions with this metastable species and

(1) Rosen, B. *Selected Constants Relative to Diatomic Molecules*; Pergamon: New York, 1970.

(2) McDermott, W. E.; Schelkin, N. R.; Benard, D. J.; Bousck, R. R. *Appl. Phys. Lett.* 1978, 32, 469.

(3) Benard, D. J.; Winker, B. K.; Seder, T. A.; Cohn, R. H. *J. Phys. Chem.* 1989, 93, 4790.

(4) Herbelin, J. M.; Klingberg, R. A. *Int. J. Chem. Kinet.* 1984, 16, 849.

a mechanism for energy pooling. Production of 528-nm NF(b-X) emission has also been demonstrated⁵ by resonant energy pooling between chemically generated NF(a) and I* obtained by pulsed laser excitation of ground-state I atoms. Another potential chemical laser is based on excitation of the IF(B-X) transitions from 520 to 720 nm by multiple collisions⁶ with O₂(a).

Metastable NCl(a¹Δ) carries approximately 1500 cm⁻¹ more electronic energy^{1,7} than O₂(a) and is of the same electronic symmetry. Consequently, NCl(a) may be used as a potential in situ pump for I* by energy transfer to ground-state I atoms (in place of an external laser) to generate NF(b) or as a replacement for O₂(a) in the O₂-I or potential IF(B-X) chemical laser systems. Use of NCl(a) to generate NF(b) or IF(B) is interesting, if it can be obtained by thermal dissociation of ClN₃, because the production and dissociation of ClN₃ and FN₃ can then be easily integrated with each other in a common reactor scheme to generate mixtures of the corresponding metastable species. Since the processes of X + N₂ reaction and thermal dissociation of XN₃ are physically similar in the exit channel and Coombe⁸ has found that metastable singlet NX molecules are produced by the reactive mechanism with X = F and Cl, our previous results on FN₃ dissociation² suggested that thermal dissociation of ClN₃ might also be expected to yield metastable singlet NCl products. Therefore, we have investigated CO₂ laser pyrolysis of ClN₃ as a potential source of NCl(a) and have studied production of the NF(b) and IF(B) states in the simultaneous presence of NF(a) and NCl(a).

Theory

Covalent azides, such as FN₃ and ClN₃, have relatively weak central bonds.^{9,10} Consequently, these species may be thought of as complexes formed from more tightly bound NX and N₂ molecules, as described in our prior work,³ which discusses the potential energy surfaces in greater detail. Since the electronic ground states of FN₃ and ClN₃ are both of singlet character,^{11,12} the spin-allowed dissociation products are either singlet (metastable) NX and singlet (ground state) N₂ or triplet (ground state) NX and triplet (metastable) N₂. The singlet products are favored, however, because the triplet states of N₂ are several electronvolts higher in energy¹ than the singlet states of NF or NCl. The heats of formation^{11,12} of these halogen azides are, however, large enough to allow dissociation into the singlet products by an exothermic reaction. Therefore, dissociation of FN₃ and ClN₃ only requires sufficient excitation to overcome the potential barrier which lies between the bound XN₃ ground state and the separated NX(a,b) and N₂ products. Since the central bond is weak, it is anticipated that thermal excitation may be adequate to induce rapid dissociation of the halogen azides at modest temperatures. Once initiated, the dissociation of FN₃ and ClN₃ is expected to proceed to completion, since the associated enthalpy change will increase the gas temperature. Consequently, the primary role of temperature is to control the rate of dissociation, rather than to compensate a thermodynamic deficit.

Ab initio self-consistent field (SCF) calculations of the equilibrium structure and potential energy surfaces of the ¹A' ground states of FN₃ and ClN₃ were performed in optimized C₂ geometry with the GAUSSIAN 88 electronic structure code¹³ using Pople's split-valence (6-31G*) basis sets.¹⁴ Gradient optimizations were performed to locate the geometries of both the equilibrium structure and the transition state. In the case of FN₃, similar

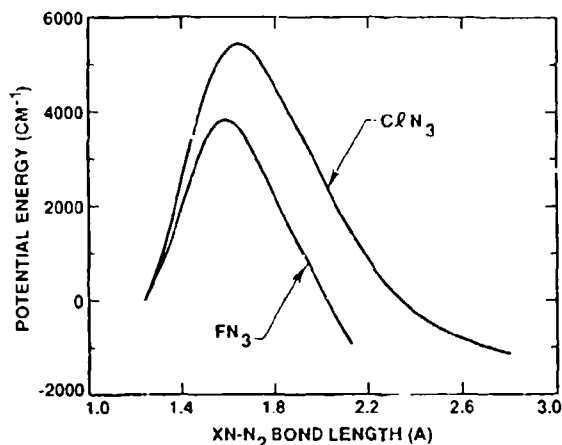


Figure 1. Results of ab initio calculations of the barriers to thermal dissociation of the halogen azides.

calculations have shown a significantly higher barrier to dissociation by stretching of the F-N₃ bond than by central bond fission.³ To ensure that stationary points of the correct curvature have been found, harmonic vibrational frequencies were computed for the equilibrium structure (all real frequencies) and for the transition structure (one imaginary frequency). The SCF calculations yielded equilibrium structures that were in close agreement with the experimental results of Christen et al.¹⁵ for FN₃ and of Cook and Gerry¹⁶ for ClN₃. The average error in the bond lengths and bond angles were 0.03 Å and 1.5°, respectively. It is well-known that SCF frequencies are uniformly too large and that a scaling of the SCF force field is required for comparison with experimental results. A uniform scaling factor of 0.86 was found to bring the calculated vibrational frequencies of FN₃ into good agreement with the data of Gholivand, Schatte, and Willner.¹⁷ This same factor was successfully applied in the ClN₃ calculations, which yielded vibrational frequencies in reasonable agreement with the matrix isolation results of Milligan and Jacox.¹⁸ Comparing the equilibrium and transition states, the classical barrier height of ClN₃ was calculated as 0.67 eV or 5444 cm⁻¹, approximately 1600 cm⁻¹ larger than in FN₃. These barrier heights are reduced slightly by corrections for zero point vibrational energy; however, correlated calculations¹⁹ of FN₃ at the CCD/6-31G* level of theory demonstrate a somewhat greater correction in the opposite direction, indicating that the actual barrier in ClN₃ may be slightly larger than the classical estimate.

The paths of steepest descent from the optimized transition-state geometry were calculated backward toward the equilibrium state and forward to dissociation into NX(a) + N₂ products, using the intrinsic reaction coordinate pathfinder of Schmidt et al.²⁰ as shown in Figure 1. At large XN-N₂ separations, these pathways are not reliable since the dissociating molecule must take on the diradical character of the NX(a¹Δ) product which cannot be correctly represented at the restricted Hartree-Fock level of theory. A multiconfiguration analysis of this dissociation region will progressively lower these potential surfaces as the molecule breaks apart into separated products. In our previous work³ on FN₃, we obtained an experimental barrier height of approximately 0.63 eV, or 1240 cm⁻¹ greater than the classical barrier shown in Figure 1. The relative heights of the calculated barriers for FN₃ and ClN₃, however, should be accurately predicted at the SCF level of theory since the electronic structure and geometry of these two halogen azides are quite similar.

In the case of FN₃, similar calculations^{3,19} have also shown that the repulsive triplet state which correlates to N₂ + NF(X³Σ)

(15) Christen, D.; Mack, H. G.; Schatte, G.; Willner, H. *J. Am. Chem. Soc.* **1988**, *110*, 707.

(16) Cook, R. L.; Gerry, M. C. L. *J. Chem. Phys.* **1970**, *53*, 2525.

(17) Gholivand, K.; Schatte, G.; Willner, H. *Inorg. Chem.* **1987**, *26*, 2137.

(18) Milligan, D. E.; Jacox, M. E. *J. Chem. Phys.* **1964**, *40*, 2461.

(19) Michels, H. H.; Montgomery, Jr., J. A. To be submitted for publication.

(20) Schmidt, M. W.; Gordon, M. S.; Dupuis, M. *J. Am. Ceram. Soc.* **1985**, *107*, 2585.

(5) Herbelin, J. M.; Kwok, M. A.; Spencer, D. J. *J. Appl. Phys.* **1978**, *49*, 3750.

(6) Whitefield, P. D.; Shea, R. F.; Davis, S. J. *J. Chem. Phys.* **1983**, *78*, 6793.

(7) Pritt, A. T.; Patel, D.; Coombe, K. D. *J. Mol. Spectrosc.* **1981**, *87*, 401.

(8) Pritt, A. T.; Patel, D.; Coombe, R. D. *Int. J. Chem. Kinet.* **1984**, *16*, 977.

(9) Haller, J. F. Ph.D. Thesis, Cornell University, Ithaca, NY, 1942.

(10) Treiren, A. *The Chemistry of the Azido Group*; Patai, S., Ed.; Interscience: New York, 1971; Chapter 1.

(11) Patel, D.; Pritt, A. T.; Benard, D. J. *J. Phys. Chem.* **1985**, *90*, 1931.

(12) Coombe, R. D.; Patel, D.; Pritt Jr., A. T.; Wodarczyk, F. J. *J. Chem. Phys.* **1981**, *75*, 2177.

(13) Frisch, M. J., et al. GAUSSIAN 88; Gaussian Inc.: Pittsburgh, PA, 1988.

(14) Hariharan, P. C.; Pople, J. A. *Theor. Chim. Acta* **1973**, *28*, 213.

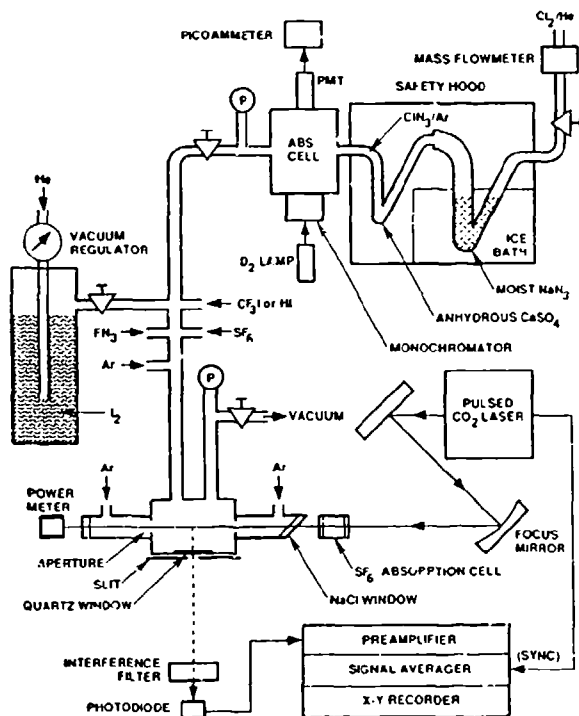


Figure 2. Schematic diagram of the apparatus used to study thermal decomposition of ClN_3 and energy-transfer reactions of $\text{NCl}(a)$.

crosses the potential surface leading to excited $\text{NF}(a,b)$ fragments on the products side of the barrier to dissociation. This condition guarantees a high yield of $\text{NF}(a)$ upon thermal dissociation of FN_3 , as observed,³ since the $\text{FN}-\text{N}_2$ molecule will pass through the spin-forbidden crossing region only once after surmounting the barrier to dissociation. In contrast, thermal dissociation of HN_3 yields primarily $\text{NH}(X^3\Sigma)$ products because the singlet-triplet crossing occurs inside the barrier to dissociation.²⁰ Although the probability of changing from the singlet to the triplet surface is typically less than 10^{-2} each time the crossing region is encountered,²¹ the azide is allowed to leak away into ground-state products because the crossing region is encountered many times before the molecule acquires enough energy to surmount the barrier to dissociation. If the triplet potential curves of ClN_3 are similar to FN_3 rather than HN_3 in this respect, then a high yield of $\text{NCl}(a)$ can also be expected upon thermal dissociation of the parent molecule.

Experimental Section

Generation of ClN_3 . The apparatus used for generation of $\text{NCl}(a)$ radicals and for studying their energy-transfer reactions is shown schematically in Figure 2. Dilute flows of ClN_3 in inert carrier gas were produced by a method following Coombe¹² in which a 10% mixture of Cl_2 in Ar was slowly passed over moist NaN_3 contained in an ice-chilled glass U-tube. An electronic mass flow meter that was calibrated with He to a wet test meter was used to measure the Cl_2 flow. The reactor was operated at approximately 350 Torr total pressure and at a net flow of 3.5 scs. Approximately 1 g of NaN_3 powder was suspended on glass wool that was loosely packed into a 10–15 cm long section at the bottom of the 2.5 cm diameter U-tube. Moisture was added to the reactor by soaking the glass wool in water and then pressing out the excess before treating it with NaN_3 . The gaseous product of the $\text{Cl}_2 + \text{NaN}_3$ reaction was dried by passage through a 5 cm diameter \times 15 cm long column of anhydrous CaSO_4 . In the absence of moisture, the yield of ClN_3 from the reactor was diminished significantly. Infrared absorption of the effluent gas from this generator was studied by using a low-pressure gas cell with IR

transmitting windows and a Fourier transform spectrometer (FTS). The IR spectra showed strong absorption bands¹⁸ at 720, 1140, and 2060 cm^{-1} , confirming the presence of ClN_3 . Mass spectra of the generator effluent also showed no significant peak at $m/e = 43$ and strong peaks at $m/e = 49, 51, 70, 72,$ and 74, which suggests a low yield of HN_3 and indicates a significantly higher yield of ClN_3 (measured as N^{35}Cl and N^{37}Cl) as well as unreacted Cl_2 . The line strengths of the chlorinated species were found to be in proportion to the natural abundance of the Cl isotopes.²³

The absolute concentration of ClN_3 in the effluent of the generator was measured by UV absorption spectroscopy using a gas cell with sapphire windows, a spectrometer-filtered deuterium lamp as the source, and a 1P28 photomultiplier tube (PMT) that was coupled to a picoammeter as the detector. The wavelength band most suitable for the ClN_3 absorption diagnostic was also significantly absorbed by HN_3 , which is a potential impurity due to the use of H_2O as a catalyst for the $\text{Cl}_2 + \text{NaN}_3$ reaction. Therefore, absorption measurements at three UV wavelengths (224, 241, and 254 nm) were performed. In this wavelength range, the absorption cross section of HN_3 varies significantly, whereas the absorption by ClN_3 is nearly constant. The relative optical densities of the effluent gas at these three wavelengths indicated that ClN_3 was the only significant absorber and that no detectable amounts of HN_3 were present. Thus, with knowledge^{12,24} of the extinction coefficient, the concentrations of ClN_3 could be measured routinely by UV absorption at 241 nm. The typical ClN_3 concentration corresponded to approximately 50% of the Cl_2 flow that was admitted to the generator.

Attempts were also made to generate ClN_3 free from Cl_2 and HN_3 by mixing the Cl_2 with dry NaN_3 in a batch reactor and allowing sufficient time for completion of the reaction. In this method, approximately 700 Torr of 10% Cl_2 in Ar was mixed with 100 g of freshly ground NaN_3 in a 2-l. Teflon-lined steel reactor. Stirring of the azide charge with a Teflon-coated magnetic rod was necessary since the azide surface was rapidly passivated. The FTS diagnostic demonstrated that the reaction was slow but complete after 5–10 h with essentially total utilization of the Cl_2 and efficient conversion to ClN_3 , which could then be withdrawn as needed. The ClN_3 decayed to one-half its initial value (70 Torr) in approximately 24 h. The rate of FN_3 decay at 300 K is significantly faster³ than the corresponding rate of ClN_3 decay, as expected, since the latter species is stabilized by a higher barrier to dissociation, as shown in Figure 1. Equivalent results were obtained with the ClN_3 obtained from either generator; however, the flowing reactor was found to offer the convenience of longer run time.

Pyrolysis Reactor. Additional Ar buffer gas and a controlled flow of SF_6 (that acts as a sensitizer) were added to the effluent of the ClN_3 generator and the mixture was admitted to a cross-shaped stainless steel reaction cell in which the reactive gas flow, the CO_2 laser beam, and the viewing axis for the emitted radiation were all mutually orthogonal. The CO_2 laser beam entered and exited the reactor through NaCl windows that were purged with Ar flows and isolated from the center of the reactor by apertures (Figure 2) so that absorption of the infrared photons only occurred within the central chamber of the reactor. The emitted radiation was detected through a quartz window that was not purged. All of the reactor gases were pumped off to vacuum via an adjustable throttling valve, and the corresponding increase in total reactor pressure with the addition of each gas was monitored via a precision capacitance manometer. Since addition of the reactive gases had little effect on the mean molecular weight of the gas mixture in the reactor, the discharge coefficient was not altered significantly. Consequently the partial pressures were taken as additive. The gas pressure in the UV absorption cell of the ClN_3 diagnostic was measured with an inductance transducer from which the mole fraction of the ClN_3 in the generator effluent was determined by using the ClN_3 concentration measurement

(21) Richardson, W. C.; Seiser, D. W. *Can. J. Chem.* 1969, 47, 2725.
(22) Kajimoto, O.; Yamamoto, T.; Fueno, T. *J. Phys. Chem.* 1979, 83, 429.

(23) Weast, R. C. *Handbook of Physics and Chemistry*; CRC Press: Boca Raton, FL, 1986.

(24) Clark, T. C.; Clyne, M. A. *Trans. Faraday Soc.* 1969, 65, 2994.

described above. Typically the total pressure in the reactor was 35–150 Torr which consisted of 5–15 Torr of SF₆, 30–300 mTorr of ClN₃, and balance Ar buffer gas and window purge.

In some experiments, a dilute mixture of FN₃ in He was added to the reactor in near equimolar concentration to the ClN₃ along with variable concentrations of HI or CF₃I and a dilute I₂/He gas mixture that was obtained by passing the carrier gas through a 4 cm diameter × 10 cm deep bed of I₂ crystals at ambient temperature and reduced pressure. The fraction of I₂ in this flow was calculated from its vapor pressure²³ and a measurement of the total gas pressure in the saturator. Typically, this procedure overestimates the I₂ mole fraction in the flow; however, prior experience²⁵ has shown by absorption measurements (similar to those used for ClN₃) that the error is less than a factor of 2. The FN₃ generator and diagnostics have been described in detail in prior publications.^{3,26}

A nominal 10-J pulsed CO₂ laser was softly focused to a 1 cm diameter spot at the center of the reactor by a 100 cm focal length concave mirror. A variable pressure SF₆ cell with NaCl windows was also interposed between the laser and the reactor to partially absorb the 10.6-μm radiation and thereby control the fluence at the reactor, since the laser itself was not easily adjusted. The cell was composed of two NaCl windows spaced 2.5 cm apart and was filled with 0–50 Torr of SF₆. The function of the CO₂ laser was to rapidly heat the gas in the reactor by excitation of the vibrational modes of SF₆, which are promptly thermalized upon collisions with the buffer gas. The suddenly increased gas temperature then triggers dissociation of the halogen azides. After passage through the reactor the laser beam was monitored for pulse energy by an electrically calibrated power (joule) meter. Only a small fraction (<33%) of the incident laser energy was actually absorbed by the SF₆ in the reactor.

Optical Diagnostics. The emission detectors included a gated optical multichannel analyzer (OMA) for collection of visible spectra and a filtered Si photodiode that was interfaced to a step-adjustable-gain preamplifier and a digital signal averager for monitoring the time profiles of the metastable products. The temporal resolution of the recording system was limited by the bandwidth of the preamplifier, which was inversely proportional to the selected gain setting. The sensitivity and temporal response of the entire recording system was determined by using a freshly calibrated Tektronix Model 2235 oscilloscope and pulse generator with a known (±1%) resistance to obtain a standard current pulse that was measured in place of the photodiode. The time profile of the ClN₃ concentration subsequent to the CO₂ laser pulse was also monitored by UV absorption (over a 2.5 cm active path length) using a D₂ lamp as the source and a filtered PMT detector that was coupled to the signal averager. The time-resolved absorption diagnostic is not shown in Figure 2 for the sake of clarity. The synchronizing electrical trigger pulses for the signal averager were obtained directly from the CO₂ laser discharge circuit.

The Si photodiode (EG&G Model SGD-444) was calibrated with a number of selected interference filters using a standard lamp that is traceable to the National Bureau of Standards (now known as the National Institute of Standards and Technology) so that the absolute NF(b) and NCl(a,b) concentrations could be calculated from the signals obtained. Our results confirmed the manufacturer's specifications in regard to the sensitivity of the detector. The recorded signals (in volts) were taken as the product of the active volume in the reactor, the concentration of the species detected, the corresponding *A* coefficient, the solid angle of the 1-cm² detector area (as measured from the center of the reactor) divided by 4π, the transmission factor of the filter for the radiation detected, the quantum efficiency of the detector (in ampere-seconds/photon), and the transconductance gain of our recording system (in volts/ampere). The filter factors were obtained by measuring their transmission as a function of wavelength on a commercial spectrophotometer and then comparing this data

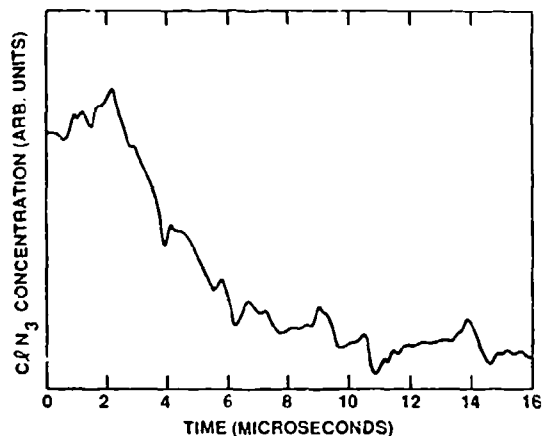


Figure 3. Time profile of ClN₃ concentration following excitation by a pulsed CO₂ laser in the presence of SF₆ as a sensitizer.

with the known emission spectra^{27,28} in the case of NCl(a,b) and by measurement of the NF(b-X) emission via the OMA with and without the corresponding filter in front of the source. Filters were selected with bandwidths that were matched to the width of the emission spectrum in each case. The active volume was taken as the product of the cross-sectional area of the exciting laser beam (as measured by thermal image paper at the center of the reactor) and the length along the beam that was within the detector's field of view, as controlled by a slit (Figure 2) that was located close to the emitting region and suitably far from the photodiode to approximately collimate the light that was detected. As will be shown, the major uncertainty in the determination of the NCl(a) yield was the lack of a reliable value for the corresponding *A* coefficient.

Results and Discussion

Dissociation Rate. Figure 3 shows the decay of a nominal initial 300 mTorr concentration of ClN₃ at a total pressure of 150 Torr in the reactor following pulsed excitation by the CO₂ laser at a fluence of approximately 1 J/cm². From parallel studies of FN₃ decomposition³ the gas temperature in the active region of the reactor is known to approach 1200 ± 100 K with similar laser pulse energies and is relatively constant during the process of dissociation since the absorbed photon energy is large compared to the chemical heat release due to the use of a high diluent ratio. Under these conditions, FN₃ dissociates roughly twice as fast³ as ClN₃. The 4-μs decay of ClN₃ at 1200 K and 150 Torr pressure (Figure 3) and the 24-h decay at 300 K and 700 Torr pressure that was observed in the dry reactor are both well fit to a dissociation rate of $(7 \times 10^{-11} \text{ cm}^3/\text{s})(T/300 \text{ K})^{0.5} \exp(-9600 \text{ K}/T)$ which corresponds to a barrier height of $0.79 \pm 0.07 \text{ eV}$. This result, which exceeds the classical estimate for dissociation of ClN₃ by 930 cm⁻¹, is in line with our theoretical expectations as described earlier. The uncertainty quoted for the barrier height reflects the accuracy of the high-temperature measurement.³ As in our previous work on FN₃, another potential source of error is the possibility of catalyzed decomposition of the ClN₃ on the walls of the dry reactor at 300 K. Corrections for this source of error, however, tend to increase both the activation energy and the prefactor of the exponential in the rate law. Since the prefactor is already at the gas kinetic limit, it follows that the decomposition at room temperature is essentially thermal. The errors in the measured decomposition rates were not deemed to be significant since these only have a weak logarithmic effect on the determination of the activation energy. The prefactor of the exponential term in the ClN₃ dissociation rate, however, is approximately 20 times larger than the corresponding quantity³ for dissociation of FN₃. This factor, which represents the rate of thermal excitation of the azide in collisions with the buffer gas, may be larger in the

(25) Patel, D.; Benard, D. J. *J. Phys. Chem.* **1985**, *89*, 3275.

(26) Benard, D. J.; Cohn, R. H. Technical Report 87-071, Air Force Astronautics Laboratory, Edwards AFB, CA, 1988.

(27) Pritt, A. T.; Coombe, R. D. *Int. J. Chem. Kinet.* **1980**, *12*, 741.

(28) Coombe, R. D.; Van Benthem, M. H. *J. Chem. Phys.* **1984**, *81*, 2985.

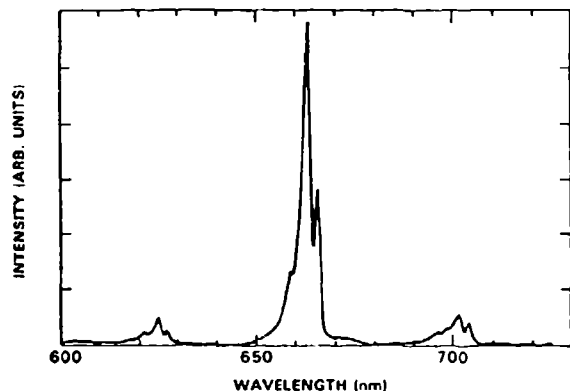


Figure 4. Visible spectrum of $\text{NCl}(b \rightarrow X)$ emission generated from thermal decomposition of ClN_3 .

present ClN_3 experiments (which used Ar buffer gas) due to a mass effect, since our prior work on FN_3 dissociation was conducted using He as the diluent.

NCl(a,b) Production. When the ClN_3 was dissociated a red flash was observed in the reactor which was confirmed by the OMA as $\text{NCl}(b \rightarrow X)$ emission.^{1,27} The emission spectrum is shown in Figure 4. Production of $\text{NCl}(b)$ essentially guarantees that a much larger yield of $\text{NCl}(a)$ will be obtained since the latter state is of the same spin as the former but is less highly excited. The visible emission was also extinguished upon elimination of the SF_6 from the reaction cell, confirming its role as a sensitizer. Direct interaction of the ClN_3 with the CO_2 laser is not expected because the halogen azide has no significant absorption¹⁸ at the 10.6- μm wavelength.

The near-infrared $\text{NCl}(a \rightarrow X)$ emission was detected by using the Si photodiode and a 1.06- μm interference filter. Since the $\text{NCl}(a \rightarrow X)$ emission^{27,28} has a very narrow wavelength distribution, similar in appearance to Figure 4, it was possible to test for overlapping emissions due to other species by first using a narrow-band interference filter that was closely matched to the spectrum of the $\text{NCl}(a \rightarrow X)$ emission and then using a second filter that is centered at the same wavelength with approximately 5 times the bandwidth. Upon comparing the results, good agreement was obtained after correcting the data for the difference in filter transmissions at the $\text{NCl}(a \rightarrow X)$ emission wavelength. This procedure demonstrates that $\text{NCl}(a)$ was indeed produced and that no other species were emitting significantly at the detection wavelength.

The time profiles of the $\text{NCl}(a)$ and $\text{NCl}(b)$ concentrations are shown in Figure 5. Since the intensity of $\text{NCl}(a \rightarrow X)$ emission was small compared to the $\text{NCl}(b \rightarrow X)$ signal, it was necessary to record the $\text{NCl}(a)$ time profile using higher gain in the preamplifier for accurate digitization. This procedure limited the temporal resolution of the $\text{NCl}(a)$ signal to 5 μs , which in turn limited the apparent rate of rise of the $\text{NCl}(a)$ concentration. The $\text{NCl}(b)$ signal was recorded at reduced gain, but with 10 \times higher bandwidth, which accounts for the lower signal to noise ratio of the data. The rise of the $\text{NCl}(b)$ time profile, however, is in good agreement with the corresponding decay of the ClN_3 concentration as shown in Figure 3. This result demonstrates that excited $\text{NCl}(b)$ and presumably $\text{NCl}(a)$ are nascent products of the dissociation process rather than the result of secondary reactions.

The $\text{NCl}(a)$ and $\text{NCl}(b)$ yields were determined from their emission intensities by using the calibration procedure described in the Experimental Section. The decay of the metastable NCl radicals is thought to be due to self-annihilation which is known to be the principal loss channel³ for $\text{NF}(a)$ obtained from thermal decomposition of FN_3 . Since the rate of $\text{NCl}(a)$ decay is relatively fast, the processes of ClN_3 dissociation and the $\text{NCl}(a)$ self-annihilation significantly overlap in time. Therefore, the correct initial concentration of $\text{NCl}(a)$ was obtained by extrapolating the decay curves back to $t = 0$. Care was taken to perform the $\text{NCl}(a)$ yield experiments at the lowest practical ClN_3 concentrations to slow the self-annihilation rate and thereby minimize the error due

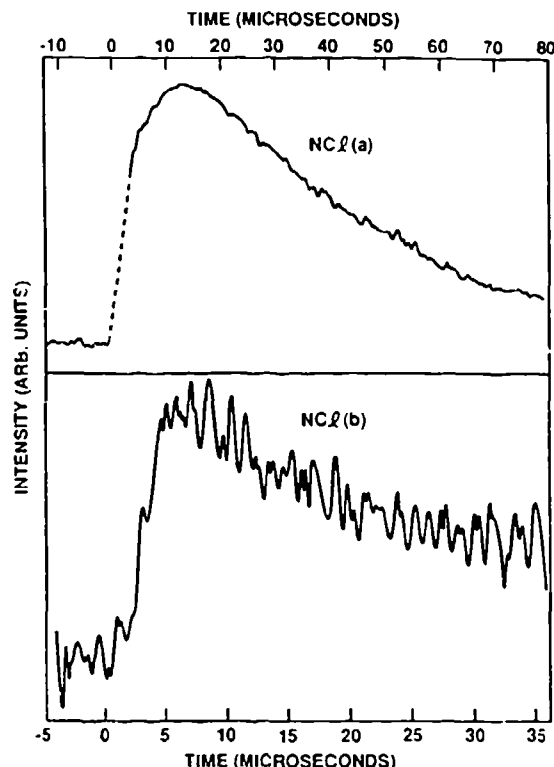


Figure 5. Temporal profiles of $\text{NCl}(a)$ and $\text{NCl}(b)$ on two different time scales. The early portion of the $\text{NCl}(a)$ signal (dashed line) was obscured by electrical noise from the CO_2 laser (fired at $t = 0$) and the corresponding rise time was limited by the bandwidth of the preamplifier.

to extrapolation. This procedure also tends to minimize errors that result from the limited bandwidth of the preamplifier.

The yield of $\text{NCl}(b)$ per ClN_3 molecule was found to be approximately 0.5%, based on the 1600/s value of the A coefficient reported by Coombe et al.¹² The A coefficients for the $\text{NCl}(a \rightarrow X)$ transition that are reported²⁸⁻³⁰ in the literature, however, vary widely from about 437/s to 0.27/s. Since this rate constant directly influences the yield calculation we found it necessary to evaluate the corresponding references. Normally the longest radiative lifetime (~ 4 s) is presumed to be correct since systematic errors due to quenching and diffusion tend to shorten the measured decay time. This result, however, was obtained in an argon matrix²⁹ which requires a significant correction based on the index of refraction for use in the gas phase and is therefore subject to error in either direction. Theoretical calculations by Yarkony³⁰ tend to support a 1.4-s lifetime, as do the reported trends in the $\text{NX}(a)$ state lifetimes and the b/a lifetime ratios^{12,28-31} in the series defined by $X = \text{F}, \text{Cl},$ and Br . Therefore, we calculated our $\text{NCl}(a)$ yield using the corresponding A coefficient of 0.7/s.

The yield of $\text{NCl}(a)$ was also found to be a complex function of the CO_2 laser energy. Initially the yield increased with pulse energy because at low laser fluences the gas temperature is too small to dissociate the ClN_3 on a time scale that is shorter than the decay time due to self-annihilation. Once dissociation becomes rapid compared to the subsequent decay, further increases in gas temperature do not increase the yield of $\text{NCl}(a)$ substantially and may potentially act to reduce the $\text{NCl}(a)$ yield by opening other dissociation channels that do not lead to metastable products. At still higher laser fluences, the yield of $\text{NCl}(a)$ apparently increases again, possibly due to a multiphoton phenomena. Therefore, relative $\text{NCl}(a)$ yields were first determined as a function of CO_2 laser energy and then absolute measurements were performed at

(29) Becker, A. C.; Schurath, U. *Chem. Phys. Lett.* 1989, 160, 586.

(30) Yarkony, D. R. *J. Chem. Phys.* 1987, 86, 1642.

(31) Malins, R. J.; Setser, D. W. *J. Phys. Chem.* 1981, 85, 1342.

(32) Tennyson, P. H.; Fontijn, A.; Clyne, M. A. A. *Chem. Phys.* 1981, 62, 171.

TABLE I: Production of NF(b) by Halogen Azide Dissociation

partial pressure, Torr				rel intensity of NF(b→X) emission
SF ₆	FN ₃	CIN ₃	I ₂	
10.7	0.10			1.0
10.7	0.10	0.14		3.7
10.7	0.10	0.14	≤0.02	27.5
7.5	0.08		≤0.02	2.5

the optimum fluence of approximately 1 J/cm², where a numerical NCl(a) state yield of 110% was obtained, using the 0.7/s value of the *A* coefficient.

If the NCl(a) yield is recalculated by using the largest value of the *A* coefficient²⁸ reported in the literature (498/s) then a 10-fold smaller yield of NCl(a) is obtained than of NCl(b). This result is physically unrealistic since reactions tend to populate the lowest energy product state that is allowed by spin selection rules. Since both NCl(a) and NCl(b) are singlets, the CIN₃ dissociation will strongly prefer the lower energy (a) state as in the case of FN₃ dissociation where typically 100 NF(a) radicals are generated for every NF(b) radical.³ Also, if the NCl(a) yield is smaller than the NCl(b) yield, the reaction would have to proceed efficiently to products that are either spin forbidden, such as NCl(X³Σ) or energetically unfavorable, such as Cl + N₃, since all of the CIN₃ dissociates (as shown in Figure 4) and the combined NCl(a,b) yield would be small compared to unity. Consequently, our yield data suggest that the largest value of the *A* coefficient reported in the literature is overestimated by 2–3 orders of magnitude.

The window purges on the reactor, which act along the path of the laser beam, have a mean velocity of approximately 100 cm/s through the apertures that are shown in Figure 2. Therefore, some of the azide molecules were swept out of the active volume of the reactor. Since we calculated our NCl(a,b) yields assuming a uniform spatial distribution of the parent molecules, the resultant yield that was measured should have been less than 100%. Prior experience with this reactor has shown that the correction factor for this effect is approximately 2. Consequently our data also suggests that the smallest values of the *A* coefficient reported in the literature^{9,30} are underestimated by less than 1 order of magnitude.

Since excited-state yields tend to either approach unity, in the case of an effective spin constraint (as expected here) or a very small statistical yield (typically less than 1%) in the absence of such constraints, it follows that dissociation of CIN₃ is at least a moderately efficient source of NCl(a). Therefore, apart from a somewhat larger activation barrier, the thermal dissociation of CIN₃ parallels the case of FN₃. Precise determination of the NCl(a) yield, however, will have to await a better measurement of the *A* coefficient for the NCl(a→X) transition.

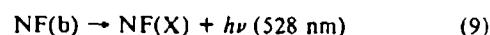
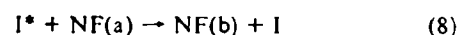
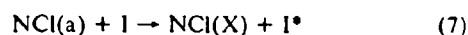
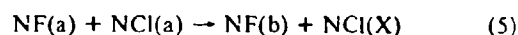
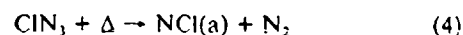
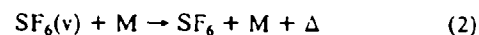
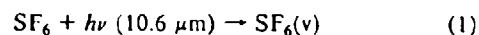
Self-Quenching. The peak NCl(a) concentration in the experiments reported above was approximately 3×10^{13} /cm³ (assuming a 100% yield from CIN₃) and a 40-μs half-life was observed, as shown in Figure 5. As in the case of FN₃, it is unlikely that this decay can be accounted for by reaction with or quenching by the buffer gas, SF₆, or N₂ by-product that is generated³ and the decay occurs well after the CIN₃ is dissociated. If the quenching of the NCl(a) is therefore attributed entirely to self-annihilation, the corresponding rate constant is about 8×10^{-12} cm³/s, somewhat faster than for NF(a) which self-annihilates^{33,34} at a rate of $(3-5) \times 10^{-12}$ cm³/s. Since other factors may still contribute to the observed decay rate and the yield of NCl(a) from CIN₃ may be less than 100%, this result should only be interpreted as an approximation. Further research is required to determine the decay kinetics of NCl(a) in detail.

NF(b) Production. Upconversion of NF(a) to NF(b) was investigated by the simultaneous dissociation of near equimolar concentrations of FN₃ and CIN₃. The NF(b→X) emission was detected with an appropriately filtered Si photodiode coupled to

the data acquisition system described previously. Table I shows that emission from NF(b) was weakly enhanced by addition of either CIN₃ or trace I₂ to the FN₃ in the reactor. Production of NF(b) from NF(a) in the presence of trace I₂ (but not CIN₃) has also recently been studied in a flow tube by Setser,³⁴ who obtained results that are comparable to the last entry in Table using the F + N₃ reaction (which also passes through iN₃ as an intermediate collision complex) to generate NF(a). In our experiment, however, simultaneous addition of both CIN₃ and trace I₂ yielded the most dramatic increase of the NF(b) concentration, by a large margin. Since the ratio of NF(b) to NF(a) obtained from thermal dissociation³ of FN₃ is approximately 1/100, Table I demonstrates that roughly one-fourth of the NF(a) radicals were upconverted to the NF(b) state.

These data also prove that the yield of NCl(a) from CIN₃ is at least 12.5%, independent of the value of the related *A* coefficient, since at most one NF(a) radical can be upconverted to the b state per NCl(a) molecule that is generated, assuming a 70% yield of NF(a) from FN₃ as measured previously.³ With this result in hand, it is now possible to place upper limits of 5.6/s on the *A* coefficient and 6.4×10^{-11} cm³/s for the self-annihilation rate of NCl(a). The actual values, however, may be up to an order of magnitude smaller in each case if the NCl(a) yield approaches unity as suggested earlier by the relative intensities of the NCl(a,b→X) emission signals.

In this system, NCl(a) may potentially contribute to the production of NF(b) via the mechanism in reactions 1–9. Reaction 1



is well-known and is based upon an optical resonance between the CO₂ laser radiation and the vibrational modes of SF₆. Since the laser fluence in our experiments was well below the threshold³⁵ for significant multiphoton dissociation of the SF₆ and the pressure was relatively high, the yield of F atoms is expected to be small in comparison to the added reactants and therefore easily scavenged by reactions with FN₃ or CIN₃ to yield N₂ and either NF₂ or NFCl as benign byproducts. Hence absorption of the CO₂ laser radiation only served to heat the bath gas upon thermalizing collisions with vibrationally excited SF₆ molecules.³⁶ The sudden addition of heat and the associated jump in gas temperature due to reactions 1 and 2 enables the dissociation of FN₃ to produce NF(a) by reaction 3 which has been demonstrated in our previous investigation.³ Reaction 4 is the analogous dissociation of CIN₃ which has been demonstrated in the present investigation to generate NCl(a) efficiently. The reaction of NF(a) and NCl(a) is sufficiently energetic to produce NF(b) but appears to occur slowly, as expected, since reaction 5 violates conservation of spin. The primary role of NCl(a) in this system, however, appears to be excitation of I atoms to the I*(5p²P_{1/2}) state by reaction 7 in a manner analogous to the pumping of I* by O₂(a) molecules in the O₂-I laser system.¹ In parallel experiments, Bower and Yang³⁷ have used the Cl + N₃ reaction to generate NCl(a) in a flow tube and have independently shown that I* is rapidly produced by resonant energy transfer from this metastable species. In our experiment, the I atoms are obtained by dissociation of I₂ which

(33) Quinones, E.; Habdas, J.; Setser, D. W. *J. Chem. Phys.* 1987, 91, 5155.

(34) Du, K. Y.; Setser, D. W. Submitted for publication in *J. Phys. Chem.*

(35) Quick, C. R.; Wittig, C. *Chem. Phys. Lett.* 1977, 48, 420.

(36) Lenzi, M.; et al. *Chem. Phys.* 1990, 142, 473.

(37) Bower, R. D.; Yang, T. T. To be submitted for publication.

may be either thermal in nature or the result of energy transfer from NCl(a) as indicated by reaction 6, since analogous multiple collisions with $\text{O}_2(\text{a})$ are known³⁸ to dissociate I_2 . Production of NF(b) by reaction 8 between I^* and NF(a) is also highly resonant and spin-allowed and has been demonstrated to occur rapidly.³ Since the I/I^* atoms can cycle back and forth between the NCl(a) and NF(a) molecules, their role is catalytic (one I atom can upconvert several NF molecules). Consequently, only trace concentrations of I_2 are required to significantly enhance the production of NF(b) .

Addition of HI in place of I_2 was also expected to enhance the yield of NF(b) , provided the concentration of F atoms present was adequate to yield a significant quantity of ground-state I atoms via the fast reaction³⁹



The effect of HI addition was found to be much less dramatic than expected, however, as the yield of NF(b) saturated with the addition of up to 250 mTorr of HI , showing only a 60% enhancement over the yield that was obtained in the absence of HI . The yield of NF(b) was also a highly nonlinear function of the iodide addition as a 30% enhancement was obtained upon adding only 50 mTorr of HI . These data reinforce the notion that the concentration of F atoms in our experiment was relatively small, since enhancement of the NF(b) production by addition of HI is limited in comparison to the results obtained upon addition of much smaller concentrations of I_2 . Also the saturation characteristic that is observed suggests that F atoms, rather than HI , are the limiting reagent. It is therefore unlikely that I atoms or IF molecules were formed in significant quantities due to the fast reaction⁴⁰



Consequently, the dissociation of I_2 into I atoms must have occurred either thermally or by the action of NCl(a) as indicated by reaction 6. This result is also significant because IF is a known fast quencher^{41,42} of NF(b) .

IF(B) Production. Several researchers^{5,43-45} have found that the $\text{B}^3\Pi_0$ states of ClF , BrF , and IF can be obtained upon addition of $\text{O}_2(\text{a})$ to processes that are likely to populate the lower $^3\Pi_1$ and $^3\Pi_2$ states of the interhalogens, such as three-body recombination of $\text{F} + \text{I}_2$ or $\text{X} + \text{O}_2(\text{a})$ reaction, where $\text{X} = \text{Cl}, \text{Br}$ or I . In each case, these investigators have theorized that $\text{O}_2(\text{a})$ acts to promote the $^3\Pi_1$ or $^3\Pi_2$ intermediates to the higher energy B state via the process of energy pooling. If these states can be accessed by energy transfer from NF(a) to ground-state interhalogens and if NCl(a) can act in the place of $\text{O}_2(\text{a})$, then it should be possible to excite the B-X transitions of a number of interhalogen species following thermal dissociation of mixtures of FN_3 and ClN_3 . Our initial investigation focused on IF , since it is a well-known lasing species,⁴⁶ although other possibilities certainly exist and deserve attention.

The potential for pumping of IF(B) by NF(a) and NCl(a) and for subsequent laser action is shown in Figure 6. The $^3\Pi_1$ state is not shown as it lies too high^{6,45,47} to be excited by NF(a) . The energy levels of the $^3\Pi_2$ states in the interhalogens are largely unknown,⁴⁸ however, the $^3\Pi_2$ state in IF has been located as the

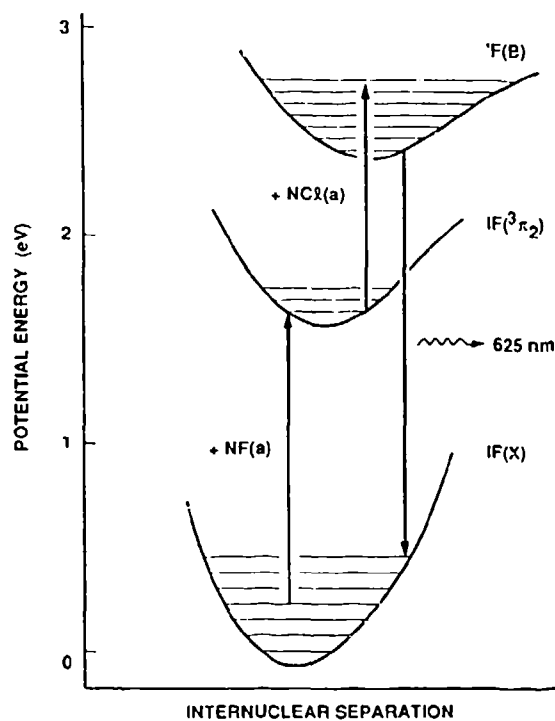


Figure 6. Energy level diagram of IF showing resonances with NF(a) and NCl(a) .

terminal energy level of a pulsed electric discharge laser transition⁴⁹ and has recently been studied in matrix by Heaven and Nicolai.⁵⁰ These authors estimate a gas-phase energy of approximately $13\,500\text{ cm}^{-1}$ between the potential minima of the $^3\Pi_2$ and $X^1\Sigma$ states of IF . Excitation of $\text{IF}(^3\Pi_2)$ by NF(a) therefore requires approximately 2000 cm^{-1} of vibrational energy in the IF(X) ground state, since prior studies⁵¹ have shown that E-E transfer from highly vertical molecules⁵² such as NF is not sensitive to the vibrational distribution of the donor species. The necessary vibrational excitation of the IF(X) ground state is obtained thermally, however, in about 1 out of 10 collisions at a temperature of 1200 K. Pumping of IF(B) from the $^3\Pi_2$ state by NCl(a) , on the other hand, is sufficiently exothermic that some of the product molecules may be generated above the $22\,300\text{ cm}^{-1}$ predissociation limit,⁶ depending on the amount of electronic energy that is converted into translational and rotational forms of excitation. Due to a lack of resonance, NF(a) is not expected to be effective at either pumping or dissociating the IF(B) state when starting from the $^3\Pi_2$ energy level.

At the high pressure of our experiment, vibrational relaxation occurs at a much faster rate than radiation from the excited B state.⁵³ Therefore, the IF(B) will preferentially decay from its lowest vibrational energy levels to vibrationally excited energy levels of the IF(X) ground state that are not thermally populated, since the Franck-Condon factors⁵⁴ strongly favor the transitions from $v' = 0$ to $v'' \sim 5-6$. This phenomenon, which helps to maintain a population inversion, results from the displacement of the potential minimum of the IF(B) state to larger internuclear separation than occurs in the ground state. Consequently, we added CF_3I to our reactor as a potential source of ground-state IF(X) molecules, to investigate the pumping of this highly desirable laser transition by NF(a) and NCl(a) .

Mixtures of SF_6 , approximately 100 mTorr each of FN_3 and ClN_3 , and trace CF_3I were subjected to pulsed CO_2 laser radiation

- (38) Heidner, R. F., et al. *J. Phys. Chem.* 1983, 87, 2348.
 (39) Jonathan, N.; Melliar-Smith, C. M.; Okuda, S.; Slater, D. H.; Timlin, D. *Mol. Phys.* 1971, 22, 561.
 (40) Foon, R.; Kaufman, M. *Prog. React. Kinet.* 1975, 8, 81.
 (41) Benard, D. J.; Chowdhury, M. A.; Pritt, A. T. *J. Appl. Phys.* 1986, 60, 405.
 (42) Cha, H.; Setser, D. W. *J. Phys. Chem.* 1987, 91, 3758.
 (43) Clyne, M. A. A.; Coxon, J. A.; Townsend, L. W. *J. Chem. Soc., Faraday Trans. 2* 1972, 2, 2134.
 (44) Coombe, R. D.; Pilipovich, D.; Horne, R. K. *J. Phys. Chem.* 1978, 82, 2484.
 (45) Coombe, R. D.; Horne, R. K. *J. Phys. Chem.* 1979, 83, 2435.
 (46) Davis, S. J.; Hanko, L. *Appl. Phys. Lett.* 1980, 37, 692.
 (47) Birks, J. W.; Gabelnick, S. D.; Johnston, H. S. *J. Mol. Spectrosc.* 1975, 57, 23.
 (48) Steinfeld, J. I. *J. Phys. Chem. Ref. Data* 1984, 13, 445.

- (49) Eden, J. G.; Dlabal, M. L.; Hutchinson, S. B. *IEEE J. Quant. Electron. QE-17*, 1981, 1085.
 (50) Heaven, M. C.; Nicolai, J. P. To be submitted for publication.
 (51) Pritt, A. T.; Benard, D. J. *J. Chem. Phys.* 1986, 85, 7159.
 (52) Andersson, A.; Ohrn, Y. *J. Mol. Spectrosc.* 1973, 45, 358.
 (53) Davis, S. J.; Hanko, L.; Shea, R. F. *J. Chem. Phys.* 1983, 78, 172.
 (54) Marinelli, W. J.; Piper, L. G. *J. Quant. Spectrosc. Radiat. Transfer* 1985, 34, 321.

to yield significant amounts of IF(B-X) emission. In addition to the cooperative mechanism outlined above, this emission could also result from pumping by NCl(a) without participation of NF(a), in a manner analogous to the known pumping of IF(B) by O₂(a), or by the action of NF(b) independent of NCl(a), as previously recorded in this laboratory.^{51,55} These prior (NF/IF transfer) experiments also demonstrated that NF(a) was not effective at producing the IF(B) state in the absence of other energetic species. In the present experiments, the IF(B-X) emission was reduced approximately 4-fold upon elimination of the FN₃. This result demonstrates that the majority of the observed IF(B-X) emission requires either NF(a) or NF(b). By adding trace I₂ to greatly enhance the NF(b) yield, at the expense of NF(a) and NCl(a), it was possible to show that only a very small fraction of the observed emission was due to transfer from the b state, since the yield of IF(B) was found to decline. Consequently, our data tends to support a cooperative mechanism involving both NF(a) and NCl(a) such as energy pooling through the ³Π₂ state as the dominant mechanism for IF(B) production under the conditions of our experiment. Since we have not observed this intermediate state directly, however, we cannot rule out other cooperative mechanisms that may be based, for example, on ground-state intermediates in a high state of vibrational excitation.

The intensity of the IF(B-X) emission was found to scale linearly with CF₃I addition up to 500 mTorr, which is well in excess of any potential for F-atom generation in our experiment. Therefore, it is unlikely that the IF(X) resulted from the fast reaction⁵⁶



because the yield of IF(B-X) emission would have saturated once the F atoms were titrated against the CF₃I. Since prior results tend to indicate a paucity of F atoms in our reactor, it appears that thermal or energy transfer induced disproportionation of CF₃I is a more likely source of ground-state IF. This mechanism, which

does not require F atoms, would yield the observed linear dependence upon CF₃I addition. Disproportionation of the perfluoroiodide, however, is expected to be a very weak (low yield) source of the ground-state interhalogen, in which case the production of IF(B) may be throttled by IF(X) generation rather than the efficiency of pumping by NF(a) and NCl(a). Also if NF(a) is required to generate the IF(X) from CF₃I, then pumping to the B state can occur (consistent with our observations) solely due to the presence of NCl(a). Therefore, an effective thermal source of IF(X) will have to be developed and characterized before the mechanism and pump rates can be evaluated quantitatively.

Summary

Reaction of Cl₂ with moist NaN₃ efficiently generates ClN₃, which has a barrier to dissociation of approximately 0.8 eV and a near gas kinetic rate of thermal excitation by collisions with the buffer gas. Thermal dissociation of ClN₃ occurs on the 1-10 μs time scale in ~100 Torr of Ar gas buffer at temperatures near 1200 K. The products are primarily NCl(a) and N₂, with a small fraction (<1%) as NCl(b). The radiative lifetime of NCl(a) is thought to be approximately 1.4 s and self-annihilation of NCl(a) may limit the kinetic lifetime of this species at high concentration. By use of a pulsed CO₂ laser and SF₆ as a sensitizer, transient concentrations of NCl(a) as large as 3 × 10¹⁵/cm³ have been obtained. The NCl(a) molecules are capable of generating I* by resonant energy transfer (similar to the O₂-I interaction) and the I* may be used to upconvert NF(a) to NF(b). Cooperative pumping of IF(B) by NCl(a) and NF(a) appears to be limited by the availability of IF(X) due to a lack of F atoms and does not involve NF(b) as a precursor, but may be the result of an energy pooling mechanism that proceeds through the IF(³Π₂) state as an intermediate. Further studies are required to determine the potential of these and similar mechanisms for the generation of visible laser radiation from the electronic energy that is stored in the singlet metastable products of thermally dissociated halogen azides.

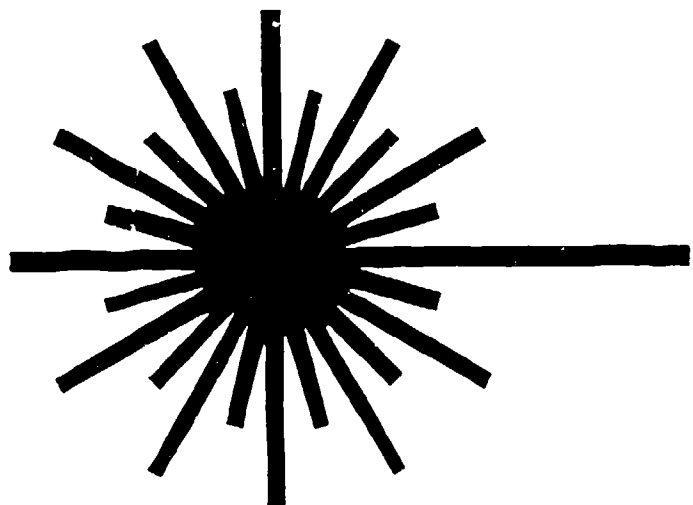
Acknowledgment. The electronic structure calculations were supported in part by the Air Force Astronautics Laboratory under contract No. F04611-86-C-0071.

(55) Pritt, A. T.; Patel, D.; Benard, D. *J. Chem. Phys. Lett.* 1983, 97, 471.
 (56) Stern, L.; Wanner, J.; Walther, H. *J. Chem. Phys.* 1980, 72, 1128.

PROCEEDINGS

OF THE
INTERNATIONAL CONFERENCE
ON

LASERS '91



SAN DIEGO, CALIFORNIA

DECEMBER 9-13, 1991

F.J. Duarte
and
D.G. Harris
Editors

CONFERENCE SPONSORED BY
THE SOCIETY FOR OPTICAL & QUANTUM ELECTRONICS

STS PRESS • McLEAN, VA • 1992

INVESTIGATION OF TWO POTENTIAL VISIBLE WAVELENGTH CHEMICAL LASER SCHEMES BASED ON THERMAL DISSOCIATION OF CHLORINE AZIDE

D.J. Benard, B.K. Winker, M.A. Chowdhury and T.A. Seder

Rockwell International Science Center
Thousand Oaks, CA 91360

and

H.H. Michels

United Technologies Research Center
E. Hartford, CT 06108

Abstract

Chlorine azide and fluorine azide were synthesized by the continuous titration of dilute HN_3 with dilute ClF and F_2 , respectively. The reaction products were analyzed by both infrared and ultraviolet absorption measurements before a CO_2 TEA laser was used to pulse heat these energetic molecules in the presence of SF_6 (sensitizer) and either I_2 or $\text{CF}_3\text{I}/\text{XeF}_2$ gas mixtures. The resulting thermal dissociation of the energetic azides produced metastable halogen nitrenes which reacted by energy transfer to pump either the $\text{NF}(\text{b})$ or $\text{IF}(\text{B})$ states, which are potentially capable of lasing at visible wavelength. Time resolved emission spectroscopy was employed to follow these emitters as well as the metastable intermediates and I^* , while the concentrations of the ground state dihalides were tracked by laser induced fluorescence. These data revealed that the global rate of I^* quenching was negligible, the rate of $\text{NF}(\text{b})$ quenching by $\text{NF}(\text{a},\text{X})$ was less than $6 \times 10^{-12} \text{ cm}^3/\text{s}$, the yield of $\text{NCl}(\text{a})$ per ClN_3 molecule was 12% and the radiative rate of the $\text{NCl}(\text{a}-\text{X})$ transition was measured as 0.9/s in good agreement with a recent theoretical estimate by Yarkony. The yield of $\text{NCl}(\text{a})$ is explained by ab initio calculations of the ClN_3 potential surfaces which demonstrate that a singlet-triplet crossing occurs inside the barrier to dissociation. Large transient concentrations of $\text{IF}(\text{X})$, generated (in situ) by the thermally initiated reaction of XeF_2 with CF_3I , were also measured absolutely by a titration technique and (using this data) the effective rate of pumping of the interhalogen to its B state (by $\text{NF}(\text{a})/\text{NCl}(\text{a})$ mixtures) was measured as $6.5 \times 10^{-13} \text{ cm}^3/\text{s}$. This low rate is explained by $\text{NF}(\text{a})$ pumping out of vibrationally excited levels of the $\text{IF}(\text{X})$ state and $\text{NCl}(\text{a})$ pumping into vibrationally excited levels of the $\text{IF}(\text{B})$ state that lie above the predissociation limit. Thermal dissociation of the stable levels of the $\text{IF}(\text{B})$ state is also likely to occur at rates that are competitive with the spontaneous radiation. Additional work, focussed on excitation of the $\text{NS}(\text{B}-\text{X})$ transition by chemical reactions of $\text{NF}(\text{a})$, is in progress.

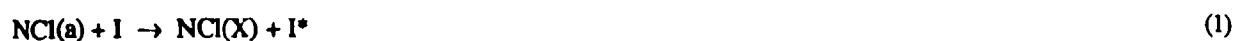
1. Introduction

In previous reports^{1,2} we have shown that both FN_3 and ClN_3 can be thermally dissociated to yield ground state N_2 and electronically excited metastable products including both the $\text{a}^1\Delta$ and $\text{b}^1\Sigma$ states of NF and NCl , respectively. These results were obtained by diluting the parent azide molecules with SF_6 and He buffer gas before exposing the gas mixtures to a pulsed CO_2 laser. Absorption of the 10.6μ laser radiation by SF_6 (followed by rapid V-T relaxation³) jumps the temperature of the bath gas and triggers dissociation of the azides on the μs time scale. In the case of FN_3 , our prior studies have demonstrated a barrier to dissociation of approximately 0.5 eV and production of $\text{NF}(\text{a})$ with near unit efficiency, while the yield of $\text{NF}(\text{b})$ is 2-3 orders of magnitude smaller. Very large ($3 \times 10^{15}/\text{cm}^3$) concentrations of $\text{NF}(\text{a})$ have been demonstrated and (using these metastables) we have studied the mechanism, kinetics and scalability of a potential blue-green $\text{BiF}(\text{A}-\text{X})$ chemical laser.^{4,5} In this system, $\text{Bi}(\text{CH}_3)_3$ is used as a volatile precursor of the active BiF species, which is pumped by successive collisions with $\text{NF}(\text{a})$ to its emitting state at an effective rate of $4 \times 10^{11} \text{ cm}^3/\text{s}$. Since the radiative decay rate⁶ of the $\text{BiF}(\text{A})$ state is $7 \times 10^5/\text{s}$, inversion of the A-X transition was expected at achievable $\text{NF}(\text{a})$ concentrations and indeed optical gain at 471 nm in the NF/BiF system was recently demonstrated in our laboratory.⁷ The large $\text{NF}(\text{a})$ concentrations required to sustain inversion in BiF , however, are problematical since they are subject to rapid self-annihilation.^{1,8} This difficulty could be alleviated, however, if an alternate transfer agent was found with either a longer radiative lifetime or potential curves⁹ that show more displacement between the excited and ground states than is characteristic of BiF , since these differences would allow inversion to be sustained at lower concentrations of $\text{NF}(\text{a})$. The $\text{Bi}(\text{CH}_3)_3$ precursor also tends to dissociate slowly and contributes to quenching of the $\text{NF}(\text{a})$ which

limits gain scaling⁵ and, finally, condensation of refractory solids (such as BiF₃) may pose an optical scattering problem. Consequently, there is ample room for improvement on the progress that has been made to date.

Our parallel studies of ClN₃ dissociation² have been motivated by the possibility that emitters other than BiF could also be pumped by metastable NCl in combination with metastable NF. We found that the barrier to dissociation of ClN₃ is about 0.7 eV and the yield of NCl(b) is comparable to the yield of NF(b). Also, once initiated, the dissociation of ClN₃ goes to completion (similar to FN₃) and the decay of the metastable NF / NCl products is due primarily to self-annihilation.^{1,2,8} The yield of the NCl(a) state, while significantly greater than 1%, however, was not determined accurately due to the lack of a reliable measurement of the A coefficient for the NCl(a-X) transition, as well as uncertainty in regard to the spatial distribution of the ClN₃ molecules in our reactor. Despite this limitation, however, we were able to demonstrate² that NCl(a) acts in a manner analogous to metastable O₂(a¹Δ) in two potential visible wavelength chemical laser schemes as described below.

Addition of I₂ to FN₃ / ClN₃ gas mixtures significantly enhanced² the yield of NF(b). Assuming that the I₂ dissociates to I-atoms, this result can be explained by the near resonant energy transfer reactions



Reaction (1), which has recently been studied by Yang and Bower,¹⁰ is similar to the well-known pumping¹¹ of I* by O₂(a); while reaction (2), which is also well-known, was first studied by Herbelin¹² and later in our laboratory as well.¹³ Under suitable conditions it is hoped that these energy transfer processes may lead to lasing on the NF(b-X) transition at 528 nm. Since the NF(b-X) transition is optically forbidden,^{14,15} it may also become inverted at (reduced) metastable concentrations that do not lead to rapid self-annihilation. The NF(b) system is free of refractory species and there are no byproducts (of the I₂ catalyst) that do not directly participate in the pumping reactions.

Substitution of CF₃I in place of I₂ also resulted² in excitation of the IF(B-X) transitions that have been operated as an optically pumped laser by Davis,¹⁶ who has recently demonstrated chemical pumping of these same bands by sequential energy transfers¹⁷ from NF(a) and O₂(a). In this case, the excitation of IF(B) proceeds via an intermediate (metastable) ³π₂ energy level^{2,18} of the interhalogen. The analogous reactions in the mixed azide system are therefore:



This candidate laser system is also free of refractory products and since inversion of the IF(B-X) transition is aided by displacement of its excited state potential curve to larger internuclear separation than the ground state,^{16,19} it may be possible to operate this scheme at more tractable metastable concentrations than are needed to support the BiF system, if the effective pump rates are comparable. In our previous work the effective rate of reactions (3) and (4) was not established because the concentration of the IF(X) ground state was indeterminate.²

In this paper we report the results of our continuing investigation of the NF(b) and IF(B) systems, which both rely on ClN₃ as a fuel. An improved method to synthesize ClN₃ is presented along with verification of the mechanism / rate of I₂ dissociation and the subsequent production and quenching of I* in the NF(b) system. Based on these results a kinetic model is developed and anchored to NF(b) time profile data to establish the yield of NCl(a), which in turn allows determination of the unknown A coefficient for the NCl(a-X) transition by absolute photometry. The effects of nonuniform spatial distributions in the photometry experiments were eliminated in the present study by comparing the yields of NF(a) and NCl(a) in the same reactor, and the yield results are explained by ab initio calculations of the halogen azide potential energy surfaces. A method to generate large in situ concentrations of IF(X) in known quantity is also described and a measurement of the effective rate of pumping of the IF(B) state by mixtures of metastable NF / NCl is reported. Finally, the rate of IF(B) excitation is explained by consideration of the relevant kinetic factors involved in the energy transfer process, and a new concept is presented which will be the subject of future investigations.

2. Experimental

The methods used in the present experiments have been documented in prior publications^{1,2,5,20} and are largely unchanged, except as noted below:

2.1 Generation of Azides

In our previous work,¹ FN_3 was generated by titrating a flow of 10% F_2 in He with a (similarly diluted) continuously generated flow of HN_3 that was obtained by reacting NaN_3 with excess stearic acid at temperatures near 100°C . Since this approach required stabilization of the HN_3 generator,²⁰ which proved to be time-consuming and inefficient, a simpler (unstabilized) HN_3 source was employed to charge a 40 liter stainless steel reservoir tank prior to dilution with He gas up to a total pressure of 25 psig. The resultant mixture of 5% HN_3 in He was then withdrawn from the tank (as needed) via an electronic vacuum regulator to generate FN_3 . The simplified HN_3 source consisted of an electrically heated and thermostated 5 liter aluminum pot (with teflon lining) that was fit with an o-ring sealed stainless steel lid which mounted a 1 RPM motor and a stainless steel stirring paddle to mix the reagents during generation. The pot was initially charged with a well-stirred mixture consisting of 3 liters loosely packed stearic acid and 30 gr NaN_3 . After sealing the lid and heating the pot to 225°F the motor was started and the first 30 minutes of gas generation were discarded to vacuum. Subsequently, the evolving gas was diverted to the (previously evacuated) storage tank which filled to 100 torr in about 60 to 90 minutes. Higher pressures of HN_3 are not advisable due to the possibility of detonation upon condensation of this energetic species. Since HN_3 is also toxic the generator and storage tank were located under a fume hood. Negligible concentrations of the usual H_2O and CO_2 impurities were found in the HN_3 gas that was withdrawn from the reservoir tank upon examination by Fourier Transform Infrared (FTIR) absorption spectroscopy using a 10 cm stainless steel gas cell with salt windows. The absolute HN_3 concentration was also measured in absorption²¹ at 204 nm using a D_2 lamp source, a 0.1 meter grating monochromator, a 3.5 mm stainless steel cell with MgF_2 windows and a 1P28 photomultiplier detector that was interfaced to a picoammeter. This diagnostic yielded results in good agreement with the initial storage tank pressure/dilution ratio and also demonstrated that the HN_3 was storable for several weeks without noticeable decomposition.

The generation of FN_3 was carried out as in previous experiments by admitting the HN_3 and F_2 flows to a 500 ml stainless steel reactor that was packed with 0.25 in. dia. stainless steel balls. Best results were obtained at ambient temperature or slightly warmer (35°C), at a total pressure of 350 torr (controlled by the dispensing HN_3 vacuum regulator) and with the F_2 flow adjusted to half the HN_3 flow. The net flow rate of the gases through the FN_3 source (as determined by an electronic mass flowmeter in the HN_3 line) was set at approximately 3.5 scc/s by the generator pressure and a 100 micron dia. pinhole that acted as a critical flow orifice downstream of the reactor. A glass frit filter was interposed between the generator and pinhole orifice to prevent clogging due to entrainment of solid byproducts in the gas stream. The product stream contained 1.5-2.0% FN_3 as measured in absorption²² at 425 nm (using a commercial spectrophotometer and a 6 cm stainless steel cell with quartz windows) while analysis by FTIR spectroscopy²³ showed negligible production of HF as a byproduct. Solid NH_4F , however, does accumulate inside the reactor and requires periodic removal. These findings are in good agreement with Haller,²⁴ who first synthesized this highly energetic and unstable azide in 1943.

Chlorine azide was previously generated by the water catalyzed reaction^{2,25} of Cl_2 with NaN_3 . In the present experiments, however, we found it much more convenient to obtain ClN_3 by reacting the HN_3/He mixture (from the storage tank) with ClF that had been prediluted to 10% in He. Substitution of Cl_2 for ClF did not produce a significant yield of the halogen azide. The ClN_3 generation was carried out in a manner that is completely analogous to the production of FN_3 (described above), except that cooling the reactor slightly to 10°C was beneficial and the optimum yield of ClN_3 was obtained upon equalizing the HN_3 and ClF flows. Analysis of the product stream in absorption (by FTIR) revealed that neither HF nor FN_3 was present in significant concentration^{22,23} and transmission measurements at 250 nm, where HN_3 absorption is negligible,²¹ demonstrated that ClN_3 was present in 1.0-1.5% concentration.

The FN_3 stream was carried in stainless steel or teflon tubing and passed through a stainless steel cold trap that was externally cooled to -73°C (by evaporation of liquid CO_2) to remove trace H_2O and HN_3 enroute to the reaction cell.²⁶ Liquid N_2 cooled traps were not used due to the potential for detonation upon condensation of the FN_3 . Also the lower vapor pressure²⁷ of the heavier azide prevented the use of any cold trap to effectively clean up impurities or byproducts in the ClN_3 flow, which included residual HN_3 and less energetic/reactive species such as nitrogen trihalides (vide infra). These thermally stable byproducts were judged to have negligible impact on the subsequent chemistry.

2.2 Reaction Cell

The FN_3 and ClN_3 flows were joined with a metered flow of SF_6 prior to the pyrolysis reactor. A mixture of 2.5% CF_3I and He was prepared in a storage tank and similarly admitted to the reactor via an electronic mass flowmeter while a carrier flow of He (which was also metered) passed through a bed of either I_2 or XeF_2 crystals on its way to the reactor. The total pressure in the reactor was measured by an inductance transducer and maintained at 75 torr by an electronic feedback loop which adjusted a metered He flow that was used to purge the reactor windows. Since there was no evidence of prereaction between any of the reagents, the partial pressures of each species in the reactor were inferred from the total pressure, the relative mass flow rates and either the ultraviolet absorption measurements, dilution ratios or vapor pressures.^{26,28} The gases were exhausted from the reactor (to vacuum) via a pair of critical flow orifices which passed 15 scc/s of He at the operating pressure. The reactor itself was constructed of stainless steel and was equipped with opposed sidearms through which the CO_2 laser beam entered and exited via purged and internally apertured salt windows. Emission from the center of the reactor was collected perpendicular to the laser beam through a quartz window and the reactive gases all entered and exited the reaction cell along a line that was mutually perpendicular to both the laser beam and the viewing direction. At the center of the reactor the laser beam had a cross sectional area of approximately 1 cm^2 and a fluence of nominally $1\text{-}2 \text{ Joules/cm}^2$. This intensity, while optimal for dissociation of the azides, is too low to cause significant multiphoton dissociation of the SF_6 at the (high) operating pressure that was maintained in the reactor.²⁹ Upon firing the CO_2 laser, with both azides and SF_6 present in the reactor, chemiluminescent emission was typically visible along the path of the beam. All of the experiments were carried out with 3-4 torr of SF_6 in the reactor, which absorbed approximately one-fifth of the incident laser radiation over a 2.5 cm path (as limited by the apertures in the sidearms). The peak temperatures achieved in this manner have been determined by spectroscopic techniques^{1,2,5} to lie in the range of 1600-2000°K. Typical azide concentrations were $5\text{-}7 \times 10^{15}/\text{cm}^3$ and the concentrations of the coreagents were either comparable to the azides or one to two orders of magnitude smaller.

2.3 Optical Diagnostics

From previous studies^{1,2,5} the emission spectra¹⁴ are well known, hence the desired emitters were isolated by use of appropriately selected narrow-band interference filters for NF(a,b) at 874 and 528 nm, NCl(a) at 1090 nm and I^* at 1315 nm, or portions of the B-X bands of IF which extend from 500 to beyond 900 nm. All the species studied were monitored by chemiluminescent emission, except IF which was measured both in chemiluminescence and laser induced fluorescence, and I_2 which was measured only by laser induced fluorescence. The I^* fluorescence measurements were done on a relative (comparison) basis only while the I_2 measurements (also relative) were done under conditions which allowed no spectroscopic interferences so that only a 550 nm long pass (absorption) filter was required to separate the fluorescence signals from scattered Ar^+ ion laser radiation. In general the weak NF(a) or NCl(a) emissions could not be isolated once either I_2 or CF_3I was added to the reactor due to spectroscopic interferences from overlapping broad band emissions.¹⁴

Approximately 2 watts of Ar^+ ion laser radiation was counterpropagated along the path of the CO_2 laser beam to induce the fluorescence signals. The lines at 514 and 476 nm were used to excite I_2 and IF, respectively. The NF , NCl and IF (chemiluminescence) signals were monitored by a 1 cm^2 active area silicon photodiode which was absolutely calibrated against a quartz halogen reference lamp.^{1,2,5} The I^* signals were detected by a fast liquid nitrogen cooled intrinsic germanium detector and the laser induced fluorescence signals were monitored via a gallium arsenide photomultiplier tube. The electrical signals from these detectors were preamplified and passed to a digital oscilloscope where they were averaged upon successive shots of the CO_2 laser. The resultant time profiles were smoothed sufficiently to remove residual noise (typically less than 5%) without losing the essential kinetic features. In most cases the data at early times (close to the firing of the CO_2 laser) was aliased by electromagnetic pickup of the capacitor discharge in the CO_2 laser. These effects, which are readily identifiable (upon blocking the CO_2 laser beam), have been removed from the data and the inferred time profiles (in the corresponding regions) are indicated by a dashed line in the figures.

The yield of NCl(a) from dissociation of ClN_3 was defined as the fraction of the parent molecules within the active volume of the reactor that generated the metastable product state. In previous experiments, the active volume was determined by the CO_2 laser beam and optical apertures that were placed between the detector and the reaction cell to restrict the field of view. Since the entire reactor was not measured, however, the data were sensitive to inhomogeneities in the spatial distribution of the parent azide molecules primarily due to the sweeping action of the window purges inside the reactor. To eliminate this source of error, the apertures were removed and the effective emitting volume was then determined by a parallel measurement of FN_3 dissociation, which prior studies¹ have shown to demonstrate a yield of NF(a) that approaches unity. The product of the yield (Y) of NCl(a) from dissociation of ClN_3 and the A coefficient for the NCl(a-X) transition was therefore evaluated as

$$Y_{\text{NCl}} = (0.18/s) \left(\frac{T_{\text{NF}}}{T_{\text{NCl}}} \right) \left(\frac{D_{\text{NF}}}{D_{\text{NCl}}} \right) \left(\frac{C_{\text{FN}_3}}{C_{\text{ClN}_3}} \right) \left(\frac{S_{\text{NCl}}}{S_{\text{NF}}} \right)$$

where the prefactor is the known yield - A coefficient³⁰ product for the NF(a-X) transition, and the T, D, C and S factors are the filter transmission, detector sensitivity, initial azide concentration and recorded signal strengths for the measurements indicated by the respective subscripts. The transmission factors and detector sensitivities were obtained by use of a commercial spectrophotometer and calibration to a reference lamp, while the azide concentrations were monitored enroute to the reactor by the ultraviolet absorption diagnostic. The signal strengths were obtained by extrapolating the NF(a) and NCl(a) time profiles back to $t = 0$ to counteract the effects of quenching during the process of dissociation. Care was taken to collect the yield data at the lowest practical azide concentrations to limit the rate of self-annihilation (in relation to the rate of dissociation) and thereby minimize the error in extrapolation. Deliberate addition of quenchers such as H₂O and HCl to the reactor significantly affected the decaying portion of the NCl(a) time profile; however, the extrapolations back to $t = 0$ were unaffected. Using these measurements, the unknown A coefficient for the NCl(a-X) transition can then be obtained given an independent determination of the corresponding yield factor.

The yields of NF(b) and IF(B) were calculated in like manner, only using the known A coefficients for the b-X and B-X transitions,^{15,31} respectively, to determine the corresponding yields from the related filter transmissions, detector sensitivities, parent concentrations and signal strengths. Since both NF(a) and NF(b) have the same parent molecule (FN₃), the concentration ratio is unity in this case. The IF(B) yields were calculated assuming that CF₃I was the parent; however, only a small fraction of the total B-X emission was detected ($v' = 0$ to $v'' = 5$ band at 625 nm). Therefore the recorded IF signal strength had to be corrected by dividing out the corresponding Frank-Condon factor¹⁹ to account for radiation from $v' = 0$ to other v'' levels of the ground state in addition to dividing out the fraction of the entire IF(B) state that was resident in the $v' = 0$ energy level. The latter correction was made by assuming a thermalized vibrational distribution of the IF(B) state at 1800°K. A relaxed distribution is expected at the high pressure of this experiment on the basis of the known radiative and collisional (V-T) rates.^{31,32} Absolute concentrations of NF(b) and IF(B) were then recovered by multiplying the corresponding yields and precursor concentrations.

3. NF(b) System

The kinetic rates of reactions (1) and (2) have been studied by other investigators, while our previous studies have elucidated the kinetics of formation and decay of the NF(a) and NCl(a) states. The potential of the system to support lasing on the b-X transition, however, also depends on the rates of quenching of the I* intermediate and the NF(b) state itself. Since the halogen azide system is relatively "clean" in relation to other chemical systems that generate metastable halogen nitrenes, the quench rates will (in this case) be minimized. Therefore our investigation should help to determine the limiting potential of the system to function as a chemical laser. Also, as will be shown, the yield of the NCl(a) state can be determined (without knowledge of the corresponding radiative rate) by modelling the NF(b) time profile.

3.1 Dissociation of I₂ and Excitation of I*

The temperatures achieved in the pulsed CO₂ laser excitation experiment are adequate¹⁴ to totally dissociate I₂; however, the rate of dissociation remains an issue, since the active species in reactions (1) and (2) are I-atoms and both the NF(a) and NCl(a) decay significantly on the time scale of tens of μs due to self-annihilation.^{1,2} To investigate this phenomenon, the azides were removed from the reactor flow and approximately 10 mtorr of I₂ was added to the SF₆ and He in the pyrolysis cell. The laser induced fluorescence signal from the I₂ was present in advance of the CO₂ laser pulse at a constant level which then declined with time (after the laser pulse) due to the thermal dissociation of the I₂ molecules. In addition to the fluorescence signal, an extraneous chemiluminescence signal was evident upon application of the CO₂ laser pulse with the Ar⁺ ion laser (used to excite the fluorescence) blocked. Data was recorded both with and without excitation by the Ar⁺ ion laser in an AC coupled mode so that the steady I₂ fluorescence in advance of the CO₂ laser pulse was not registered. Figure 1 presents the transient changes in the (recorded) sum of the chemiluminescence (ΔS_{chem}) and laser induced fluorescence (ΔS_{lif}) signals both with and without excitation by the Ar⁺ ion laser. The vertical difference between these two curves, therefore, is a measure of the amount of I₂ that has been dissociated. From these data, it is apparent that I₂ dissociates rapidly and completely with a time constant of approximately 3 μs .

Since Yang and Bower¹⁰ indicate a gas kinetic rate for reaction (1) and since significant (10^{15} - $10^{16}/\text{cm}^3$) concentrations² of NCl(a) appear within 4 μs after the firing of the CO₂ laser, the I* concentration is expected to rise in less than 10 μs . Figure 2 illustrates the chemiluminescence time profile of the emission at 1315 nm, due to CO₂ laser excitation of a SF₆ / He / FN₃ / ClN₃ gas mixture both with and without the addition of approximately 10 mtorr of I₂. Subtraction of these two time profiles to separate the desired signal (from extraneous chemiluminescence) demonstrates the anticipated rise of the I*

concentration (in approximately 6 μs) followed by a relatively slow decay. From this result, it also follows that quenching of I^* is not a significant factor in this system.

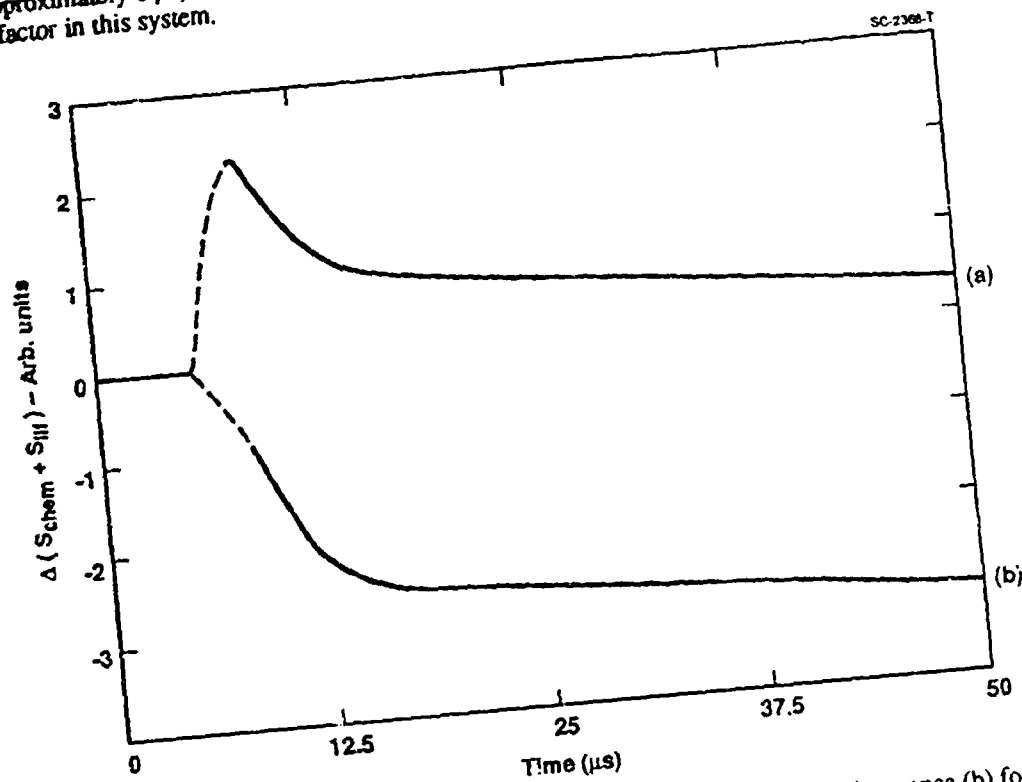


Fig. 1 Time profiles of I_2 chemiluminescence (a) and laser induced fluorescence / chemiluminescence (b) following pulsed CO_2 laser excitation of a $\text{He} / \text{SF}_6 / \text{I}_2$ gas mixture.

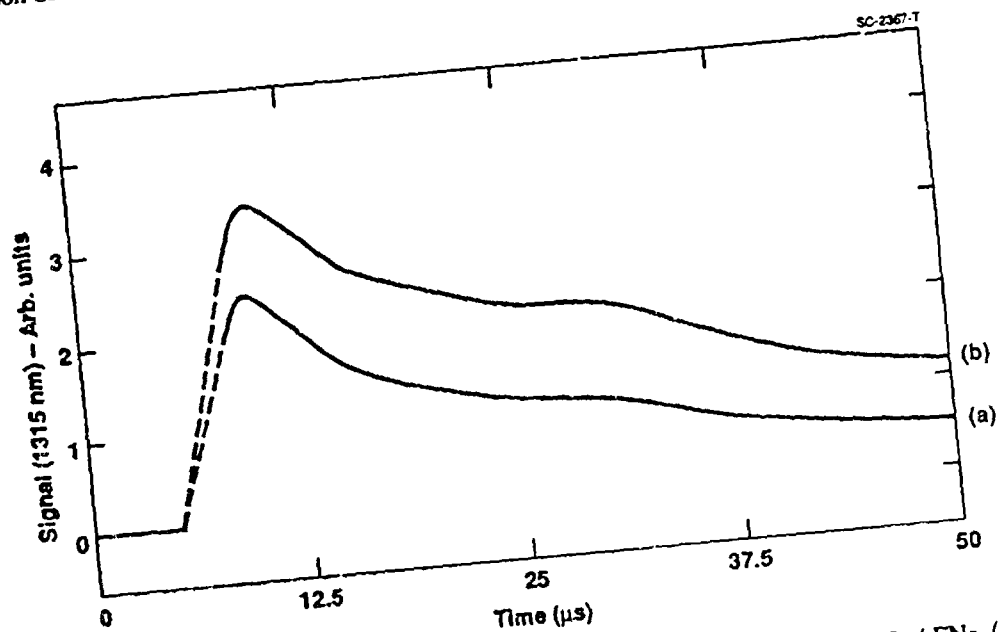


Fig. 2 Time profiles of 1315 nm emission following pulsed CO_2 laser excitation of a $\text{He} / \text{SF}_6 / \text{FN}_3 / \text{CIN}_3$ gas mixture with (a) and without (b) the addition of I_2 .

3.2 NF(b) Time Profile

Addition of ICl to an $\text{FN}_3 / \text{ClN}_3 / \text{SF}_6 / \text{He}$ mixture in the reactor enhanced the yield of NF(b), but the rate of rise and the optimized peak concentrations were both less than could be obtained upon addition of I_2 . The optimum yield of NF(b), with initial FN_3 and ClN_3 concentrations of 7 and $5 \times 10^{15}/\text{cm}^3$, respectively, was obtained upon addition of approximately 50 mtorr of I_2 . The absolutely calibrated NF(b) time profile for this condition is shown in Fig. 3. Upon substituting CH_4 in place of He in the reactor to a concentration of $3 \times 10^{17}/\text{cm}^3$, the peak yield of NF(b) was approximately halved. Setser³³ reports that quenching of NF(a) by CH_4 is negligible, while NF(b) is quenched at a rate of $1.6 \times 10^{-13} \text{ cm}^3/\text{s}$ at 300°K . Assuming that this rate scales as the square root of temperature and that CH_4 has negligible impact on NCl(a) or I^* (as might be expected), it follows that the reduction in the peak yield was due to quenching of NF(b) by the added methane at a rate near $10^5/\text{s}$. The sensitivity to methane addition therefore suggests that NF(b) is quenched (in the absence of CH_4) in approximately $10 \mu\text{s}$. To further evaluate these findings a kinetic model for the NF(b) system was assembled and anchored to the data.

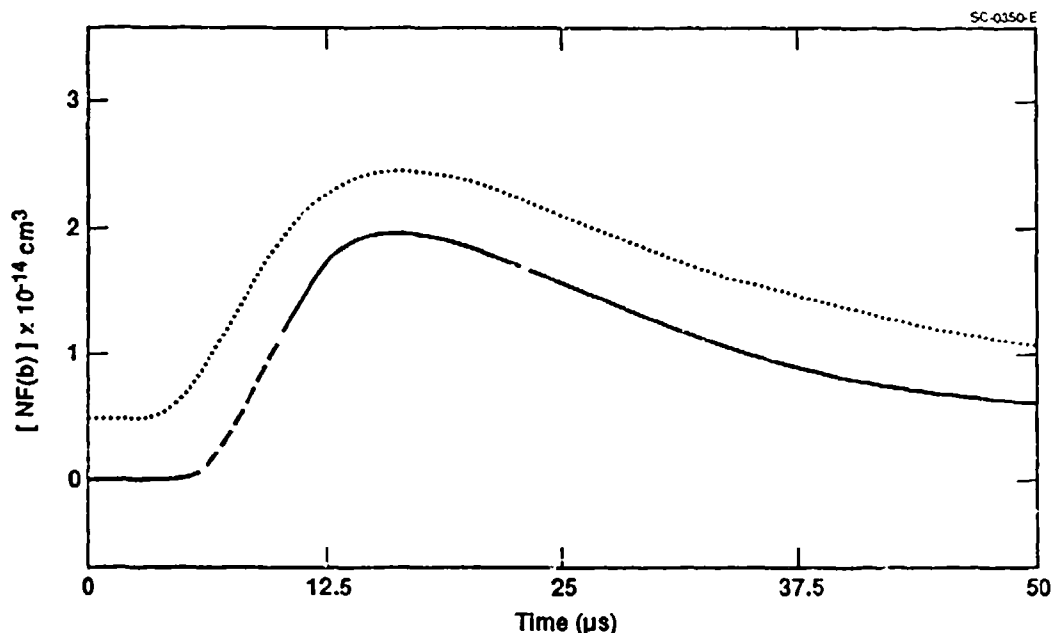


Fig. 3 Time profile of NF(b-X) emission (solid / dashed line) following pulsed CO_2 laser excitation of a $\text{He} / \text{SF}_6 / \text{FN}_3 / \text{ClN}_3 / \text{I}_2$ gas mixture compared to a best fit calculation (dots) based on a kinetic model. Note the modelling result has been vertically displaced for comparison.

The reactions included in the NF(b) kinetic model were thermal dissociation of the FN_3 , ClN_3 and I_2 to yield NF(a), NCl(a,X) and ground state I-atoms, annihilation of both NF(a) and NCl(a) by halogen nitrenes, reaction (1), both the forward and reverse processes for reaction (2), and global quenching of the NF(b) by its environment. Quenching of I^* was not included on the basis of the data in Fig. 2. The reverse process for reaction (1) was not considered because, like NF(X), the triplet ground state NCl(X) molecules are believed to be highly reactive and therefore chemically self-annihilate at a near gas kinetic rate.³⁴ Consequently the NCl(X) concentration (and the rate of the back reaction with I^*) is reduced to insignificant values. The slow radiative decays^{2,15,30,35} of the NF(a,b), NCl(a) and I^* were all considered to be negligible on the μs time scale of the experiment as was the slow quenching of these metastable intermediates by inert collision partners such as SF_6 , He or N_2 . Prior modeling of the FN_3 dissociation process⁵ revealed that the parent azide and the NF(a) product overlapped for too brief a period to contribute any significant interaction. This approximation was generalized (in the present case) to exclude all potential reactions between the metastable intermediates and their parent molecules. Finally, since the experiment was premixed and of limited duration, no transport processes, such as diffusion to the reactor walls, were considered to be significant.

The rates of FN_3 , ClN_3 and I_2 dissociation were taken from our prior studies^{1,2,5} and the data in Fig. 1 as 5.0 , 2.5 and $3.3 \times 10^5/\text{s}$, respectively. The yield of NF(a) from dissociation of FN_3 was taken as unity and the yield of NCl(a) from ClN_3 was taken as an adjustable fitting parameter to be determined empirically by comparison of the calculated and observed NF(b) time profiles. Both the NF(a) and NCl(a) metastables were assumed to self-annihilate at a common rate of $3 \times 10^{-12} \text{ cm}^3/\text{s}$

multiplied by the total initial azide concentration, which is consistent with Setser's data⁸ for self-annihilation of NF(a). This approximation, which is equivalent to assuming that all collisions between either of the metastable species and any halogen nitrene (excited or ground state) are equally effective at quenching the electronic excitation, is also consistent with our observations of metastable decay rates^{1,2} in FN₃, ClN₃ and mixed FN₃ / ClN₃ systems. The rate of reaction (1) was taken from the work of Yang and Bower¹⁰ as 1.0×10^{-10} cm³/s, while the forward rate of reaction (2) was taken as 6×10^{-11} cm³/s on the basis of current work by Koffend and Herbelin.³⁶ The reverse rate for reaction (2) was calculated from the known forward rate, state degeneracies and energy levels¹⁴ by detailed balance assuming a temperature of 1800°K consistent with our prior measurements.^{1,2,5,7} Finally, the global quench rate for NF(b) was taken as a second adjustable fitting parameter. In contrast to the analogous quenching³⁷ process in O₂, the NF(a) state was not assumed to be repopulated by quenching of the NF(b) state, since in the former case the quenching is physical (and hence constrained by spin rules) while in the latter case the quenching is more likely to be reactive (and due to the presence of other halogen nitrenes^{1,2,8,33}). The differential rate equations corresponding to the set of reactions described above was numerically integrated (via computer) starting from the experimentally established initial conditions in 0.1 μs steps.

Exercising the kinetic model described above revealed that the calculated peak yield of NF(b) was sensitive to both fitting parameters (NCl(a) yield, NF(b) quenching) while the relative rate of decay of the NF(b) time profile was only significantly affected by the quenching parameter. A good fit to the decaying portion of the relative NF(b) time profile (data in Fig. 3) was obtained for a global NF(b) quench rate of 4×10^4 /s in reasonable agreement with the results of the CH₄ quenching experiment. Once the global quench rate was fixed, agreement with the data on the absolute peak yield of NF(b), however, required adjusting the yield of NCl(a) from dissociation of ClN₃ to approximately 12%. It was not possible to obtain a good fit to both the amplitude and the relative decay rate of the NF(b) time profile for yield parameters that were significantly larger or smaller as (with the quenching parameter fixed) the calculated peak NCl(a) concentrations scaled in almost direct proportion to the adjustable yield parameter. Also with the yield parameter fixed at either 8.5% or 17%, agreement on the peak NCl(a) concentration could only be obtained for values of the (adjustable) quenching parameter that resulted in substantial errors in the relative decay rate. The corresponding best-fit (calculated) NF(b) time profile is shown in Fig. 3 for comparison to the data. The I* time profile that was calculated for this condition also demonstrated a good fit to the relative data that is shown in Fig. 2, since it rose with a 7 μs time constant and showed negligible decay out to 50 μs after initiation.

The origin of the observed quenching of the NF(b) state is not resolved in this study; however, based on the species concentrations and Setser's extensive rate data³³ it appears that quenching by He, SF₆, N₂, F₂, ClF, HF, CO₂, H₂O, nitrogen trihalides and very likely HN₃ can all be ruled out as insufficient to account for the observed decay rate. Quenching of NF(b) by I₂ or the halogen azides may be rapid^{33,38} but these interactions would not persist to long times and since significant quenching by I or I* is unlikely, it is most probable that quenching of NF(b) is dominated by the halogen nitrenes, similar to the quenching^{1,8,33} of NF(a). The observed global decay rate of NF(b) is consistent with quenching by NF(a,X) and NCl(a,X) at a common rate of 3×10^{-12} cm³/s, which sets an upper limit on the rate of NF(b) quenching by NF(a,X) of 6×10^{-12} cm³/s, if quenching by NCl(a,X) is insignificant. These results are reasonable in light of the known rate of NF(a) self-annihilation which is of the same magnitude.^{1,8} This finding is significant to the design of other NF(b-X) lasers,³⁹ that may use a more efficient source of I* (than dissociation of ClN₃) and in which the efficiency of power extraction is limited by the competition between photon emission and quenching of the NF(b). While the 45/s spontaneous rate¹⁵ of the forbidden NF(b-X) transition is too small to compete with quenching, the stimulated emission rate (given by the product of the cross section and photon flux) can be made large enough, in principle, to extract the majority of the energy that is deposited in the NF(b) state. In practice, however, the required intracavity intensities (which scale in proportion to the rate of NF(b) quenching) may become excessive if the cross section is too small. Based on an estimated NF(b-X) cross section^{39,40} of 3×10^{-20} cm² and 50% efficient power extraction with [NF(a,X)] = 10^{16} /cm³, the required (worst case) intensity is 750 kW/cm².

The absolute photometry experiments described in the experimental section demonstrated a yield - A coefficient product for dissociation of ClN₃ into NCl(a) of 0.11/s. Therefore the radiative rate of the NCl(a-X) transition is determined as 0.9/s, in close agreement with the theoretical estimate of 0.7/s made by Yarkony.⁴¹ The yield result obtained by modelling the NF(b) time profile also implies a significant difference between FN₃ and ClN₃ with respect to metastable production and is, unfortunately, not favorable for the efficient operation of a chemical laser.

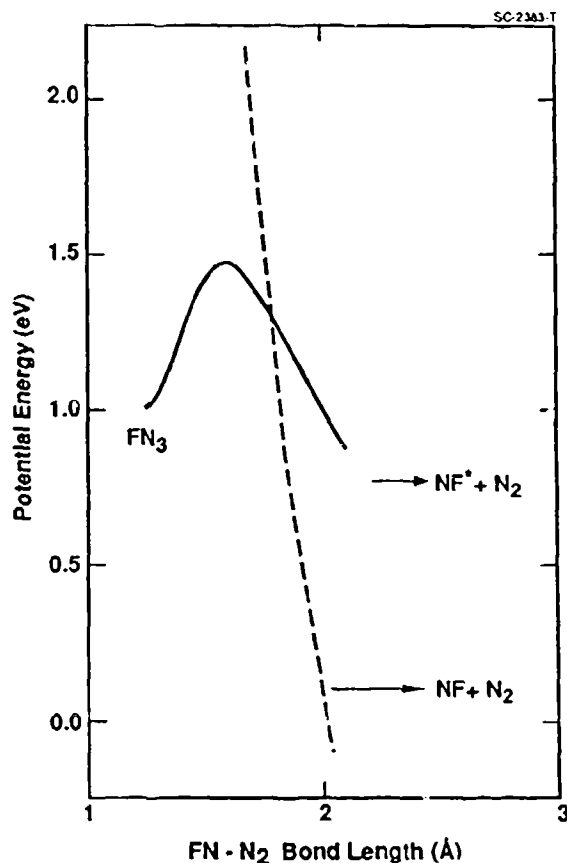
3.3 Electronic Structure Calculations

The apparent differences between dissociation of FN₃ and ClN₃ with respect to metastable yield can be related^{1,2} to the interaction between the singlet surface (that connects the ground state azide parent to metastable halogen nitrene products) with a dissociative triplet surface (that is an excited state of the azide but connects to the electronic ground states of either NF or NCl).

As shown in Fig. 4, the dissociative triplet state in FN_3 passes above the barrier in the singlet surface and crosses it on the products side. Consequently, when a FN_3 molecule acquires sufficient thermal energy to surmount the barrier, the molecule passes through the crossing region only once as it dissociates. Since the probability of crossing between surfaces of different spin is low (per each encounter) the yield of metastable $\text{NF}(a,b)$ products approaches unity.

Fig. 4

Ab initio calculation of the singlet (solid) and triplet (dashed) surfaces of FN_3 which dissociate to excited and ground state NF .



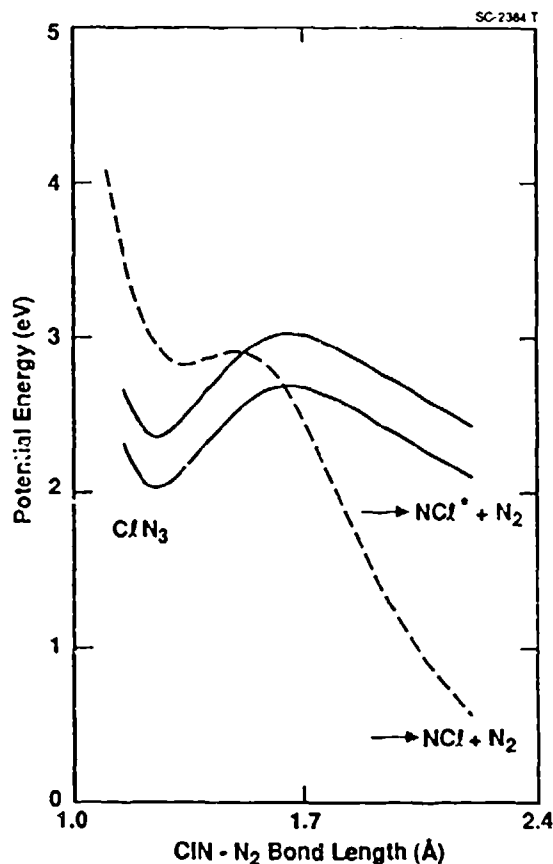
In FN_3 , the central bond is weakest due to withdrawal of electron density by the strongly electronegative halogen. Since Cl is less electronegative than F, the bonding of ClN_3 tends to resemble HN_3 more than FN_3 . The H-N_3 and HN-N_2 bonds are of near equal strength and thermal dissociation of HN_3 is known to yield predominantly ground state $\text{NH}(X^3\Sigma)$ because the dissociative triplet surface in this azide crosses the singlet surface inside the potential well.⁴² In this case, the azide molecules oscillate through the crossing region many times before surmounting the potential barrier and consequently the products "leak out" through the singlet-triplet crossing even at low probability per encounter in preference to dissociating on the singlet surface which requires a greater activation energy. This reasoning suggests that the yield of $\text{NCl}(a)$ from dissociation of ClN_3 is possibly reduced because of a singlet-triplet crossing that occurs near the peak but on the azide side of the potential barrier. The crossing is unlikely to occur well inside the barrier (similar to HN_3) since in that limit the yield of $\text{NCl}(a)$ would be reduced to well below 10%. As shown in Fig. 5 this expectation is borne out by a parallel calculation of the ClN_3 potential surfaces.

The calculations of the minimum energy (dissociation) pathways for the lowest singlet and triplet states of FN_3 and ClN_3 were performed with the GAUSSIAN 90 electronic structure code⁴³ using Pople's split-valence plus polarization (6-31G*) basis sets.⁴⁴ Gradient optimizations were performed to locate the equilibrium structure for the ground $^1A'$ state. To ensure that stationary points of the correct curvature have been found, harmonic vibrational frequencies were computed for the transition structures. The results of these calculations are given in Table 1. For comparison, the experimental structures of Christen, et al.⁴⁵ for FN_3 and Cook and Geny⁴⁶ for ClN_3 are also reported. It is clear that the SCF predictions are an accurate representation of the molecular geometries for both FN_3 and ClN_3 . The bond lengths and bond angles are calculated with an average error of 0.03 Å and 1.5 degrees, respectively. The SCF frequencies are well known to be uniformly too large and that a scaling of the SCF force field is required for comparison with experiment. We find that a uniform scaling factor of ~ 0.86 brings our calculated SCF frequencies for FN_3 in good agreement with the data of Christen, et al.⁴⁵ Applying this same factor to ClN_3 yields the predictions shown in Table 1. Calculations were then carried out to locate the transition state corresponding to the decomposition

of ClN_3 into $\text{NCl}[\text{a}^1\Delta] + \text{N}_2[\text{X}^1\Sigma_g^+]$. Starting from the location of the transition state, both forward and backward minimum energy pathways were followed along the intrinsic reaction coordinate;⁴⁷ the forward pathway leading to dissociation, the backward pathway leading back to the equilibrium structure. The results of these and prior⁴⁸ calculations are shown in Figs. 4 and 5, respectively. As previously reported,^{1,2} we find that the barrier height of the transition state in ClN_3 is approximately 1600 cm^{-1} larger than in FN_3 . However, in contrast to our findings in FN_3 , the triplet surface in ClN_3 crosses on the inside portion of the singlet surface that leads to dissociation. The location of this crossing is sensitive to the correlation treatment of the system since the triplet surface, corresponding to an open valence-shell electron pair, can be expected to exhibit a smaller total correlation energy.

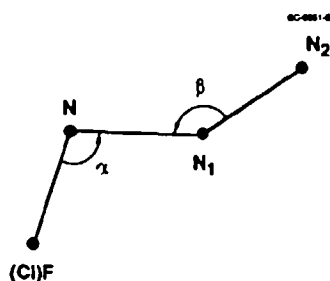
Fig. 5

Ab initio calculation of the singlet (solid) and triplet (dashed) surfaces of ClN_3 which dissociate to excited and ground state NCl . The two curves for the singlet state represent the limits of uncertainty in the thermodynamic potential relative to the triplet state.



To estimate upper and lower bounds for the location of the singlet-triplet crossing, correlated calculations were carried out at the equilibrium geometry of the singlet $^1A'$ surface. The method employed is based on the G1 theory of Pople, et al^{49,50} which has been shown to predict heats of formation of first- and second-row compounds containing multiple bonds with an accuracy of $\pm 2 \text{ kcal/mol}$. The triplet $^3A''$ surface was then located at the equilibrium geometry of the ground $^1A'$ state using this same G1 procedure. The calculated G1 singlet-triplet splitting at the equilibrium geometry was then used to determine the separation of the $^1A'$ and $^3A''$ dissociation surfaces calculated at the SCF level of theory. The results, shown in Fig. 5, represent the upper and lower bounds corresponding to the G1 calibration and SCF theory, respectively. As SCF methods will underestimate the singlet energy relative to the triplet, they can be regarded as providing a lower bound to the actual splitting. In previous studies⁴⁸ of FN_3 , we have observed that correlated treatments of the $^1A'$ state result in a lowering of this state by 0.6-0.8 eV relative to the triplet $^3A'$ surface.

Table 1
Optimized RHF/6-31G* Structures and Properties for FN₃ and ClN₃



Optimized C _s Geometry [¹ Å]						
	NF(NCl)	NN ₁	N ₁ N ₂	α	β	Energy
FN₃						
eq-calc	1.3820	1.2536	1.0995	104.315	174.108	-262.602488
eq-exp ⁴⁵	1.4440	1.2530	1.1320	103.800	170.900	—
ts-calc	1.3618	1.5891	1.0774	100.170	169.890	-262.585108
ClN₃						
eq-calc	1.7341	1.2470	1.0978	108.998	174.111	-622.689393
eq-exp ⁴⁶	1.7450	1.2520	1.1330	108.700	171.900	—
ts-calc	1.7204	1.6495	1.0768	103.905	167.385	-622.664592
Harmonic Frequencies						
	a'					a''
	(Cl)F-N-N ₁	N-N ₁ -N ₂	(Cl)F-N	N-N ₁	N ₁ -N ₂	out-of-plane
	bend	bend	stretch	stretch	stretch	bend
FN₃						
eq-calc	281	757	1045	1225	2386	606
eq-exp	241	658	876	1090	2044	504
ts-calc	186	610	1114	561 i	2690	295
ClN₃						
eq-calc	248	617	817	1237	2449	626
scaled by 0.86	213	531	703	1064	2106	538
ts-calc	163	480	789	513 i	2717	263

Bond lengths are in angstroms, bond angles are in degrees, energies are in hartrees and vibrational frequencies are in wavenumbers.

It is interesting to compare the FN_3 and ClN_3 molecules at the transition state for central bond dissociation. As described above, we find a classical barrier height of 0.675 eV for ClN_3 , a value ~ 40% larger than the 0.473 eV barrier found for FN_3 . The FN-N_2 and ClN-N_2 bond lengths are very similar at the transition state geometry: 1.59 Å for FN_3 as compared with 1.65 Å for ClN_3 . Thus the major factor influencing the singlet-triplet crossing on the inside of the barrier for ClN_3 is the repulsive character of the triplet surface. The triplet interaction, corresponding to $\text{NCl}[\text{X}^3\Sigma^-] + \text{N}_2[\text{X}^1\Sigma_g^+]$, is less repulsive than in the FN_3 system and even shows a small minimum in the region of the singlet-triplet surface crossing. A second derivative analysis, carried out at this stationary point on the triplet surface, indicated that it was a saddle region rather than a true local minimum. Analysis of the normal coordinate modes at this point indicates that the molecule is bending out-of-plane, breaking C_s symmetry. The nature of the singlet-triplet crossing in ClN_3 is similar to that found by Alexander, et al⁵¹ for HN_3 . They argue that the planarity of the molecule should be retained during the dissociation process since the N-N and N-H bonds are nearly perpendicular at the crossing point. Further studies of the triplet surface are in progress but they are not expected to alter our conclusion that the singlet-triplet crossing occurs on the inside region of the reaction barrier.

4. IF(B) System

Our principal goal in evaluating the $\text{FN}_3 / \text{ClN}_3 / \text{CF}_3\text{I}$ system was to determine the effective pump rate of the IF(B) state. This parameter, which influences the achievable gain, is determined by treating the excitation of the IF(B-X) transition as if it occurs by energy transfer from a single (effective) metastable species (M) whose concentration is given by

$$[\text{M}] = \frac{[\text{NF(a)}][\text{NCl(a)}]}{[\text{NF(a)}] + [\text{NCl(a)}]}$$

and by equating (in steady state) the rate of photon emission on the B-X transition to the product of an effective rate constant (k_e), the concentration of effective metastables and the IF(X) concentration. Therefore, the effective rate is determined as

$$k_e = \frac{A_{\text{IF}}[\text{IF(B)}]}{[\text{IF(X)}][\text{M}]}$$

where A_{IF} is the known ($1.4 \times 10^5/\text{s}$) radiative decay rate of the IF(B) state.³¹ This value of k_e , which sets an upper limit on the slower rate of reactions (3) or (4), assumes negligible quenching of the IF(B) state and is defined in terms of the generation of products (photons). It therefore reflects both the rates of reaction (removal of reagents) and the branching ratios that lead to formation of IF(B). Both $[\text{IF(B)}]$ and $[\text{M}]$ are readily determined by absolute photometry (as discussed in the experimental section) and since only the ratio of these quantities is significant, many of the elements (in common to both measurements) cancel. The difficult aspect of the measurement is determining the IF(X) concentration. Our approach was to monitor the concentration of this species on a relative basis by laser induced fluorescence and then obtain an absolute calibration by use of a titration technique based on the $\text{F} + \text{CF}_3\text{I}$ reaction which is known to yield IF(X) efficiently.⁵²

4.1 Production and Measurement of IF(X)

In our previous work we concluded that the CF_3I precursor was not quantitatively converted to IF(X) due to a lack of F-atoms in the azide system.² In the present study, this difficulty was rectified by adding XeF_2 to the reaction cell, since this weakly bound⁵³ noble gas dihalide is readily dissociated (at the temperatures achieved by the CO_2 laser excitation) to yield F-atoms and inert gas byproducts. Use of XeF_2 in combination with CF_3I dramatically enhanced the laser induced fluorescence signals which confirms a significant increase of IF(X) concentration. The fluorescence data shown in Fig. 6 was collected without azides present in the reactor (to suppress chemiluminescence), either with or without addition of 28 mtorr of XeF_2 and with an excess (90 mtorr) of CF_3I present. These time profiles reveal that the IF(X) which is formed in the absence of F-atoms appears much more rapidly ($\sim 5 \mu\text{s}$) than the much larger IF(X) concentration which derives from the $\text{F} + \text{CF}_3\text{I}$ reaction in 15-20 μs (when XeF_2 is present in the reactor). Based on the rate⁵⁴ of the $\text{F} + \text{CF}_3\text{I}$ reaction and the CF_3I concentration, it follows that the later source of IF(X) is rate limited by the dissociation of the XeF_2 .

Figure 7 shows the result of an experiment conducted with 120 mtorr of XeF_2 in the reactor in which the IF(X) fluorescence signal (at 20 μs after the laser pulse) is plotted as a function of the CF_3I addition. The data are characteristic of a titration experiment except that the knee in the curve occurs at a higher CF_3I addition than anticipated ($[\text{CF}_3\text{I}] = 2 [\text{XeF}_2]$) and the yield of IF(X) continues to grow, although more slowly, as a function of the CF_3I addition above the knee in the curve. The results in Fig. 7, however, reflect the sum of two processes, one which (promptly) generates CF_3I (in the absence of F-atoms) as

indicated by the dashed line while the other (delayed) process depends on the slower dissociation of the XeF_2 followed by the fast $\text{F} + \text{CF}_3\text{I}$ reaction. The dashed line through the origin representing the prompt yield of $\text{IF}(\text{X})$ has the same slope as the data that was collected for CF_3I concentrations in excess of the titration point, consistent with our prior studies² that showed linear scaling between the intensity of $\text{IF}(\text{B-X})$ emission and CF_3I addition. The knee in the curve (corresponding to the titration point for the delayed process) occurs at a higher CF_3I concentration than anticipated due to consumption of the iodide by the prompt reaction, which is responsible for the destruction of approximately three (out of ten) CF_3I molecules per $\text{IF}(\text{X})$ molecule that is formed. The mechanism by which the prompt reaction occurs, however, is unknown. Nonetheless, the data in Fig. 7 can be used to normalize the relative $\text{IF}(\text{X})$ fluorescence signal by equating the difference between the solid and dashed lines to twice the XeF_2 concentration at high values of CF_3I addition.

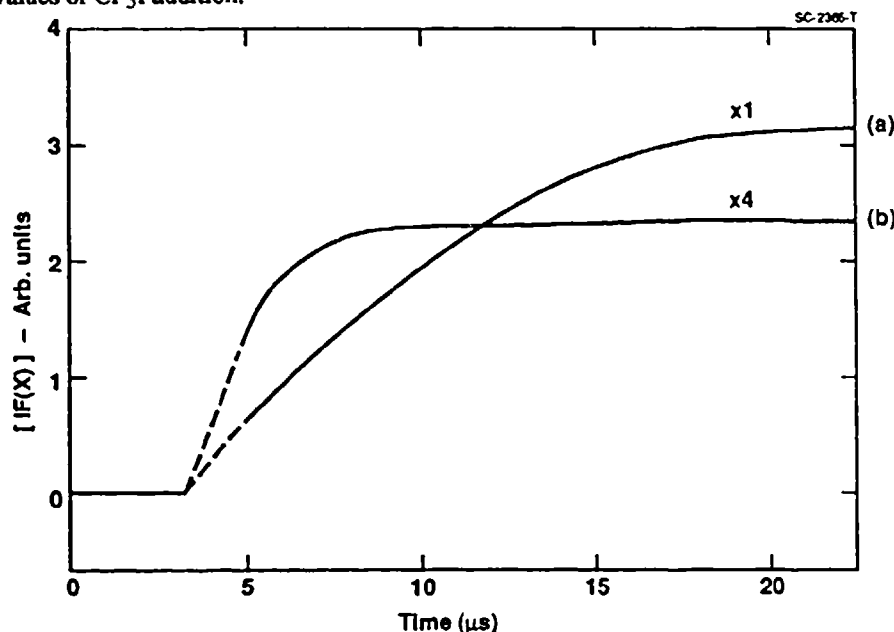


Fig. 6 Time profiles of $\text{IF}(\text{X})$ following pulsed CO_2 laser excitation of a $\text{He} / \text{SF}_6 / \text{CF}_3\text{I}$ gas mixture with (a) and without (b) the addition of XeF_2 .

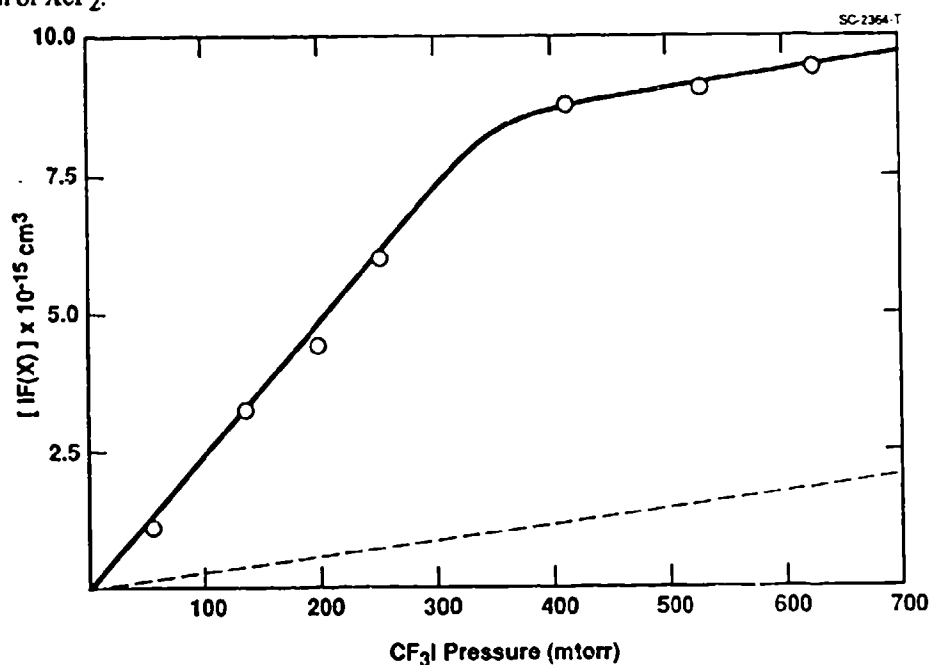


Fig. 7 Yield of $\text{IF}(\text{X})$ measured $20 \mu\text{s}$ after pulsed CO_2 laser excitation of a $\text{He} / \text{SF}_6 / \text{XeF}_2$ gas mixture as a function of CF_3I addition.

4.2 Effective Pump Rate

The yield of IF(B) was measured with initial azide concentrations that yielded peak concentrations of NF(a) and NCl(a) of 7×10^{15} and $5 \times 10^{14}/\text{cm}^3$, respectively, using 30 mtorr of CF_3I with excess addition of XeF_2 . The effective concentration of metastables was therefore $4.7 \times 10^{14}/\text{cm}^3$ and the prompt and delayed concentrations of IF(X) were 1.1 and $8.5 \times 10^{14}/\text{cm}^3$, respectively. The resulting absolutely calibrated IF(B) time profile is shown in Fig. 8. From this data, it follows that only the prompt component of the IF(X) generation contributed significantly to the IF(B-X) emission. Even though the IF(X) concentration increases by nearly an order of magnitude from 2 to 20 μs after the CO_2 laser pulse, the yield of IF(B) continues to diminish in the same time period because of declining concentrations of NF(a) and NCl(a). The kinetic lifetime of these metastables must be significantly attenuated, however, to produce this result since (in the absence of coreagents) the NF(a) and NCl(a) concentrations are typically still at 50% of their early (peak) values after 20 μs . The rate of NF(a) quenching by CF_3I , as measured by Setser,³³ is too small to be significant, therefore either NCl(a) is rapidly quenched by CF_3I or (more likely) the byproducts of the prompt reaction effectively quench the metastables. Consistent with this analysis the peak yield of IF(B) was found to be insensitive to elimination of XeF_2 from the reactor. Since the IF(B) is only in steady state at the peak of its time profile, which occurs promptly after the laser pulse, the effective rate is most accurately calculated using the peak metastable concentrations (in the absence of coreagents) and the (smaller) prompt yield of IF(X), which gives a value for k_e of $6.5 \times 10^{-13} \text{ cm}^3/\text{s}$. This result is approximately two orders of magnitude less than the equivalent rate in the BiF system. Consequently, it is unlikely that the NF / NCl / IF system will be able to function adequately as a laser.

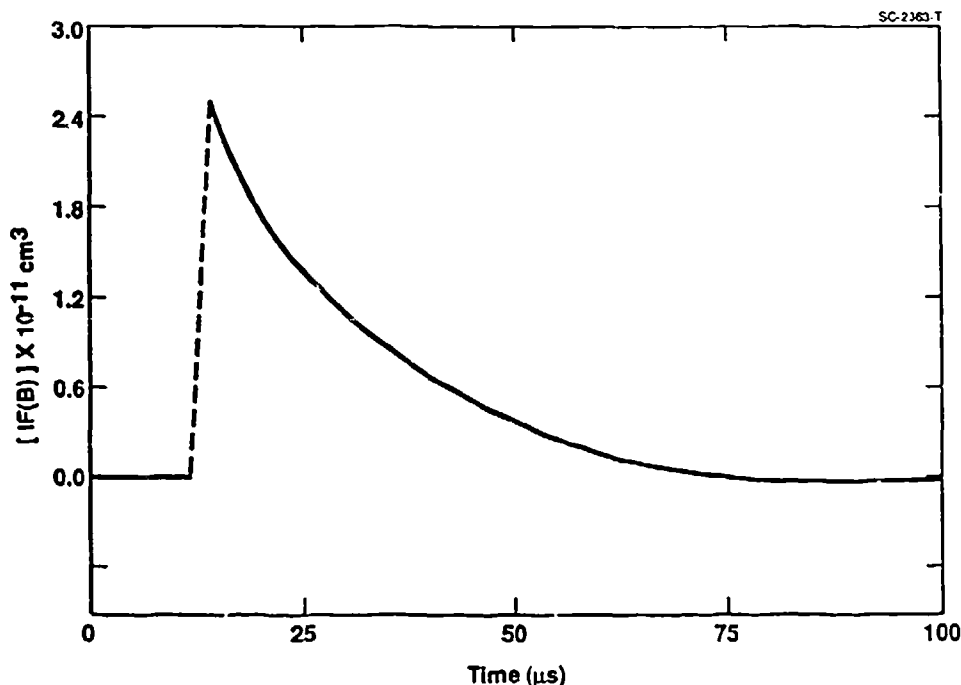


Fig. 8 Time profile of IF(B) following pulsed CO_2 laser excitation of a He / SF_6 / FN_3 / ClN_3 / CF_3I / XeF_2 gas mixture.

Several factors may account for the low effective rate in this IF(B) system. Since the IF(B) state has a radiative lifetime³¹ of 7 μs , it is not likely to be effectively quenched by any of the species present in the reactor. The position¹⁸ of the $3\pi_2$ state in IF is such that only molecules with $v'' \geq 4$ in the ground state¹⁴ will be pumped by NF(a). The IF(X) ground state, however, is rapidly thermalized³² at the high pressure of our experiment, and approximately 10% of the (Boltzmann) vibrational distribution can participate in reaction (3) at the (1800°K) temperatures used to initiate the dissociation process.² Since the NF(a) concentration is an order of magnitude larger than the NCl(a) concentration, no bottleneck should result if the rate of reaction (3) for molecules with $v'' \geq 4$ is comparable to the rate of reaction (4). The difficulty, however, is more likely to originate with reaction (4) since it is capable of producing IF(B) in vibrational energy levels that lie well above the predissociation limit.^{14,55} Therefore, although the rate of reaction (4) may be large, it is likely to have a low branching ratio into the lower (stable) vibrational energy levels of the IF(B) state, while the majority of the molecules that are generated at higher energy levels will be prone to either spontaneous dissociation or (more likely) reaction with the NCl(a) to form a mixed nitrogen dihalide in preference to energy transfer. This phenomenon is similar to the resonant pumping of IF(B) by NF(b) which consumes the metastable at a

rate that is large in comparison to the yield of IF(B-X) photons.^{13,56,57} Finally, even the stable levels of the IF(B) state are subject to (subsequent) rapid thermal dissociation since less than 0.3 eV of vibrational energy is required to access the region of predissociation⁵⁵ and the excited interhalogens are born into an environment whose temperature and pressure are adequate to dissociate FN₃ (which has a 0.5 eV bond energy¹) in approximately 2 μ s. Therefore the actual rate of production of the IF(B) state may be significantly larger than the observed rate of IF(B-X) emission. These findings suggest that NCl(a) is too energetic to be used in place of O₂(a) to pump IF, and azide driven systems which require high temperatures for rapid dissociation are incompatible with the use of IF as an emitting species.

5. New Directions

It is indeed unfortunate that the yield of NCl(a) from dissociation of ClN₃ is smaller than desired and that neither of the mixed azide systems involving NF(b) or IF(B) appears to have kinetics that are appropriate to a practical laser system. Some valuable lessons, nonetheless learned, have helped to guide our selection of new candidates. Molecules that are pumped by NF(a) at near gas kinetic rates and that have radiative lifetimes shorter than about 10 μ s (to compete with quenching) and longer than 1 μ s (to obtain inversion at achievable metastable concentrations) will have to be identified. Viable candidates will also require electronically excited states that are strongly bound and not predissociated at or near vibrational energies up to 0.5 eV and that are preferably characterized by displaced potential curves. Finally, it is still desirable to obtain the active molecules from precursors with adequate vapor pressure which are also capable of rapid and efficient dissociation to yield the transfer agents without the formation of refractory species or byproducts that act as significant quenchers.

Our plans are to proceed along three tracks which include (1) demonstration of lasing in the FN₃ / Bi(CH₃)₃ reaction system, (2) testing of alternative BiF donors that dissociate more rapidly and produce more benign byproducts than Bi(CH₃)₃ and (3) investigation of reaction schemes such as



which may potentially support lasing on the NS(B-X) transition at 415 nm.¹⁴ This emitter meets many (if not all) of the qualifications listed above and has the advantage of requiring only one reaction with one metastable species to generate the emitter. Although our investigations at this stage are preliminary, feasibility appears to depend most critically on scaling the HS concentration to adequate levels via the F + H₂S reaction or thermal dissociation of weakly bonded R-SH parent molecules. The known rate of NF(a) quenching by H₂S is acceptable³³ and the radiative lifetime⁵⁸ of the NS(B) state is close to 1 μ s, hence it is not likely to be quenched directly. The NS(B) state is favorably displaced to larger internuclear separation⁵⁹ than the ground state, but is coupled to two bound non-radiating states (via curve crossings) that act as a reservoir and the majority of the excited state population resides in these energy levels which lie slightly below the B state.⁶⁰ Consequently, the effective kinetic lifetime of the coupled radiating and non-radiating states is approximately 30 μ s at 1800°K and decreases with increasing temperature. While no energy is lost by the population of these reservoir states, the probability of quenching the excited NS molecules is nonetheless increased. The system, however, is tolerant of the high temperatures required for dissociation of azides since there are no predissociations of the NS(B) state (or its non-radiating reservoir states) for vibrational energy levels within 1.3 eV of the lowest potential minimum.⁶⁰ Preliminary estimates (for trace concentrations of HS) show an effective pump rate in the range of 10⁻¹¹ to 10⁻¹² cm³/s (which may be acceptable) and current effort is focused on scaling up the HS concentration to levels consistent with efficient utilization of the NF(a) metastables.

6. Acknowledgments

This work was supported by the Innovative Science and Technology Office of the Strategic Defense Initiative through Contract No. F49620-90-C-0025 with the Air Force Office of Scientific Research. The electronic structure calculations were supported in part by the Propulsion Directorate of the Air Force Phillips Laboratory under Contract No. F04611-90-C-0009.

7. References

1. D.J. Benard, B.K. Winker, T.A. Seder and R.H. Cohn, *J. Phys. Chem.* **93** (1989) 4790.
2. D.J. Benard, M.A. Chowdhury, B.K. Winker, T.A. Seder and H.H. Michels, *J. Phys. Chem.* **94** (1990) 7507.
3. M. Lenzi, E. Molinari, G. Piciacchia, V. Sessa and M.L. Terranova, *Chem. Phys.* **142** (1990) 473.
4. J.M. Herbelin and R.A. Klingberg, *Int. J. Chem. Kinetics*, **16** (1984) 849.
5. B.K. Winker, D.J. Benard and T.A. Seder, *High Power Gas Lasers*, Proceedings of the SPIE, **1225** (1990) 543.
6. R.F. Heidner, H. Helvajian, J.S. Holloway and J.B. Koffend, *J. Chem. Phys.* **84** (1986) 2137.
7. D.J. Benard and B.K. Winker, *J. Appl. Phys.* **69** (1991) 2805.

8. E. Quinones, J. Habdas and D.W. Setser, *J. Phys. Chem.* **91** (1987) 5155.
9. W.E. Jones and T.D. McLean, *J. Mol. Spectrosc.* **90** (1981) 481.
10. T.T. Yang and R.D. Bower, High Power Gas Lasers, Proceedings of the SPIE, **1225** (1990) 430.
11. R.G. Derwent and B.A. Thrush, *Disc. Faraday Soc.* **53** (1972) 162.
12. J.M. Herbelin, M.A. Kwok and D.J. Spencer, *J. Appl. Phys.* **49** (1978) 3760.
13. D.J. Beuard, M.A. Chowdhury and A.T. Pritt, *J. Appl. Phys.* **60** (1986) 4051.
14. B. Rosen, Spectroscopic Data Relative to Diatomic Molecules (Pergamon, 1970).
15. P.H. Tennyson, A. Fontijn and M.A.A. Clyne, *Chem. Phys.* **62** (1981) 171.
16. S.J. Davis and L. Hanco, *Appl. Phys. Lett.* **37** (1980) 692.
17. S.J. Davis, Physical Sciences Inc. (Andover, MA) private communication.
18. J.P. Nicolai and M.C. Heaven, *J. Chem. Phys.* **87** (1987) 3304.
19. W.J. Marinelli and L.G. Piper, *J. Quant. Spectrosc. Radiat. Transfer*, **34** (1985) 321.
20. D.J. Benard and R.H. Cohn, Model Studies of CBES Decomposition, AFAL-TR-87-071 (February, 1988).
21. R.D. Coombe, D. Patel, A.T. Pritt and F.J. Wodarczyk, *J. Chem. Phys.* **75** (1981) 217..
22. K. Gholivand, G. Schatte and H. Willner, *Inorg. Chem.* **26** (1987) 2137.
23. S.D. Ross, Inorganic Infrared and Raman Spectra (McGraw-Hill, 1972).
24. J.F. Haller, Ph.D. Dissertation, Cornell University (Ithaca, NY) 1943.
25. D.E. Milligan and M.E. Jacox, *J. Chem. Phys.* **40** (1964) 2461.
26. R.C. Weast, Handbook of Physics and Chemistry (CRC Press, 1980).
27. W.J. Frierson, Ph.D. Dissertation, Cornell University (Ithaca, NY) 1943.
28. J.F. Weeks and M.S. Matheson, Inorganic Synthesis VII (McGraw-Hill, 1966).
29. C.R. Quick and C. Wittig, *Chem. Phys. Lett.* **48** (1977) 420.
30. R.J. Malins and D.W. Setser, *J. Phys. Chem.* **85** (1981) 1342.
31. M.A.A. Clyne and I.S. McDermid, *J. Chem. Soc. (Faraday Trans. II)* **74** (1978) 1644.
32. P.J. Wolf and S.J. Davis, *J. Chem. Phys.* **87** (1987) 3492.
33. K.Y. Du and D.W. Setser, *J. Phys. Chem.* **94** (1992) 2425.
34. C.T. Cheah, M.A. Clyne and P.D. Whitefield, *J. Chem. Soc. (Faraday Trans. II)* **76** (1980) 711.
35. R.H. Garstang, *J. Res. Nat. Bur. Stand.* **68A** (1964) 61.
36. J.B. Koffend, Aerospace Corporation (El Segundo, CA) private communication.
37. F. Stuhl and H. Niki, *Chem. Phys. Lett.* **7** (1979) 473.
38. H. Cha and D.W. Setser, *J. Phys. Chem.* **91** (1987) 3758.
39. J.M. Herbelin, Aerospace Corporation (El Segundo, CA) private communication.
40. D. Copeland, Rocketdyne (Canoga Park, CA) private communication.
41. D.R. Yarkony, *J. Chem. Phys.* **86** (1987) 1642.
42. O. Kajimoto, T. Yamamoto and T. Fueno, *J. Phys. Chem.* **83** (1979) 429.
43. M.J. Frisch, et al, Gaussian 90, Gaussian Inc., Pittsburgh, PA, 1990.
44. P.C. Hariharan and J.A. Pople, *Theor. Chem. Acta* **28** (1973) 213.
45. D. Christen, H.G. Mack, G. Schatte and H. Willner, *J. Am. Chem. Soc.* **110** (1988) 707.
46. R.L. Cook and M.C.L. Gerry, *J. Chem. Phys.* **53** (1970) 2525.
47. M.W. Schmidt, M.S. Gordon and M. Dupuis, *J. Am. Chem. Soc.* **107** (1985) 2585.
48. H.H. Michels and J.A. Montgomery, Jr., to be published.
49. J.A. Pople, M. Head-Gordon, D.J. Fox, K. Raghavachari and L.A. Curtiss, *J. Chem. Phys.* **90**, 5622 (1989).
50. L.A. Curtiss, C. Jones, G.W. Trucks, K. Raghavachari and J.A. Pople, *J. Chem. Phys.* **93**, 2537 (1990).
51. M.H. Alexander, H. Werner and P.J. Dagdigan, *J. Chem. Phys.* **89**, 1388 (1988).
52. L. Stern, J. Wanner and H. Walther, *J. Chem. Phys.* **72** (1980) 1128.
53. J.E. Huheey, Inorganic Chemistry (Harper & Row, 1978).
54. J.W. Bozelli and M. Kaufmann, *J. Phys. Chem.* **77** (1973) 1748.
55. P.D. Whitefield, R.F. Shea and S.J. Davis, *J. Chem. Phys.* **78** (1983) 6793.
56. A.T. Pritt, D. Patel and D.J. Benard, *Chem. Phys. Lett.* **97** (1983) 471.
57. A.T. Pritt and D.J. Benard, *J. Chem. Phys.* **85** (1986) 7159.
58. J.B. Jeffries and D.R. Crosley, *J. Chem. Phys.* **86** (1987) 6839.
59. K. Raghuvver and N.A. Narasimham, *J. Astrophys. Soc.* **3** (1982) 13.
60. Y. Matsumi, T. Munakata and T. Kasuya, *J. Phys. Chem.* **88** (1984) 264.

PROCEEDINGS REPRINT

 SPIE—The International Society for Optical Engineering

Reprinted from

High-Power Gas Lasers

15-17 January 1990
Los Angeles, California



Volume 1225

©1990 by the Society of Photo Optical Instrumentation Engineers
Box 10, Bellingham, Washington 98227 USA. Telephone 206/676-3290.

Chemical pumping of potential visible laser transitions in bismuth monofluoride
by thermal dissociation of fluorine azide

B.K. Winker, D.J. Benard and T.A. Seder

Rockwell International Science Center
Thousand Oaks, CA 91360

ABSTRACT

A visible chemical laser on the BiF(A-X) transitions at 430-470 nm can potentially be generated by the interaction of Bi-atoms with metastable species such as NF(a¹Δ). Experiments were performed in which these constituents were obtained in situ by fast pulsed CO₂ laser pyrolysis of FN₃ and Bi(CH₃)₃, respectively. Time-resolved optical diagnostics were used to follow the concentrations of FN₃, NF(a¹Δ), Bi(CH₃)₃, Bi(²D) and BiF(A). The optimal concentrations of FN₃ and Bi(CH₃)₃ were limited by NF(a¹Δ) self-annihilation and Bi(²D) quenching reactions, respectively. The Bi(CH₃)₃ was found to be only 20 % dissociated at the peak of the NF(a¹Δ) time profile and the yield of Bi-atoms from dissociated Bi(CH₃)₃ was determined to be approximately 5 %; however, significant recycling of the active Bi/BiF species was observed at a limiting rate of $4 - 5 \times 10^{-11}$ cm³/s, driven by NF(a¹Δ). On the basis of these results, a peak BiF(A) concentration of 10¹³/cm³ was predicted by kinetic modeling and subsequently observed. The model also predicts an absolute population inversion of the BiF(A-X) transition at high NF(a¹Δ) concentration with unsaturated gains of approximately 10⁻³/cm. Intracavity experiments have verified that the BiF(X) ground state concentration is low enough relative to the excited state to generate at least a partial inversion, and initial evidence for an absolute population inversion has been obtained.

1. INTRODUCTION

Since chemical reactions follow the same spin-selection rules as optical transitions, it is difficult to produce electronically excited products with high efficiency unless they are optically metastable, because the reaction will preferentially populate any lower energy product state that is of the same spin. Consequently, the generation of electronic transition chemical lasers typically involves a two-step process consisting of efficient chemical production of an optically metastable species, which acts as an energy store, followed by some form of energy transfer from the store to a more suitable radiating species. In our work, the a¹Δ state of nitrogen monofluoride (NF) is the energy store and bismuth monofluoride (BiF) is the radiating species. The transfer of energy from NF(a¹Δ) to BiF was initially discovered by Herbelin¹ who used the reaction of H-atoms with NF₂ radicals to generate the NF(a¹Δ). Recently, we have developed a new source of NF(a¹Δ) that is based on thermal dissociation of fluorine azide (FN₃), which is capable of achieving unusually high NF(a¹Δ) concentrations.² Large yields of NF(a¹Δ) are important to this application since the BiF(A) state has a radiative lifetime³ near 1 μs and the rate of BiF excitation (which must approach 10⁶/s) is controlled by the NF(a¹Δ) concentration. In this work, we have used the FN₃ source of NF(a¹Δ) to extend Herbelin's work to higher NF(a¹Δ) concentrations and to investigate any differences in the mechanism of BiF excitation that may occur between the two chemical sources of metastable NF.

2. EXPERIMENTAL

Figure 1 shows schematically how the experiments were performed. A variable gas mixture of FN₃, Bi(CH₃)₃ and SF₆ in He buffer gas was admitted to a slowly flowing reactor that was exhausted to a vacuum. The gas flow in the reactor was optically pumped by a pulsed CO₂ laser at a rate of 1-2 Hz, so that gas flow in the reactor changed the active sample between shots.

The functions of the SF₆ additive were to absorb the incident CO₂ laser radiation and to heat the gas upon subsequent collisional relaxation. The laser fluence in these experiments was well below the threshold for significant production of F-atoms by multiphoton dissociation.⁴ The excited states of NF and BiF were detected in emission at 874/528 and 450 nm, respectively,⁵ by an optical multichannel analyzer (OMA) for spectral analysis and by a filtered silicon photodiode interfaced to a fast preamplifier and digital signal averager for temporal analysis. The diode/filter combinations were absolutely calibrated by comparison to a standard lamp of known emissivity that is traceable to the National Bureau of Standards. Therefore, absolute NF(a¹Δ, b¹Σ) and BiF(A) concentrations could be inferred with knowledge of the relevant A coefficients,^{3,6,7} and the gas sample / photon collection geometry. Ground state species such as Bi(CH₃)_x and FN₃ were followed by time-resolved ultraviolet absorption using a D₂ lamp source and a filtered IP28 photomultiplier tube as the detector. The absorption signals were processed in the same manner as the emission signals from the silicon detector, and absolute concentrations were inferred from these data with knowledge of the active path length and the relevant extinction coefficients.^{8,9} Detection of Bi(²D) was accomplished by ultraviolet absorption since the emission signal was prone to spectroscopic interference due to overlapping HF emissions. In this case, the D₂ lamp was replaced by a Bi-hollow cathode lamp which was electronically pulsed to enhance its intensity. The lamp current was pulsed to approximately 500 ma for about 500 μs with a 200 μs lead on the CO₂ laser pulse used to initiate the chemical reactions to be monitored. Hence, the lamp intensity was essentially constant during the time of data collection. In these experiments, the 289.8 nm line was selected by the filter that was placed over the detector, and the absolute concentration of Bi(²D) was determined from the absorption data using a cross section that was calculated from the radiative rate¹⁰ assuming a Doppler broadened line profile. The gas temperature was determined with ± 50 K accuracy by comparison of a section of the BiF(A-X) emission spectrum to a set of synthetically generated emission spectra, provided by Koffend,¹¹ as described in a prior publication.² Worst case propagation of errors in the concentration measurements suggests an accuracy of approximately ± 35 %.

The reactor was designed for wall-free operation by admitting the reactive gas flows to a central 2.5 mm × 2.5 cm rectangular duct that was surrounded by a velocity matched Ar shield flow. All gas flows were electronically monitored by mass flow meters and the reactor pressure was monitored by an inductance transducer. The Bi(CH₃)₃ was eluted from a cold trap at ice temperature by bubbling a flow of He carrier gas through the liquid. The mole fraction of the Bi(CH₃)₃ in the He flow was determined from the vapor pressure¹² of the Bi(CH₃)₃ and a measurement of the total pressure in the trap, assuming complete saturation of the He flow. Prior experience has shown this method to overestimate the Bi(CH₃)₃ mole fraction by a factor of less than two. Typical conditions in the reactive jet were 0-0.1 torr Bi(CH₃)₃, 1.5 torr FN₃, 13.5 torr SF₆ and balance He to a net pressure of 150 torr. The jet was side pumped by the CO₂ laser with a soft line focus (2.5 mm × 2.5 cm) at a fluence of approximately 1 joule/cm². The SF₆ concentration was chosen so that approximately 66 % of the incident laser energy was transmitted through the reactor to a retroreflecting cylindrical mirror that refocused and counterpropagated the beam through the reactor. This procedure was used to insure uniform excitation of the reactive flow across its short dimension. The optical measurements were taken along the 2.5 cm long axis of the reactive flow (perpendicular to the CO₂ laser beam).

The FN₃ flow was generated by reacting commercial grade sodium azide with stearic acid at 110°C to yield hydrogen azide (HN₃) gas in a He carrier stream, which subsequently reacted with a dilute F₂/He gas stream to yield HF, which was eliminated in a cold trap, and FN₃. This is a somewhat hazardous and complex operation that is described in detail in prior publications.^{2,13} The mole fraction of FN₃ in the He carrier stream was determined by absorption measurements at 425 nm using the extinction data of Gholivand.⁸ The materials of construction were limited to stainless steel, teflon/viton and glass/quartz to prevent undesired reaction, and care was taken to avoid even mild heating of the FN₃ flow to prevent disproportionation¹⁴ into

N_2F_2 and N_2 . The FN_3 gas flow at the laser pyrolysis reactor showed negligible decomposition as determined by mass spectroscopy.

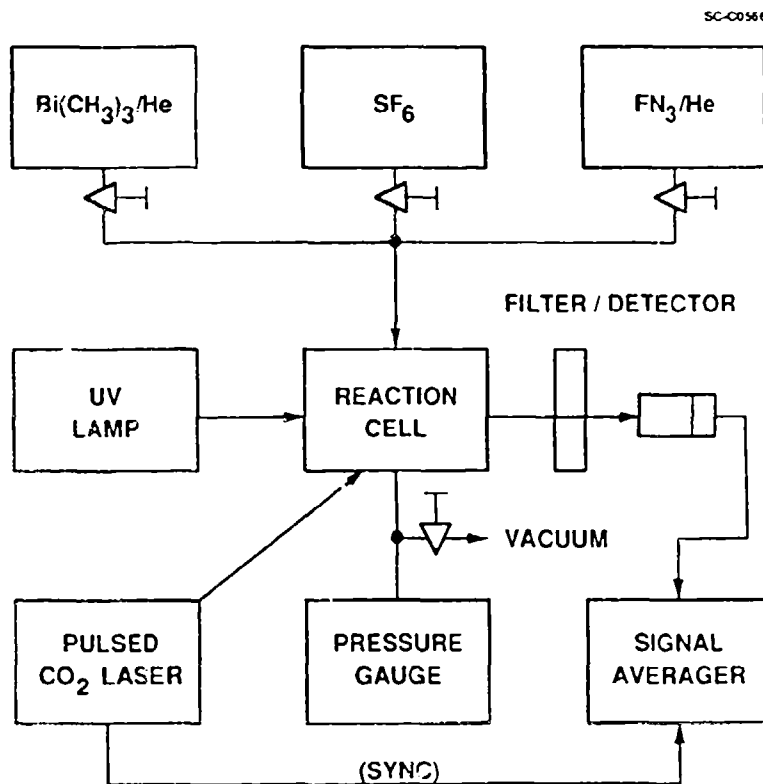
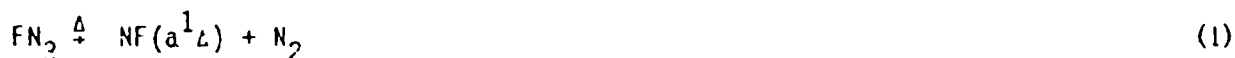


Fig. 1 Block diagram of experiment used to investigate energy transfer from $NF(a^1\Delta)$ to BiF .

3. GENERATION OF $NF(a^1\Delta)$

Figure 2 shows the typical emission spectrum that is obtained in the vicinity of the $NF(a-X)$ transitions at 874 nm by CO_2 laser excitation of FN_3/SF_6 gas mixtures. It is characteristically free of overlapping $N_2(B-A)$ emissions that are common to other $NF(a^1\Delta)$ sources, which is consistent with the very simple mechanism of excitation just described.

Typical time profiles of the FN_3 and $NF(a^1\Delta)$ following the CO_2 laser pulse (in the absence of $Bi(CH_3)_3$) are shown in Fig. 3. These data were collected with 100 ns resolution; however, the $NF(a^1\Delta)$ time profile has been smoothed since $NF(a^1\Delta)$ is a weak emitter and the statistical noise is significant on the sub- μs time scale. The error bar indicates the magnitude of the peak-to-peak noise at 100 μs resolution. The FN_3 absorption data is relatively noise free but does experience some electrical interference from the CO_2 laser at early times as indicated by the error bar and the dashed portion of the line. The yield of $NF(b^1\Sigma)$ in these experiments was approximately 10^{-2} of the $NF(a^1\Delta)$, and the peak temperature was estimated at 1200 K using trace addition of $Bi(CH_3)_3$. The rise of the $NF(a^1\Delta)$ is seen to coincide with the decay of the FN_3 indicating a simple mechanism, namely:



The subsequent decay of the $NF(a^1\Delta)$ due to self-annihilation



has been observed by Setser¹⁵ in low density flowtube experiments. The products of this reaction are not known; however, the yield of $NF(b^1\Sigma)$ obtained in both Setser's and our experiments is too low to account for the $NF(a^1\Delta)$ loss due to energy pooling. Because of the self-annihilation process, high densities of $NF(a^1\Delta)$ can be achieved only if the FN_3 is dissociated rapidly.

6C50041

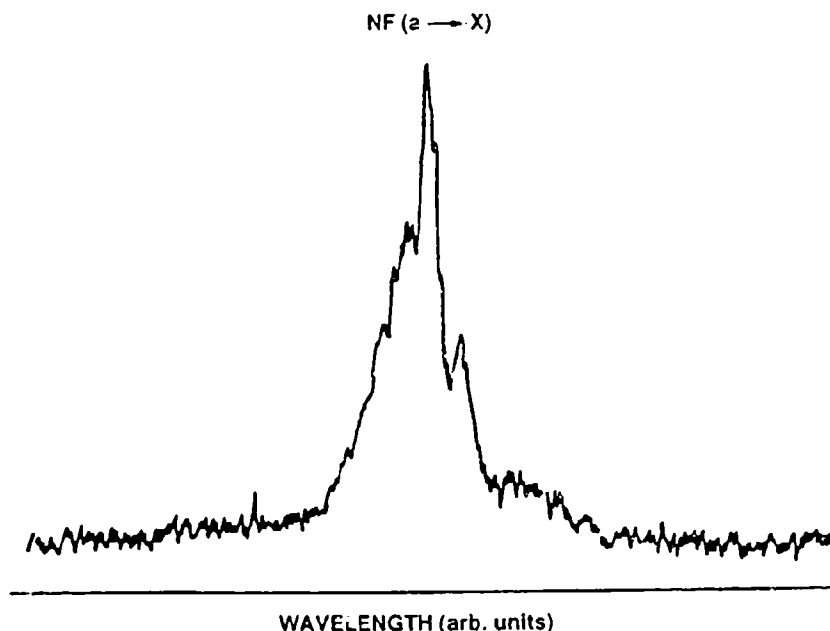


Fig. 2 Emission spectrum of $NF(a^1\Delta)$ obtained by thermal dissociation of FN_3 .

The principal factors that govern the dissociation rate are the collision frequency, the barrier height for activation of the dissociation reaction and the gas temperature. Michels¹⁶ has calculated the barrier to FN_3 dissociation by ab initio methods to be approximately 0.5 eV. The dissociation of FN_3 and the production and decay of the $NF(a^1\Delta)$ can therefore be described by the following set of coupled differential rate equations which treat temperature as a dynamic variable and assume 100% conversion of FN_3 to $NF(a^1\Delta)$ upon dissociation with negligible loss of reactants or heat due to transport phenomena.

$$\frac{d}{dt} [FN_3] = -k_d e^{-T/T_0} [FN_3] [M] \quad (3)$$

$$\frac{d}{dt} [NF(a)] = -\frac{d}{dt} [FN_3] - k_q [NF(a)]^2 \quad (4)$$

$$\frac{d}{dt} T = \frac{1}{C} (\sigma I(t) [SF_6] - H_d \frac{d}{dt} [FN_3] + H_q k_q [NF(a)]^2) \quad (5)$$

The terms are defined as follows: k_d is the collision rate between FN_3 molecules and other species (M), T is temperature and T_0 is the barrier height expressed in terms of temperature, k_a is the self-annihilation rate, C is the heat capacity of the gas, $I(t)$ is the intensity time profile of the incident CO_2 laser radiation, σ is the cross section for absorption by SF_6 , and $H_{d,a}$ are the heat releases associated with the dissociation of FN_3 and the self-annihilation reactions, respectively. The thermodynamic factors are available in large part from the JANAF tables. The products of reaction (2) are assumed to be N_2 and two F-atoms. The heat of formation of FN_3 was obtained as +120 kcal/mole from prior work involving ArF photolysis of the azide at low pressure.¹⁷ The cross section (σ) was determined by actual transmission measurements since its value is somewhat dependent on the intensity of the CO_2 laser. Finally, $I(t)$ was modeled as the sum of two linearly decaying time profiles that correspond to the fast and slow components of the CO_2 laser output. The principal fitting parameters are k_d , which can be estimated at 10^{-11} cm^3/s by kinetic theory, T_0 , which is approximately 6000 K on the basis of Michel's calculation and k_a , which was measured by Setser and confirmed in our laboratory to have a value near 3×10^{-12} cm^3/s . Figure 4 shows the typical result obtained by computer integration of equations (3-5) subject to the initial values defined by the experimental conditions. Table 1 provides a more detailed comparison between theory and experiment under conditions which optimize the yield of $\text{NF}(a^1\Delta)$. These results were obtained with only modest variation of the rate parameters ($\pm 25\%$) and the activation barrier ($\pm 10\%$). Therefore, the general agreement that is obtained as well as the ability of the model to reproduce the qualitative trends that are observed with variation of laser energy and initial FN_3 concentration suggest that reactions (1) and (2) are the dominant processes and that the rate constant/barrier height estimates are approximately correct. Since our gas sample was heavily diluted, the rise in gas temperature was primarily due to laser heating rather than the induced reactions, as shown in Fig. 4. If this condition were not satisfied, the time profiles would be considerably more complex and difficult to model accurately.

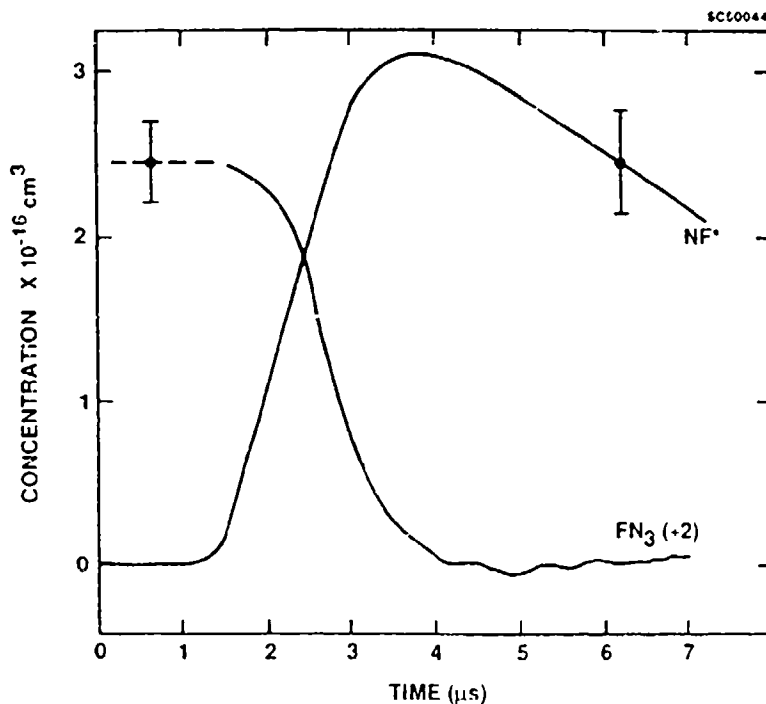


Fig. 3 Characteristic time profiles of FN_3 and $\text{NF}(a^1\Delta)$ following pulsed CO_2 laser excitation.

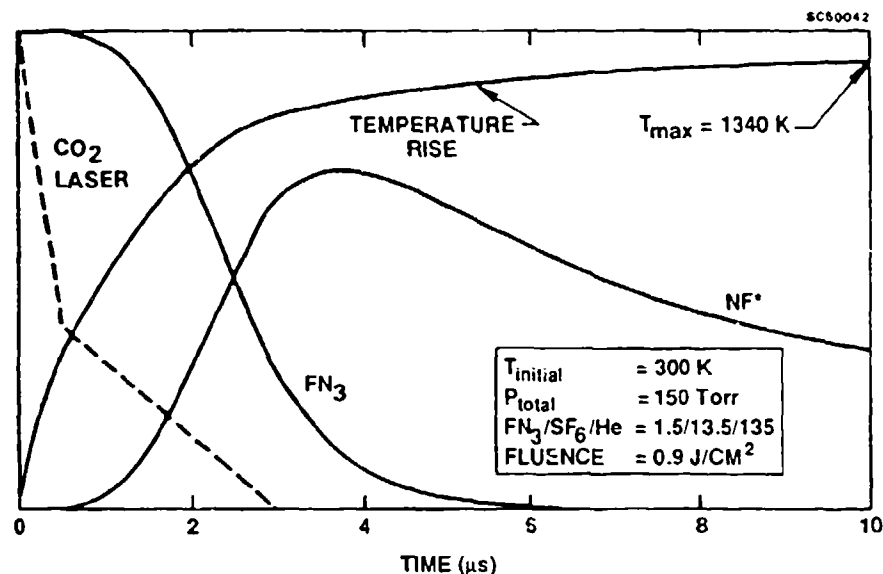


Fig. 4 Time profiles of FN_3 , $\text{NF}(a^1\Delta)$ and gas temperature obtained by kinetic modeling.

Table 1
Comparison of Modeling Results to Experimental Data
for CO_2 Laser Driven Pyrolysis of FN_3

Result	Model	Data	Units
Peak [$\text{NF}(a^1\Delta)$]	4×10^{16}	3×10^{16}	cm^{-3}
Rise Time (10-90 %)	2.6	2.4	μs
Decay Time (100-50 %)	5.7	5.0	μs
Temperature at Peak	1237	1150	K

4. EXCITATION OF $\text{BiF}(A)$

Upon addition of $\text{Bi}(\text{CH}_3)_3$ to the FN_3 and SF_6 in the reactor very intense $\text{BiF}(A-X)$ emission was observed. The mechanism of excitation of this species is considerably more complex than that of $\text{NF}(a^1\Delta)$, as shown by the processes indicated on the energy level diagram given as Fig. 5. Once Bi-atoms are introduced into the system, the reactions



set up a complex equilibrium between Bi-atoms, BiF , BiF_2 and BiF_3 . From a strictly thermodynamic standpoint, the majority of the Bi is expected to be in the form of BiF_2 and

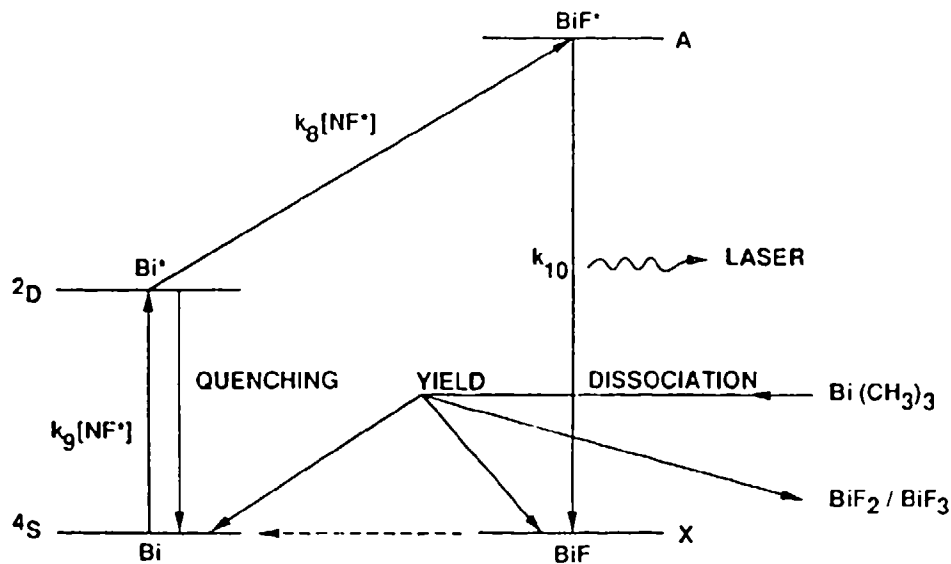


Fig. 5 Energy levels and kinetic processes involved in the excitation of the BiF(A) state. The reactions responsible for recycling active Bi/BiF are shown by the dashed line.

BiF₃ which do not participate in the observed chemiluminescence. Therefore, the efficiency of converting dissociated Bi(CH₃)₃ into active Bi/BiF is a key concern. Related issues are the rate and mechanism of Bi(CH₃)₃ dissociation and the quenching of NF(a¹Δ) and other significant electronically excited species by undissociated Bi(CH₃)₃ or its dissociation by-products. Herbelin¹¹ has suggested that the actual mechanism responsible for the BiF(A) generation is



where the Bi(²D) is generated by the fast resonant transfer reaction



first studied by Sutton and Capelle.¹⁸ Once produced, BiF(A) decays radiatively



and there is a potential for recycling of the Bi-atoms if reactions such as (7, x = 1) or



occur at a significant rate. It is therefore important to know which step in the cycle is rate limiting and the associated rate constant. Reactions such as (7, x = 1) and (11) also help to

remove BiF(X) and thereby to maintain population inversion of the A-X transition. Our investigation is aimed at a resolution of these issues.

5. RESULTS AND DISCUSSION

Measurements of the time profiles of Bi(CH₃)_x, Bi(²D) and BiF(A) were collected under conditions of both high ($3 \times 10^{16}/\text{cm}^3$) and low ($3 \times 10^{15}/\text{cm}^3$) peak NF(a¹Δ) concentration to resolve the kinetic issues described above. The peak NF(a¹Δ) concentrations were changed by adjusting the initial FN₃ concentration. The principal reason for this alteration was to slow the self-annihilation reaction (2) which occurs at a rate comparable to the Bi/BiF kinetics for high NF(a¹Δ) concentrations. Since the experimental observables reflect both the time evolution of the NF(a¹Δ) as well as the Bi/BiF species, this condition was necessary in some cases to effect a deconvolution of these phenomena. The data are presented and analyzed in the order that yields the simplest interpretation of the results.

5.1 Production of BiF(A) from Bi(²D)

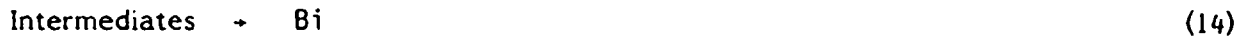
The time profiles of Bi(²D) and BiF(A) at high peak NF(a¹Δ) concentration are shown in Fig. 6. The initial Bi(CH₃)₃ concentration in these experiments was set to $6 \times 10^{14}/\text{cm}^3$ to optimize the Bi(²D) measurement. At this concentration of Bi(CH₃)₃, the NF(a¹Δ) time profile is not significantly altered, as will be shown later. Since the BiF(A) time profile follows the Bi(²D) by approximately one radiative lifetime in the vicinity of the peak emission regime, our data are compatible with reaction (8) as the principal pumping mechanism. The rate of the pumping reaction (k_8) of Bi(²D) with NF(a¹Δ) to yield BiF(A) can be determined by applying the steady state relation

$$k_8 [\text{NF}(a^1\Delta)] [\text{Bi}({}^2\text{D})] = A [\text{BiF}(A)] \quad (12)$$

at the peak of the BiF(A) time profile. Taking $A = 7 \times 10^5/\text{s}$ as measured by Koffend,³ $[\text{NF}(a^1\Delta)] \sim 3 \times 10^{16}/\text{cm}^3$ and $[\text{BiF}(A)] \sim 2 [\text{Bi}({}^2\text{D})]$ from Fig. 6 gives $k_8 \sim 4.7 \times 10^{-11} \text{ cm}^3/\text{s}$ in reasonable agreement with an independent determination of the same rate as measured by Herbelin¹¹ using the H + NF₂ reaction to generate the NF(a¹Δ). The sum of the Bi(²D) and BiF(A) concentrations, however, is only about 1 % of the initial Bi(CH₃)₃ concentration. The other 99 % must therefore be accounted for by incomplete dissociation of the Bi(CH₃)₃, the yield of active Bi/BiF from the Bi(CH₃)₃ that was dissociated, and the production of ground state Bi/BiF species. The latter is believed to be negligible, however, since Sutton found complete disappearance of ground state Bi in the presence of NF(a¹Δ). A similar situation may also exist in regard to ground state BiF(X) at high NF(a¹Δ) concentrations, due to reactions (7, x = 1) and (11). Therefore, we will proceed on the assumption of negligible BiF(X) concentration and will address this point independently later.

5.2 Dissociation of Bi(CH₃)₃

The disappearance of the Bi-donor was tracked at 270 nm where FN₃ absorption^{6,9} is weak compared to Bi(CH₃)₃. Background data were collected and subtracted to account for residual FN₃ absorption and ultraviolet chemiluminescence emitted by the reactor. The absorption vs time after the CO₂ laser pulse was found to increase initially and then to decline to zero as shown in Fig. 7. This behavior is attributed to sequential loss of the methyl groups and a higher absorption coefficient in the intermediate Bi(CH₃)₂ or Bi(CH₃)₁ species than in Bi(CH₃)₃. To deal with this complication, a simple model of the form



was constructed. The rates k_{13} and k_{14} were assumed to be fixed, owing to a thermal dissociation mechanism, since the absorption data were not influenced by the presence or lack of FN_3 . In other words, $\text{NF}(a^1\Delta)$ does not contribute significantly to the dissociation of $\text{Bi}(\text{CH}_3)_3$ as a result of energy transfer or chemical reactions. The absorption signal was normalized to unity at $t = 0$ and the ratio of the ultraviolet absorption cross sections (intermediates to initial $\text{Bi}(\text{CH}_3)_3$) was used as a fitting parameter along with k_{13} and k_{14} . The rate equations corresponding to reactions (13) and (14) were solved analytically, and the absorption signal was calculated and also normalized to unity at $t = 0$. The cross section ratio was analytically selected to yield an absorption time profile that peaked in time at the same point as the data. Trial values of k_{13} and k_{14} were then selected and the solutions were compared against the data for relative peak height and overall decay rate. The best fit to the absorption data shown in Fig. 6 corresponds to $k_{13} = 4.2 \times 10^5/\text{s}$ and $k_{14} = 3.9 \times 10^5/\text{s}$. While the values of k_{13} and k_{14} could be co-varied somewhat without significantly affecting the agreement with the data, the yield of Bi-atoms, which was then calculated analytically, did not vary significantly. Therefore, as shown in Fig. 7, the $\text{Bi}(\text{CH}_3)_3$ is completely converted to Bi-atoms in about 10 μs . At high $\text{NF}(a^1\Delta)$ concentrations, however, the peak $\text{BiF}(A)$ emission occurs at about 2 μs . Consequently, only about 20 % of the $\text{Bi}(\text{CH}_3)_3$ contributes to the pumping of the $\text{BiF}(A)$ state when the $\text{NF}(a^1\Delta)$ yield is optimized. Since the overall yield of active Bi/ BiF from initial $\text{Bi}(\text{CH}_3)_3$ is 1 %, it then follows that the yield of active Bi/ BiF from dissociated $\text{Bi}(\text{CH}_3)_3$ is about 5 %.

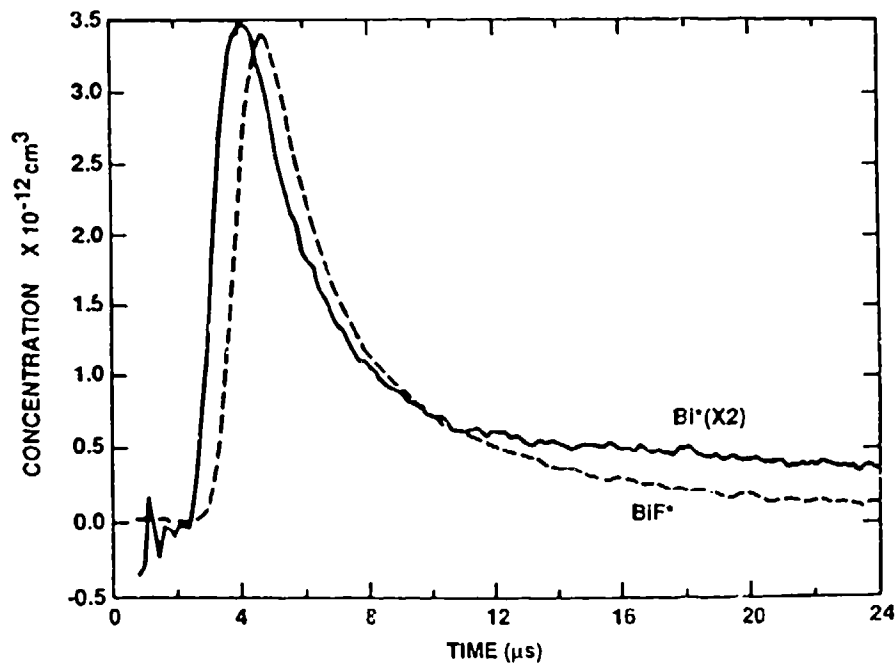


Fig. 6 Time profiles of $\text{Bi}(^2\text{D})$ and $\text{BiF}(A)$ following pulsed CO_2 laser excitation.

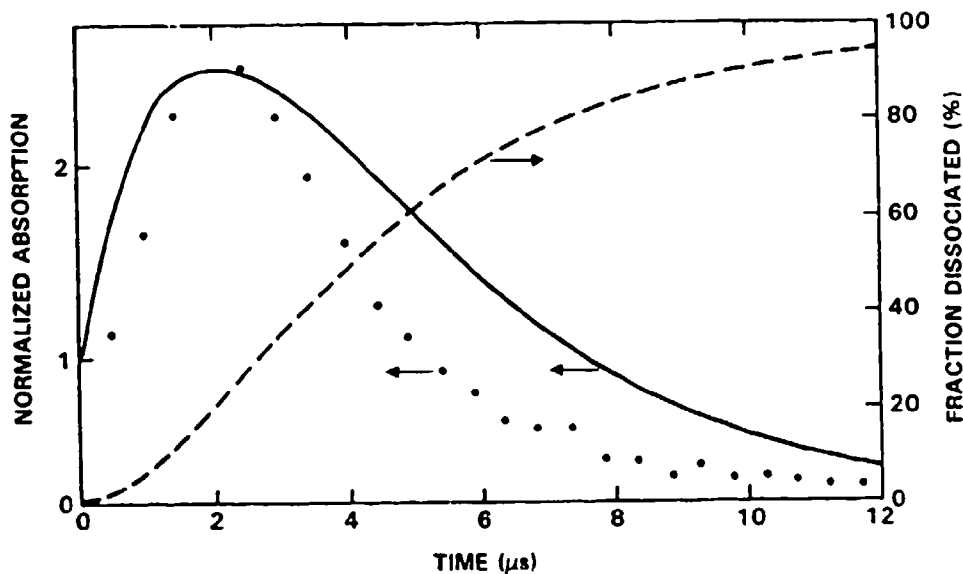


Fig. 7 Time profile of ultraviolet absorption due to $\text{Bi}(\text{CH}_3)_3$ species (dots) and related kinetic modeling results (solid and dashed lines).

5.3 Recycling of Active Bi/BiF

By reducing the initial $\text{NF}(a^1\Delta)$ concentration an order of magnitude and using trace concentrations of $\text{Bi}(\text{CH}_3)_3$, essentially all of the $\text{Bi}(\text{CH}_3)_3$ is dissociated before the peak $\text{NF}(a^1\Delta)$ concentration decays significantly. When this is done, a $10 \mu\text{s}$ rise in the $\text{BiF}(A)$ time profile is observed, which can be assigned to the dissociation of the $\text{Bi}(\text{CH}_3)_3$, as shown in Fig. 8. Following this rise, the decay of the $\text{BiF}(A)$ essentially follows the decay of the $\text{NF}(a^1\Delta)$. Consequently, a near steady state is achieved, which suggests that active Bi/BiF is recycled following the emission step; otherwise a more rapid decay of the $\text{BiF}(A)$ would be observed. By integrating the $\text{BiF}(A)$ time profile, the net yield of $\text{BiF}(A-X)$ photons per unit volume was found to equal 70 % of the initial $\text{Bi}(\text{CH}_3)_3$ concentration. Since all the $\text{Bi}(\text{CH}_3)_3$ dissociates in this experiment but only 5 % of the dissociated $\text{Bi}(\text{CH}_3)_3$ yields active Bi/BiF, approximately 14 photons were generated per each active Bi/BiF species, which demonstrates effective recycling. Under these conditions, the rate of photon emission is governed by the limiting rate in the cycle. The radiative step (10) is not limiting in this case as all of the other reactions are driven by low $\text{NF}(a^1\Delta)$ concentrations. The excitation of $\text{Bi}(^2D)$ by $\text{NF}(a^1\Delta)$, reaction (9), is known to be fast¹⁸ by comparison to reaction (8). Therefore, the limiting rate is either the pumping step (8) or the conversion of $\text{BiF}(X)$ back into Bi-atoms due to reactions (7, $x = 1$) and (11). Without determining which rate is limiting, the limiting rate constant (k_0) can be determined under cycling/total dissociation conditions by applying the steady state relation

$$I = k_0 Y [\text{Bi}(\text{CH}_3)_3] [\text{NF}(a^1\Delta)] \quad (15)$$

where I is the rate of $\text{BiF}(A-X)$ photon emission per unit volume and Y is the dissociation yield of active Bi/BiF or about 5 %. Applying the above analysis to the data in Fig. 7 yields $k_0 \sim 5 \times 10^{-11} \text{ cm}^3/\text{s}$ in close agreement with the measured rate of reaction (8). It therefore follows that the rates of the $\text{BiF}(X)$ removal reactions (7, $x = 1$ and 11) are at least this fast or possibly faster. Consequently, at high $\text{NF}(a^1\Delta)$ concentrations, the rate of $\text{BiF}(X)$ removal exceeds $(5 \times 10^{-11} \text{ cm}^3/\text{s}) \times (3 \times 10^{16}/\text{cm}^3)$ or $1.5 \times 10^6/\text{s}$, which is twice the radiative rate of

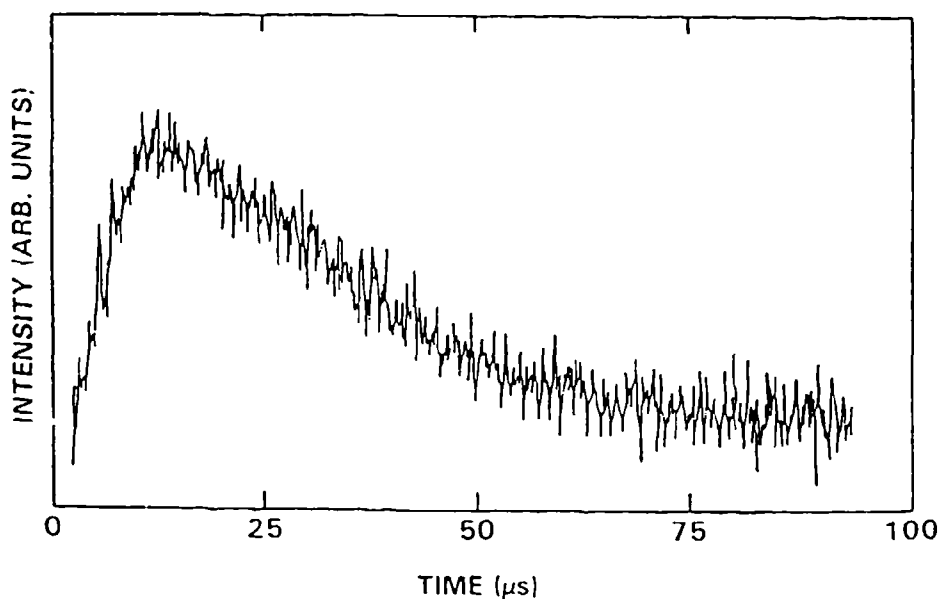


Fig. 8 Time profile of BiF(A) at reduced $NF(a^1\Delta)$ concentration showing a $10 \mu s$ rise due to the dissociation of $Bi(CH_3)_3$.

the BiF(A-X) transition. This result, which implies an absolute population inversion at high $NF(a^1\Delta)$ concentration, is consistent with the earlier assumption of negligible BiF(X) concentration.

5.4 Scaling of BiF(A)

The peak achievable yield of BiF(A) depends critically on the amount of $Bi(CH_3)_3$ that can be productively added to the FN_3 . This factor is controlled primarily by the associated quenching of $Bi(^2D)$ and BiF(A) by $Bi(CH_3)_3$ and its by-products. Since BiF(A) decays radiatively at a high rate, it is less subject to quenching than $Bi(^2D)$ which has a much longer kinetic lifetime. Optimum addition of $Bi(CH_3)_3$ will therefore be limited by the competition between the reaction of $Bi(^2D)$ with $NF(a)$ and its quenching by $Bi(CH_3)_3$ according to the relation

$$k_8 [NF(a^1\Delta)] = k_s [Bi(CH_3)_3]_{optimal} \quad (16)$$

where k_s is the quenching rate constant that controls scaling. Taking $k_s = 3 \times 10^{-10} \text{ cm}^3/\text{s}$ based on Trainor's work¹⁹ yields $3 \times 10^{15}/\text{cm}^3$ as the optimum $Bi(CH_3)_3$ concentration for $[NF(a^1\Delta)] \sim 3 \times 10^{16}/\text{cm}^3$. Higher concentrations of $Bi(CH_3)_3$ will promote quenching at a rate that is competitive with the pumping reaction and therefore will not increase the yield of BiF(A) significantly. Consequently, the peak yield of BiF(A) is expected to be $3 \times 10^{15}/\text{cm}^3$ multiplied by 0.2 to account for the dissociation fraction, 0.05 to account for the yield of active Bi/BiF and 0.66 to account for the fraction of active Bi/BiF in the BiF(A) state. In practice, this steady-state estimate must be discounted by an additional factor of 2, since under optimal $Bi(CH_3)_3$ loading the time duration (FWHM) of the BiF(A) pulse is comparable to the radiative lifetime. The net result is an expected BiF(A) yield of $10^{13}/\text{cm}^3$, which was indeed observed as shown in Fig. 9 where the rollover with initial $Bi(CH_3)_3$ concentration occurs at the predicted $3 \times 10^{15}/\text{cm}^3$ concentration.

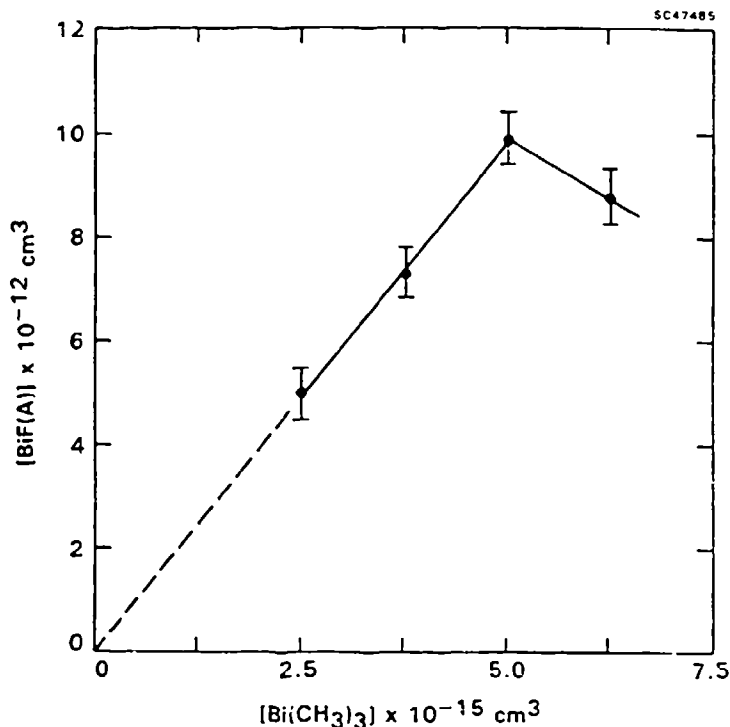


Fig. 9 Scaling of BiF(A) yield vs addition of Bi(CH₃)₃.

The scaling of the BiF(A) yield was also investigated at fixed Bi(CH₃)₃ concentration with respect to varied initial FN₃ concentration as shown in Fig. 10. Here the scaling is apparently nonlinear in [NF(a¹Δ)] at low concentrations because quenching dominates the decay rate of the Bi(²D) intermediate. In this limit, [Bi(²D)] scales proportional to [NF(a¹Δ)] since the metastable species drives its production, and [BiF(A)] produced via the reaction of Bi(²D) with NF(a¹Δ) then scales as [NF(a¹Δ)]². As the NF(a¹Δ) concentration is increased, the pumping reaction (8) begins to compete with the quenching of the Bi(²D). The Bi(²D) concentration then saturates and the BiF(A) state begins to scale linearly with [NF(a¹Δ)]. At high NF(a¹Δ) concentrations, a saturation of the BiF(A) yield could set in if a destructive reaction between NF(a¹Δ) and BiF(A) were to occur with a sufficiently high rate constant to compete with the radiative decay of the BiF(A) state. No evidence of such reaction was obtained, however, up to NF(a¹Δ) concentrations of 3 × 10¹⁶/cm³.

Under optimal Bi(CH₃)₃ loading conditions, the BiF(A) time profile is shorter than the NF(a¹Δ) time profile in the absence of Bi(CH₃)₃ by roughly a factor of two, as shown in Fig. 11. This result indicates that Bi(CH₃)₃ quenching of NF(a¹Δ) is also a significant factor. The NF(a¹Δ) data has been smoothed to eliminate peak-to-peak noise as indicated by the error bar. The BiF(A-X) emission is quite intense and therefore noise free. The vertical scale for the BiF emission is substantially reduced in sensitivity relative to the NF data.

The typical per BiF(A, v' = 0) stimulated emission cross sections for the most favored transitions are approximately 10⁻¹⁶ cm² at 1200 K. At this temperature, roughly 35 % of the BiF(A) state concentration is in v' = 0; however, this figure increases with reduced temperature as does the cross section due to the combined effects on the rotational distribution and Doppler width. Therefore, with careful optimization, 10¹³/cm³ concentrations of BiF(A) are capable of generating unsaturated gain coefficients that approach 10⁻³/cm, adequate for large scale high energy laser devices, provided the concentration of BiF(X) is not excessive.

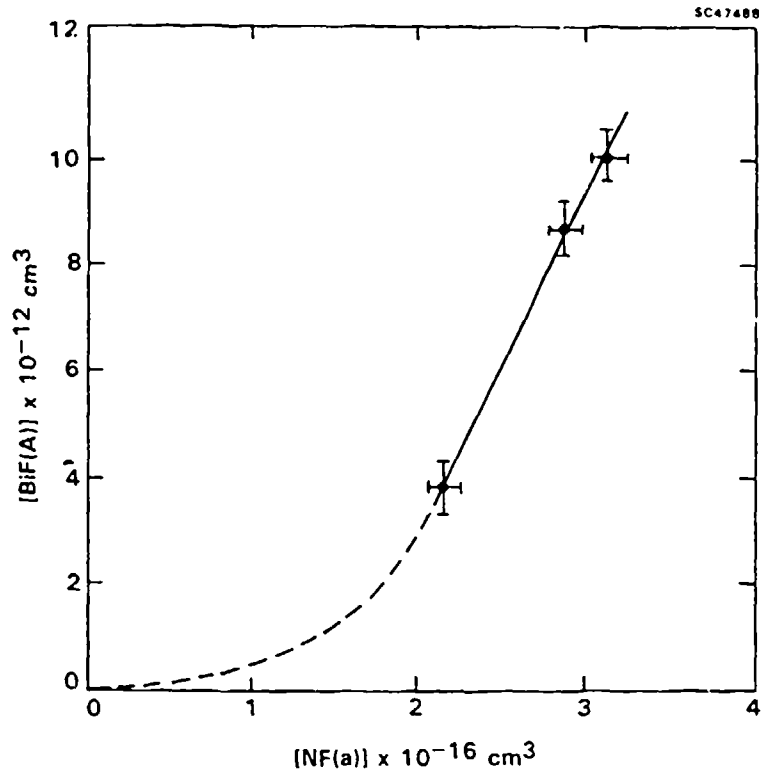


Fig. 10 Scaling of BiF(A) yield vs initial FN_3 concentration.

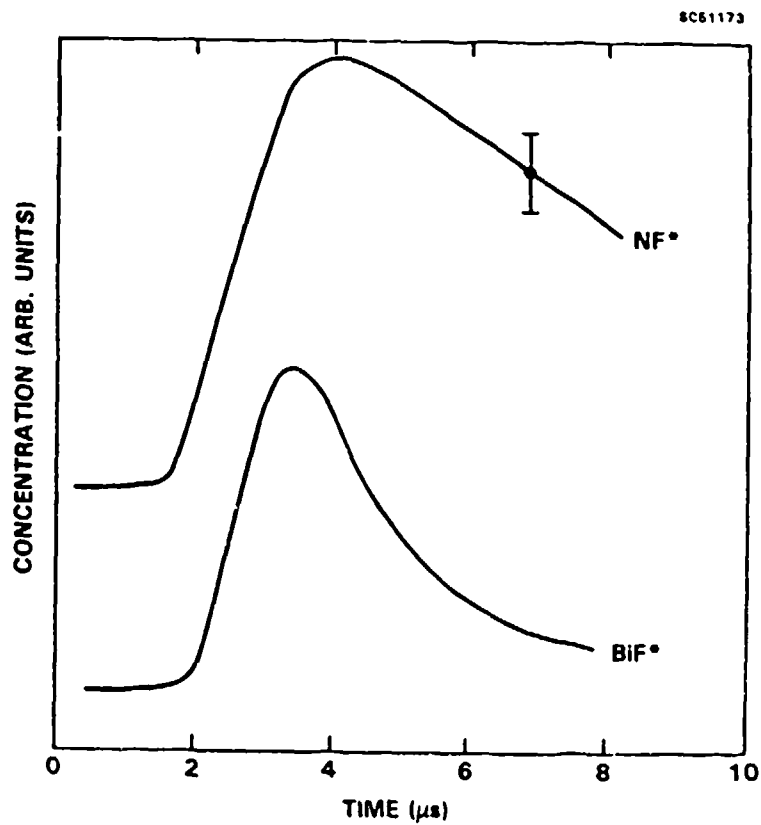


Fig. 11 Time profiles of $\text{NF}(a^1\Delta)$ in the absence of $\text{Bi}(\text{CH}_3)_3$ - upper curve and $\text{BiF}(A)$ with optimal loading of $\text{Bi}(\text{CH}_3)_3$ - lower curve.

5.5 Population Inversion

To test for excess population of the BiF(X) ground state, the reactor used in the above studies was enclosed inside an optical cavity formed by a pair of concave dielectric mirrors. The mirrors were sealed to the reactor without use of intracavity windows by long, purged stainless steel bellows so that the optical axis of the resonator passed through 2.5 cm of the reacting flow. The mirror separation was set at 50 cm so that the $c/2L$ spacing of the cavity modes was approximately 25 % of the Doppler width of the BiF(A-X) transitions to insure that a cavity mode was located near line center where the cross section is at a maximum. Mirrors were selected with constant $R = 95$ % reflectivity over the wavelength band of the BiF(A-X) transitions so that on the average, a photon would execute $1/(1-R^2) \sim 10$ roundtrips inside the cavity before escaping to an external detector. The effective path length through the active medium was therefore 50 cm. The OMA was used to collect on-axis radiation leaking from the cavity and to compare the spectrum of the cavity emissions to a direct chemiluminescence spectrum obtained without use of an optical cavity. The intensifier section of the OMA was gated to detect only the peak of the BiF(A) time profile in each case. The region of the $v' = 0$ to $v'' = 0$ transitions was then analyzed for signs of spectroscopic distortion due either to intracavity self-amplification or self-absorption. Band-to-band comparisons were not used because slight departures from vibrational equilibrium, which are possible due to the short duration of the experiment, would lead to erroneous results. Distortion of the shape of a single band, however, depends on the rotational distribution which is more rapidly thermalized. In the $v' = 0$ to $v'' = 0$ band, the cross section is peaked to the red of the bandhead at $J = 30$ (437 nm). Therefore, the presence of gain or loss in the cavity will distort the shape of the band as seen through the mirrors. Contrary to first intuition, the presence of gain initially increases the width of the band by enhancing the $J = 30$ radiation relative to the bandhead.

Within the signal-to-noise ratio of the experiment, which was 20 to 1 or better, no significant distortion of the band shape was observable, as shown in Figs. 12(a) and 12(b). An upper limit on the BiF(X) concentration was therefore established by assuming a trial value for [BiF(X)] and then calculating the absorption of $J = 30$ and bandhead radiation over a 50 cm path, assuming [BiF(A)] = $10^{13}/\text{cm}^3$ and rotational-vibrational equilibrium at 1200 K. The cross sections were calculated from knowledge of the radiative rate³ and the spectroscopic parameters²⁰ of the BiF(A-X) band system. The trial concentration of BiF(X) was then adjusted so that the differential absorption matched twice the signal-to-noise ratio of the experiment. By following this procedure, the concentration of BiF(X) was shown to be less than $4 \times 10^{13}/\text{cm}^3$. This result does not rule out an absolute inversion, but tends to suggest at least partial inversions on the $v' = 0$ to $v'' \geq 3$ transitions, assuming a near thermal vibrational distribution in the BiF(X) ground state.

More sensitive experiments have been conducted with mirrors of 99.9 % reflectivity in which the potential peak gains can actually exceed the cavity threshold. Saturated lasing is not expected in this case, however, because the peak gain lasts for only about 2 μs (Fig. 11) during which the photons can execute approximately 600 roundtrips. At a peak gain per roundtrip of $(3 \times 10^{-4}/\text{cm})(5 \text{ cm}) \sim 0.15$ %, neglecting mirror losses, the initial spontaneous emission can only experience a net enhancement of order unity. Therefore, no significant laser output is expected, but spectroscopic distortion of the cavity output due to optical gain can be substantial. In these final experiments, the production of BiF(A) was also enhanced by using a KrF laser to partially photodissociate the $\text{Bi}(\text{CH}_3)_3$ with a variable lead in time relative to the peak of the NF(a) time profile. The best results were obtained when the KrF laser pulse was applied approximately 1 μs ahead of the peak NF(a) signal, resulting in a 50% enhancement of the peak BiF(A) concentration. The BiF(A) signal disappeared entirely, however, when the KrF laser was applied with the CO_2 laser beam blocked, confirming that NF(a) production by thermal dissociation of FN_3 was necessary to excitation of the metal fluoride. This result is not surprising since

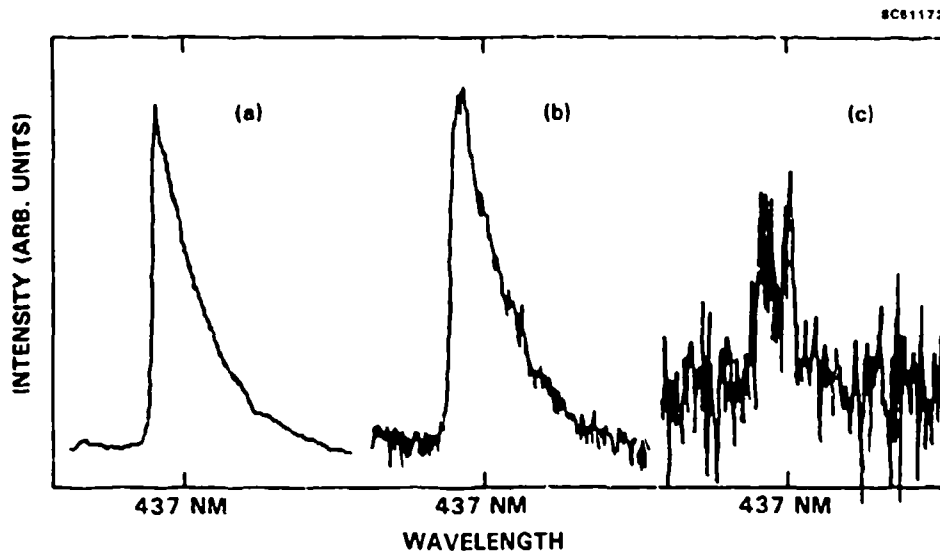


Fig. 12 Comparison of BiF(A-X, $v' = 0$ to $v'' = 0$) bands in the absence of a cavity (a) and with a cavity using mirrors of 99.5 % reflectivity (b) and 99.9 % reflectivity (c).

the KrF radiation is strongly absorbed^{8,9} by $\text{Bi}(\text{CH}_3)_3$, but only very weakly by FN_3 . Time profiles of $\text{Bi}(^2\text{D})$ collected with and without use of the KrF and CO_2 lasers revealed that the KrF laser did yield a prompt source of $\text{Bi}(^2\text{D})$ that was comparable to the $\text{Bi}(^2\text{D})$ produced by reaction (9), which accounts for the enhanced BiF(A) production. The KrF laser, however, does not help to clear the BiF(X) ground state and since the photon lifetime in the high reflectance cavity is comparable to the radiative lifetime of BiF(A), the intracavity experiment constitutes a valid test for chemical removal of the BiF(X) ground state. The corresponding cavity emission data, shown in Fig. 12(c), is characterized by a lower signal-to-noise ratio because of the reduced transmission through the high reflectance mirrors. Nonetheless, a significant distortion of the $v' = 0$ to $v'' = 0$ band at 437 nm is evident, which is presumably the result of amplification, since it is a reproducible feature of the cavity emission spectrum and is not present in background scans taken with the CO_2 laser blocked. This result implies an absolute inversion of the BiF(A-X) transition. Work is currently proceeding to use a pulsed dye laser to charge the optical cavity with resonant photons so that amplification during the cavity ring down can be sensitively detected with a high signal-to-noise ratio. Details of this experiment will be reported in a subsequent publication.

6. CONCLUSIONS

The results we have obtained using the FN_3 source of $\text{NF}(a^1\Delta)$ to excite BiF(A) with $\text{Bi}(\text{CH}_3)_3$ as a starting material are basically compatible with Herbelin's findings in the same system driven by $\text{NF}(a^1\Delta)$ obtained from the $\text{H} + \text{NF}_2$ reaction, and support the conclusion that energy transfer from $\text{NF}(a^1\Delta)$ to BiF is a viable mechanism for the generation of a visible wavelength chemical laser. Further work will be required to develop the laser, however, in three key areas. Since the potential gains are small, larger gain lengths and gain times will be required for efficient power extraction. In a high energy system, it will also be desirable to replace the CO_2 laser heating mechanism with supersonic mixing between a preheated primary gas stream and secondary injection of FN_3 at 300 K. The nozzle design will be critical in several regards. First, due to the self-annihilation reaction, it will be necessary to accomplish mixing on the μs time scale to dissociate the FN_3 efficiently; second, careful optimization of temperature is required to tradeoff dissociation rate with gain cross section; and third, adiabatic expansion and the use of an inert diluent gas as a thermal buffer will have a strong

influence on the coupling between Mach number as influenced by reactive heat release and dissociation rate as influenced by changes in gas temperature due to pressure recovery. Finally, it will be desirable to replace the $\text{Bi}(\text{CH}_3)_3$ with superheated Bi vapor that consists primarily of Bi-atoms, to eliminate the kinetic bottleneck and by-product quenching reactions that are associated with use of the organometallic Bi donor.

7. ACKNOWLEDGEMENTS

This work was partially supported under a contract from the Air Force Weapons Laboratory and the Air Force Astronautics Laboratory.

8. REFERENCES

1. J.M. Herbelin and R.A. Klingberg, "Efficient Production of Electronically Excited $\text{BiF}(A)$ via Collisions with $\text{NF}(a^1\Delta)$," *International Journal of Chemical Kinetics*, vol. 16, pp. 849-866, 1984.
2. D.J. Benard, B.K. Winker, T.A. Seder and R.H. Cohn, "Production of $\text{NF}(a^1\Delta)$ by Dissociation of Fluorine Azide," *Journal of Physical Chemistry*, vol. 93, pp. 4790-4796, 1989.
3. R.H. Heidner, H. Helvajian, J.S. Holloway, and J.B. Koffend, "BiF(A) Radiative Lifetimes and Rate Coefficients for V-T Transfer and Electronic Quenching," Technical Report 87-19, Aerospace Corporation, El Segundo, CA, 1987.
4. C.R. Quick and C. Wittig, "Time-Resolved HF Vibrational Fluorescence from the IR Photodissociation of SF_6/H_2 Mixtures," *Chemical Physics Letters*, Vol. 48, pp. 420-424, 1977.
5. B. Rosen, *Selected Constants Relative to Diatomic Spectra*, Pergamon Press, New York, 1970.
6. R.J. Malins and D.W. Setser, "Rate Constants, Branching Ratios and Energy Disposal for $\text{NF}(b,a,X)$ and $\text{HF}(v)$ Formation from the $\text{H} + \text{NF}_2$ Reaction," *Journal of Physical Chemistry*, vol. 85, pp. 1342-1349, 1981.
7. P.H. Tennyson, A. Fontijn and M.A.A. Clyne, "Radiative Lifetimes of Metastable States of Free Radicals. I. $\text{NF}(b^1\Sigma)$," *Chemical Physics*, vol. 62, pp. 171-177, 1981.
8. K. Gholivand, G. Schatte and H. Willner, "Properties of Triazadienyl Fluoride, N_3F ," *Inorganic Chemistry*, vol. 26, pp. 2137-2140, 1987.
9. J. Connor, P.J. Young and O.P. Strausz, "Flash Photolysis of Trimethylanitmony and Trimethylbismuth and the Quenching of Excited Antimony and Bismuth Atoms," *Journal of the American Chemical Society*, vol. 93, pp. 882-828, 1971.
10. M. Stanek, K. Musiol and S. Labuz, "Experimental Determination of Transition Probabilities in Bi I and Bi II," *Acta Physics Polonica*, vol. A59, pp. 239-245, 1981.
11. J.M. Herbelin and B. Koffend, Aerospace Corporation, El Segundo, CA, private communication.
12. Alfa Catalog, "Research Chemicals and Materials," pg. P-168, Morton Thiokol, Danvers, MA, 1986/87.
13. D.J. Benard and R.H. Cohn, "Model Studies of CBES Decomposition," Technical Report 87-071, Air Force Astronautics Laboratory, Edwards Air Force Base, CA, 1987.
14. J.F. Haller, "A Study of the Preparation, Structure, Properties, and Decomposition of Azine Fluoride and of Difluorodiazene," Ph.D. thesis, Cornell University, Ithaca, NY, 1942.
15. E. Quinones, J. Habjas and D.W. Setser, "Gas-Phase Chemistry of $\text{NF}(a^1\Delta)$: Quenching Rate Constants," *Journal of Physical Chemistry*, vol. 91, pp. 5155-5158, 1987.
16. H. Michels, United Technologies Research Laboratories, E. Hartford, CT, private communication.
17. D. Patel, A.T. Pritt, and D.J. Benard, "Photolysis of FN_3 at 193 nm," *Journal of Physical Chemistry*, vol. 90, pp. 1931-1934, 1986.

18. G.A. Sutton, D.G. Capelle and J.I. Steinfeld, "Near-Resonant Electronic Energy Transfer from $\text{NF}(a^1\Delta)$ to Bi," *Journal of Chemical Physics*, vol. 69, pp. 5140-5146, 1978.
19. D.W. Trainor, "Collisional Relaxation of Electronically Excited Bismuth: $6p^3(^2D^{\circ}_{3/2})$ and $6p^3(^2D^{\circ}_{5/2})$," *Journal of Chemical Physics*, vol. 66, pp. 3094-3099, 1977.
20. W.E. Jones and T.D. McLean, "The Electronic Spectrum of Bismuth Monofluoride: A Reinvestigation of the A-X System," *Journal of Molecular Spectroscopy*, vol. 90, pp. 481-506, 1981.

Chemical generation of optical gain at 471 nm

D. J. Benard and B. K. Winker

Rockwell International Science Center, Thousand Oaks, California 91360

(Received 26 October 1990; accepted for publication 21 November 1990)

Stimulated emission on the $P(43)$ and $R(70)$ transitions of the $\text{BiF}(A-X, v' = 1 \text{ to } v'' = 4)$ band was demonstrated, using the reaction of premixed FN_3 and $\text{Bi}(\text{CH}_3)_3$. The transient chemistry was thermally initiated by a pulsed CO_2 laser, using SF_6 as a sensitizer, while amplification was detected using an étalon-tuned pulsed dye laser probe and a sensitive cavity ringdown technique. The magnitude of the peak gain, estimated at $3.6 \times 10^{-4}/\text{cm}$, was consistent with a negligible concentration of the terminal $\text{BiF}(X, v'' = 4)$ state, based on the calculated optical cross section and the peak concentration of the $\text{BiF}(A, v' = 1)$ state, as measured by absolute photometry.

I. INTRODUCTION

The development of the $\text{O}_2(a^1\Delta)-I^*$ energy transfer laser,¹ which operates at 1315 nm in the near infrared, demonstrates that electronic transitions can be efficiently pumped by chemical reaction. Despite a decade of intense effort, no new chemical lasers have appeared at shorter wavelength; however, recently considerable progress has been made on the chemical generation of metastable species that are higher-energy analogs of $\text{O}_2(a^1\Delta)$. In prior reports^{2,3} we have demonstrated that gaseous FN_3 can be safely generated in the laboratory and that very large concentrations of metastable $\text{NF}(a^1\Delta)$ can be obtained by rapid (pulsed CO_2 laser-initiated) pyrolysis of $\text{FN}_3/\text{SF}_6/\text{He}$ gas mixtures. In this system, the SF_6 absorbs the infrared laser radiation and then heats the He bath gas upon rapid thermalization.⁴ The sudden increase in gas temperature then triggers efficient dissociation of the FN_3 molecules into $\text{NF}(a^1\Delta)$ and N_2 on the μs time scale. In a subsequent report,⁵ we also demonstrated (following the work of Herbelin⁶) that intense blue $\text{BiF}(A-X)$ chemiluminescence was obtained upon generating $\text{NF}(a)$ by dissociation of FN_3 in the presence of $\text{Bi}(\text{CH}_3)_3$. Consequently we have focused our efforts on the $\text{FN}_3/\text{Bi}(\text{CH}_3)_3$ reaction system as a potential gain generator for a visible wavelength chemical laser.

II. EXPERIMENT

A. Chemical pumping

The best results [in terms of $\text{BiF}(A)$ production] were obtained using approximately 2–3 Torr of FN_3 , 15 Torr of SF_6 , 30–50 mTorr of $\text{Bi}(\text{CH}_3)_3$, and balance He to a total pressure of 150 Torr, with an excitation fluence of approximately $300 \text{ mJ}/\text{cm}^2$. The active region of our reactor was approximately a rectangular parallelepiped of dimensions $0.3 \times 0.3 \times 2.5 \text{ cm}^3$. The CO_2 laser was pulsed at a 2 Hz repetition rate and the incident $10.6 \mu\text{m}$ radiation was transmitted normal to the long axis of the reaction zone, while the reagent gases were allowed to flow through the reactor at a nominal velocity of 20 cm/s. The direction of gas flow in the reactor was normal to both the long axis of the reaction zone and the direction of propagation of the CO_2 laser beam. The active flow was also enclosed by a velocity-matched Kr

shield flow, while the cylindrically focused CO_2 laser beam entered and exited the stainless-steel reactor through NaCl windows at normal incidence. Since the FN_3 and $\text{Bi}(\text{CH}_3)_3$ were subject to slow prereaction on the 100–500 ms time scale, these reagents were separately ducted to the reaction zone where mixing occurred in approximately 5–10 ms prior to initiation by the CO_2 laser. In the absence of $\text{Bi}(\text{CH}_3)_3$, the $\text{NF}(a)$ time profile consisted of a smooth rise to a peak concentration of $3 \times 10^{16}/\text{cm}^3$ in approximately 2 μs followed by a decay to half its peak concentration in about 5–10 μs . Addition of optimal $\text{Bi}(\text{CH}_3)_3$ produced a $\text{BiF}(A)$ time profile which rose to a peak concentration of $3.5 \times 10^{13}/\text{cm}^3$ with a nominal 1 μs rise time and a 2–3 μs (FWHM) pulse duration. Both the $\text{NF}(a)$ and $\text{BiF}(A)$ concentrations were determined by absolute photometry from the measured intensities and the known radiative rates^{7,8} of the transitions^{6,7} at 874 and 437 nm, respectively. The intensity data was collected using interference filters, a calibrated Si photodiode, and a transient digitizer or oscilloscope. These measurements are fully described in prior publications, which also detail the generation and measurement of the initial reagent species.^{3,5} The gas temperature at the time of peak $\text{BiF}(A-X)$ chemiluminescence was also estimated, with knowledge of the relevant Franck-Condon factors,⁹ as $1800 \pm 200 \text{ K}$ by analysis of the emission spectrum¹ that was captured by a gated optical multichannel analyzer (OMA).

B. Gain generation

Inversion of the 1.4- μs $\text{BiF}(A-X)$ transition was expected in the $\text{FN}_3/\text{Bi}(\text{CH}_3)_3$ reaction system because (under selected conditions) we were able to observe the emission of several photons per organometallic donor molecule in the active volume of our reactor. This result suggests that $\text{BiF}(X)$ is repumped to the $\text{BiF}(A)$ state by $\text{NF}(a)$ following the emission of an $A-X$ photon. Therefore, at sufficiently high $\text{NF}(a)$ concentration the cycling reactions would compete with the spontaneous decay rate, leading to A/X concentration ratios greater than unity. Prior work has also suggested a rate coefficient for the pumping reaction⁵ of $4 \times 10^{-11} \text{ cm}^3/\text{s}$, which would be sufficient to yield a weak inversion of the $A-X$ electronic transition, for $\text{NF}(a)$ concentrations $\geq 2 \times 10^{16}/\text{cm}^3$. This condition, however, would

be adequate for the generation of a strong inversion on selected vibrational transitions from low v' to higher v'' energy levels, if thermal distributions are obtained in both electronic states. Vibrational relaxation is expected to occur on the μs time scale at the high operating pressure of our reactor⁸ and time gated spectroscopic analysis of the $\text{BiF}(A-X)$ emission has revealed a near thermal distribution of the $v' = 0-3$ energy levels in our experiment. The $v' = 1$ to $v'' = 4$ transition was selected for study because it offered the highest gain cross section on a transition with a high probability of inversion. Transitions to lower v'' energy levels or from higher v' energy levels are less likely to be inverted, while transitions from $v' = 0$ or $v' = 1$ to energy levels with $v'' > 4$ have low optical cross sections due to declining Franck-Condon factors. The $v' = 1$ to $v'' = 4$ transition was selected over the $v' = 0$ to $v'' = 3$ or $v'' = 4$ transitions, because the latter have anomalously low transition probabilities. Also, the vibrational spacing⁹ in the $\text{BiF}(A)$ state is relatively small (384 cm^{-1}) and, consequently, the $v' = 1$ and $v'' = 0$ concentrations are comparable at the peak temperatures achieved in our reactor. Finally, the degenerate $P(43)$ and $R(70)$ rotational transitions at $21\,218.906\text{ cm}^{-1}$ (in the $v' = 1$ to $v'' = 4$ band) were selected since the corresponding J levels lie near the peak of the rotational distribution at 1800 K and the accidental spectroscopic alignment of these transitions enhances the sensitivity of our measurement. In this region of the $\text{BiF}(A-X)$ spectrum, the adjacent pairs of P/R rotational lines are spaced by approximately 1.7 cm^{-1} .

C. Gain diagnostic

The measurement of optical gain or loss was accomplished by using a variant of the cavity ringdown method¹⁰ reported by O'Keefe and Deacon. In our experiment, the active volume of the reactor was located at the center of a symmetrical resonator formed by two maximum-reflectance

dielectric mirrors of 50 cm radius of curvature that were spaced 50 cm apart. The mirrors were sealed directly to the reactor by stainless-steel bellows that were purged with Ar to prevent surface contamination and eliminate any intracavity optical losses due to imperfectly transmitting windows. The axis of symmetry of the optical cavity was aligned to pass through the center of the active region of our reactor (along the long axis), perpendicular to both the CO_2 laser beam and the direction of gas flow. A pulsed dye laser probe beam was also aligned to the axis of symmetry of the optical cavity and upon exiting the cavity was directed to the OMA. As shown in Fig. 1, a coaxial HeNe laser beam was used to align the cavity mirrors to each other as well as the dye laser, reactor, and OMA.

The dye laser was similar in design to the device originally reported¹¹ by Hansch except that we used a XeCl laser rather than an N_2 laser for excitation and we replaced the grating reflector with a prism/flat reflecting mirror combination. The dye laser included an intracavity telescope and a temperature stabilized solid étalon with a free spectral range of 3.1 cm^{-1} and a finesse of 40. The energy of the XeCl laser was adjusted to yield nominal $50\text{ }\mu\text{J}$ output pulses of 5 ns duration. Coarse tuning of the rear mirror defined a lasing envelope in the vicinity of 471 nm under which as many as 20-30 modes of the étalon were observed in the output. The dye laser output was attenuated by a neutral density filter to prevent saturation of the OMA, while isolation between the dye laser and the reactor cavity was obtained using an optical delay long enough to insure that the dye laser pulse was terminated before any retroreflection could affect its spectral content. Also the separation of the mirrors in the reactor cavity was chosen for efficient interaction with the gain medium by insuring a small enough mode spacing so that a cavity resonance is always located near the peak of the selected (Doppler broadened) BiF transition. Finally, the dye laser radiation (upon exiting the reactor cavity) was condensed to a spot that was slightly larger than the entrance slit

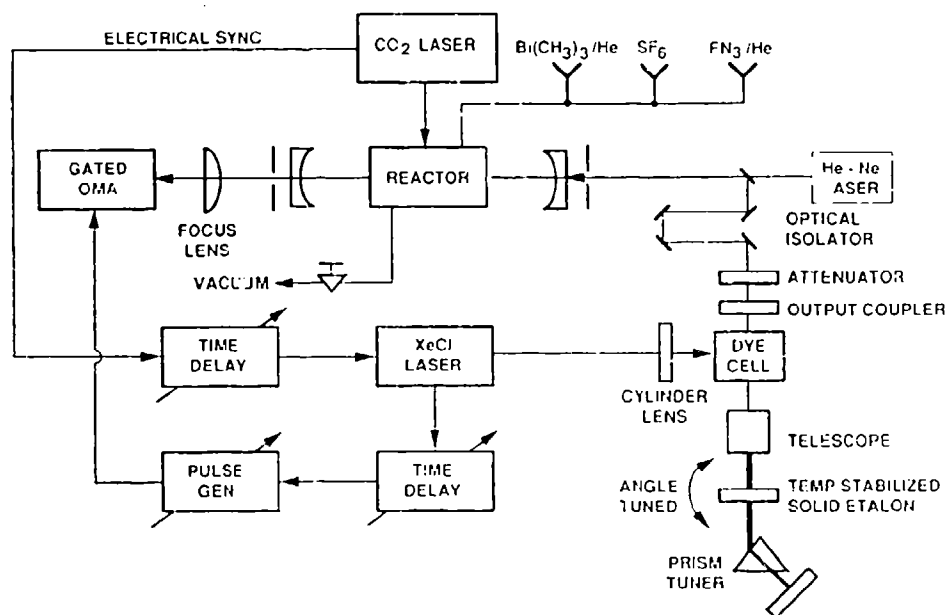


FIG. 1. Schematic diagram of the cavity ringdown experiment used to demonstrate optical gain in BiF .

of the OMA to eliminate any gas lens effects due to local heating of the reactants by the CO₂ laser.

An electronic signal derived from the CO₂ laser discharge was used to trigger a circuit which fired the XeCl laser after a variable time delay. The function of this delay was to allow time for the chemistry (initiated by the CO₂ laser) to build up a maximum inversion before the gain medium was interrogated by the dye laser. A second time delay, triggered off the XeCl laser discharge, was used to fire a pulse generator to open the gate of the OMA for a 100 ns period following a 200 ns delay. Therefore, on the average, the detected photons were inside the optical cavity for 250 ns, corresponding to 150 passages through the 2.5-cm-long gain medium. Consequently, the effective gain length was 375 cm. By using a fast Si photodiode and oscilloscope to monitor the dye laser beam that exited the cavity (with the reactor at vacuum), the exponential decay time of the optical resonator was found to be approximately 1 μs, which is consistent with the mirror spacing and the > 99.8% reflectivity quoted by the manufacturer.

By tilting the étalon, a selected laser mode was positioned near the wavelength of the target BiF transition, using the OMA and a Ne hollow cathode lamp as an absolute wavelength reference.¹² The spectroscopic resolution of the OMA was adequate to separate the modes of the étalon, but not the individual rotational lines of the BiF molecule. Since the rotational spacing of the BiF molecule and the free spectral range of the étalon do not agree, only one mode of the probe laser can be aligned to one BiF transition (that is measured) while the adjacent modes of the dye laser fall between the nearby BiF transitions. These nonaligned modes therefore provide a convenient zero gain/zero loss reference. Both the active (measuring) mode and the adjacent (reference) modes were captured simultaneously by the OMA for direct comparison.

The presence of gain or loss is detected by using the OMA to record the enhancement or diminution of the aligned mode of the dye laser in relation to its adjacent reference modes, after passage through the reactor during the period of chemical reaction. Since detector noise is negligible, the sensitivity of the experiment depends primarily on the stability of the dye laser probe. Blocking the dye laser beam (ahead of the reactor cavity) while passing the CO₂ laser into the reactor (to initiate chemistry) demonstrated that chemiluminescence was not detectable on the sensitivity scale of the OMA that was employed to monitor the probe beam. Therefore, the magnitude of the gain coefficient is inferred from the effective path length discussed above and the relative magnitude of the observed enhancement, taking into account the interaction of the probe beam with the BiF transitions. The efficiency of this interaction is roughly given by the ratio of the Doppler width of the BiF transitions to the width of the convolved laser mode and target transition. Based on Hansch's data,¹¹ and the characteristics of our étalon, we expect a probe linewidth (for a single mode) of 0.03–0.06 cm⁻¹. Since the Doppler width of the BiF transitions at the temperature of our experiment is approximately 0.05 cm⁻¹, the efficiency factor is in the range of 60%–90%.

The gain experiment was performed by first setting a

long-time delay between the CO₂ and dye laser and using an excess of Bi(CH₃)₃ in the reactor to generate a large absorption signal that could be used for final tuning of the laser without the benefit of signal averaging. Once the laser was tuned to the target transitions (in absorption), the Bi(CH₃)₃ flow was reset to optimize the gain and the time delay was adjusted so that the dye laser photons were injected into the reactor cavity in near temporal coincidence with the peak of the BiF(*A*) time profile. Data was then collected in both a signal and baseline mode. The baseline data was obtained by blocking the CO₂ laser beam to turn off the chemistry in the reactor and establish the mode to mode pattern of the unperturbed dye laser probe. With the exception of the deliberately aligned mode, infrequent (accidental) near resonances between the dye laser and nearby BiF transitions, and a strong absorption line¹² at 472.2 nm [due to the presence of Bi(³D) as an intermediate species^{5,6}] the signal/baseline intensity ratio of each individual mode was close to unity for all the étalon modes in the output of the dye laser. There was, however, an observable trend due to the presence of undissociated FN₃ (in the baseline experiment), which progressively increased the intensity of the signal modes (in relation to the corresponding baseline data) as the wavelength decreased. This effect, which did not depend on the tuning of the étalon, is due to a weak continuum absorption¹³ by FN₃ that is increasing towards a maximum at 425 nm. The resultant deviation was a weak (near-linear) function of wavelength that produced a net 10% change in the signal/baseline ratio over approximately 20 free spectral ranges. Consequently, there was negligible (< 0.5%) effect on the relative signal/baseline intensity ratios between any two adjacent modes. Since this absorption is very weak at 471 nm, and the FN₃ is largely dissociated⁵ by the time the concentration of the BiF(*A*) state peaks, the signal absorption (due to residual azide) is conservatively estimated at less than 5 × 10⁻⁵/cm.

III. RESULTS

The experimental method was initially developed by measurements conducted on overlapping *P/R* transitions in the *v'* = 0 to *v''* = 0 band (near 437 nm) at peak NF(*α*) concentrations of 6 × 10¹⁵/cm³. Under these conditions gain is not expected and was not observed; however, relatively large absorption signals were detected which facilitated testing of the apparatus. Verification experiments were employed, as detailed below, to insure that the measurements are valid and not the result of experimental artifacts. The sensitivity of the reactor cavity to weak internal absorbers was verified by using a fast silicon photodiode and oscilloscope to monitor the exponential decay of the cavity emission following pulsed dye laser excitation. In these experiments the CO₂ laser was initially blocked and a FN₃/SF₆/He gas mixture was admitted to the reactor. Using the known extinction coefficient¹³ of FN₃, a sufficient amount of the gas was added to the reactor to approximately halve the decay time. Upon observing that the decay time was indeed halved, the CO₂ laser was then unblocked (to dissociate the FN₃) and the decay time was found to return

to its original value. Upon addition of $\text{Bi}(\text{CH}_3)_3$ to the reactor, we also confirmed (by tuning the étalon) that the features being probed in absorption were narrow in comparison to a free spectral range. Further, the correct rotational spacing between adjacent pairs of BiF rotational lines was confirmed and the lines appeared (to within $\pm 0.5 \text{ cm}^{-1}$) of the predicted absolute wavelengths. We also observed that the magnitude of the absorption signals were reduced in other portions of the band where the P and R lines are well separated, and the signals were found to disappear entirely at wavelengths just below the bandhead as expected. The signals also disappeared if the dye laser was fired ahead of the CO_2 laser in time, and the absorption signals increased with increasing delay of the dye laser in relation to the CO_2 laser. No signals were obtained if $\text{Bi}(\text{CH}_3)_3$ was eliminated from the reactor, and use of larger $\text{Bi}(\text{CH}_3)_3$ concentrations increased the magnitude of the measured absorption. Consequently, we can be assured that the observed signals are due only to the presence of BiF molecules in the reactor.

The results shown in Table I were obtained on the $v' = 1$ to $v'' = 4$ transition, with a peak $\text{NF}(a)$ concentration of $3 \times 10^{16}/\text{cm}^3$ and a $\text{Bi}(\text{CH}_3)_3$ flow that was chosen to yield a peak $\text{BiF}(A-X)$ emission intensity approaching 60% of optimal. The donor concentration was reduced to prevent excessive formation of the $\text{BiF}(X)$ ground state since addition of $\text{Bi}(\text{CH}_3)_3$ eventually saturates⁵ the peak yield of $\text{BiF}(A)$. The dye laser was also fired approximately 100–200 ns ahead of the peak of the $\text{BiF}(A)$ time profile and data was collected in 128 shot averages that were typically reproducible (for any one mode) to within 1%–2% of the peak intensity registered on the OMA. The experiment was repeated eight times, each consecutive run consisting of a signal and baseline average, without significant anomalies. The data presented in Table I corresponds to the largest gain signal that was achieved (by appropriate adjustment of the CO_2 laser energy and reactor stoichiometry/pressure), and measurable gain was found on each of the eight runs in this sequence. The spectroscopic data used in Table I are from an atlas of the BiF transitions compiled by Jones⁹ and, as shown in the table, alignment of the étalon to the degenerate $P(43)$ and $R(70)$ transitions results in mistuning errors ($\Delta\lambda^{-1}$) that are typically 5–10 Doppler widths for the two adjacent modes. Correspondingly, there is little difference in the signal and baseline data for the reference modes that register at

OMA pixel numbers 490 and 510. The aligned mode at pixel number 500, however, shows a 10% enhancement over the corresponding baseline data. This result demonstrates optical amplification of the probe beam by the chemical medium with a signal-to-noise ratio greater than 5 to 1. The corresponding (two-line) gain coefficient is $3.6 \pm 1.0 \times 10^{-4}/\text{cm}$, depending primarily on the coupling efficiency. Based on an effective cross section of $8 \times 10^{-17}/\text{cm}^2$, which is derived from the known radiative rate⁸ and Franck-Condon factors⁹ by assuming rotational equilibrium, negligible hyperfine splitting, and a Honl-London factor of 0.5 (for high J values), an inversion density of $4.5 \pm 1.3 \times 10^{12}/\text{cm}^3$ is inferred for the $v' = 1$ to $v'' = 4$ transition. Since this value agrees favorably with the measured peak value of the $\text{BiF}(A, v' = 1)$ concentration, which is approximately $4.2 \pm 1.0 \times 10^{12}/\text{cm}^3$, we can infer (by comparison) that the concentration of the terminal $\text{BiF}(X, v'' = 4)$ state is negligible and that a strong ($N_u/N_l > 2$) inversion is present.

The magnitude of the gain signal was observed to roughly track the peak concentration of the $\text{BiF}(A)$ state, which increased with increasing CO_2 laser energy (temperature) over a limited range. This dependence provides additional evidence that a strong inversion is present, since a weak ($N_u \sim N_l$) inversion would be adversely affected by increasing thermal population of the terminal $v'' = 4$ state. Since the gain cross sections decrease at higher temperature, due to increased Doppler linewidth and rotational dilution, the improvement in gain is due to enhancement of the $\text{BiF}(A)$ population. Also since prior work⁷ has shown that the yield of $\text{NF}(a)$ is saturated (versus CO_2 laser energy), while the initial dissociation of $\text{Bi}(\text{CH}_3)_3$ is both thermally activated and slower than the rate of $\text{NF}(a)$ self-annihilation^{1,14} (for initial FN_3 concentrations greater than approximately 0.1 Torr), we attribute the increased $\text{BiF}(A)$ population at higher temperature to more rapid (and hence more complete) dissociation of the donor molecule, resulting in larger concentrations of active Bi species by the time of peak inversion.

IV. DISCUSSION

In the case of the $\text{O}_2(a^1\Delta)-I^*$ system, lasing was obtained within a year of the first demonstration of optical

TABLE I. Comparison of étalon/ $\text{BiF}(A-X, v' = 1 \text{ to } v'' = 4)$ wavenumbers and related signal/baseline intensities in the vicinity of 471 nm.

Pixel	Line	$h\nu$ (cm^{-1})	Étalon (cm^{-1})	$\Delta\lambda^{-1}$ (cm^{-1})	Signal (baseline)	Difference (%)
510	$R(68)$	21 222.436		+ 0.432		
	$P(41)$	21 222.270	21 222.004	+ 0.266	166 (165)	+ 0.6
	$R(69)$	21 220.691		- 1.313		
	$P(42)$	21 220.598		+ 1.692		
500	$R(70)$	21 218.906	21 218.906	0.000		
	$P(43)$	21 218.906	21 218.906	0.000	176 (160)	+ 10.0
	$P(44)$	21 217.146		- 1.760		
	$R(71)$	21 217.146		+ 1.338		
490	$P(45)$	21 215.391	21 215.308	- 0.417	178 (175)	+ 1.7
	$R(72)$	21 215.280		- 0.528		

gain.^{15,16} Based on the present result, efforts now under way to demonstrate lasing in BiF are expected to be successful. The demonstration of optical gain at 471 nm in a reacting medium also establishes the feasibility of other new chemical lasers that may operate at visible and near ultraviolet wavelengths. The low-gain coefficients, which are inherent to chemically pumped diatomic short wavelength emitters, will pose significant problems in the area of resonator design; and a number of additional challenges (specific to the NF/BiF system) will have to be addressed before such a laser can be operated efficiently. These difficulties include identification of a more efficient means to thermally initiate reaction than by use of a CO₂ laser and extraction of optical power on the μ s time scale before the excited state concentrations can decay significantly. The principal losses in the NF/BiF system include spontaneous radiation⁸ of the BiF(*A*) state, self-annihilation^{3,14} of the NF(*a*) radicals and quenching¹⁷ due to the addition of Bi(CH₃)₃. Further research to identify alternatives to BiF that can generate higher gain coefficients from lower concentrations of NF(*a*) over longer periods of time is therefore definitely warranted. Recent discoveries¹⁸ of mechanisms involving NF(*a*) and NCl(*a*) obtained from FN₃ and ClN₃, which pump interhalogens (such as IF), may be of interest in this regard, however, since these molecules have longer radiative lifetimes¹⁹ and larger cross sections than BiF. Also, the Franck-Condon factors²⁰ in these molecules help to sustain inversion by favoring transitions that terminate at higher vibrational energy levels of the ground state than in BiF. Consequently, the ability to generate a sufficient quantity of metastable species (to invert BiF) suggests that other (more efficient) chemical lasers can also be developed by exploring the appropriate transfer mechanisms to allow excitation of superior emitting species.

ACKNOWLEDGMENTS

This work was supported by the Strategic Defense Initiative Office and the U.S. Army MICOM Office through the Air Force Office of Scientific Research Contract No. F49620-90-C-0025.

- ¹D. J. Benard, W. E. McDermott, N. R. Pchelkin, and R. R. Bousek, *Appl. Phys. Lett.* **34**, 40 (1979).
- ²D. J. Benard and R. H. Cohn, Air Force Astronautics Laboratory Technical Report No. AFAL-TR-87-071 (February, 1988).
- ³D. J. Benard, B. K. Winker, T. A. Seder, and R. H. Cohn, *J. Phys. Chem.* **93**, 4790 (1989).
- ⁴M. Lenzi, E. Molinari, G. Piciacchia, V. Sessa, and M. L. Terranova, *Chem. Phys.* **142**, 473 (1990).
- ⁵B. K. Winker, D. J. Benard, and T. A. Seder, *Proc. SPIE* **1225**, 543 (1990).
- ⁶J. M. Herbelin and R. A. Klingberg, *Int. J. Chem. Kinet.* **16**, 849 (1984).
- ⁷R. J. Malins and D. W. Setser, *J. Phys. Chem.* **85**, 1342 (1981).
- ⁸R. F. Heidner, H. Helvajian, J. S. Holloway, and J. B. Koffend, *J. Chem. Phys.* **84**, 2137 (1986).
- ⁹W. E. Jones and T. D. McLean, *J. Mol. Spectrosc.* **90**, 481 (1981).
- ¹⁰A. O'Keefe and D. A. G. Deacon, *Rev. Sci. Instrum.* **59**, 2544 (1988).
- ¹¹T. W. Hansch, *Appl. Opt.* **11**, 895 (1972).
- ¹²G. R. Harrison, *MIT Wavelength Tables* (Wiley, New York, 1960); C. E. Moore, *Atomic Energy Levels* (National Bureau of Standards, Washington, DC, 1949).
- ¹³K. Gholivand, G. Schatte, and H. Willner, *Inorg. Chem.* **26**, 2137 (1986).
- ¹⁴E. Quinones, J. Habdas, and D. W. Setser, *J. Phys. Chem.* **91**, 5155 (1987).
- ¹⁵A. T. Pritt, R. D. Coombe, D. Pilipovich, R. I. Wagner, D. J. Benard, and C. Dymek, *Appl. Phys. Lett.* **31**, 745 (1977).
- ¹⁶W. E. McDermott, N. R. Pchelkin, D. J. Benard, and R. R. Bousek, *Appl. Phys. Lett.* **32**, 467 (1978).
- ¹⁷D. W. Trainor, *J. Chem. Phys.* **66**, 3094 (1977).
- ¹⁸D. J. Benard, M. A. Chowdhury, B. K. Winker, T. A. Seder, and H. H. Michels, *J. Phys. Chem.* **94**, 7507 (1990).
- ¹⁹M. A. A. Clyne and I. S. McDermid, *J. Chem. Soc. (Faraday Trans. II)* **72**, 2252 (1976).
- ²⁰W. J. Marinelli and L. G. Piper, *J. Quant. Spectrosc. Radiative Transfer* **34**, 321 (1985).

Threshold oscillation of an $\text{NF}(a^1\Delta)/\text{BiF}$ visible wavelength chemical laser

D. J. Benard

Rockwell International Science Center, Thousand Oaks, California 91358

(Received 22 February 1993; accepted for publication 7 May 1993)

A novel shock tube reactor was used to pulse heat a gaseous mixture of He, FN_3 , and $\text{Bi}(\text{CH}_3)_3$ along a 40 cm optical path between two highly reflective mirrors. Production of $\text{NF}(a^1\Delta)$ by dissociation of the azide was found to occur in a "delayed avalanche" approximately 50 μs after shock reflection, and weak lasing at 470 nm was observed that is assignable to electronic transitions in the $\text{BiF}(A-X, \Delta v=3)$ band.

I. INTRODUCTION

Since demonstration of the near-infrared (electronic transition) oxygen-iodine chemical laser¹ in the late 1970s, efforts to develop an alternative reaction system that operates at a visible wavelength have met with little success. Because efficient production of optically active species in direct reactions is forbidden by spin-selection rules, electronic transition laser concepts typically involve a "chemical generator" to produce a metastable (energy-storage) species, which, in turn, transfers its excitation to a suitable "emitter." Use of $\text{NF}(a^1\Delta)$ as the metastable in visible wavelength laser schemes is favored by the high electronic energy content (1.4 eV), low self-annihilation rate,² in comparison with higher energy (N_2) triplet metastables,³ and availability of two efficient pumping reactions [$\text{F} + \text{N}_3 \rightarrow \text{NF}(a^1\Delta) + \text{N}_2$ and $\text{F} + \text{NF}_2 \rightarrow \text{NF}(a^1\Delta) + \text{HF}$], which can be used for chemical generation.^{4,5} In the early 1980s, Herbelin⁶ discovered that addition of $\text{Bi}(\text{CH}_3)_3$ to $\text{NF}(a^1\Delta)$ yields the diatomic BiF emitter, which is rapidly pumped ($k \sim 4 \times 10^{-11} \text{ cm}^3/\text{s}$) to the radiating A state by energy transfer and energy pooling reactions. Heidner⁷ also recently determined the radiative rate of the $\text{BiF}(A-X)$ transition to be $A = 7 \times 10^5/\text{s}$. Production of a strong (absolute) inversion therefore requires $\text{NF}(a^1\Delta)$ concentrations well in excess of $A/k \sim 2 \times 10^{16}/\text{cm}^3$. In this case, optimum gain is generated on vibrational transitions with $\Delta v=0$. Partial inversions, on transitions with $\Delta v > 0$, can also be obtained at somewhat lower concentrations of $\text{NF}(a^1\Delta)$, depending on temperature, if the pressure is high enough to maintain thermalized vibrational distributions. The highest Δv transitions, however, have diminished gain cross sections due to declining Franck-Condon factors.⁸ Consequently, at temperatures from 1200–1800 K; the $\Delta v=3$ band is optimal for gain generation and requires $[\text{NF}(a^1\Delta)] \sim 3 \times 10^{16}/\text{cm}^3$ to support a strong (partial) inversion. During most of the 1980s, however, the known $\text{NF}(a^1\Delta)$ generator concepts were not easily scaled to the required metastable concentration because of inherent limitations associated with initiation by slow mixing and parasitic side reactions.

A superior chemical source of $\text{NF}(a^1\Delta)$, based on rapid thermal dissociation of FN_3 , was discovered during the late 1980s in our laboratory.^{9,10} This premixed and chemically pristine generator scheme overcame the difficulties cited above and achieved record $\text{NF}(a^1\Delta)$ concen-

trations. Subsequently, Benard and Winker¹¹ were able to demonstrate optical gain on a selected $\text{BiF}(A-X)$ transition in the 1–4 band by using a pulsed CO_2 laser to rapidly heat a mixture of He, SF_6 , FN_3 , and $\text{Bi}(\text{CH}_3)_3$ inside a subthreshold cavity that was probed by a dye laser. Unfortunately, the achievable gain coefficients were very small, because addition of $\text{Bi}(\text{CH}_3)_3$, and hence inversion density, are both limited by rapid quenching¹² due to the methyl radicals. The amplification obtained using the organometallic donor, however, was still adequate to support a lasing demonstration, and the high vapor pressure of $\text{Bi}(\text{CH}_3)_3$ represents a significant experimental convenience. The CO_2 laser heating method, on the other hand, is both highly inefficient and impractical as a means to generate a large gain length. Therefore, the present work relies on shock heating, since the gasdynamic approach is more capable of supporting a laboratory demonstration of spontaneous lasing. The experiments were performed using the tabletop scale shock tube reactor described below.

II. EXPERIMENT

A. Shock tube

The reactor was constructed of welded stainless steel plates, with an internal 50 cm \times 1.25 cm rectangular cross section and with a net length in the flow direction of 48 cm. As shown in Fig. 1, the shock tube was continuously evacuated through a line of small holes in the top plate running parallel to and 5 cm upstream of the wall at the driven end of the reactor. Surge tanks containing He, H_2 , 20% F_2 in He and 3% FN_3 in He were each slowly filled to regulated pressures from on-line storage tanks or generators. The 3 l tank containing the FN_3 was teflon lined and cooled to -15°C by an external heat exchanger. A slow flow of He was also bubbled through liquid $\text{Bi}(\text{CH}_3)_3$ at the bottom of a surge tank that was chilled to temperatures in the range of -15°C to -45°C using a variable external stream of cooled nitrogen. With the surge tanks fully charged and the shock tube evacuated, electronically controlled solenoid valves were opened for ~ 0.8 s, allowing all gases to rush into the reactor. The flow of each gas was individually controlled either by a critical flow orifice or an adjustable needle valve. The H_2 and F_2 flows were mixed (on the fly) with a variable flow of He and a small but continuous flow of O_2 inside a 3/8 in. o.d. \times 20 ft long coiled copper tube, which exhausted to a manifold in the back wall of the

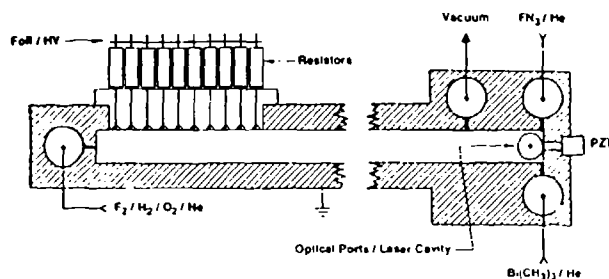


FIG. 1. Side view of the shock tube reactor.

shock tube. The mixed gases were then injected into the reactor through a series of small orifices in the back wall of the driver section. The O_2 flow was adjusted to the minimum value, which prevented spontaneous ignition of the H_2 and F_2 flows upon contact. Finally, the FN_3 and $Bi(CH_3)_3$ gas streams were each separately admitted to the shock tube through two similar manifolds, above and below the channel, adjacent to the end wall of the driven section.

The optical ports consisted of two aligned 1-cm-diam holes in the sidewalls of the reactor that were located tangent to the end wall along the midline of the channel in the driven section. These ports were purged by a slow continuous flow of He that was increased tenfold while the reactants were being admitted to the shock tube. The pressure in the reactor during the gas charging operation was measured by a capacitance manometer and an electronic peak detection circuit. The peak pressures of the individual gas components, when admitted to the shock tube one at a time, are given in Table I for a nominal condition. The total peak pressure in the shock tube when all gases were admitted simultaneously was approximately 50 Torr, prior to shock initiation.

The driver section of the shock tube extended from the back wall a distance of 16 cm and within this section the top plate of the reactor was replaced by a fiberglass panel, which mounted a hexagonally close packed array of 1392 resistively loaded pin cathodes that each discharged across the channel to ground. Each cathode pin was connected to a $330 \Omega/2 W/5\%$ carbon resistor that was potted in epoxy and connected in turn to all the other resistors via a copper foil. A 10 mac/30 KV power pack was used to charge a low-inductance 0.5 ufd energy storage capacitor through a high impedance current limiting resistor. The capacitor

TABLE I. Preignition pressures of reagents used in the shock tube reactor.

Driver	(Torr)	Laser	(Torr)
20% F_2^a	8.7	3.0% FN_3^a	22.0
H_2	4.5	0.4% $Bi(CH_3)_3^a$	17.0
O_2	0.8	He (purge, low)	0.2
He ^b	0-3.8	He (purge, high)	2.0

^aDiluted in He.

^b($M \sim 3$ to $M \sim 2$, respectively).

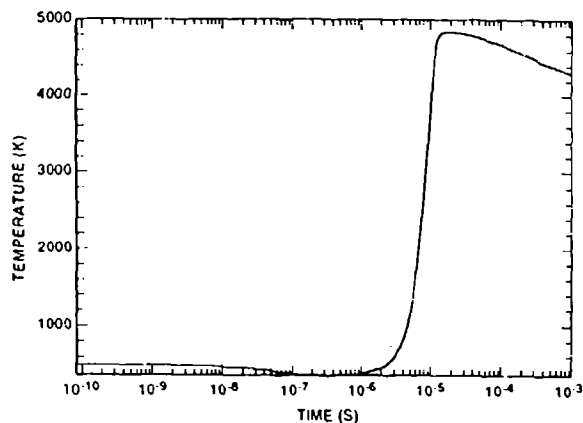


FIG. 2. Calculated time profile of the driver gas temperature.

was discharged to the copper foil through a triggered hydrogen spark gap, which was electronically fired at the end of the gas charging period. The function of the pulsed discharge in the driver section was to volume initiate the $H_2 + F_2$ chain reaction and rapidly increase the gas temperature. Figure 2 presents modeling results of the driver gas temperature versus time for a typical shock tube condition.¹³ The calculation was performed using a HF chemical laser rate package/kinetics code and the results show that peak temperatures of 4000-5000 K, depending on He diluent, are achievable in less than $10 \mu s$. No diaphragm was required to generate a shock because the driver gas could not expand effectively on this short time scale. Therefore, with density fixed by inertia, the pressure of the gas in the driver section was suddenly increased by the $H_2 + F_2$ reaction in relation to the pressure of the (cooler) gas in the driven section.

As shown in the wave diagram, Fig. 3, the resultant spatial discontinuity in pressure launches a compression shock with a Mach number ($M \sim 2.5$) toward the end wall and a diffuse rarefaction wave backward into the driver, both waves starting from the downstream edge of the discharge at time zero. For the sake of simplicity only the leading edge of the rarefaction wave is shown in this figure. The rarefaction reflects off the back wall of the driver and then begins to overtake the compression shock from behind. The compression shock moves into the driven gas,

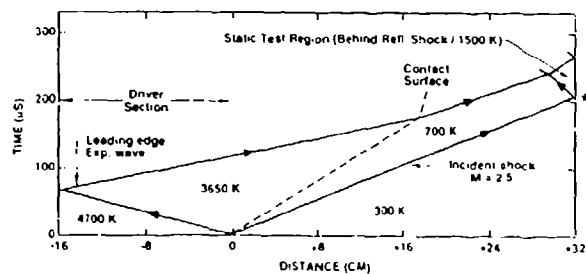


FIG. 3. Wave diagram showing propagation of disturbances in the shock tube reactor.

leaving the contact surface, which separates the driver and driven gas, following behind. The length of the shock tube was selected so that the incident compression shock arrived at the end wall of the driven section [where the FN_3 and $\text{Bi}(\text{CH}_3)_3$ were injected] ahead of the rarefaction wave. The passage of a shock compresses, heats, and accelerates the gas in the direction of shock motion. Therefore, when the incident shock reflected off the end wall (*), a region of static gas was created (adjacent to the wall) that had been heated and compressed twice, and accelerated twice in opposing directions. This condition was subsequently maintained until the rarefaction arrived, and the gas began to cool as it expanded back toward the driver. A more analytical presentation of shock tube theory by Kantrowitz¹⁴ shows that at $M=2.5$, the temperature of the reflected shock region is ~ 1500 K, while the corresponding gas density is increased by roughly a factor of 5 over its pre-shock condition. The shock tube was designed to operate in the range of $M\sim 2$ to $M\sim 3$ and achieve temperature/density conditions (behind the reflected shock) that approximated the CO_2 laser heated experiment, where optical gain was previously demonstrated. The intermediate temperatures behind the incident shock, however, were too low to promote rapid reaction of the FN_3 and $\text{Bi}(\text{CH}_3)_3$.

The arrival of the incident shock at the end wall of the reactor was sensed by five uniformly spaced, high-speed (PZT) piezoelectric transducers mounted across the shock tube. The signals from any three of the PZT monitors were used to trigger electronic threshold circuits that generated standard square pulses of differing amplitudes, which were summed and displayed on a storage scope with a delayed time base that was triggered by the capacitor discharge. The recorded "staircase" patterns were monitored to ensure that the incident shock was both flat and parallel to the back wall of the reactor. Shocks that were synchronized to $\pm 2 \mu\text{s}$ over 40 cm (in the optical direction) were obtained with care by symmetrically feeding the high voltage capacitor to both the right and left sides of the copper foil in the driver section, by controlling the flow of $\text{H}_2 + \text{F}_2$ into the right versus left side of the driver manifold, and by inserting tapered fiberglass liners along the reactor walls on either side of the shock channel. Feeding the capacitor discharge to the copper foil in the center of the channel resulted in less intense discharges on either side of the driver due to varying (electrical) inductances in the discharge current loops. Consequently the chemical "induction time" of the $\text{H}_2 + \text{F}_2$ reaction was increased on the sides of the driver relative to the center, which resulted in launching a transversely arched shock wave. Adjusting the $\text{H}_2 + \text{F}_2$ flow to favor the right or left side of the driver was effective in correcting any transverse "tilt" in the shock, and the tapered liners compensated for curvature due to viscous drag by increasing the pressure behind the incident wave in the vicinity of each sidewall. Angled liners with tapers of 7° to 15° (decreasing channel area in the direction of flow) were effective if the slope was chosen to conserve the area behind the shock, and if the taper was begun at a point on the sidewall, where a line to the center of the end wall was also at the Mach angle.

B. Chemistry

The FN_3 used in this work was generated on line in a half-liter column of 0.25 in. diam stainless steel balls by the ambient temperature reaction¹⁵ of 5% HN_3 with 10% F_2 (both in He diluent) at a total pressure of 350 Torr. The F_2 flow was controlled by an electronic mass flow meter and was set to yield a HN_3 to F_2 molar stoichiometry of 2/1. The ~ 3.5 scc/s (total) gas flow was passed through a teflon filter, and approximately 50 ft of standard $\frac{1}{4}$ in. o.d. stainless steel and teflon tubing to a 6 cm optical cell, where its transmission at 425 nm was measured to determine the FN_3 concentration using the absorbance data of Gholivand.¹⁶ The FN_3 flow then passed through a 100 μm diam critical flow orifice before entering the surge tank. When the pressure in the surge tank reached 172 Torr, the shock tube was fired automatically, and, following each shot, the tank pressure recovered slowly from approximately 95 Torr. The continuous flow of FN_3 and He into the reservoir caused the shock tube to fire at a rate of approximately one shot every five minutes. All of the other surge tanks held enough gas for three to ten shots each and were fully recharged within 1–2 min after each firing.

The HN_3 (used to form the FN_3) was generated in batch mode by reacting 30 g of powdered NaN_3 with 3 l of loosely packed stearic acid flakes¹⁷ in a vacuum-sealed, resistively heated and teflon-lined aluminum pot. With stirring by a 1 rpm paddle and heating to $\sim 225^\circ\text{F}$, the NaN_3 reacted to completion in approximately 45 min, if the reactants were initially well mixed before heat was applied. The first and last "thirds" of the HN_3 that evolved were discarded to vacuum, while the middle "third" was collected into a pre-evacuated 40 l stainless steel tank. Care was taken not to accumulate more than 100 Torr of HN_3 in this reservoir to avoid hazardous condensation. When the azide generation was complete, He was added to the HN_3 tank to a total pressure of 25 psig. The yield of HN_3 was subsequently verified by its known ultraviolet absorbance,¹⁸ and did not measurably decay after storage in the tank for several weeks. During operation of the shock tube the azide flow was controlled by an electronic pressure regulator and the HN_3 tank bled down at approximately 1 psig per hour.

Great care was exercised at all times to avoid personal exposure to any of the azides, F_2 or $\text{Bi}(\text{CH}_3)_3$, because of toxicity, and no cold traps that might condense or detonate the gaseous azides were used.

C. Optical

The diagnostics used with the shock tube included a GaAs photomultiplier tube (PMT) with selected interference filters and a wideband preamplifier to record time profiles on the storage scope and a time gated optical multichannel analyzer (OMA) for spectral analysis. These detection systems were used, with either quartz windows or maximum reflectance dielectric mirrors (450–490 nm), in place over the optical ports. One mirror was flat and the other mirror had a 100 cm concave radius of curvature. The mirrors, spaced 60 cm apart, were aligned by colli-

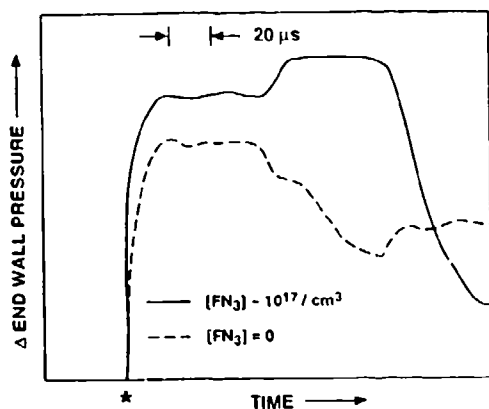


FIG. 4. Gasdynamic effect of heat release caused by dissociation of FN_3 .

mated radiation from a 476 nm Ar^+ laser, and measurements were taken of both single mirror and multimode cavity throughputs, using calibrated optical power meters and detectors, to determine the reflectance and transmission coefficients. Each mirror reflected 99.9%, in agreement with the manufacturer's specifications, and transmitted ~ 4 ppm of the incident radiation. Therefore $\sim 10^{-3}$ of the incident radiation was diffusely scattered due to surface roughness.

III. RESULTS

A. Gasdynamic

The end wall pressures sensed by the PZT monitors were significantly affected by the heat release, which accompanied dissociation of the FN_3 molecules. As shown in Fig. 4, with $M \sim 2$ and no azide present, the end wall pressure jumped suddenly upon reflection of the incident shock (*) and then held steady for $\sim 50 \mu\text{s}$ until the rarefaction arrived, after which the pressure began to decay smoothly. With nominal FN_3 present in the reactor, the prompt jump in pressure increased about 20%, showing that some of the azide was dissociated in the immediate vicinity of the shock. This reaction was not self-sustaining, however, because subsequently the pressure held constant. At about the same time when pressure began to decrease, the pressure with FN_3 present increased again, until it was more than twice the pressure that was originally maintained without azide in the reactor. The temporal coincidence between arrival of the rarefaction and the onset of secondary heat release is only accidental, however, as it is unlikely that the rarefaction triggers any new chemistry. The relative magnitudes of the pressure differences therefore demonstrate that a much larger fraction of the FN_3 is consumed by the delayed dissociation reaction than by the prompt chemistry. Also, the delayed reaction appears to be self-sustaining and the heat release a more gradual process, suggesting that chemical energy was temporarily stored in intermediate metastable states.

B. Metastables

With FN_3 present, and $\text{Bi}(\text{CH}_3)_3$ replaced by He, the faint chemiluminescence from the shock tube was rose colored, and identical time profiles were obtained at wavelengths of 590, 660, and 770 nm using the PMT detector. These wavelengths correspond to the $\Delta v = 4, 3,$ and 2 transitions, respectively, of the $\text{N}_2(B-A)$ band system,¹⁹ as subsequently confirmed by the OMA. The $\text{N}_2(B)$ chemiluminescence is most likely due to energy pooling³ between $\text{N}_2(A)$ metastables that are formed in the decomposition of two or more FN_3 molecules. The mechanism of $\text{N}_2(A)$ formation, however, is uncertain. The time profile of the $\text{N}_2(B-A)$ emission consisted of two overlapping pulses with relatively sharp leading edges that were separated by typically $50 \mu\text{s}$. The leading pulse was temporally coincident with the arrival and reflection of the incident shock, while the second or delayed pulse was coincident with the onset of the delayed FN_3 dissociation monitored by the PZT signals. Since the intensity of the delayed pulse (relative to the prompt pulse) was optimized at lower Mach numbers, all subsequent data was therefore taken at $M \sim 2$.

The 874 nm chemiluminescence was due to a combination of $\text{N}_2(B-A, \Delta v = 1)$ and $\text{NF}(a-X)$ emission.¹⁹ By comparing the 874 nm time profiles to the $\text{N}_2(B-A, \Delta v = 2-4)$ time profiles, the intensity of the second or delayed pulse (at 874 nm) was found to be enhanced relative to the shorter wavelength data. This result indicated that $\text{N}_2(A,B)$ was produced in the prompt pulse, while both $\text{N}_2(A,B)$ and $\text{NF}(a^1\Delta)$ were produced in the delayed pulse. Since the NF emission is very strongly forbidden²⁰ compared to the rates of $\text{N}_2(A)$ energy pooling³ or $\text{N}_2(B-A)$ emission,²¹ the concentration of $\text{NF}(a^1\Delta)$ in the delayed pulse was much larger than the concentration of $\text{N}_2(A,B)$ in either pulse. This result is consistent with limited dissociation of FN_3 in the prompt pulse, as well as the much slower self-annihilation rate of $\text{NF}(a^1\Delta)$ compared to metastable N_2 .

C. BiF emission

Addition of $\text{Bi}(\text{CH}_3)_3$ to the shock tube with FN_3 present yielded intense blue chemiluminescence, with both initial and delayed pulses in temporal synchronization with the N_2 and NF pulses described above. The emission spectra on either the prompt or delayed pulse consisted of $\text{BiF}(A-X)$ bands^{6,8,19} from 425 to 475 nm and an atomic line²² of Bi at 472 nm. The Bi-atom emission was enhanced relative to the molecular BiF chemiluminescence at high $\text{Bi}(\text{CH}_3)_3$ additions, and was suppressed at the lowest $\text{Bi}(\text{CH}_3)_3$ mole fraction. Moreover, as shown in Fig. 5, the yield of BiF emission on the prompt pulse declined, while the intensity of the same emission on the delayed pulse was enhanced, as an addition of $\text{Bi}(\text{CH}_3)_3$ was increased by warming the organometallic liquid reservoir. Post-shock $\text{Bi}(\text{CH}_3)_3$ concentrations in the optical region of the reactor were estimated from the known vapor pressure curve²³ of the organometallic liquid, the measured temperature and pressure of its surge tank, the data in Table I, and shock tube theory¹⁴ anchored to PZT time profiles. With

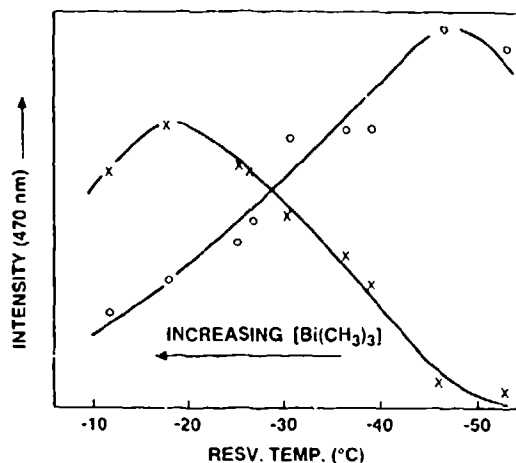


FIG. 5. Effect of donor concentration on initial (O) and delayed (X) chemiluminescence.

[FN₃] ~ 10¹⁷/cm³ behind the reflected shock, optimum emission on the delayed pulse occurred in the vicinity of [Bi(CH₃)₃] ~ 10¹⁶/cm³, assuming that none of the donor species was lost due to prior reaction or dissociation. The simplest interpretation of the chemiluminescence data, however, is that the initial pulse was due to excitation of active Bi/BiF, derived from Bi(CH₃)₃, by a relatively small concentration of N₂(A), while the delayed pulse was due to a much larger concentration of NF(a¹Δ) acting on a significantly attenuated concentration of Bi/BiF, due to intervening reactions that consumed the active emitters between the prompt and delayed pulses. In this case, increasing the donor concentration in effect "swamps" the N₂(A) during the initial pulse, while the delayed pulse is "starved" for active emitters, consistent with the observed trends in the data.

D. Cavity emission

Figures 6 and 7 compare the emission spectra and time profiles (at 470 nm) from shock excitation of FN₃ and Bi(CH₃)₃, both with and without an optical cavity installed, under the conditions that generated optimum delayed BiF(A-X) chemiluminescence. As can be seen, only the delayed pulse escapes from the optical cavity. This result was anticipated on the basis of the preceding analysis, since a small concentration of N₂(A) acting on a large concentration of Bi(CH₃)₃ is unlikely to sustain a population inversion. Therefore, photons generated in the prompt pulse (*) were reabsorbed inside the optical cavity before escaping through the maximum reflectance dielectric mirrors. On the other hand, the delayed pulse, which is due to a much larger concentration of NF(a¹Δ) acting on a lean concentration of emitters, was able to sustain a population inversion. Since in this case stimulated emission occurs faster than absorption, the generated radiation continues to bounce back and forth inside the optical cavity (while increasing in intensity) until escaping at the mirrors, either by transmission or surface scattering. Based on the mea-

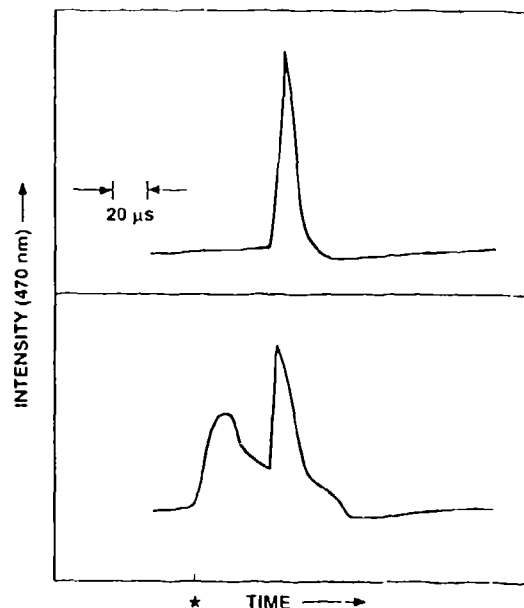


FIG. 6. Time profiles of chemiluminescence (lower) and cavity emission (upper).

sured mirror transmission and cavity output, the peak intracavity power (at 470 nm) was approximately 180 mW on the delayed pulse. The total stimulated emission power (due to both mirror transmission and scatter) was therefore approximately a third of a milliwatt.

The emission spectra with and without an optical cavity were recorded at different resolutions, as can be seen by comparing the Bi-atom lineshape in Fig. 7 to the Hg-atom

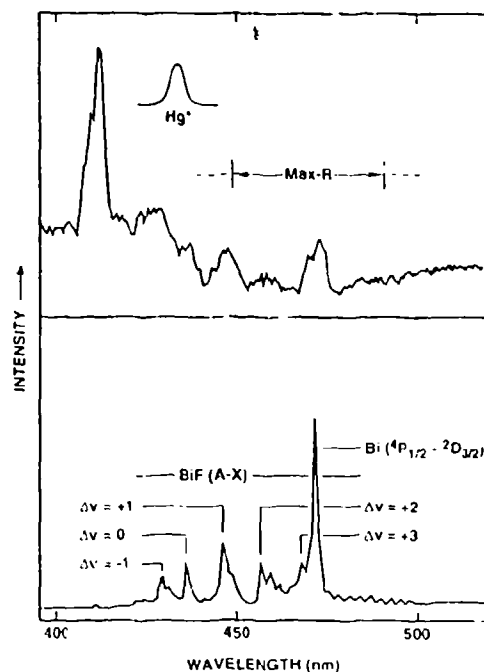


FIG. 7. Spectra of chemiluminescence (lower) and cavity emission (upper).

emission lineshape that was obtained from a discharge lamp in place of the cavity emission. Within the reflectance band of the mirrors, all the BiF($A-X$) bands in the cavity output were suppressed, except the $\Delta v=3$ band. The vibrational transitions within this band, including $0 \rightarrow 3$, $1 \rightarrow 4$, and $2 \rightarrow 5$, are not resolved. The $0 \rightarrow 3$ subband, however, has a small Franck-Condon⁸ factor and, therefore, a low gain cross section. The $1 \rightarrow 4$ subband, on the other hand, has a larger gain cross section as well as larger inversion density than any of the higher subbands in the $\Delta v=3$ sequence, if the vibrational distributions are thermal. Therefore the cavity output is most likely derived from the BiF($A-X, 1-4$) transition, which, coincidentally, is the band that demonstrated optical amplification in prior gain measurements.¹¹ The absence of any significant emission from the $\Delta v=2$ or $\Delta v=4$ bands in the cavity output suggests that lasing has indeed commenced; however, the apparent structure of the 470 nm cavity output (compared to the Hg-atom lineshape) suggests that lasing may not be restricted to a single wavelength. Therefore stimulated emission may also be occurring on other $\Delta v=3$ subbands, particularly if the vibrational distributions in the BiF(A) state are nonthermal. Lasing apparently does not occur on transitions of the BiF($A-X$) band system if $\Delta v < 3$, because the inversion relies on a Boltzmann factor (associated with the ground state vibrational distribution) that favors higher values of Δv . Lasing is also not seen for $\Delta v > 3$, because, as Δv increases, the Franck-Condon factors for transitions out of $v'=0$ decrease. Therefore, either the inversion densities or the cross sections are diminished and, as a result, there is too little optical gain to overcome the cavity loss at the mirrors.

IV. DISCUSSION

A. Threshold oscillation

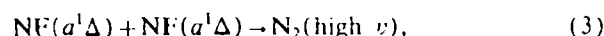
In a pulsed low-gain laser the output may typically be controlled by the kinetics of cavity buildup from initial spontaneous chemiluminescence to the (10^4 – 10^5 W/cm²) saturation intensity²⁴ that causes stimulated emission at rates comparable to the spontaneous decay. Typically, this buildup spans eight to nine orders of magnitude in intensity. If the mirrors are lossless and the gain (γ) is constant from mirror to mirror, as well as across the cavity aperture, intracavity intensity initially grows as $\exp(\gamma ct)$, where c is the speed of light and t is time. The exponential trend, of course, is modified as the laser begins to approach saturation. Based on the prior gain measurement, $\gamma \sim 3 \times 10^{-4}$ /cm is generated¹¹ by the reaction of FN₃ with Bi(CH₃)₃. This figure, however, must be discounted in the present experiment for mirror losses as well as nonconstant gain in both the optical and flow directions. The actual working gain length in the reactor is ~ 40 cm rather than 50 cm because of the tapered walls used to correct shock curvature. Consequently, gain only exists over two-thirds of the distance from mirror to mirror. In the flow direction, a delayed reaction wave follows $\sim 50 \mu\text{s}$ behind the reflected shock at a velocity of ~ 0.8 mm/ μs and based on prior time resolved chemiluminescence studies,²⁵ the width

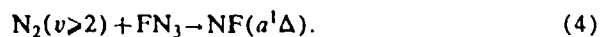
of the reaction (or gain) zone is $\sim 2 \mu\text{s}$. The transit time (t) of the reaction wave across the 1 cm aperture is therefore approximately 12.5 μs and the gain zone only fills 16% of the working region of the optical cavity. Finally, subtracting the distributed 0.1% loss at each mirror (over 60 cm) yields $\bar{\gamma} \sim 1.5 \times 10^{-5}$ /cm for the average gain over threshold and $\exp(\bar{\gamma} ct) \sim 850$ for the expected cavity buildup ratio. These results are relatively insensitive to shock curvature, if the deviations from flatness are small compared to the transit time of the reaction wave through the cavity, because the spatially averaged gain is not significantly affected in this case. Since the estimated buildup ratio is much less than 10^8 , the laser cannot achieve saturation or extract power efficiently. Increasing the value of $\bar{\gamma}$ by roughly a factor of 3 to 4, however, would allow much larger saturated outputs to be obtained.

The amount of light initially in the cavity at the start of the buildup process can be estimated from a number of factors, including prior chemiluminescence data,²⁵ which gives [BiF(A)] $\sim 5 \times 10^{13}$ cm³, active volume ~ 5 cm³, photon energy = 4.2×10^{-19} Watt s, BiF(A) radiative rate = 7×10^5 /s, Franck-Condon factor⁸ for the $1 \rightarrow 4$ transition = 0.149, fraction of BiF(A) in the $v'=1$ energy level $\sim 24\%$ for a thermal distribution at 1200 K with 384 cm⁻¹ vibrational spacing,⁸ fraction of the rotational lines in the "center" of the Maxwell-Boltzmann distribution $\sim \frac{1}{2}$, probability of emission into a cavity mode $\sim 2 \times 10^{-7}$ (based on resonator theory²⁶), and cavity $Q \sim 500$. Multiplying these factors yields approximately 0.13 mW, which is the intracavity power that can be supported on lasable transitions in steady state by the peak concentration of BiF(A), if there is neither gain nor loss in the medium. Use of a steady-state estimate for the initial light in the cavity is valid because the $\sim 2 \mu\text{s}$ photon lifetime of the empty resonator is small compared to the time over which the cavity builds up due to the presence of gain. Multiplying the estimated initial intensity by the estimated cavity buildup ratio yields an anticipated intracavity power of ~ 110 mW, which compares favorably with the observed value of 180 mW. While these results are only approximate, the analysis shows that the observed cavity output is of an appropriate magnitude for unsaturated lasing or threshold oscillation.

B. Delayed avalanche

Another interesting aspect of the shock tube chemistry is the delayed appearance of NF($a^1\Delta$), which has also been observed in prior experiments,¹⁰ where FN₃ was dissociated by contact with vibrationally excited HF molecules. Since the BiF(A) state also tracked the NF($a^1\Delta$) concentration in previous studies,²⁵ the data in Fig. 6 suggests that delayed appearance of the metastables has a sharp leading edge characteristic of an avalanche. A hypothetical mechanism that might account for this phenomenon is based on the following four chemical reactions:





Here Δ is used to represent heat, Q is a generalized quencher, and only the active products are shown in each case. The "delay and switch" characteristics of the $\text{NF}(a^1\Delta)$ generator derive from the nonlinear coupling and positive feedback processes inherent to this mechanism as follows. Reaction (1), thermal dissociation of FN_3 , is essentially a very slow process that serves only to initiate production of $\text{NF}(a^1\Delta)$. At low metastable concentration, first-order quenching²⁷ of $\text{NF}(a^1\Delta)$ by other species, Reaction (2), dominates over second-order self-annihilation, reaction (3). The feedback to reaction (1) is therefore essentially thermal, and hence subject to significant dilution by the He buffer gas. Consequently, reactions (1) and (2) do not satisfy the "loop gain greater than unity" criterion, and the $\text{NF}(a^1\Delta)$ concentration builds up only very slowly. Eventually, as the $\text{NF}(a^1\Delta)$ concentration increases, a point is reached where reaction (3) begins to compete with reaction (2), and the feedback then shifts from a thermal to a vibrational mode. Reaction (3) is highly exothermic²⁸ and may yield N_2 products in states of vibrational excitation up to $v \sim 20$ that are not diluted by contact with He buffer gas. Further, only two vibrational quanta of N_2 are required in reaction (4) to overcome the 0.5 eV barrier^{10,29} to dissociation of the azide. Therefore each self-annihilation event can subsequently generate several new molecules of $\text{NF}(a^1\Delta)$. Consequently, once reaction (3) is activated, the "loop gain" quickly becomes large compared to unity, and reactions (3) and (4) constitute a branched chain that drives swiftly to completion. This mechanism, although physically appealing and consistent with the data, must remain speculative, however, until the products of reaction (3) are verified and reaction (4) is studied in isolation. The rate of removal of $\text{NF}(a^1\Delta)$ by reaction (3) is known to be approximately 3×10^{-12} cm³/s, based on work by Setser,² as well as our own prior observations,¹⁰ but the products have not been determined experimentally.

Regardless of the mechanism, the appearance of $\text{NF}(a^1\Delta)$ in what amounts to a "delayed avalanche," nonetheless aids the design of continuous flow supersonic lasers by allowing premixed chemistry to occur in conventional nozzles. In this concept, secondary FN_3 is injected into a hot flow of primary gas from a precombustor (or heat exchanger) just upstream of the nozzle throat to initiate the dissociation process. Donors such as $\text{Bi}(\text{CH}_3)_3$ can also be injected at the same point and functions, such as mixing, donor chemistry, and gas expansion/cooling are accomplished in route during the delay period. The subsequent premixed lasing chemistry is then triggered farther downstream by the $\text{NF}(a^1\Delta)$ avalanche in cold supersonic flow where optical quality and gain cross sections are both maximized. This concept is valuable because elimination of slow mixing is critical in $\text{NF}(a^1\Delta)$ powered lasers (such as BiF), since large metastable concentrations that decay rapidly due to self-annihilation are needed to support inversion.

C. Conclusions

In summary, shock induced dissociation of FN_3 yields metastable $\text{NF}(a^1\Delta)$ after a 50 μs delay, and weak lasing at 470 nm has been achieved in the shock initiated chemical reaction between FN_3 and $\text{Bi}(\text{CH}_3)_3$. The principal factors limiting the laser output were the low gain coefficient and short gain duration, which prevented building up intracavity intensity to saturate the inverted medium. These conditions, in turn, derive from rapid quenching^{12,27} associated with the use of an organometallic donor. Consequently, replacement of $\text{Bi}(\text{CH}_3)_3$ by an alternate BiF precursor could improve both the gain coefficient as well as gain duration, and thereby significantly increase power extraction efficiency. Efforts are also underway to identify higher gain emitters³⁰ and variations to the shock tube experiment, which might lead to much larger (saturated) outputs. While the rate of cavity buildup is not as important a factor in continuous wave lasers, there is still a critical need to replace $\text{Bi}(\text{CH}_3)_3$ by a more suitable donor to generate larger gain coefficients and promote more efficient utilization of $\text{NF}(a^1\Delta)$, since, with limited BiF concentration, most of the metastables are lost to self-annihilation rather than the productive energy transfer and lasing reactions.^{2,25}

ACKNOWLEDGMENTS

This work was sponsored by the Innovative Science and Technology and the Directed Energy Offices of the Strategic Defense Initiative Organization; and the U.S. Army MICOM Office, under the Air Force Office of Scientific Research Contract No. F49620-90-C-0025. Special thanks go to W. Smith, W. Warren, and J. Herbelin for advice on driver chemistry, shock tubes, and BiF kinetics, respectively, and to B. R. Graves, who provided able assistance and encouragement in the laboratory when most needed.

- ¹D. J. Benard, W. E. McDermott, N. R. Pchelkin, and R. R. Bousek, *Appl. Phys. Lett.* **34**, 40 (1979).
- ²E. Quinones, J. Habdas, and D. W. Setser, *J. Phys. Chem.* **91**, 5155 (1987).
- ³W. G. Clark and D. W. Setser, *J. Phys. Chem.* **84**, 2225 (1980), and references therein.
- ⁴J. Habdas, S. Wategaonkar, and D. W. Setser, *J. Phys. Chem.* **91**, 451 (1987).
- ⁵J. M. Herbelin, D. J. Spencer, and M. A. Kwok, *J. Appl. Phys.* **48**, 3050 (1977).
- ⁶J. M. Herbelin and R. A. Klingberg, *Int. J. Chem. Kinet.* **16**, 849 (1984).
- ⁷R. F. Heidner, H. Helvajian, J. S. Holloway, and J. B. Koffend, *J. Chem. Phys.* **84**, 2137 (1986).
- ⁸W. E. Jones and T. D. McLean, *J. Mol. Spectr.* **90**, 481 (1981).
- ⁹D. Patel, A. T. Pritt, and D. J. Benard, *J. Phys. Chem.* **90**, 1931 (1986).
- ¹⁰D. J. Benard, B. W. Winker, T. A. Seder, and R. H. Cohn, *J. Phys. Chem.* **93**, 4790 (1989).
- ¹¹D. J. Benard and B. K. Winker, *J. Appl. Phys.* **69**, 2805 (1991).
- ¹²J. M. Herbelin and M. A. Kwok, *Proceedings of the Conference on High Power Gas Lasers* (SPIE, Los Angeles, CA January 1990), Vol. 1225, p. 560.
- ¹³W. Smith, R. Acebal, D. J. Benard, and B. R. Graves, *American Institute for Aeronautics and Astronautics 23rd Plasmadynamics and Lasers Conference* (AIAA, Nashville, TN, July 1992), Paper No. AIAA 92-2996.

- ¹⁴E. L. Resler, S. C. Lin, and A. Kantrowitz, *J. Appl. Phys.* **23**, 1350 (1952).
- ¹⁵J. F. Haller, Ph.D. thesis, Cornell University, 1942.
- ¹⁶K. Gholivand, G. Schatte, and H. Willner, *Inorg. Chem.* **26**, 2137 (1987).
- ¹⁷R. S. Konar, S. Matsumoto, and B. de B. Darwent, *Trans. Faraday Soc.* **67**, 1698 (1971).
- ¹⁸J. R. McDonald, J. W. Rabalais, and S. P. McGlynn, *J. Chem. Phys.* **52**, 1332 (1970).
- ¹⁹R. Rosen, *Selected Constants Spectroscopic Data Relative to Diatomic Molecules* (Pergamon, New York, 1970).
- ²⁰R. J. Malins and D. W. Setser, *J. Phys. Chem.* **85**, 1342 (1981).
- ²¹M. Junnehomme and A. B. F. Duncan, *J. Chem. Phys.* **41**, 1692 (1964).
- ²²M. Stanek, K. Musiel, and S. Lubuz, *Acta Phys. Polon. A* **59**, 239 (1981).
- ²³Alfa Catalog, 1986/87, p. P-168, available from Morton Thiokol, Danvers, MA.
- ²⁴Saturation intensity based on spectroscopic parameters in Ref. 8.
- ²⁵B. K. Winker, D. J. Benard, and T. A. Seder, in *Pet.* **12**, p. 543.
- ²⁶A. Yariv, *Quantum Electronics* (Wiley, New York, 1967), Chap. 14.
- ²⁷K. Y. Du and D. W. Setser, *J. Phys. Chem.* **94**, 2425 (1990).
- ²⁸M. W. Chase, C. A. Davies, J. R. Downey, D. J. Frump, R. A. McDonald, and A. N. Syverud, *JANAF Thermochemical Tables* (3rd ed.), *J. Phys. Chem. Ref. Data* **14**, Supplement No. 1 (1985).
- ²⁹D. J. Benard, M. A. Chowdhury, B. K. Winker, T. A. Seder, and H. H. Michels, *J. Phys. Chem.* **94**, 7507 (1990).
- ³⁰Substitution of B_2H_6 in place of $Bi(CH_3)_3$ excites the $BH(A-X)$ transition at 433 nm, unpublished results.

Journal of Physical Chemistry

Energy Transfer from Metastable NF to Boron Hydride

D.J. Benard and E. Boehmer
Rockwell International Science Center
Thousand Oaks, CA 91358

and

H.H. Michels and J.A. Montgomery, Jr.
United Technologies Research Center
E. Hartford, CT 06108

ABSTRACT

Gas phase reaction of B_2H_6 with HN_3 at $400^\circ C$ yields tetraazidodiborane (TADB), which subsequently dissociates into two diazidoborane molecules. Exposure of TADB to vibrationally excited SF_6 generates free BH radicals that may be pumped by energy transfer from metastable $NF(a^1\Delta)$ molecules, obtained by simultaneous dissociation of FN_3 . Even though BH radicals are rapidly consumed, the transient yields approach 2% of initial donor concentration. The rate constants for sequential excitation of the $a^3\Pi$ and $A^1\Pi$ states of BH by $NF(a^1\Delta)$ are estimated to be $\sim 8 \times 10^{-10}$ and $\sim 3 \times 10^{-11}$ cm^3/s , respectively, and transient populating inversions with peak optical gains of 10% /cm are developed on the $BH(A - X)$ transition at 4300 nm.

INTRODUCTION

Resonant electronic energy transfer from chemically generated metastable species to emitting atoms or molecules is the basis for a number of potential visible wavelength chemical laser systems. Production of metastable $O_2(a^1\Delta)$ by the base-catalyzed reaction of Cl_2 with H_2O_2 , followed by resonant transfer to I-atoms, produces an efficient laser at 1315 nm.¹ Similarly, production² of metastable $NF(a^1\Delta)$ by dissociation of FN_3 , followed by energy transfer to (and energy pooling with) BiF has led to recent demonstrations of both optical gain³ and unsaturated lasing⁴ at 471 nm. The BiF gain coefficients which have been achieved to date, however, are still quite small due to rotational/vibrational dilution of the inversion density and quenching of the electronically excited species⁵ by the organometallic donor used for *in-situ* formation of BiF. Consequently, there has been a strong motivation to identify alternative emitting molecules for which these difficulties can be circumvented.

Metal hydrides are interesting transfer partners for $NF(a^1\Delta)$ because of the large rotational/vibrational spacings which significantly reduce the dilution factor. Also, these transfer partners are favored by availability of volatile inorganic precursors which are less likely to act as efficient quenchers. The BH radical, in particular, is interesting because of a double resonance between its excited states and the 11,442 cm^{-1} excitation of $NF(a^1\Delta)$, which permits efficient pumping of an allowed transition at 433 nm. Referring to Fig. 1, the spectroscopic constants of the $X^1\Sigma^+$ and $A^1\Pi$ states of BH are well-known⁶, as is the ($A_{BH} \sim 6/\mu s$) radiative rate⁷. Recent independent *ab initio* calculations by Michels⁸ and Saxon⁹ have also located the potential minimum of the metastable intermediate $BH(a^3\Pi)$ state at $11,000 \pm 200 cm^{-1}$ excitation relative to the $X^1\Sigma^+$ ground state. Based on these results, the spin-allowed pumping reactions



are each shown to be nearly resonant¹⁰ and therefore potentially able to occur at gas kinetic rates. Transfer between NF and BH is also favored by large thermal velocities due to a low reduced mass factor, strong chemical bonding forces, and minimized reliance on specific internuclear motions due to highly vertical potential energy surfaces in each of the diatomics.^{6,7,11} Consequently, the interaction between NF($a^1\Delta$) and BH should be faster than the ($\sim 10^{-11}$ cm³/s) rate of energy transfer from NF($b^1\Sigma^+$) to the heavier IF molecule, which involves weaker chemical forces and greater dependence on internuclear separation.¹² Also, the generally high rates of BH($A^1\Pi$) electronic quenching, measured by Douglass and Rice,¹³ suggest that energy transfer processes involving this species are likely to be rapid as well.

The degeneracy ratio for Reaction (1) is much larger than for Reaction (2). Consequently, it is anticipated that $k_1 \gg k_2$ and the overall rate of BH($A^1\Pi$) production is therefore limited by k_2 . Inversion of the BH($A - \dots$, $\Delta v = 0$) transitions, however, requires removal of the $X^1\Sigma^+$ state at a rate faster than the radiative decay of the $A^1\Pi$ state. Therefore, with NF($a^1\Delta$) concentrations $> 10^{16}$ /cm³ obtainable by dissociation of FN₃, inversion is expected if k_1 approaches the gas kinetic limit. In this case, large gain coefficients may be generated on the 433 nm ($v' = 0$ to $v'' = 0$) transition, provided adequate concentrations of the BH radical and NF($a^1\Delta$) are cogenerated without inducing excessive quenching of the excited species.

Since the BH radical is highly energetic ($\Delta H_f = + 105$ kcal/mole),¹⁴ its efficient production requires a precursor or donor molecule of significant chemical energy content, and removal of the BH radical by highly exothermic chemical reactions is likely to occur rapidly. Consequently, dissociation of the donor molecules must be done both *in situ* and in temporal synchronization with production of the metastables. The donor must therefore be capable of coexisting with FN₃ (in a premixed state) for periods long enough to transport the gases through a suitable reactor. In this paper, we report our observations on the synthesis of an improved donor molecule, tetraazidodiborane, and the kinetics of its dissociation into BH as well as the subsequent interaction of BH with vibrationally excited SF₆ and metastable NF($a^1\Delta$).

EXPERIMENTAL

As in previous experiments²⁻⁴, gaseous HN_3 was generated in batch mode by the reaction of powdered NaN_3 with excess stearic acid between 100-120 °C. The azide product was diluted to 5% in He and stored in a stainless steel tank for later use. Gaseous FN_3 (~3% in He) was then generated on-line at 25°C and 350 Torr total pressure by titrating the HN_3/He flow with a secondary flow of 10% F_2 in He from a commercially available gas cylinder. The FN_3 flow was expanded across a pinhole orifice and mixed with continuous flows of SF_6 and donor molecules (diluted in He) at a system pressure of 100 Torr. The combined flows were directed via teflon tubing to a windowed stainless steel reaction cell where the gas stream was excited at the rate of 0.5 pps by (0.5 - 2.0 Joule) pulses of 10.6 μ radiation from a CO_2/TEA laser. The beam was softly focused to a 1cm x 1cm cross sectional area at the center of the reaction cell, which exhausted continuously to vacuum. Within the reactor, SF_6 molecules become vibrationally excited (after absorption of laser photons) and contribute to subsequent dissociation of both FN_3 and donor molecules by energy transfer. The CO_2 laser was operated at constant output energy, but the beam was attenuated by passage through a variable pressure SF_6 absorption cell before entering and exiting the reactor through NaCl windows, and terminating on a pulse calorimeter. The intensity time profile of the laser was also monitored by a fast Ge detector.

The donor molecules were formed on-line by continuously passing a mixture of HN_3 and B_2H_6 , both diluted in inert gas, through a 400°C capillary oven (residence time ~ 10 ms) that was closely coupled to the subsequent reaction cell. The rapidly cooled effluent from the capillary oven could also be diverted to a low residence time (10 cm long) absorption cell with NaCl windows that was positioned inside an FT-IR instrument for analysis of the product stream. Typical (unreacted) mole fractions in the reactor were 0.7% FN_3 , 4.5% SF_6 , 0.06% B_2H_6 , 0.25% HN_3 and balance inert gas, approximately half of which was used to purge the windows. All gas flows were electronically measured and controlled, and previous work² revealed that peak $[\text{NF}(a^1\Delta)]$ is ~70% of the initial FN_3 concentration within 1-2 μ s following the laser pulse, after which the

metastable decay is dominated by self-annihilation¹⁵ at a rate of approximately $3 \times 10^{-12} \text{ cm}^3/\text{s}$.

Chemiluminescence from the reactor was monitored at 874 nm to track the $\text{NF}(a^1\Delta)$ produced by CO_2 laser excitation of the SF_6/FN_2 /inert gas mixture. The gas flow, laser beam and direction of optical detection were along three mutually orthogonal axes passing through the center of the reactor. The chemiluminescence was transmitted through an interference filter and detected by a silicon photodiode. When a donor species was added to the flow, $\text{BH}(A - X)$ emission at 433 nm was similarly monitored using a second interference filter and either the photodiode or a 1P28 photomultiplier tube (PMT). A spectrometer was also employed to ensure that no overlapping emissions from other species occurred within the bandwidth of either filter. The wavelength dependence of the silicon photodiode's quantum efficiency was provided by the manufacturer (EG & G), and the detector was mounted on a rigid stand which maintained its spatial relationship to the reacting (emitting) volume to insure reproducibility and comparability of the data. Since both the $\text{NF}(a - X)$ and $\text{BH}(A - X)$ emission bands are confined to very narrow spectroscopic regions,¹⁰ the transmission factors for the corresponding filters were easily determined by use of a commercial spectrophotometer.

Light from a resonance lamp¹⁶ was also focussed into the reacting volume and re-imaged at the PMT detector which was filtered to respond to the $\text{BH}(A - X)$ emission. The ~ 5 cm long by 1 cm ID lamp was energized by applying a pulsed discharge to 10 Torr of 70% Ne and 30% He gas that was passed through a column of SiO_2 and decaborane ($\text{B}_{10}\text{H}_{14}$) at ambient temperature. Two electrical drivers for the lamp were available. The first produced a constant current (5 ampere) hollow-cathode discharge of 150 μs duration, that was electronically initiated approximately 100 μs in advance of the CO_2 laser. Therefore, during the time of reaction following the laser pulse, the lamp intensity was essentially constant. A second, much more intense lamp driver, produced an approximately square (135 ampere / 15 μs) pulsed coaxial discharge which could also be synchronized with the chemiluminescence from the reactor. The operation of each lamp was stabilized by drawing a continuous current of ~ 1 ma, either between the main electrodes in the

hollow cathode lamp or between the cathode and a secondary pin anode in the coaxial lamp. To separate the 433 nm chemiluminescence (originating in the reactor) from the probing 433 nm radiation (originating in the lamp), data from the PMT was electronically directed to Channel A on even numbered shots (Channel B grounded) and to Channel B on odd numbered shots (Channel A grounded). The lamp was then fired on even numbered shots only, and data corresponding to Channel A minus Channel B was averaged in the oscilloscope over a large (even) number of laser pulses so that the chemiluminescence contribution was cancelled. The amplifier gains on Channels A and B were carefully balanced to within 1% and care was taken to ensure that neither channel was saturated. Consequently, the lamp diagnostic was sensitive to the difference in (degeneracy weighted) populations between the $A^1\Pi$ and $X^1\Sigma^+$ states of BH.

THEORETICAL

Wiberg and Michaud¹⁷ have shown that HN_3 and B_2H_6 react in ether by abstracting H_2 to form azidoboranes. The corresponding gas phase reaction could therefore proceed as



provided the reaction products are stable. *Ab initio* calculations¹⁸ were performed to explore the possible existence and stability of the tetraazido-borane (TADB) structure suggested in Reaction (3). Our calculations indicate the likely existence of a vibrationally stable D_2 structure for TADB. The RHF/6-31G* optimized geometry for TADB is shown in Table 1, and the calculated vibrational frequencies and intensities, which can be used to characterize experimental absorption bands, are given in Table 2. SCF calculations are well-known to yield vibrational frequencies which are overestimated. The frequencies listed in Table 2 should therefore be multiplied by a uniform scaling factor of 0.8929 for comparison with experimental data. This correction is most accurate for the high frequency bands where a variance of 5-10% is anticipated. Also, at this level of calculation, the intensity results are qualitative at best. The results obtained are, nonetheless, adequate for identification of product molecules. Calculated heats of reaction and heats of

formation are reported in Table 3. These data include scaled vibrational zero-point corrections obtained from calculated vibrational frequencies. The MP2/6-31+G**/RHF/6-31G* heat of formation for TADB, given in Table 3, indicates that Reaction (3) is exothermic by 73.2 kcal/mole. In a fashion similar to B₂H₆, the TADB molecule can also dissociate upon heating, yielding diazidoborane (DAB):



Ab initio calculations of DAB indicate a vibrationally stable C_{2v} structure as shown in Tables 1 and 2. The calculated energies in Table 3 indicate that Reaction (4) is exothermic by about 9.8 kcal/mole.

The above findings suggest that TADB is a potential (nascent) product of reacting gaseous HN₃ with B₂H₆. Since TADB is thermodynamically unstable with respect to dissociation into DAB molecules, it is not expected to persist for long periods, except possibly at cryogenic temperatures. Therefore, reaction time and temperature may be critical factors influencing the yield of TADB.

Similar to the halogen azides, DAB can eliminate a terminal N₂ group. At the RHF/6-31G* level of theory, the reaction



has a barrier of 17.9 kcal/mole, slightly greater than the 13.6 kcal/mole (expt) and 10.8 kcal/mole (calc) values^{2,18} found for FN₃. The molecular fragments resulting from DAB, upon N₂ elimination, may then undergo a conformational change by migration of the lone N-atom away from the azide group, and insertion into the H-B bond to form planar HNBN₃. Calculations at the RHF/6-31G* level of theory, shown in Tables 1 and 2, indicate that this compound is vibrationally stable. The overall reaction (DAB → HNBN₃ + N₂) is exothermic by 41.1 kcal/mole, as calculated from the data in Table 3. Once formed, the HNBN₃ molecule is not expected to yield a significant quantity of BH radicals upon further fragmentation.

RESULTS

Donor Chemistry

On-line mixing of HN_3 and B_2H_6 , upstream of the capillary oven and FT-IR absorption cell, revealed no reaction at ambient temperature as shown by the upper trace in Fig. 2, where the observed bands are all assignable to reactants.^{19,20} The middle trace was obtained with HN_3 in excess and the oven temperature at 400°C . Rapid cooling of the gas (from the capillary oven) as well as fast transport through the FT-IR cell was necessary to record this data, which shows that B_2H_6 has reacted completely and the intermediate product is lacking a vibration at $\sim 2600\text{ cm}^{-1}$. This frequency can be assigned to a free B-H stretch by analogy to the corresponding modes^{21,22} in HBF_2 (2619 cm^{-1}), HBCl_2 (2625 cm^{-1}) and HBBr_2 (2600 cm^{-1}). The dihaloboranes are comparable to azidoboranes, since the N_3 radical is a pseudo-halogen. The lower trace in Fig. 2 was obtained by continued heating of the intermediate product at 400°C in a second oven of much longer residence time. This final product is characterized by a B-H stretch, and the major absorption bands are reasonably correlated with the frequencies of the four strongest bands of DAB, as shown in Table 2. A static charge of DAB was trapped in the FT-IR cell (at ambient temperature) and its decay was monitored over the course of a day. The measured attenuation ($\sim 5\%$ /hr) was in fair agreement with the analogous decay of ClN_3 , which has a similar barrier to dissociation.¹⁸

The intermediate product, obtained by reaction of HN_3 and B_2H_6 , is thought to be TADB based on its decomposition into DAB, as well as the lack of a free B-H stretch in the corresponding FT-IR data. Since the two H-atoms in TADB are bridge bonded, as in B_2H_6 , this donor molecule does not show a characteristic absorption at $\sim 2600\text{ cm}^{-1}$. Our theoretical investigation also demonstrated that both DAB and TADB are sufficiently energetic to yield $\text{BH} + \text{N}_2$ products. Consequently, these donors are preferable to B_2H_6 , at least on the basis of thermodynamics. The bridge bonds in TADB, however, are likely to increase the kinetic probability of azide-azide annihilation (leading to $\text{BH} + \text{N}_2$ fragments) relative to DAB, by hindering the migration process

which allows formation of non-productive HNBN₃ molecules.

To evaluate these potential donors, equimolar concentrations of DAB, TADB and unreacted B₂H₆ were each separately mixed with SF₆ / FN₃ / inert gas and exposed to pulsed CO₂ laser radiation, while monitoring production of BH(A - X) chemiluminescence. As expected, the yields of BH(A¹Π) from B₂H₆ and DAB were comparable, while the yield of BH(A¹Π) from TADB was enhanced by nearly an order of magnitude under optimized conditions, which corresponded to a stoichiometry of approximately 4 parts HN₃ to 1 part B₂H₆ into the heated capillary oven. Therefore, with the exception of the gain measurements, all subsequent experiments were performed using the intermediate (short-time) product of the thermally activated reaction of HN₃ with B₂H₆ as the donor of choice.

Reaction Mechanism

Figure 3 shows data collected using the (constant intensity) lamp diagnostic with inert gas, SF₆ and TADB only in the reactor. All three traces show an electrical noise spike at time zero from the CO₂ laser discharge, and the electronic signal processing for each of the traces was identical. The lower trace, however, was collected with the lamp blocked (to test the chemiluminescence cancellation) while the uppermost trace was collected with the laser blocked (to test constancy of the lamp output). The peak intensity of the uncanceled BH(A - X) chemiluminescence (not shown in Fig. 3), due to weak transfer from vibrationally excited SF₆ molecules, was about 25% of the lamp signal. The intermediate trace in Fig. 3 therefore reflects absorption of lamp radiation by ground state BH(X¹Σ⁺) radicals. This signal also approximately measures the total concentration of BH radicals, since (in the absence of FN₃) no NF(a¹Δ) is formed, and we may therefore assume the concentration of both BH(a³Π) and BH(A¹Π) to be negligible. The rise and fall times of the BH(X¹Σ⁺) concentration are approximately 0.3 and 2.2 μs, respectively, and the peak yield of BH(X¹Σ⁺) was estimated at approximately 2% of the B₂H₆ used to generate the TADB. This result is based on an active 1 cm optical path length and an averaged cross section of $\sim 3 \times 10^{-14}$ cm², which assumes the lamp and reaction cell are each characterized by rotational/translational

temperatures of 600°C. Since these temperatures are uncertain within a factor of two, the estimated yield may in fact vary between 50 and 200% of the quoted value. The vibrational temperatures produced by CO₂ laser excitation of SF₆ are higher;²³ however, the error due to population of $v' > 0$ levels in the A¹Π state is small due to the large (2367 cm⁻¹) vibrational spacing^{6,10} of the BH radical, as confirmed by measuring relative intensities of the 0-0 and 1-1 bands. Finally, since heating of B₂H₆ catalyzes formation of higher weight boranes²⁴ and the TADB may precipitate out of the flow due to polymerization (a white deposit forms between the oven and reactor), the quoted yield figure is actually a lower limit for the concentration ratio of peak BH to active TADB in the flow.

The rates of rise and fall of the BH(X¹Σ⁺) time profile correspond to the time constants for dissociation of the TADB and subsequent removal of the BH radicals. The data in Fig. 3 alone, however, do not determine which process corresponds to the rise and which to the fall of the BH(X¹Σ⁺) time profile, except that the faster of the two determines the rate of rise and the slower the rate of fall. This uncertainty can be resolved in two ways. First, by comparing the laser intensity and BH(X¹Σ⁺) time profiles in the absence of FN₃, as given in Fig. 4(a), it is found that both decays occur on a similar time scale. This result suggests that BH(X¹Σ⁺) is destroyed more rapidly than it is generated, so that a steady-state relationship between [BH(X¹Σ⁺)] and the laser-driven rate of formation is established. In this case, the rate of rise of BH(X¹Σ⁺) is linked to the time constant for removal, while the rate of fall reflects the time constant for dissociation of TADB, as influenced by the time profile of the CO₂ laser intensity. This assignment can be further verified, as shown in Fig. 4(b), which compares two [BH(X¹Σ⁺)] time profiles (still in the absence of FN₃) at different CO₂ laser energies. Here, the rate of dissociation of the donor is altered significantly (via the laser intensity) while the rate of BH(X¹Σ⁺) removal remains approximately fixed. Since the time profiles show a near-constant rise time, but widely-varied decay rates, the above assignment is proved to be correct. Also, as expected in the steady state limit, increasing laser intensity enhances the yield of vibrationally excited SF₆, and therefore also the rate of donor dissociation as well as the peak yield of BH(X¹Σ⁺). If, on the other hand, the rate of rise were due

to the formation step, the yield of BH radicals would saturate, and become nearly independent of laser power, since dissociation of the donor would complete before significant loss due to the slower removal process. The data in Figs. 3 and 4, therefore, establish that $\text{BH}(X^1\Sigma^+)$ is consumed approximately seven times faster than it is generated. Consequently, if the removal process were eliminated, the concentration yield of $\text{BH}(X^1\Sigma^+)$ would rise from $\geq 2\%$ to match that actual branching ratio from TADB to $\text{BH}(X^1\Sigma^+)$, which is $\geq 14\%$.

Since the densities of boron-containing molecules and F-atoms (from multiphoton dissociation^{25,26} of the SF_6) are too low to account for the observed fast removal process, even at gas kinetic rates, it follows (by elimination) that SF_6 molecules are responsible for consuming the BH radicals. A likely mechanism for this reaction is abstraction of F-atoms, which are more tightly bonded to boron than sulfur.¹⁴ Measurements by Rice,²⁷ however, indicate a low rate of reaction between BH and SF_6 at 300°K. Consequently, the high temperatures and vibrational excitations (associated with CO_2 laser pumping) appear to play a role in surmounting an activation barrier for the removal process.

Figure 5(a) shows the time profile of $\text{NF}(a^1\Delta)$ in the absence of any BH donor, and Fig. 5(b) compares the time profiles of $\text{BH}(A^1\Pi)$ with FN_3 present and two different concentrations of TADB donor. Note that the $\text{BH}(A^1\Pi)$ signal decays more rapidly than the $\text{NF}(a^1\Delta)$ time profile. This difference is due to removal of BH radicals discussed above, as well as to possible removal of $\text{NF}(a^1\Delta)$ catalyzed by addition of the donor. Since the $\text{BH}(A^1\Pi)$ concentration scales in proportion to the donor concentration and neither the rate of rise nor the rate of fall are affected when the donor concentration is altered, it follows that varying the concentration of TADB (under these conditions) does not appreciably change either the peak yield of $\text{BH}(X^1\Sigma^+)$ per donor molecule or the $\text{NF}(a^1\Delta)$ time profile. Therefore, significant removal of $\text{BH}(X^1\Sigma^+)$ by boron-containing molecules is ruled out (as expected), and the donor molecule as well as its byproducts do not appear to be highly efficient quenchers of $\text{NF}(a^1\Delta)$.

Figure 6 compares the measured time profile of $\text{BH}(A^1\Pi)$, with FN_3 present, to the calculated product of the $\text{BH}(X^1\Sigma^+)$ and $\text{NF}(a^1\Delta)$ time profiles, from Figs. 3 and 5, respectively. Since $\text{BH}(A^1\Pi)$ decays radiatively in 160 ns, its concentration is in steady-state with its precursors, namely $\text{BH}(X^1\Sigma^+)$ and $\text{NF}(a^1\Delta)$, on longer time scales. Therefore, the measured $\text{BH}(A^1\Pi)$ time profile should proportionately track the calculated-product time profile, unless NF either removes $\text{BH}(X^1\Sigma^+)$ chemically, or $\text{NF}(a^1\Delta)$ assists the dissociation of TADB. Since the actual yield of $\text{BH}(A^1\Pi)$ exceeds the calculated yield at long times, $\text{NF}(a^1\Delta)$ aids dissociation of the donor, although this secondary effect is of little consequence at early times. Chemical removal of BH by NF apparently does not proceed at a significant rate because the potential reactions are either four-centered (to form $\text{BN} + \text{HF}$), tri-molecular (to form FNBH), or endothermic (to form atomic + triatomic products).¹⁴

Pump Rate

When FN_3 was admitted to the reaction cell, in addition to TADB and SF_6 , the yield of $\text{BH}(A^1\Pi)$ increased by approximately two orders of magnitude. Heating of the FN_3 flow to $\sim 100^\circ\text{C}$, in route between the generator and the point of SF_6 /donor addition, also eliminated this $\text{BH}(A - X)$ chemiluminescence. Since the azide is thermally decomposed to N_2F_2 and N_2 under these conditions,²⁸ the anticipated role of $\text{NF}(a^1\Delta)$ as a pumping species is verified and other ground-state chemiluminescence mechanisms are ruled out. The rate constant k_2 may therefore be extracted from the data shown in Fig. 6 by combining the steady state relation

$$k_2 [\text{NF}(a^1\Delta)] [\text{BH}] \sim A_{\text{BH}} [\text{BH}(A^1\Pi)] \quad (6)$$

at early time with the intensity relations

$$S_{\text{BH}} = C_{\text{FBH}} D_{\text{BH}} G_{\text{BH}} A_{\text{BH}} [\text{BH}(A^1\Pi)] \quad (7)$$

$$S_{\text{NF}} = C_{\text{FNF}} D_{\text{NF}} G_{\text{BH}} A_{\text{NF}} [\text{NF}(a^1\Delta)] \quad (8)$$

to yield the expression

$$k_2 \sim \frac{A_{NF}}{[BH]} \left(\frac{S_{BH}}{S_{NF}} \right) \left(\frac{F_{NF}}{F_{3H}} \right) \left(\frac{D_{NF}}{D_{BH}} \right) \left(\frac{G_{NF}}{G_{BH}} \right) \quad (9)$$

where S_{BH}/S_{NF} is the recorded emission signal ratio at 433 and 874 nm, and the terms F, D and G are the corresponding filter transmission, detector quantum yield and electronic amplification (gain) factors, respectively. As used here, C is a common geometric collection factor and [BH] represents the total concentration of boron hydride radicals, since with $k_1 \gg k_2$ the majority of the population will be in the $a^3\Pi$ state when high densities of $NF(a^1\Delta)$ are present. Also, quenching of the $A^1\Pi$ state is ignored in this analysis due to its fast radiative decay. Using $A_{NF} = 0.2$ /s for the radiative rate of the $NF(a - X)$ transition,²⁹ and peak [BH] from the absorption measurement, Equation (9) yields $k_2 \sim 3 \times 10^{-11}$ cm³/s.

Population Inversion

Due to the high yield of $BH(A - X)$ emission that was achieved with FN_3 present in the reactor, the constant intensity lamp diagnostic could not be used to monitor transmission at 433 nm because the probing radiation was swamped by intense chemiluminescence. Therefore, the high intensity coaxial lamp was employed to monitor the reacting medium, using an (OD = 2) neutral density filter in series with the interference filter to prevent detector saturation. Since small differences in signal intensity were critical in these experiments, the data was collected in 128 shot averages to suppress statistical fluctuation, and unreacted B_2H_6 was used as the donor in place of the more efficient TADB precursor to suppress instabilities in the reactor arising from growth of polymer films. No significant reaction between FN_3 and B_2H_6 (prior to the laser pulse) was evident under the conditions of the experiment, and the reduced donor efficiency could be partially compensated by approximately tripling the concentration of B_2H_6 that was added to the reactor flow, since the B_2H_6 did not quench the $NF(a^1\Delta)$ appreciably.

The upper/dashed trace in Fig. 7 shows the time profile of the lamp intensity as measured

by the difference between Channels A and B with the laser beam blocked from entering the reactor. The lower/dashed trace is the uncanceled chemiluminescence from the reactor (Channel B only) and the lower/solid trace is the canceled chemiluminescence signal (Channel A minus Channel B) taken under identical conditions with the lamp optically blocked. The upper/solid trace in Fig. 7 is the data collected (Channel A minus Channel B) with both the lamp and laser coupled into the reaction cell and, as previously, all traces show electrical noise spikes at time zero due to the CO₂ laser discharge. These data demonstrate positive optical gains of up to ~ 10% /cm for the first ~ 1.5 μs of the chemiluminescence pulse, since the monitored signal (with both the lamp and laser active) exceeds the intensity of the lamp signal alone by a margin that is too wide to explain by either fluctuations in the data or by imbalance of the chemiluminescence signals in Channels A and B of the oscilloscope. At longer times, the medium regains transparency due to the removal of BH radicals, as expected. The data were reproducible, and the appearance of transient optical gain was eliminated when FN₃ was not admitted to the reactor. Consequently, an absolute population inversion of the BH(A – X) transition was obtained; and the system will likely operate as a laser. These results are significant because the optical gain coefficient generated by the NF/BH system is large in comparison to the (~ 3 x 10⁻⁴ /cm) gain factor that was obtained³ by interaction of NF(a¹Δ) with F₂.

DISCUSSION

A simple model of the NF/BH transfer-pooling system is based on the following three physical approximations. First, since the removal rate of BH is slower than the radiative rate, total BH concentration at the chemiluminescence peak is unaffected by the presence of NF(a¹Δ), which serves only to alter the distribution between the X¹Σ⁺, a³Π and A¹Π states. Second, neither BH(a³Π) nor BH(A¹Π) are quenched significantly, because the former is metastable (low quenching cross section) and the latter decays optically at a very high rate. Consequently, the BH kinetics are dominated by the radiative decay and interaction with NF(a¹Δ). Pumping of NF(X³Σ⁻) by either the a³Π or A¹Π states of BH, the reverse of Reactions (1) and (2), are negligible due to

the fast removal³⁰ of $NF(X^3\Sigma^-)$, as well as the fast radiative decay of $BH(A^1\Pi)$ and the 9 to 1 degeneracy ratio of Reaction (1) which strongly favors production of $BH(a^3\Pi)$ over $NF(a^1\Delta)$. Third, steady-state relations apply to all three BH states at the peak of the chemiluminescence time profile. The $BH(A^1\Pi)$ concentration is in steady-state (by definition), and since this state follows the product of the $BH(a^3\Pi)$ concentration, and a more slowly varying $NF(a^1\Delta)$ time profile, the $a^3\Pi$ state is also approximately peaked. Finally, applying conservation of total BH density, it follows that the $X^1\Sigma^+$ ground state is simultaneously minimized. Consequently, at the peak of the chemiluminescence time profile the energy transfer system is governed by the relations

$$[BH] = [BH(X^1\Sigma^+)] + [BH(a^3\Pi)] + [BH(A^1\Pi)] \quad (10)$$

and

$$A_{BH} [BH(A^1\Pi)] = k_1 [NF(a^1\Delta)][BH(X^1\Sigma^+)] = k_2 [NF(a^1\Delta)][BH(a^3\Pi)]. \quad (11)$$

It is useful to define an inversion parameter

$$y = \{[BH(A^1\Pi)] - 2 [BH(X^1\Sigma^+)]\} / [BH] \quad (12)$$

where the factor of two accounts for the different degeneracies of the upper and lower states of the potential $BH(A - X)$ laser transition. Solving equations (10 - 12) simultaneously yields

$$k_1 / k_2 = (2 + y) / (x - y(1 + x)) \quad (13)$$

where

$$x = k_2 [NF(a^1\Delta)] / A_{BH}. \quad (14)$$

The above relations are essentially an "equation of state" for the NF/BH system which relates the metastable concentration to the unsaturated optical transmission properties (at 433nm) through the dimensionless parameters x and y , respectively. From the prior intensity data ($k_2 \sim 3 \times 10^{-11}$ cm³/s, $[NF(a^1\Delta)] \sim 1.5 \times 10^{16}$ /cm³) and $A_{BH} \sim 6 \times 10^6$ /s, the value of x is small compared to unity. Without use of this approximation, however, one may still require $y > 0$

for positive gain in Equations (13) and (14), which yields

$$k_1 [NF(a^1\Delta)] \geq 2 A_{BH} \quad (15)$$

after suitable algebraic manipulations. Equation (15) is the condition for inversion to occur at the peak of the $BH(A^1\Pi)$ time profile and may be employed to evaluate k_1 as $\geq 8 \times 10^{10} \text{ cm}^3/\text{s}$, given the data above. The corresponding cross section ($\sim 100 \text{ A}^2$) is consistent with the very favorable dynamics of the energy transfer process as detailed in the introduction.

CONCLUSIONS

The rate constants for excitation of BH by energy transfer from $NF(a^1\Delta)$ are conducive to formation of a population inversion with high optical gain on the 433 nm (A – X) transition at achievable metastable concentrations. The intermediate product, tetraazidodiborane, formed in the thermally-activated reaction of HN_3 and B_2H_6 , is shown to be a superior donor of free BH radicals, which are rapidly consumed by the vibrationally excited SF_6 molecules that are used (in the current experiments) to trigger dissociation of the metastable precursor and donor species. Clearly, more work is needed to establish optimal conditions for synthesis and transport of the TADB donor, since high concentrations of BH are necessary to efficiently extract the metastable energy in competition with the loss due to self-annihilation. Also, more scalable methods to initiate dissociation of the BH donor and FN_3 need to be applied to optimize the performance of the laser system.

ACKNOWLEDGMENTS

This work was supported by the Innovative Science and Technology Office of the Ballistic Missile Defense Organization which provided funding through the Air Force Office of Scientific Research, Contract No. F49620-90-C-0025, and by the High Energy Density Materials Office of the Air Force Phillips Laboratory, Contract No. F04611-90-C-0009.

REFERENCES

1. D.J. Benard, W.E. McDermott, N.R. Pchelkin and R.R. Bousek, *Appl. Phys. Lett.* 34 (1979) 40.
2. D.J. Benard, B.K. Winker, T.A. Seder and R.H. Cohn, *J. Phys. Chem.* 93 (1989) 4790.
3. D.J. Benard and B.K. Winker, *J. Appl. Phys.* 69 (1991) 2805.
4. D.J. Benard, *J. Appl. Phys.* 74 (1993) 2900.
5. J.M. Herbelin and M.A. Kwok, Proceedings of the Conference on High Power Gas Lasers (SPIE, Los Angeles, CA/January 1990) Vol. 1225, pg. 560.
6. W.T. Luh and W.C. Stwalley, *J. Molec. Spectrosc.* 102 (1983) 212.
7. C.H. Douglass, H.H. Nelson and J.K. Rice, *J. Chem. Phys.* 90 (1989) 6940.
8. H.H. Michels, United Technologies Research Center (E. Hartford, CT) private communication.
9. R. Saxon, SRI International (Menlo Park, CA) private communication.
10. B. Rosen, Spectroscopic Data Relative to Diatomic Molecules (Pergammon Press, NY) 1970.
11. M. Bettendorf and S.D. Peyerimhoff, *Chem. Phys.* 99 (1985) 55.
12. A.T. Pritt and D.J. Benard, *J. Chem. Phys.* 85 (1986) 7159.
13. C.H. Douglass and J.K. Rice, *J. Phys. Chem.* 93 (1989) 7659.
14. M.W. Chase, et al. JANAF Thermochemical Tables, *J. Phys. Chem. Ref. Data* (Vol. 14, Third Edition) 1985.

15. E. Quinones, J. Hablas and D.W. Setser, *J. Phys. Chem.* 91 (1987) 5155.
16. J.W.C. Johns, F.A. Grimm and R.F. Porter, *J. Molec. Spectrosc.* 22 (1967) 435.
17. E. Wiberg and H. Michaud, *Z. Naturf.* 9B (1954) 497.
18. D.J. Benard, M.A. Chowdhury, B.K. Winker, T.A. Seder and H.H. Michels, *J. Phys. Chem.* 94 (1990) 7507, and references therein.
19. W.C. Price, *J. Chem. Phys.* 16 (1948) 894.
20. D.A. Dows and G.C. Pimentel, *J. Chem. Phys.* 23 (1955) 1258.
21. B. deMançirola and J.F. Westerkamp, *Spectrochim. Acta* 24A (1964) 1633.
22. L. Lynds, *J. Chem. Phys.* 42 (1965) 1124.
23. M. Lenzi, E. Molinari, G. Piciacchia, V. Sessa and M.L. Terranova, *Chem. Phys.* 142 (1990) 473.
24. J.F. Stanton, W.N. Lipscomb and R.J. Bartlett, *J. Am. Chem. Soc.* 111 (1989) 5165.
25. C.R. Quick and C. Wittig, *Chem. Phys. Lett.* 48 (1977) 420.
26. P. Bado and H. Van den Bergh, *J. Chem. Phys.* 68 (1978) 4188.
27. J.K. Rice, N.J. Caldwell and H.H. Nelson, *J. Phys. Chem.* 93 (1989) 3600.
28. J.F. Haller, Ph.D. Thesis (Cornell University, Ithaca NY) 1942.
29. R.J. Malins and D.W. Setser, *J. Phys. Chem.* 85 (1981) 1342.
30. Since the ground state of NF is a triplet, its rate of self-annihilation is expected to be much faster than the rate of removal for metastable (singlet) NF reported in references 2 and 11.

CAPTIONS

- Fig. 1 Excitation of BH(A - X) chemiluminescence by NF($a^1\Delta$) energy pooling mechanism. The potential curves for the BH($A^1\Pi$) and BH($X^1\Sigma^+$) states are from Ref. 6 by Stwalley and Luh.
- Fig. 2 Infrared absorption spectra of a reacting hydrogen azide and diborane gas mixture.
- Fig. 3 Time profiles of 433 nm signals due to transmission of resonance lamp through the laser driven reactor in the absence of FN₃.
- Fig. 4 Comparison of smoothed BH($X^1\Sigma^+$) and laser intensity time profiles (a), and BH($X^1\Sigma^+$) at two different laser energies (b), in the absence of FN₃.
- Fig. 5 Time profiles of NF($a^1\Delta$) in the absence of donor (a), and BH($A^1\Pi$) at two levels of donor concentration (b).
- Fig. 6 Comparison of measured BH($A^1\Pi$) time profile with the calculated product time profile of NF($a^1\Delta$) and BH($X^1\Sigma^+$).
- Fig. 7 Time profiles of 433 nm signals from transmission of the resonance lamp through the laser-driven reactor with FN₃ present.
- Table 1 Calculated RHF/6-31G* geometries (angstroms and degrees)
- Table 2 Calculated RHF/6-31G* vibrational frequencies (cm^{-1}) and intensities (km/mole).
- Table 3 Calculated energies (hartrees) and thermochemistry (kcal/mole).

Table 1
Calculated RHF/6-31G* Geometries (angstroms and degrees)

TADB (D ₂)		DAB (C _{2v})		HNBN ₃ (C _s)	
B-B	1.821	H-B	1.179	H-N	0.980
H-B	1.332	B-N ₁	1.439	N-B	1.225
B-N ₁	1.464	N ₁ -N ₂	1.237	B-N ₁	1.409
N ₁ -N ₂	1.230	N ₂ -N ₃	1.095	N ₁ -N ₂	1.233
N ₂ -N ₃	1.097	H-B-N ₁	115.4	N ₂ -N ₃	1.054
H-B-N ₁	103.5	B-N ₁ -N ₂	123.6	H-N-B	180.0
B-N ₁ -N ₂	118.8	N ₁ -N ₂ -N ₃	173.1	N-B-H ₁	177.4
N ₁ -N ₂ -N ₃	174.7			B-N ₁ -N ₂	120.1
H-B-N ₁ -N ₂	-168.2			N ₁ -N ₂ -N ₃	173.9
B-N ₁ -N ₂ -N ₃	-179.5			N-B-N ₁ -N ₂	180.0

Table 2**Calculated RHF/6-31G* Vibrational Frequencies (cm⁻¹) and Intensities (km/mole)****DAB****A₁** 2845(162), 2588(924), 1401(556), 919(16), 824(81), 506(10), 122(0)**A₂** 674(0), 60(0)**B₁** 952(59), 686(63), 311(3)**B₂** 2532(194), 1435(900), 1279(13), 1043(27), 693(1), 181(0)**TADB****A** 2580(0), 2260(0), 1442(0), 1103(0), 835(0), 674(0), 532(0), 262(0), 186(0), 70(0),
42(0)**B₁** 2533(633), 2003(106), 1442(262), 1158(18), 730(47), 668(33), 497(25), 315(1), 155(3),
34(1)**B₂** 2537(440), 1744(4), 1450(843), 1312(385), 1080(90), 724(1), 667(8), 453(0), 181(0),
110(1), 33(0)**B₃** 2560(2145), 1831(2335), 1357(3117), 1160(391), 877(659), 800(368), 668(90),
485(15), 134(10), 48(2)**HNBN₃****A'** 4146(336), 2592(728), 2178(882), 1432(300), 900(30), 695(11), 559(154), 517(19),
153(0)**A''** 651(19), 490(0), 435(210)

Table 3
Calculated Energies (Hartrees) and Thermochemistry (kcal/mole)

TADB

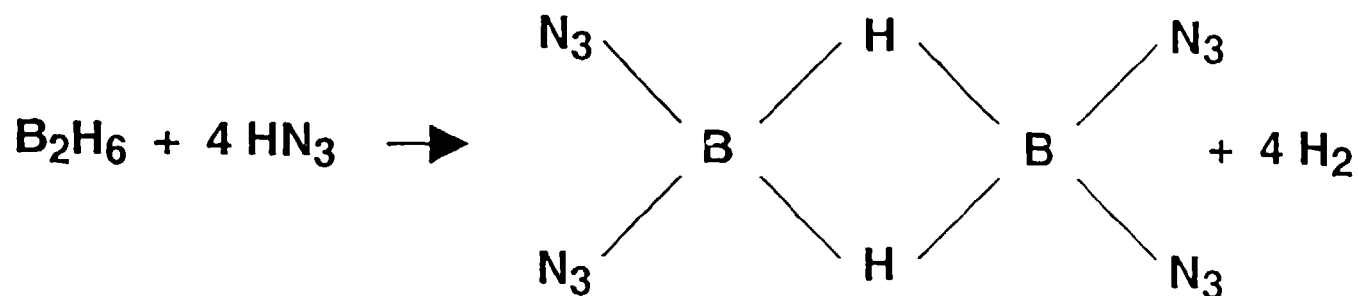
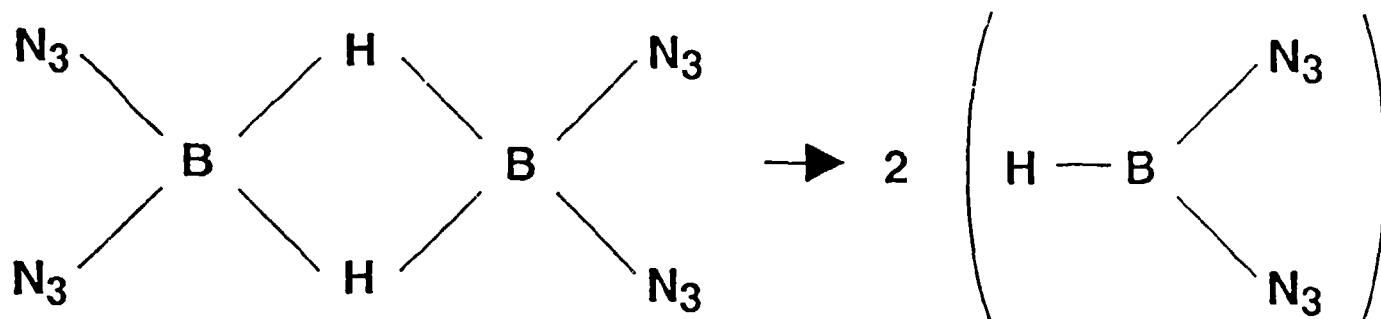
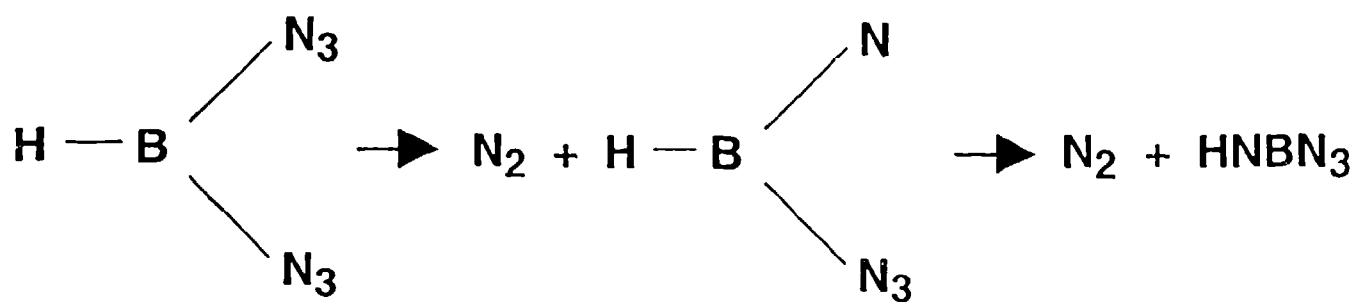
<i>Level of Theory</i>	<i>E</i>	$\Delta H_r[\text{Eq.}(3)]$	ΔH_f
RHF/6-31G*	-703.68903	-33.3	266.2
MP2/6-31G**/RHF/6-31G*	-705.83842	-75.0	224.5
MP2/6-31+G**/RHF/6-31G*	-705.87845	-73.2	226.3

DAB

<i>Level of Theory</i>	<i>E</i>	$\Delta H_r[\text{Eq.}(4)]$	ΔH_f
RHF/6-31G*	-351.86757	-31.0	117.6
MP2/6-31G**/RHF/6-31G*	-352.92725	-12.2	106.2
MP2/6-31+G**/RHF/6-31G*	-352.94539	-9.8	108.3

HNBN₃

<i>Level of Theory</i>	<i>E</i>	$\Delta H_r[\text{Eq.}(5)]$	ΔH_f
RHF/6-31G*	-243.01229	-57.6	40.4
MP2/6-31G**/RHF/6-31G*	-243.73651	-38.0	60.0
MP2/6-31+G**/RHF/6-31G*	-243.75290	-41.1	56.0

GRAPHIC AGRAPHIC BGRAPHIC C

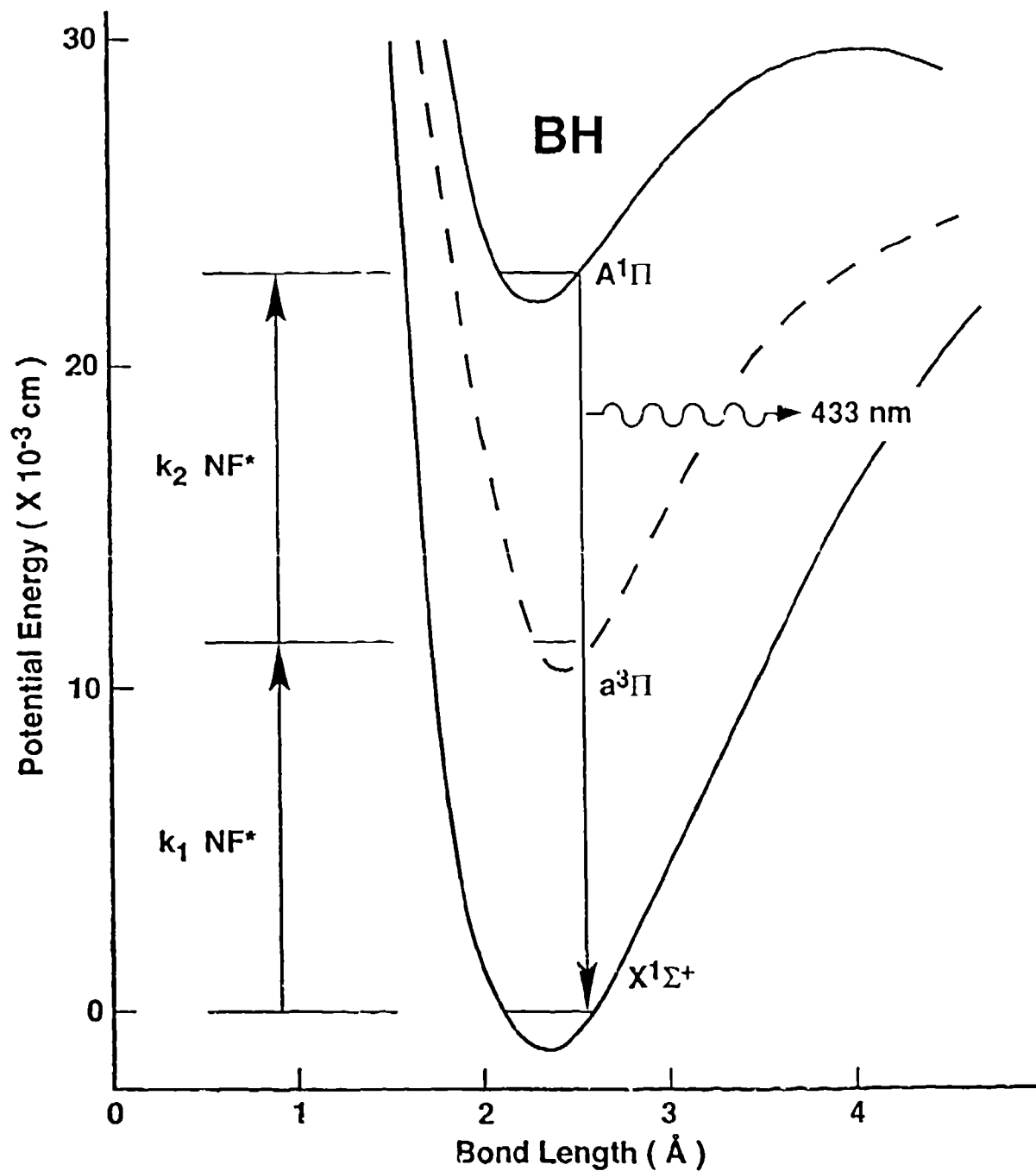


Fig. 1 Excitation of BH(A - X) chemiluminescence by NF($a^1\Delta$) energy pooling mechanism. The potential curves for the BH($A^1\Pi$) and BH($X^1\Sigma^+$) states are from Ref. 6 by Stwalley and Luh.

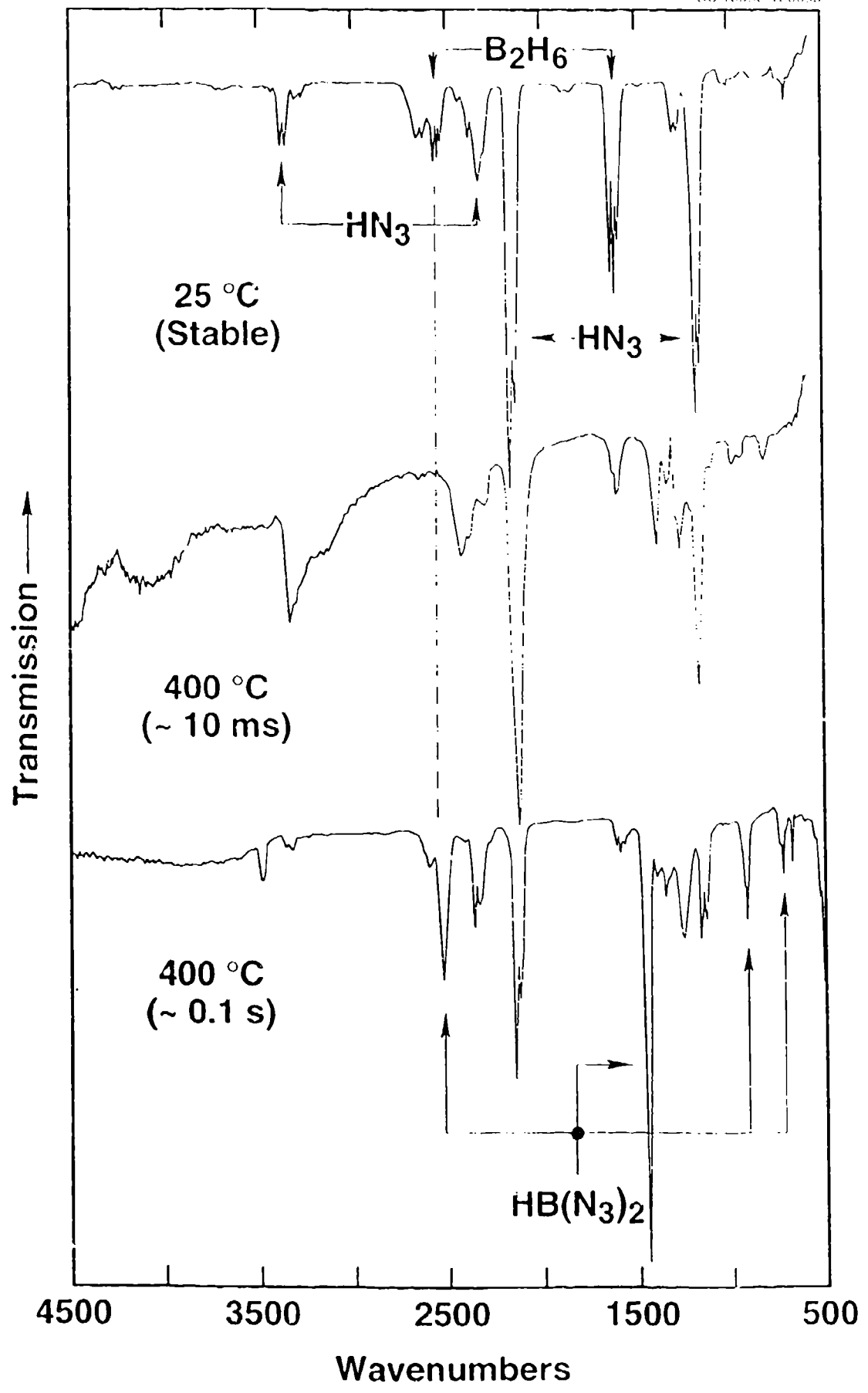


Fig. 2 Infrared absorption spectra of a reacting hydrogen azide and diborane

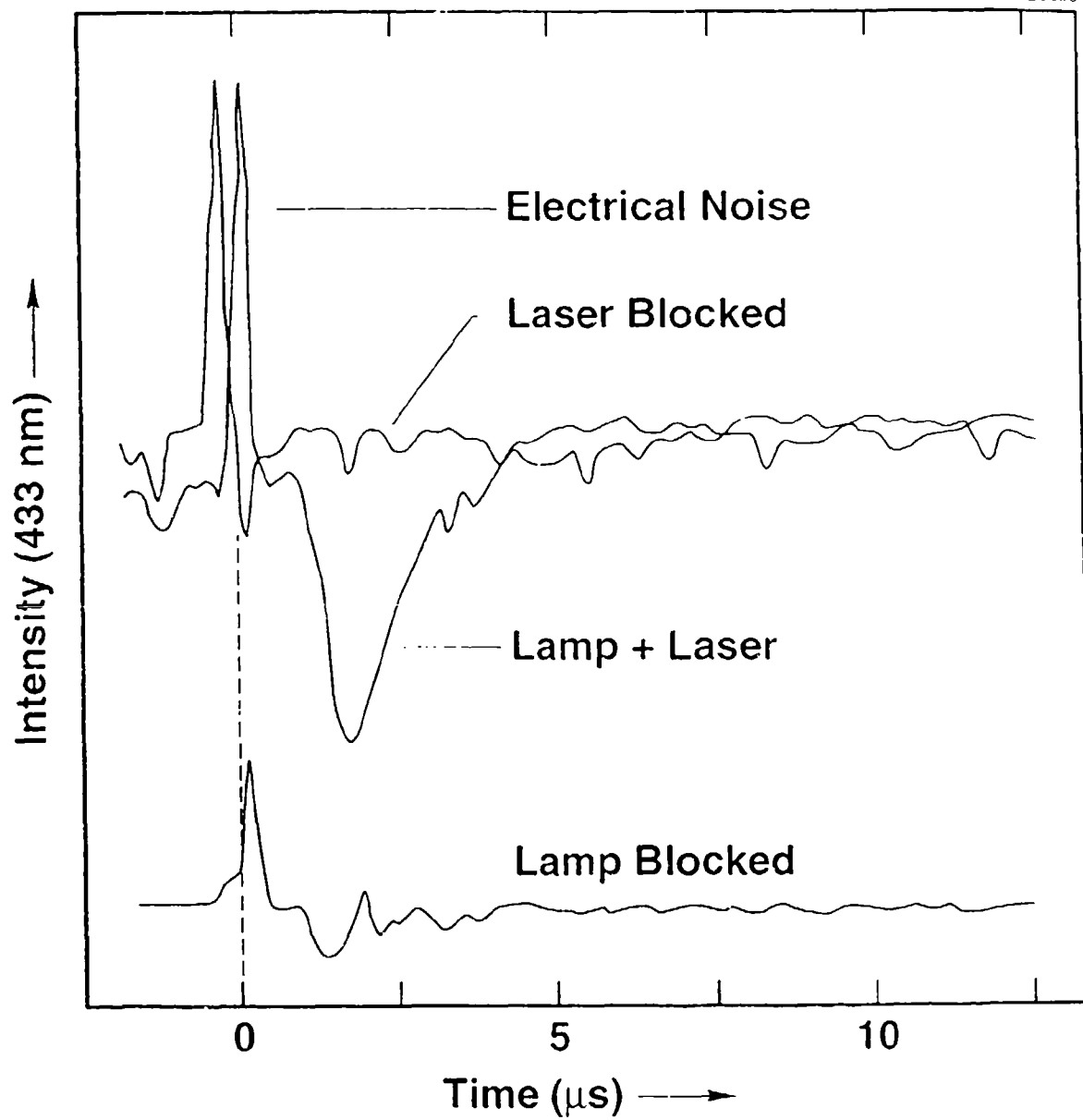


Fig. 3 Time profiles of 433 nm signals due to transmission of resonance lamp through the laser driven reactor in the absence of FN_3 .

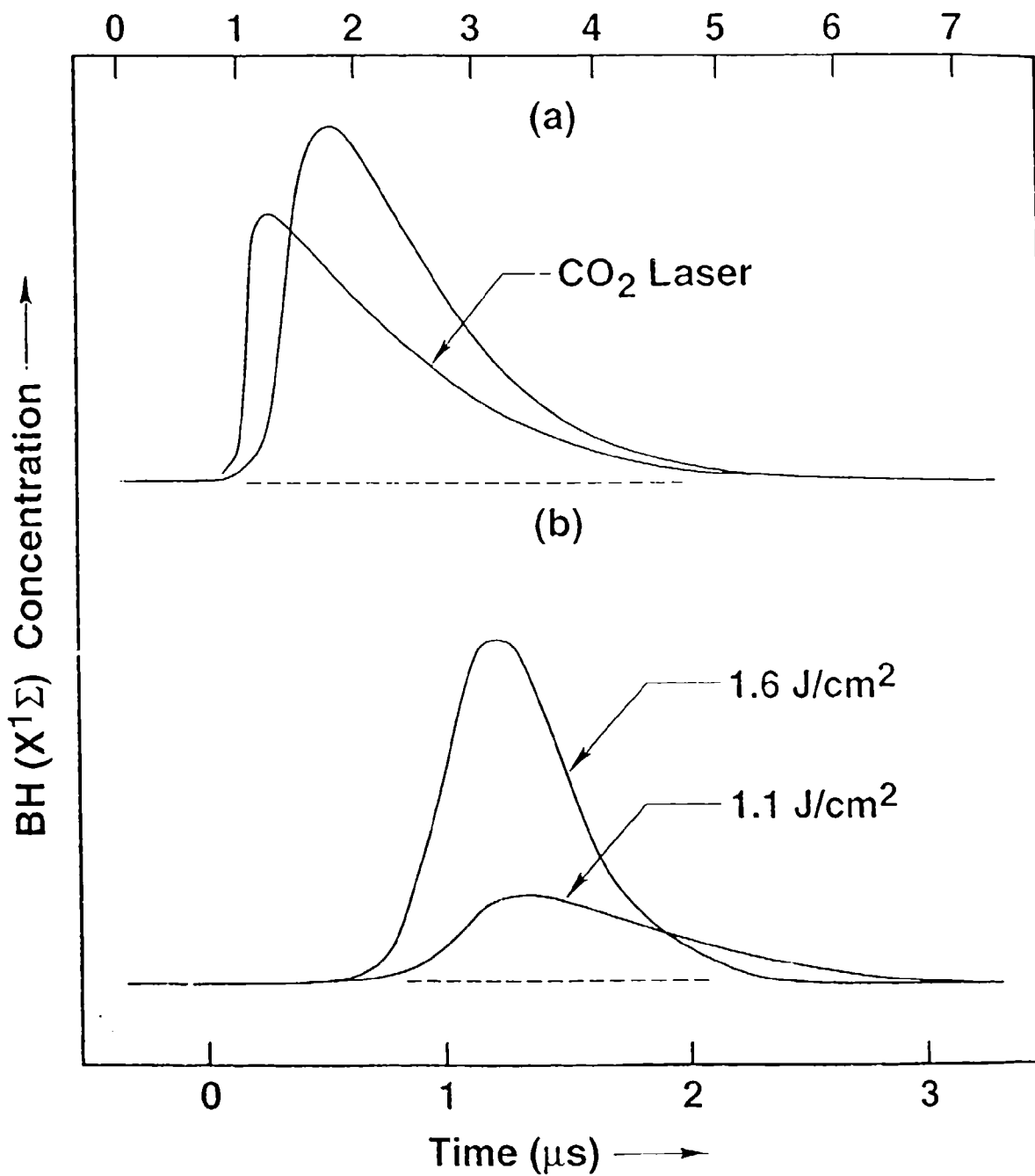


Fig. 4 Comparison of smoothed BH($X^1\Sigma^+$) and laser intensity time profiles (a), and BH($X^1\Sigma^+$) at two different laser energies (b), in the absence of FN₃.

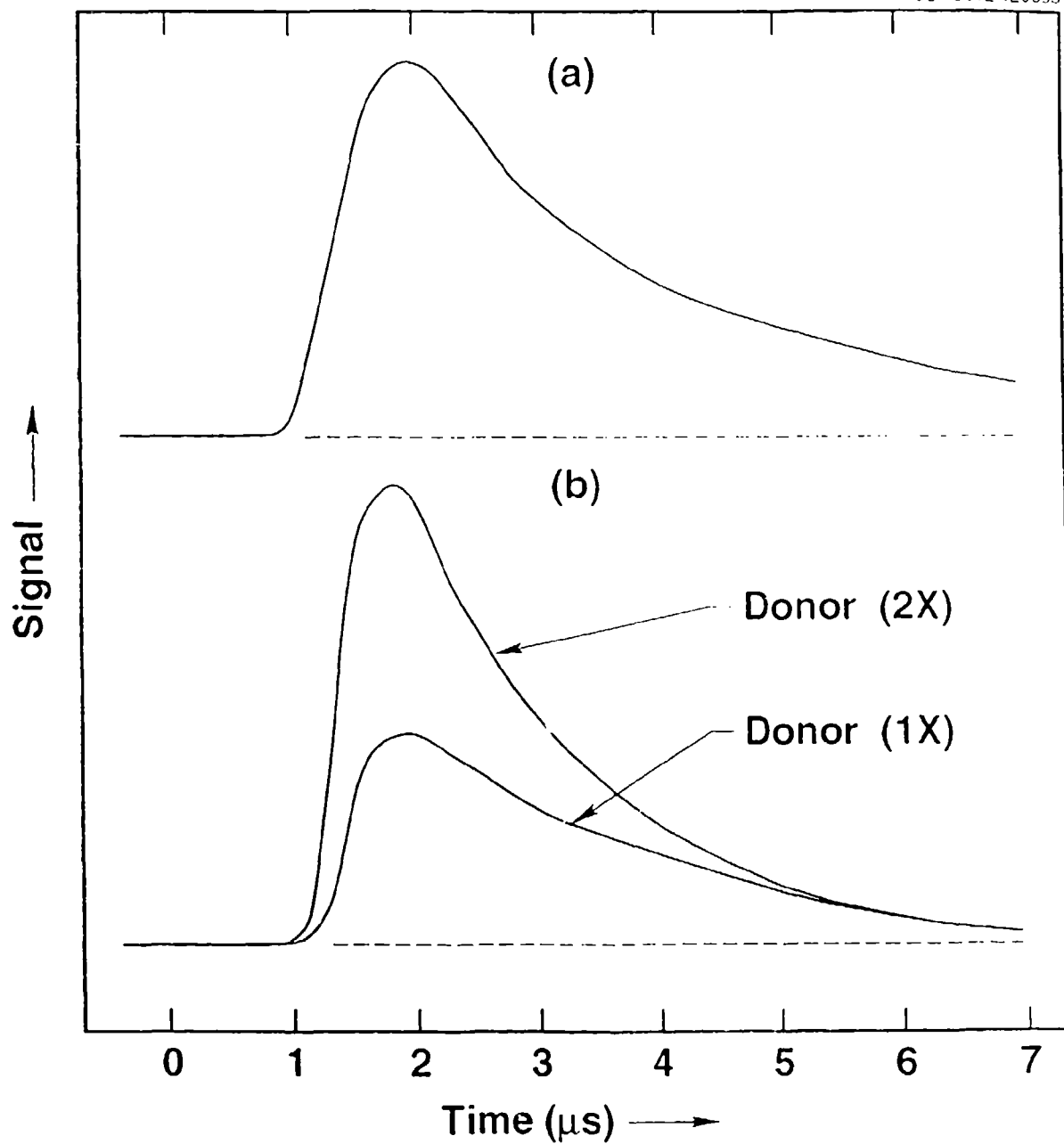


Fig. 5 Time profiles of $\text{NF}(a^1\Delta)$ in the absence of donor: (a), and $\text{BH}(A^1\Pi)$ at two levels of donor concentration (b).

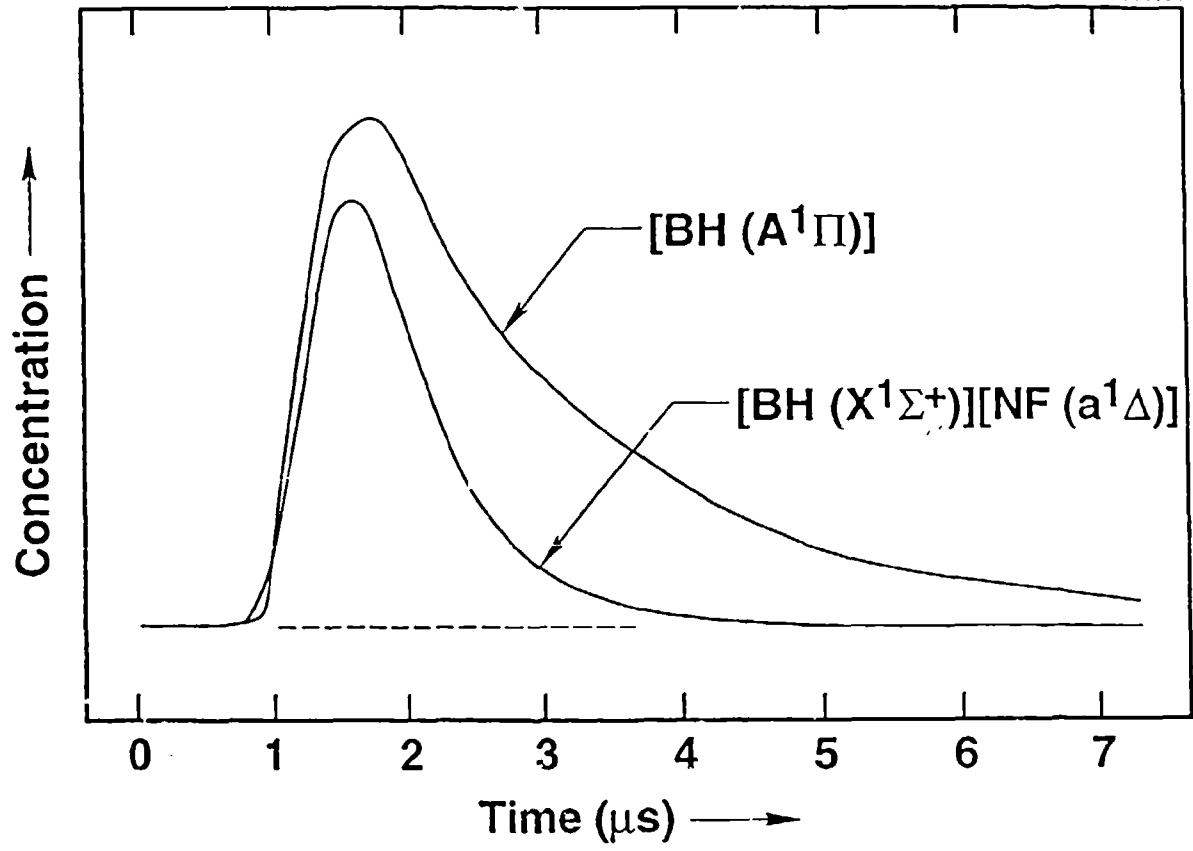


Fig. 6 Comparison of measured $\text{BH}(A^1\Pi)$ time profile with the calculated product time profile of $\text{NF}(a^1\Delta)$ and $\text{BH}(X^1\Sigma^+)$.

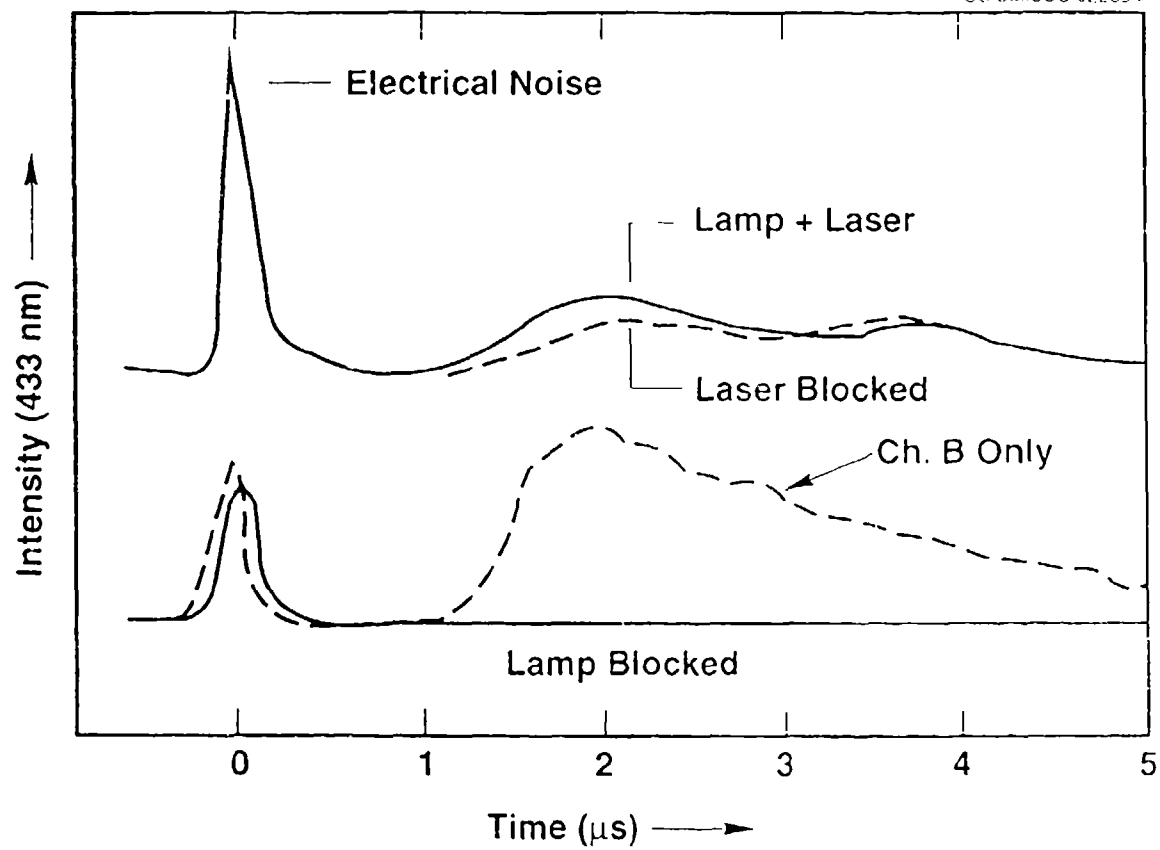


Fig. 7 Time profiles of 433 nm signals from transmission of the resonance lamp through the laser-driven reactor with FN_3 present.

Applied Physics Letters

A Chemically-Pumped Visible-Wavelength Laser with High Optical Gain

D.J. Benard and E. Boehmer

Rockwell International Science Center

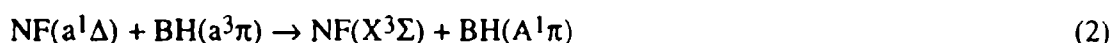
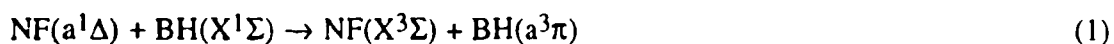
Thousand Oaks, CA 91358

ABSTRACT

Excitation of a mixture of FN_3 , B_2H_6 , SF_6 and He by a pulsed CO_2 laser generates a transient gain medium capable of supporting laser oscillation at 433 nm in an optical cavity with threshold gain of 2.5% / cm.

INTRODUCTION

Previous studies¹ have shown that large concentrations of the 1.4 eV metastable species, $\text{NF}(a^1\Delta)$, can be efficiently generated by rapid dissociation of the energetic FN_3 molecule. Also, energy transfer² from $\text{NF}(a^1\Delta)$ to ground state BH radicals pumps the allowed $\text{BH}(A-X)$ transition at 433 nm by the rapid (resonant) pooling reactions:



The FN_3 is produced by first reacting solid NaN_3 with excess stearic acid at $\sim 100^\circ\text{C}$ to generate HN_3 , and then reacting the gaseous azide product with F_2 diluted in He. The FN_3 is subsequently dissociated by mixing with SF_6 and exposure to 10.6μ radiation from a pulsed CO_2 laser. The infrared photons are resonantly absorbed by the SF_6 molecules, which become vibrationally excited, and collisional transfer of this excitation to the FN_3 causes dissociation to occur on the μs time scale.¹ If B_2H_6 is also present as a donor, a small yield of BH radicals is co-generated. Since the $\text{NF}(a^1\Delta)$ and BH radicals are liberated under premixed conditions, the rate of formation of the emitting $\text{BH}(A^1\pi)$ state is limited only by Reactions (1) and (2). Encouraged by recent measurements² of high optical gain ($\sim 10\%/cm$) in this transient chemical system, we have attempted to demonstrate laser oscillation in an optical cavity with a relatively large threshold gain to validate our previous conclusions.

The NF/BH laser concept (described above) is interesting in relation to other visible wavelength chemical laser systems, such as NF/BiF, which operate in a similar manner, because the achievable gain coefficients are substantially larger. In prior work, we obtained a gain coefficient of $\sim 3 \times 10^{-4}/cm$ at 471 nm in the NF/BiF system.³ While a detailed analysis of the NF/BiF and NF/BH systems is beyond the scope of this paper, the following approximate

comparison may nonetheless be useful. The peak $\text{NF}(a^1\Delta)$ concentrations and limiting pump rates in the two systems are nearly identical. The density of active emitter molecules in the BH system, however, is about an order of magnitude larger than in the BiF system, owing to reduced quenching by the precursor.^{2,3} This difference approximately cancels the larger radiative rate of BH (~ 6 vs 0.7 / μs in BiF) resulting in comparable inversion densities. The difference in gain therefore primarily reflects terms which influence the cross section, such as the radiative rates already mentioned, the Franck-Condon factors (0.99 for the $v' = 0$ to $v'' = 0$ transition in BH vs 0.15 for the $v' = 1$ to $v'' = 4$ transition in BiF), and the rotational spacings (~ 12 vs 0.23 cm^{-1}) which account for a seven-fold reduction of the number of transitions excited within the thermal manifold of BH. Other less critical factors influencing the cross section such as wavelength are nearly equal, while the Doppler widths (favoring BiF) and the vibrational distributions (favoring BH) tend to approximately cancel.^{3,4}

The principal difficulty in the NF/BH laser concept stems from reliance on high concentrations of $\text{NF}(a^1\Delta)$ to maintain an absolute population inversion against the fast radiative decay. These high metastable densities increase the rate of $\text{NF}(a^1\Delta)$ self-annihilation⁵ and thereby limit the time available for Reactions (1) and (2) to transfer energy to the emitting transition. Efficient power extraction is therefore critically dependent on achieving an adequate concentration of BH radicals. In general, this is a difficult (but not impossible) criterion to satisfy. For the present experiments, however, we have chosen to use B_2H_6 as a convenient BH precursor, even though the low yield of emitting molecules precludes efficient power extraction. Reliance on SF_6 as a sensitizer for the CO_2 laser also results in rapid scavenging of the BH radicals that are released.² An alternate approach that eliminates this difficulty is use of gas-dynamic shock heating to dissociate the reagents in lieu of CO_2 laser excitation. Although feasible, this approach is much more complicated experimentally,⁶ and the simpler CO_2 laser / SF_6 method of triggering the reactions was preferred to demonstrate the high optical gain of the system.

EXPERIMENTAL

The reagents (FN_3 , B_2H_6 , SF_6 and He) were transported by 0.25 inch OD stainless steel and teflon tubing at a total pressure (flow rate) of 100 Torr (15 sccm) and were mixed on-the-fly at or near the reactor inlet. The mole fractions were: $\text{FN}_3 \sim 1\%$, $\text{B}_2\text{H}_6 \sim 0.05\%$, $\text{SF}_6 \sim 5\%$ and balance He of which approximately half was used for window purges. A schematic of the reactor is shown in Fig. 1. A stainless steel cube approximately 8 cm on a side was bored along three mutually perpendicular axes to pass the gas flow, the CO_2 laser beam, and the axis of the optical resonator through a common point. The gas flow exited the reactor via a sonic orifice in route to a vacuum pump, and the ~ 2 Joule / 0.5 pps CO_2 laser beam was focused to ~ 1 cm dia. at the center of the reactor (through a NaCl window) before exiting to a beam dump and calorimeter. The optical resonator was formed by using o-rings to seal two dielectric mirrors onto support tubes extending from either side of the reactor. Both internal apertures and He purge flows were used to protect the optical surfaces. The resonator cavity, tuned to 433 nm, consisted of a totally reflecting / flat mirror and a 95% reflecting / concave (50 cm radius of curvature) mirror, spaced 26 cm apart with the gain zone midway between them. The gain length, corresponding to the diameter of the CO_2 laser beam, was ~ 1 cm. The calculated mode diameter in the gain zone is ~ 0.4 mm, and the corresponding gain volume is therefore $\sim 1.6 \mu\ell$. The limiting aperture in the resonator was 6 mm in dia.; and assuming no other losses than mirror transmission, the threshold gain was $\sim 2.5\%$ / cm, about two orders of magnitude larger than the amplification achieved in the NF/BiF system.³ Both mirrors were aligned to each other and to the limiting apertures by use of an external He-Ne laser. The cavity emission was monitored through a fiber optic cable by an optical multichannel analyzer (OMA) for spectral content, or by a 430 ± 5 nm filtered photomultiplier tube for intensity time profile. A photographic camera was used to record the spatial distribution of the output beam.

RESULTS

When the reactor was operated under nominal conditions, with the output mirror replaced by a quartz window, intense pulses of blue chemiluminescence filled the cavity aperture coincident with each shot of the CO₂ laser. Full-aperture chemiluminescence was also visible through the output mirror; however, in this case a much brighter spot of blue radiation, of ~ 1 mm diameter, also appeared in the field of view. The "lasing" spot was sensitive to mirror alignment and exhibited threshold behavior upon varying the B₂H₆ flow into the reactor (i.e., the chemiluminescence persisted over a wider range of stoichiometry than the lasing action). The OMA scan verified the cavity emission was at 433 nm, coincident with the $v' = 0$ to $v'' = 0$ band of the BH(A-X) transition.

The lasing spot was approximately isolated by a 1 mm dia. brass pinhole and the relative intensity time profile, shown in Fig. 2(a), was recorded by signal averaging on a digital oscilloscope. The measured strength of the initial sharp lasing spike (~ 250 ns duration) was subject to large (> twofold) fluctuations from shot to shot. This result is attributable to variations in the spatial profile of the CO₂ laser beam, which induced index gradients in the gain medium and observable movement of the cavity mode. In the average over several shots, therefore, the lasing signal was attenuated by random vignetting of the cavity mode on the pinhole. The time dependence of the cavity signal, however, is accurate. By comparison, the intensity of the chemiluminescence signal was nearly constant from shot to shot. Figure 2(b) shows the chemiluminescence time profile taken with a window in place of the output mirror. The cavity and chemiluminescence time profiles in Fig. 2 have been normalized at long times to allow examination of the early time differences due to stimulated emission. The onset of cavity emission is delayed (relative to the chemiluminescence) and rises more steeply, but peaks later, than the spontaneous emission time profile. Consequently, there is time interval during which the cavity output is growing while the chemiluminescence is decaying. The initial cavity output peak is also narrower in time than the corresponding pulse of spontaneous chemiluminescence.

Photographs of the aperture (in room light) and the laser beam (single shot) were taken using a camera and lens that were fixed in relation to the reactor hardware. The negatives were developed and rephotographed on a transmission microscope at fixed magnification to produce the comparison images that are shown in Fig. 3. Multiple exposures in which the number of shots was adequate to compensate the transmission of the output mirror were also recorded, and in these cases, no evidence of full-aperture chemiluminescence was recorded on the film. Since the beam is small compared to the aperture, has well-defined edges, and is more intense than chemiluminescence, it is clearly the result of laser oscillation.

DISCUSSION

The peak energy stored by $\text{NF}(a^1\Delta)$ in these experiments is about $5 \text{ J}/\ell$. With an active volume of $1.6 \mu\ell$ and a pulse width of 250 ns, maximum output at 100% efficient power extraction could be as high as 32 watts. Since B_2H_6 was used in place of an efficient BH donor, the output power was certainly much smaller. The goals of the present experiment, however, were to establish lasing and to demonstrate high levels of optical gain, both of which have been achieved. In the near future, we expect to be able to increase the output significantly by utilizing more efficient donors than B_2H_6 , and increasing the active volume of the laser mode. On a longer time scale, we envision supporting a CW laser demonstration in which shock recovery in a supersonic flow is used to dissociate the FN_3 and BH donor. In this case, outputs of up to $500 \text{ Watts}/\text{cm}^2$ of nozzle area are achievable based on a sonic velocity of approximately 10^5 cm/s (He @ 300 K), efficient power extraction, and equivalent $5 \text{ J}/\ell$ energy storage in $\text{NF}(a^1\Delta)$.

ACKNOWLEDGEMENT

This work was supported by the Innovative Science and Technology Office of the Ballistic Missile Defense Organization through the Air Force Office of Scientific Research, Contract No. F49620-90-C-0025.

REFERENCES

1. D.J. Benard, B.K. Winker, T.A. Seder and R.H. Cohn, *J. Phys. Chem.* 93, 4790 (1989).
2. D.J. Benard, E. Bochmer, H.H. Michels and J.A. Montgomery, *J. Phys. Chem.* (in press).
3. D.J. Benard and B.K. Winker, *J. Appl. Phys.* 69, 2805 (1991).
4. C.H. Douglass, H.H. Nelson and J.K. Rice, *J. Phys Chem.* 90, 6940 (1989) and references therein.
5. E. Quinones, J. Habdas and D.W. Setser, *J. Phys. Chem.* 91, 5155 (1987).
6. D.J. Benard, *J. Appl. Phys.* 74, 2900 (1993).

FIGURE CAPTIONS

Fig. 1 Schematic of the CO₂ laser driven reactor and visible laser cavity.

Fig. 2 Time profiles of 433 nm cavity emission (a) and chemiluminescence (b).

Fig. 3 Photographic comparison of the cavity aperture and output beam.

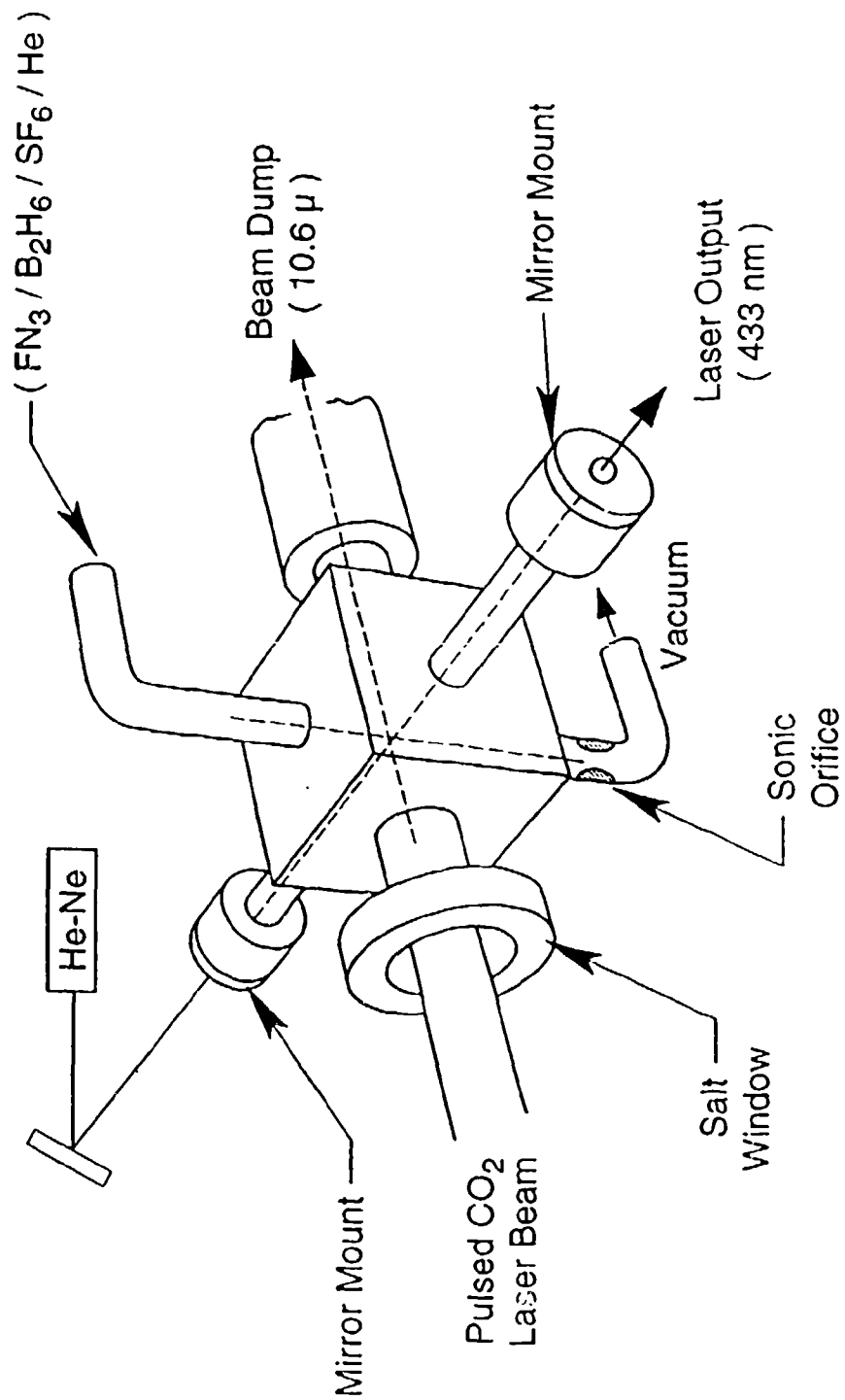


Fig. 1 Schematic of the CO_2 laser driven reactor and visible laser cavity.

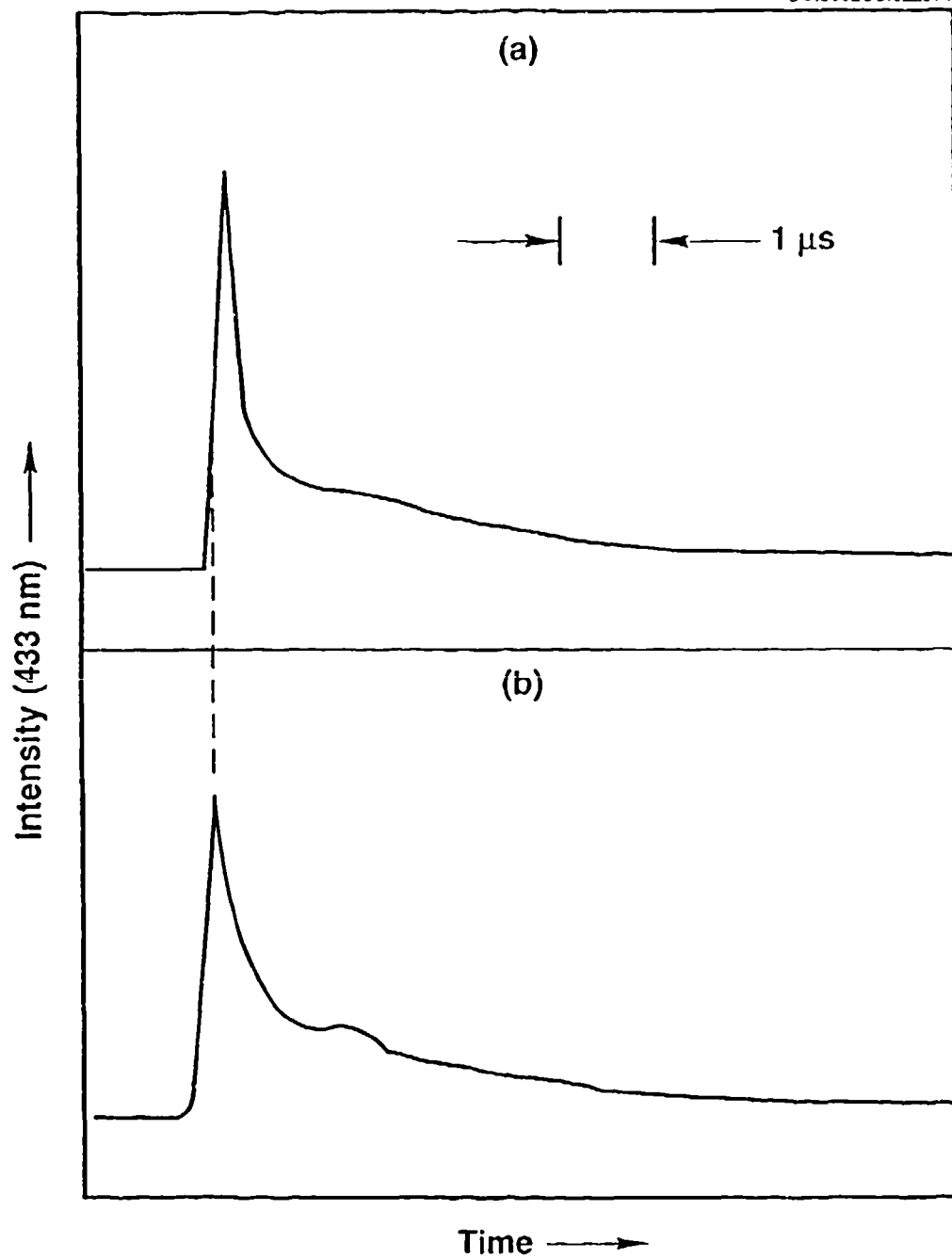
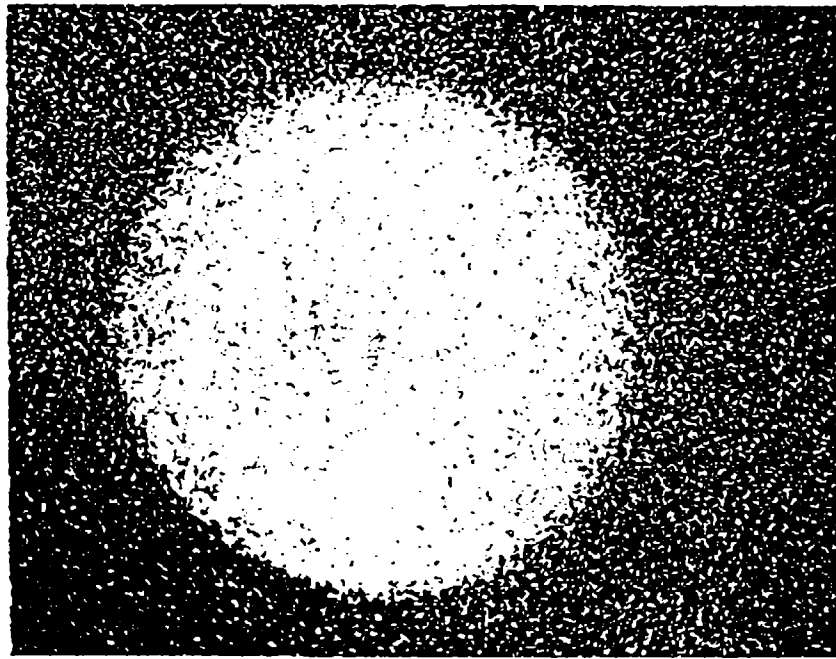
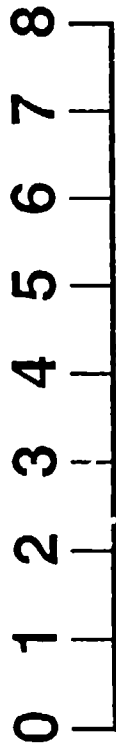


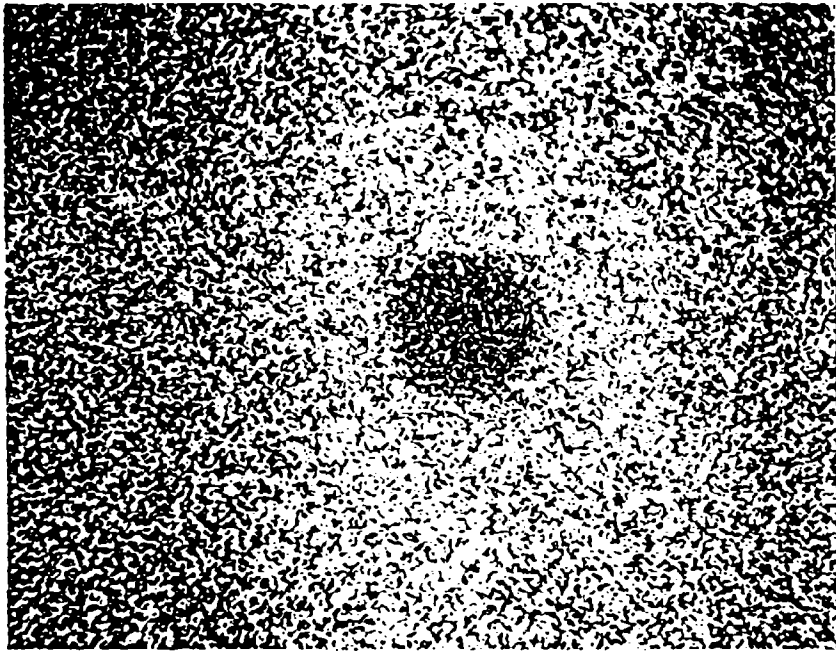
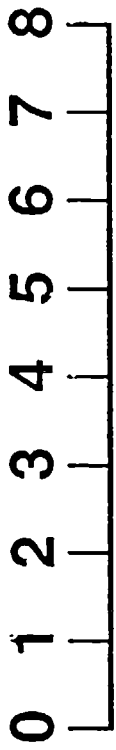
Fig. 2 Time profiles of 433 nm cavity emission (a) and chemiluminescence (b).

mm



Aperture

mm



Beam

Fig. 3 Photographic comparison of the cavity aperture and output beam.

**Investigation of the BH($a^3\Pi$) State in the Presence of
Metastable NF($a^1\Delta$)**

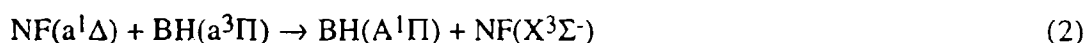
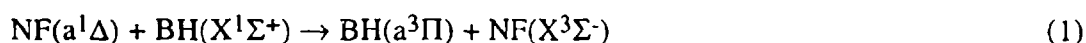
E. Boehmer and D.J. Benard
Rockwell International Science Center
Thousand Oaks, CA 91358

Abstract

Recently both gain and lasing have been demonstrated in the NF($a^1\Delta$)/BH energy transfer system. In this paper, measured emission and absorption time profiles are presented for all key electronic BH states involved in the transfer mechanism. The highly metastable BH($a^3\Pi$) state has for the first time been monitored directly by resonance absorption using a spin-allowed transition to the $b^3\Sigma^-$ state. These measurements show, in the absence of pump species NF(a), that both the BH(a) and BH($A^1\Pi$) concentrations are negligible, and the total BH concentration is adequately reflected by the BH($X^1\Sigma$) state. Also under lasing conditions, with high densities of NF(a) present, the BH(a) state is efficiently populated by collisions with NF(a) and functions as a reservoir for most of the total BH concentration. An effective absorption cross section of $\sim 1.7 \times 10^{-14} \text{ cm}^2$ has been estimated for the BH(a \rightarrow b) transition and the time profile of the total BH radical concentration is controlled by a competition between the dissociation of its precursor and rapid chemical removal. Finally, our experimental results are compared with a simple kinetics model which assumes sequential excitation of the BH(a) and BH(A) states by NF(a), leading to BH(A - X) emission and optical gain at 433 nm.

Introduction

Resonant energy transfer from metastable $\text{NF}(a^1\Delta)$ to BH radicals forms the basis for a collisionally pumped high gain visible wavelength chemical laser.^{1,2} The $\text{NF}(a)/\text{BH}$ energy transfer system is favored by high rates of energy transfer/pooling as well as the large rotational parameter and vertical nature of the BH system, which minimizes dilution of $\text{NF}(a)$ pump energy among BH rotational and vibrational degrees of freedom. The key processes in this lasing system are two spin-allowed pumping reactions followed by fast radiative decay of the $\text{BH}(A^1\Pi)$ state via emission of 433 nm photons.



The energy transfer reaction (1) is close to resonance with excitation energies of $\sim 11,442 \text{ cm}^{-1}$ and $\sim 11,000 \text{ cm}^{-1}$ for $\text{NF}(a)$ and the highly metastable $\text{BH}(a^3\Pi)$ state, respectively.³⁻⁶ The transfer rate was estimated in our previous study¹ and, as expected, is close to the gas kinetic limit with $k_1 \sim 8 \times 10^{-10} \text{ cm}^3/\text{s}$. The energy pooling reaction (2) is thought to be slower, with $k_2 \sim 3 \times 10^{-11} \text{ cm}^3/\text{s}$, because this process is slightly endothermic and the degeneracy ratio for reaction (1) is much larger than for reaction (2). The subsequent radiative decay of $\text{BH}(A)$ is fast,^{6,7} with $A_{\text{BH}} \sim 6 \times 10^6 / \text{s}$.

The reaction scheme outlined above demonstrates that $\text{BH}(a)$ is a key species in the pumping system, but this critical state has not yet been probed directly. In our previous work,¹ the role of $\text{BH}(a)$, both in the absence and presence of $\text{NF}(a)$, was inferred from observations of gain or absorption and chemiluminescence at 433 nm on the $\text{BH}(A - X)$ transition. These studies were based on a steady-state analysis, negligible quenching or back reaction, and no significant population of the $\text{BH}(a)$ state in the absence of $\text{NF}(a)$. To

confirm these assumptions, we present here results from direct absorption studies of the BH(a) state, which use a spin-allowed transition to the higher lying $b^3\Sigma^-$ state. The measured BH(X, a, A) species concentrations and inversion densities as a function of time are then compared to calculated results obtained from a kinetics code using reactions (1)–(3). These studies profited considerably from recent progress in both experimental⁸ and *ab initio*⁶ studies of the BH triplet system.

Experimental

A detailed description of the apparatus and technique for generation of NF(a) has previously been published in this journal^{1,9} and herein only details necessary to clarify the experimental results and calculations will be mentioned. Metastable NF(a) and BH radicals were generated by transient dissociation of FN₃ and B₂H₆; typical precursor concentrations were either zero or $\sim 5 \times 10^{16}$ /cm³, and either zero or $\sim 3 \times 10^{15}$ /cm³, respectively. The dissociation reactions were activated by collisions with vibrationally hot SF₆^{*} molecules produced by a pulsed CO₂ laser, and translationally hot He atoms generated by SF₆^{*} collisions with the bath gas. The chemiluminescence from the reactor was imaged onto the entrance slit of a monochromator ($\Delta\lambda = 4$ nm FWHM), and then detected using a GaAs photomultiplier tube. The generation and decay of the metastable and emitting species was monitored via NF(a \rightarrow X) emission at 874 nm and BH(A \rightarrow X) emission at 433 nm as a function of time. Both of these emissions were confined to narrow spectral regions within the resolution of the spectrometer. Absolute concentrations of both species were also recovered by photometry using calibrated filters and detectors as described in our previous publications.^{1,9} The peak NF(a) yield was $\sim 3 \times 10^{16}$ /cm³.

The time profiles of BH(X) and BH(a) were monitored by resonance absorption, both with and without NF(a) metastables present in the reactor. The resonant probe light was obtained from a pulsed 150 μ s-long high-current discharge in 10 Torr of 70% Ne and 30% He gas that was passed through a column of SiO₂ and decaborane (B₁₀H₁₄) at

ambient temperature. The lamp was fired 50 μ s prior to the CO₂ laser and delivered approximately constant intensity on the time scale of the reactive chemistry. The radiation from the resonance lamp was focused into the reactive volume and reimaged at the entrance slit of the monochromator. Assignment of the lamp emission was achieved by comparing low resolution spectra with results from the literature.⁷ The primary visible emitter was BH(A) at 433 nm. Emissions observed from 369 to 372 nm. were also assigned to the BH(b \rightarrow a) system in comparison with spectroscopic data published by Almy and Horsfall¹⁰ and recently confirmed by Brazier et al.⁸

The NF(a)/BH chemiluminescence system did not measurably emit into the spectral region of the BH(b \rightarrow a) band. Therefore, absorption of 370 nm lamp light by BH(a) in the reactor could be observed without difficulty and was used to measure the concentration of this intermediate state. Measurements at 433 nm with NF(a) present, however, were sensitive to the difference between the degeneracy weighted BH(A) and BH(X) concentrations. Consequently, the BH(X) concentration was measured without NF(a) present in the reactor to insure that [BH(X)] \gg [BH(A)]. The 433 nm data were nonetheless aliased by a background (SF₆* induced chemiluminescence) signal at the same wavelength, which was about 25% of the lamp intensity. Therefore, to measure the BH(X) absorption accurately, data from the PMT was analyzed using a two channel digital storage oscilloscope as follows. The amplified signals were directed to Channel A on even numbered CO₂ laser shots (Channel B grounded) and to Channel B on odd numbered shots (Channel A grounded) while the lamp was fired on the even numbered shots only. The data (Channel A minus Channel B) was then collected over a large (even) number of CO₂ laser pulses so that the chemiluminescence contribution was canceled. The amplifier gains on Channels A and B were carefully balanced to within 1%, and care was taken not to saturate either channel.

Results

Chemiluminescence time profiles were measured for NF(a) and BH(A), and absorption time profiles were measured for both the A - X and b - a transitions of BH. Peak amplitudes and rates of rise and fall are derived from the data and discussed briefly with respect to general observations made during previous studies.¹

Emission Typical NF(a) and BH(A) chemiluminescence signals as a function of time are shown Fig. 1. Both signals are peaked at $\sim 2 \mu\text{s}$ relative to the CO₂ laser trigger. This delay is in part due to the laser itself as well as the subsequent chemical reactions. The NF(a) decay, either in the absence or presence of B₂H₆, is dominated by NF(a) self-annihilation at a rate of $\sim 2.2 \times 10^{-12} \text{ cm}^3/\text{s}$ as given by Setser.¹¹ The B₂H₆ and its byproducts (other than BH) do not appear to be highly efficient quenchers of NF(a) as shown by earlier investigations, which found a linear scaling relationship between the chemiluminescence intensity and the initial donor concentration. Consequently, although the energy transfer from NF(a) to BH radicals is rapid, the concentration of BH is too small in these experiments for reactions (1) or (2) to compete with the loss of NF(a) due to self-annihilation. Alternate (ground state) pump mechanisms leading to BH(A) can nonetheless be excluded since the BH(A) chemiluminescence background was increased by \sim two orders of magnitude upon addition of NF(a) to the reaction system.

Single exponential fits to the measured BH(A \rightarrow X) chemiluminescence decay curve yielded a fall constant of $\sim 0.7 / \mu\text{s}$. The BH(A) signal also clearly decays more rapidly than the NF(a) signal, which can be attributed to fast chemical removal of the BH radicals. Our prior investigations¹ demonstrated that BH removal was independent of the initial FN₃ and B₂H₆ concentrations, and was therefore most likely due to reactions involving the SF₆ sensitizer.

Absorption Figure 2 shows representative BH(X - A) and BH(a - b) absorption time profiles collected with the pulsed lamp diagnostic. The temporal jitter of both the CO₂ laser and lamp discharge circuit is responsible for an uncertainty in reaction time of $\pm 0.3 \mu\text{s}$ in these data. A rising and falling exponential fit to the 433 nm absorption time profile, taken without NF(a) present in the system, yielded rise and decay constants of ~ 1.2 and $\sim 0.8 \mu\text{s}$, respectively, for the BH(X) state. The measured rate of rise of the BH(X) time profile reflects the rapid approach to a steady state relationship between BH production and fast chemical removal, while the decay reflects the slower rate of B₂H₆ dissociation as influenced by the CO₂ laser intensity time profile.¹ The peak BH(X) concentration ($\sim 0.5\%$ of initial B₂H₆) is determined using Beer's law in the limit of small absorption, based on an optical path length of ~ 1 cm and an averaged or effective absorption cross section of $\sigma_{XA} \sim 3 \times 10^{-14} \text{ cm}^2$. The largest error in this calculation is due to the assumption of ~ 600 °C rotational/translational temperatures in both the lamp and reaction cell, which are uncertain within a factor of two. The vibrational temperatures produced by the CO₂ laser are clearly higher, but the BH(A¹Π, v' > 0) populations are insignificant due to the large vibrational spacing (2367 cm^{-1})^{6,7} of this radical, as confirmed by independent measurements of the 0-0 and 1-1 band intensities.

The presence of BH(a) was monitored both with and without NF(a) present in the reactor. In the absence of NF(a), the BH(a) concentration was below the experimental detection limit. The much larger absorption signal recovered in the presence of NF(a) is shown in Fig. 2, with a statistically determined maximum fractional absorption ($\Delta I_{\text{max}}/I_0$) at 370 nm of 0.23 ± 0.05 . These results demonstrate that pumping by NF(a) dominates BH(a) production, and only negligible amounts of BH(a) are due to pumping by other energetic species such as vibrationally hot SF₆. Consequently, in the absence of NF(a) the total concentration of BH radicals is measured accurately by the BH(X) state. The rates of rise and decay of the BH(a) state were determined to be ~ 1.2 and $\sim 0.5 \mu\text{s}$, respectively.

Discussion

BH(a) State Theoretical estimates by Yarkony et al.⁶ show comparable radiative rates for the A - X and b - a transitions in B¹H. Consequently, the yield of BH(a) in the presence of NF(a) is shown to be substantial by the data in Fig. 2, since the absorption cross sections scale in proportion to the A-coefficients. Since the BH(a), BH(X) and BH(A) time profiles also approximately track each other it then follows that all three BH states are dominated by reactions (1)–(3). In this case, the approximate relations $[BH(a)] \sim (k_1/k_2) [BH(X)]$ and $[BH(A)] \sim (k_2/A_{BH}) [NF(a)] [BH(a)]$ can be derived by applying the steady state approximations ($d[BH(A)]/dt$ and $d[BH(a)]/dt \approx 0$). Favorable comparisons between these steady state estimates and the measured BH(a) and BH(A) time profiles are shown in Figs. 3 and 4, respectively.

Kinetic Model The purpose of this calculation is to remove the steady state approximations and to evaluate the adequacy of reactions (1)–(3) as a valid description of the NF(a)/BH energy transfer system. The calculation will first be anchored to the observed NF(a) concentration time profile in the absence of BH and the observed BH(X) time profile in the absence of NF(a).

Dissociation of FN₃ to NF(a) and N₂ has a barrier³ of $E_a \sim 4800 \text{ cm}^{-1}$. An estimate of the dissociation rate,⁹ as a function of temperature (T) and the concentration of collision partners [M] is given by

$$d[FN_3]/dt = -k_5 \exp(-E_a/RT) [M] [FN_3] \quad (4)$$

where $k_4 = 1.0 \times 10^{-11} \text{ cm}^3/\text{s}$. The NF(a) time profile is described by equation (5), where FN₃ dissociation (with unit branching ratio) and the self-annihilation process between two NF(a) metastables ($k_a = 2.2 \times 10^{-12} \text{ cm}^3/\text{s}$) are the only significant contributing factors.

Quenching of NF(a) by FN₃ is negligible since these species do not overlap for a significant period of time.

$$d[\text{NF(a)}]/dt = -d[\text{FN}_3]/dt - k_a [\text{NF(a)}]^2 \quad (5)$$

Heat generation in this reaction system is initiated by pulsed CO₂ laser production of vibrationally hot SF₆, which in turn heats the bath gas due to rapid V-T relaxation.^{12,13} Terms that contribute to the temperature time profile are given by the equation

$$dT/dt = \{ \sigma [\text{SF}_6] I(t) + Q_d d[\text{FN}_3]/dt + k_a [\text{NF(a)}]^2 Q_a \} / C \quad (6)$$

where the SF₆ absorption cross section for 10.64 μm light can be estimated according to Lenzi et al. ($\sigma \sim 4.6 \times 10^{-19} \text{ cm}^2$)¹² and I(t) represents the experimentally determined CO₂ laser energy time profile. The terms $Q_d \sim 12,000 \text{ cm}^{-1}$ and $Q_a \sim 50,000 \text{ cm}^{-1}$ correspond to heat released by the FN₃ dissociation and NF(a) self-annihilation processes, respectively, and C is the heat capacity of the gas. Figure 5 presents a comparison between the measured NF(a) chemiluminescence time profile and a satisfactory fit to a computer solution of equations (4)–(6) in which the critical parameters of the model (k_a , E_a) were varied only slightly ($\pm 10\%$) from their independently established values.

The B₂H₆ dissociation is likely to be a two-step process leading initially to BH₃, which subsequently dissociates to BH and H₂.^{13,14} The kinetics of B₂H₆ dissociation in the presence of a pulsed CO₂ laser field, vibrationally hot SF₆ and translationally hot He is complex, and a satisfactory model is beyond the scope of this paper. Consequently, the total BH radical concentration time profile data (see Fig. 2, open circles) was fit to a double exponential function of time, [BH(t)], as shown in Fig. 6. The fit parameters (a, b, c) were then frozen and held constant in all subsequent calculations. The resulting conservation relation

$$[\text{BH}(t)] = \{ a \exp(-bt) - \exp(-ct) \} = [\text{BH(A)}] + [\text{BH(a)}] + [\text{BH(X)}] \quad (7)$$

was subsequently combined with the rate equations for the BH(a) and BH(A) states

$$d[\text{BH(a)}]/dt = k_1 [\text{BH(X)}] [\text{NF(a)}] - k_2 [\text{BH(a)}] [\text{NF(a)}] \quad (8)$$

$$d[\text{BH(A)}]/dt = k_2 [\text{BH(a)}] [\text{NF(a)}] - A_{\text{BH}} [\text{BH(A)}] \quad (9)$$

corresponding to reactions (1)–(3) to yield a kinetic model for the time dependence of all three BH states.

Modeling of the coupled NF(a)/BH system can then be performed by simultaneous computer integration of equations (4)–(9) with knowledge of the initial experimental parameters, provided the presence of NF(a) does not affect [BH(t)], since it has previously been established that BH radicals, as well as the associated donors and byproducts, do not influence the NF(a) concentration. A prior comparison,¹ however, of the BH(A) chemiluminescence time profile with the calculated product of the measured NF(a) time profile and the measured BH(X) time profile (without NF(a) present) demonstrated that NF(a) does not impact the production of BH radicals significantly except at long reaction times, well after the peak chemiluminescence. The correlation of this model with the coupled NF(a)/BH data therefore depends primarily on the rate parameters k_1 and k_2 .

Figure 7 shows the results of a fully coupled NF(a)/BH calculation, based on the original estimates for k_1 and k_2 (from our prior work)¹ using no other variable rate parameters except those that were fixed by correlation of the model to the uncoupled NF(a) and BH(X) time profile data. In this case, most of the BH concentration is resident in the intermediate $a^3\Pi$ state. Figures 8 and 9, respectively, present a comparison of the measured 433 nm chemiluminescence and 370 nm absorption data (both with NF(a) present) vs the corresponding calculated time profiles. The BH(A) concentrations in Fig. 8 are based on absolute photometry using the data in Fig. 1 and the known value of the transition rate,¹⁴ while the BH(a) concentrations in Fig. 9 are derived from the data in Fig. 2 (closed circles) using $\sigma_{\text{ab}} \sim 1.7 \times 10^{-14} \text{ cm}^2$ as a fitting parameter. Figure 10 compares the calculated

inversion density on the BH(A - X) transition with the previously measured experimental gain time profile, which is converted to equivalent concentration data by dividing out a best fit stimulated emission cross section. Use of an alternative high-intensity (short-pulse) resonance lamp in the gain experiment (to overcome the intense 433 nm chemiluminescence)¹ unfortunately precludes an absolute comparison with this gain model, since the effective cross sections are sensitive to rotational/vibrational temperatures which vary widely in these radiation sources. The temporal correlation of the experimental data to the model calculations in Figs. 8 - 10, however, clearly demonstrates that the previously estimated values of k_1 and k_2 are satisfactory, and moreover that interactions of BH(a) and BH(A), with species other than NF(a), is insignificant compared to the rates of metastable induced transfer/pooling or radiative on the A - X transition. Therefore, all the approximations used and results obtained in our previous analysis have been verified.

Summary

For the first time relative concentration time profiles were measured for all three key electronic states in the NF(a)/BH system. The highly metastable BH(a) state was directly monitored by resonance absorption, and an effective absorption cross section for the BH(a \rightarrow b) transition was estimated as $1.7 \times 10^{-14} \text{ cm}^2$. In the absence of NF(a), the BH(a) and BH(A) densities were both negligible, and the total BH population was estimated adequately by measurements of the BH(X) concentration. With NF(a) present, the BH(a) state concentration was controlled by collisions with the metastable pump species and this state functions as a reservoir for most of the total BH population. The measured time evolution of the relative BH(X, a, A) concentrations (as well as inversion density) was adequately reproduced by a simple kinetics model based on a two-step cyclic pumping mechanism to populate the BH(A) state by energy pooling through the BH(a) intermediate state, followed by radiative decay at 433 nm to the BH(X) ground state. Details regarding the production and decay of the net BH population, however, remain to be determined.

Acknowledgements

This work was supported by the Innovative Science and Technology Office of the Ballistic Missile Defense Organization, which provided funding through the Air Force Office of Scientific Research, Contract No. F49620-90-C-0025.

References

1. D.J. Benard, E. Boehmer, H.H. Michels and J.A. Montgomery, Jr. *J. Phys. Chem.* (in press).
2. D.J. Benard and E. Boehmer *J. Appl. Phys.* (in press).
3. H.H. Michels, United Technologies Research Center (E. Hartford, CT) private communication.
4. R. Saxon, SRI International (Menlo Park, CA) private communication.
5. M. Bettendorf and S.D. Peyerimhoff, *Chem. Phys.* **1985**, *99*, 55.
6. L.A. Pederson, H. Heetema and D.R. Yarkony *J. Phys. Chem.* (submitted).
7. W.T. Luh and W.C. Stwalley *J. Molec. Spectrosc.* **1983**, *102*, 212.
8. C.R. Brazier and P.G. Carrick *Abstracts of the High Energy Density Matter Contractors Meeting* **1994**.
9. D.J. Benard, B.K. Winker, T.A. Seder and R.H. Cohn, *J. Phys. Chem.* **1989**, *93*, 4790.
10. G.M. Almy and R.B. Horsfall *Phys. Rev.* **1937**, *51*, 491.
11. K. Du and D.W. Setser *J. Phys. Chem.* **1993**, *97*, 5266.
12. U. Lenzi, E. Molinari, G. Picciacchia, V. Sessa and M.L. Terranova *Chem. Phys.* **1990**, *142*, 463 and 473.
13. J.K. Rice, N.J. Caldwell and H.H. Nelson *J. Phys. Chem.* **1989**, *93*, 3600.
14. C.H. Douglas, H.H. Nelson and J.K. Rice *J. Chem. Phys.* **1989**, *90*, 6940.

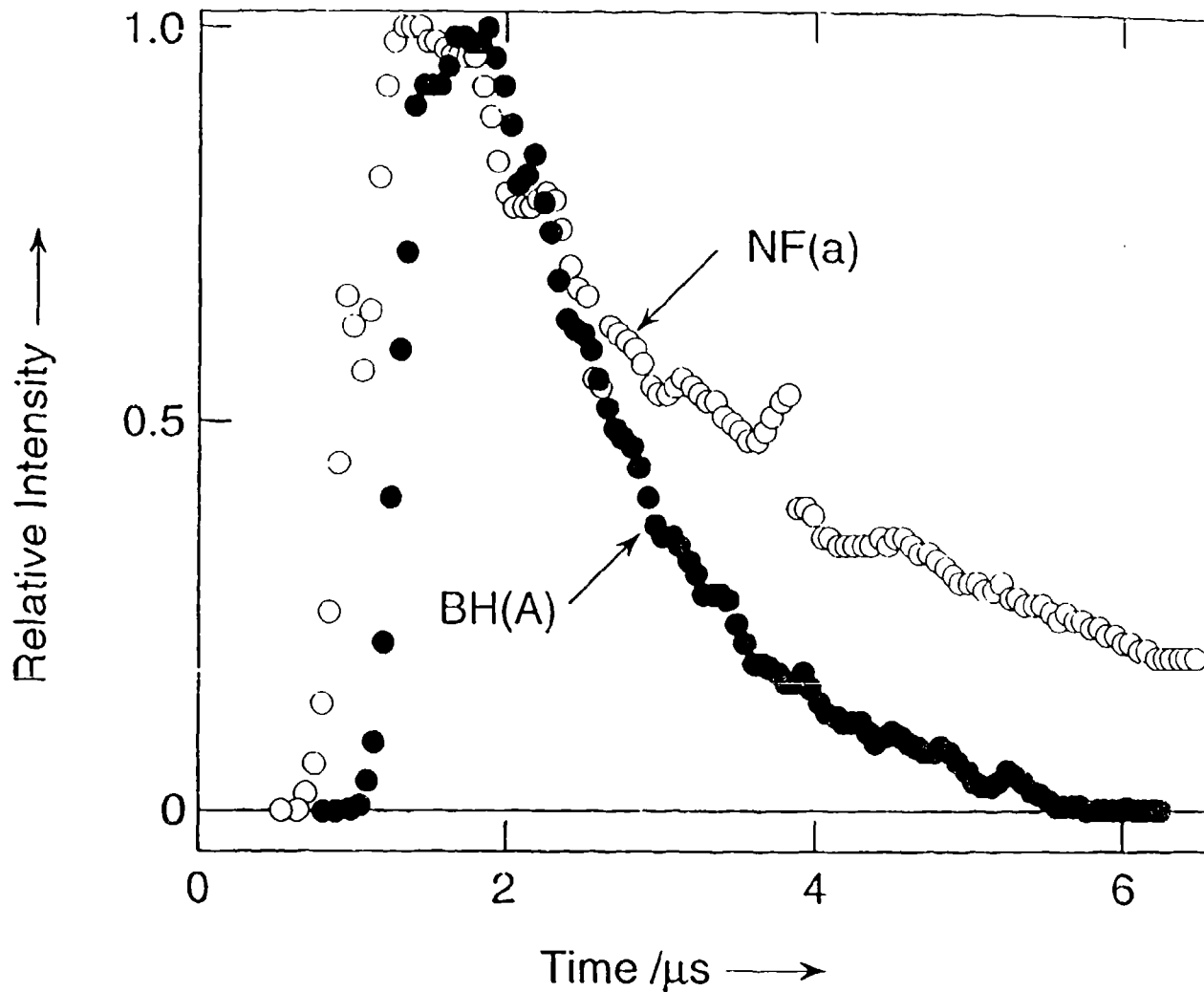


Fig. 1 NF(a) and BH(A) chemiluminescence signals as a function of time after the CO₂ laser trigger. The NF(a) intensity time profile was adjusted to appear on the same ordinate scale as the BH(A) intensity time profile.

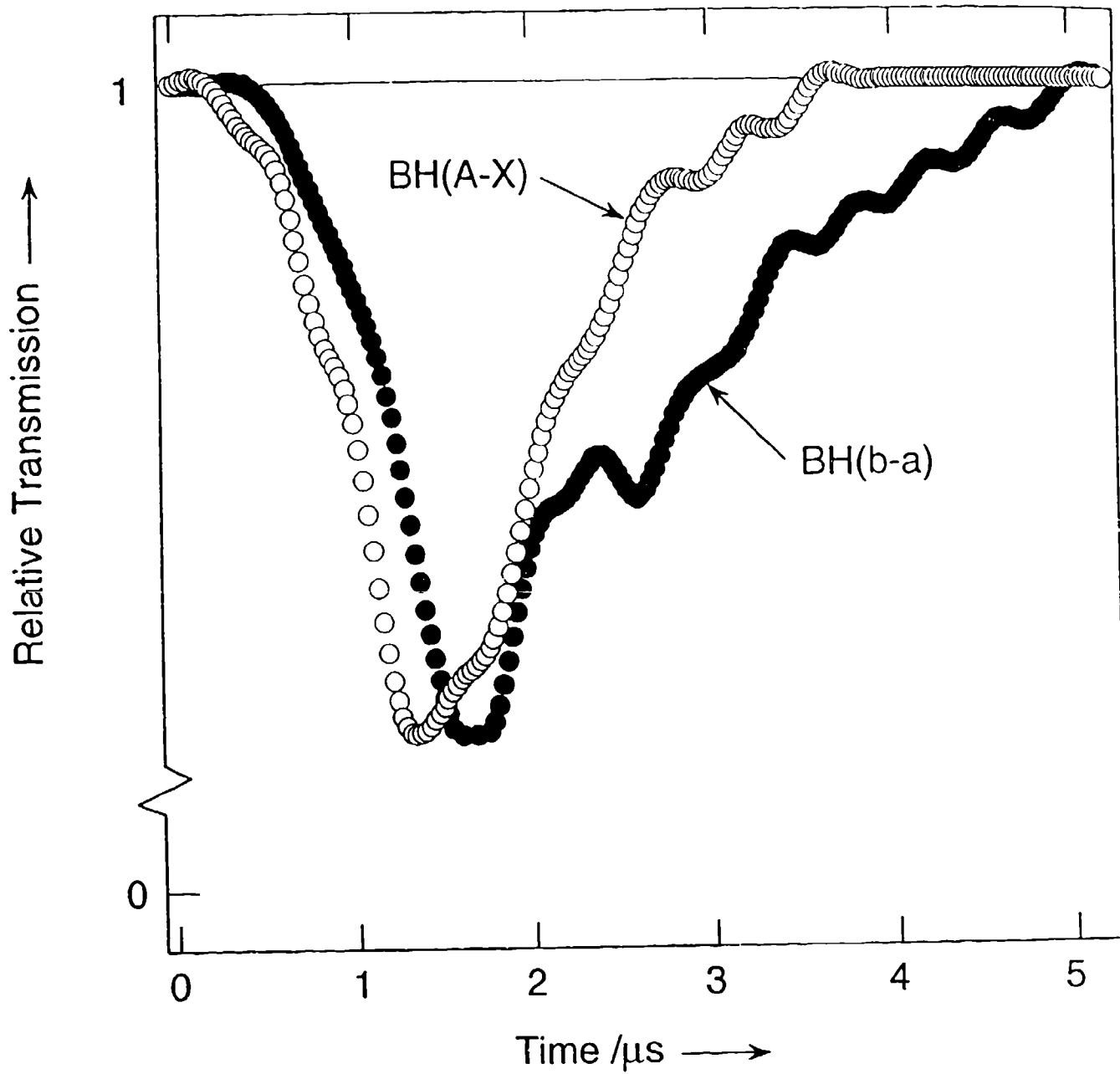


Fig. 2 Typical unscaled experimental absorption time profiles at 433 nm (open circles, $NF(a) = 0$) and 370 nm (filled circles, peak $[NF(a)] \sim 3 \times 10^{16} / \text{cm}^3$).

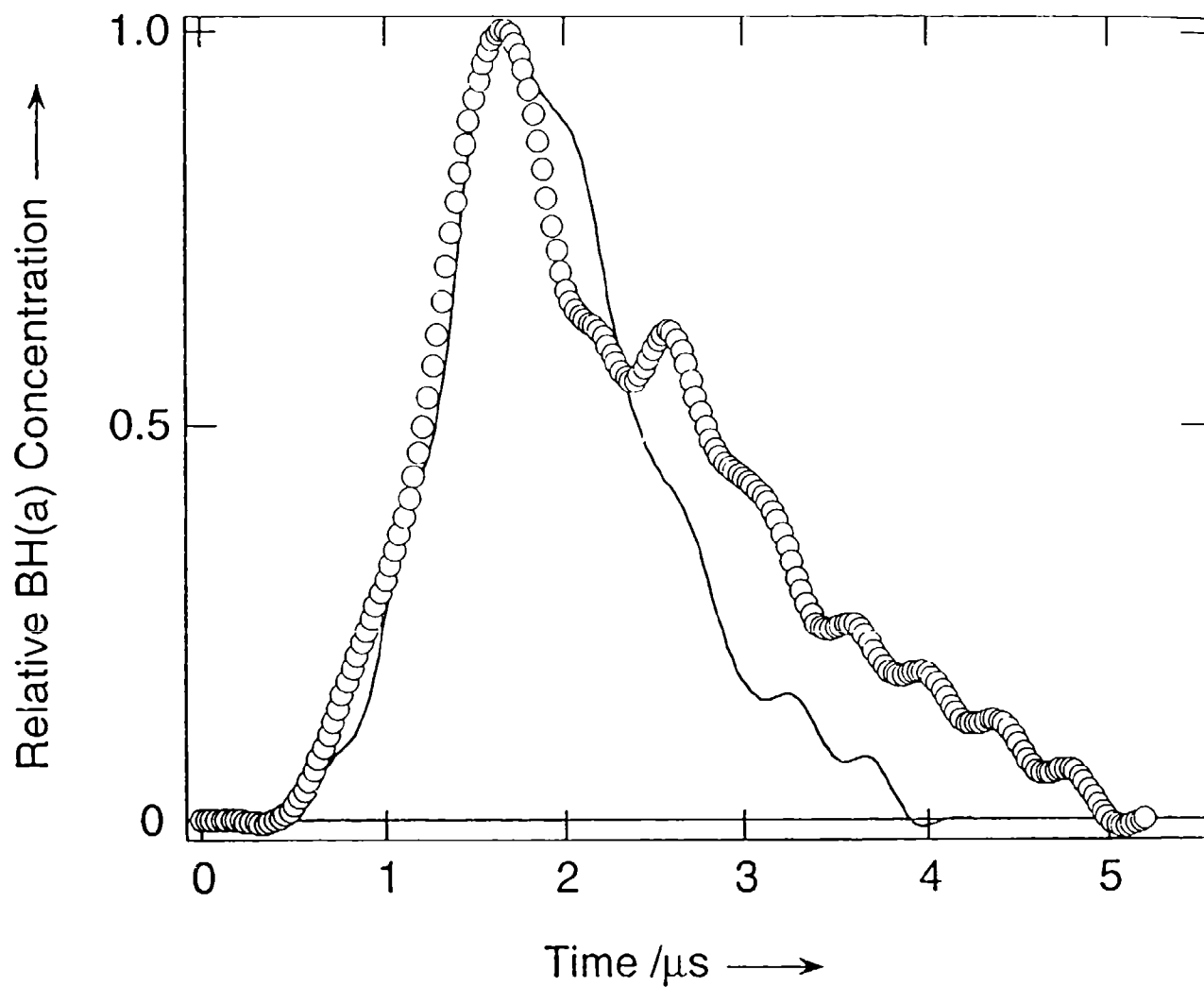


Fig. 3 Normalized BH(a) populations as a function of time. Experimental values are represented by open circles. The solid line shows the BH(a) population calculated using a steady state approximation.

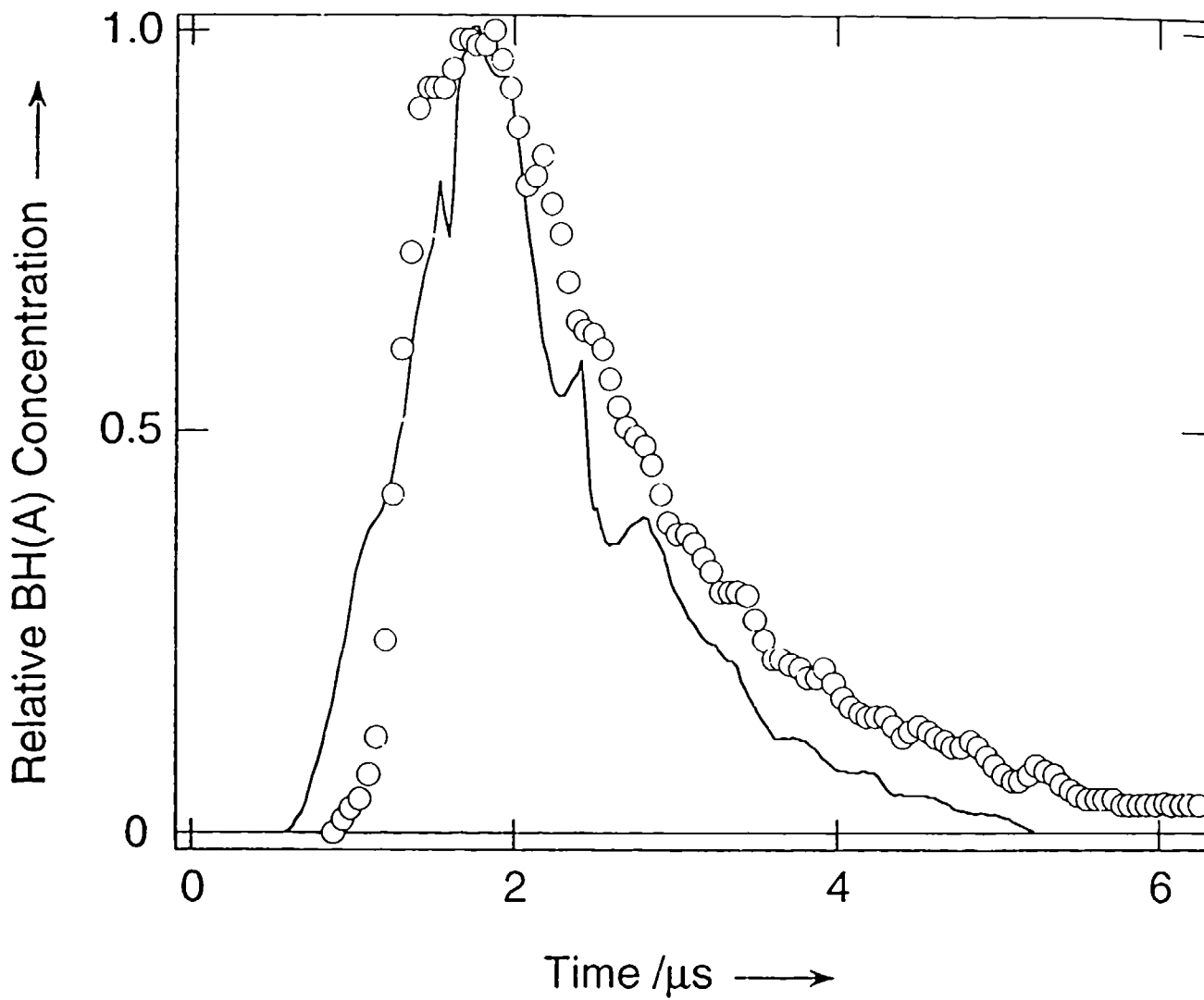


Fig. 4 Normalized BH(A) populations as a function of time. The measured BH(A) population is represented by open circles. The solid line indicates the BH(A) population calculated using a steady state approximation.

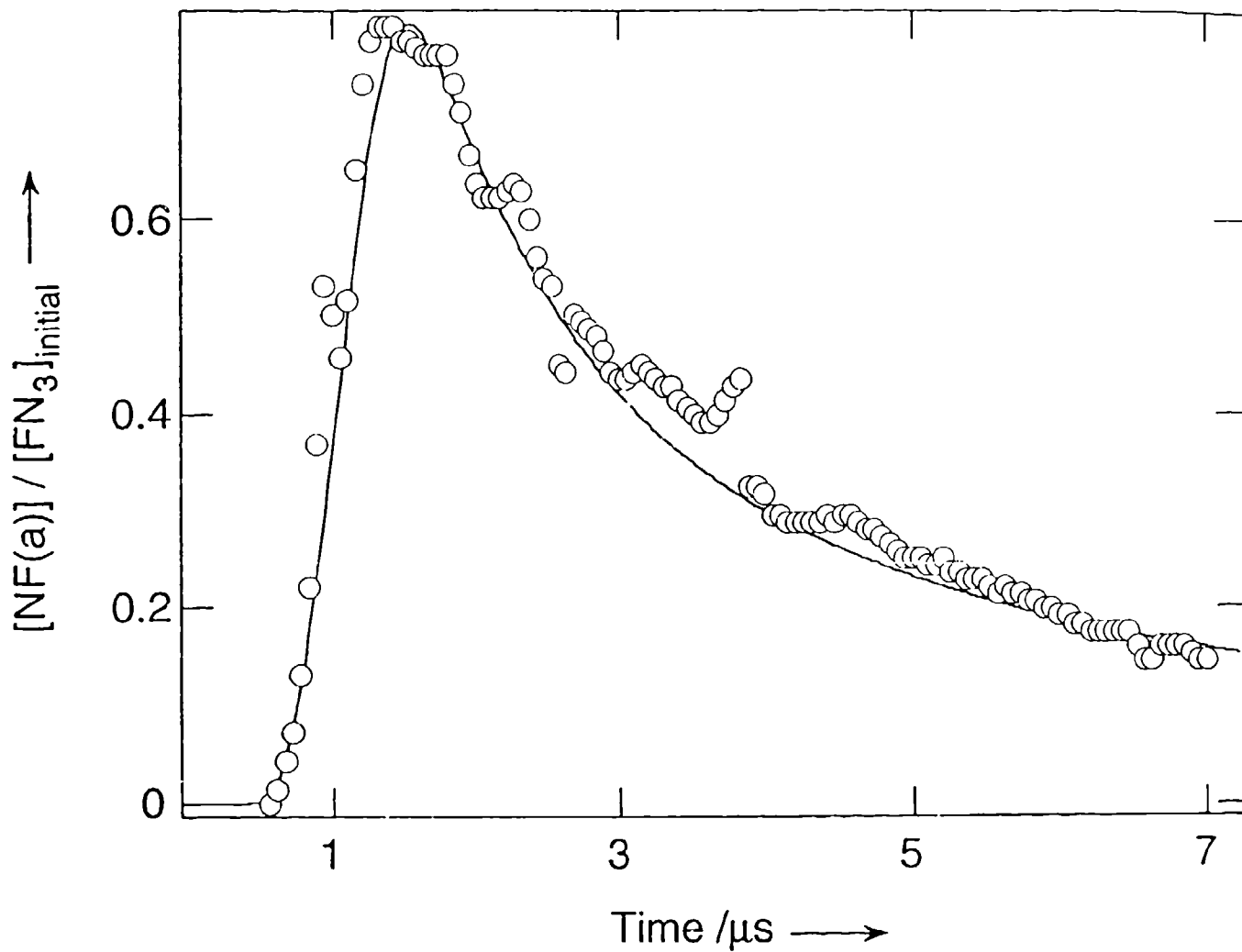


Fig. 5 NF(a) time profiles in the absence of B_2H_6 . The experimental values are represented by open circles and the solid line is from a kinetics model.

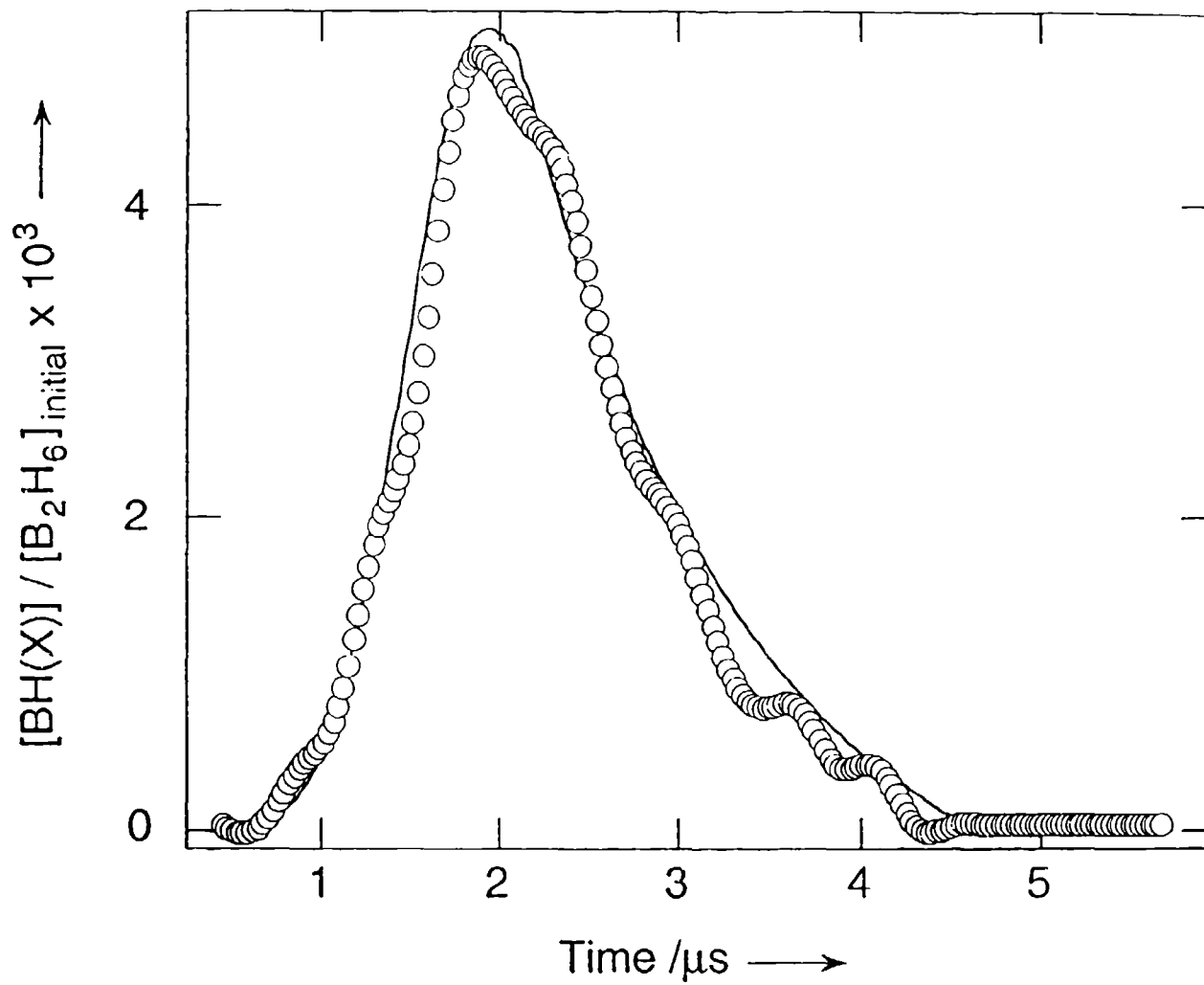


Fig. 6 BH(X) time profiles in the absence of NF(a). The experimental values are represented by open circles and the solid line is a fit to a rising and falling exponential.

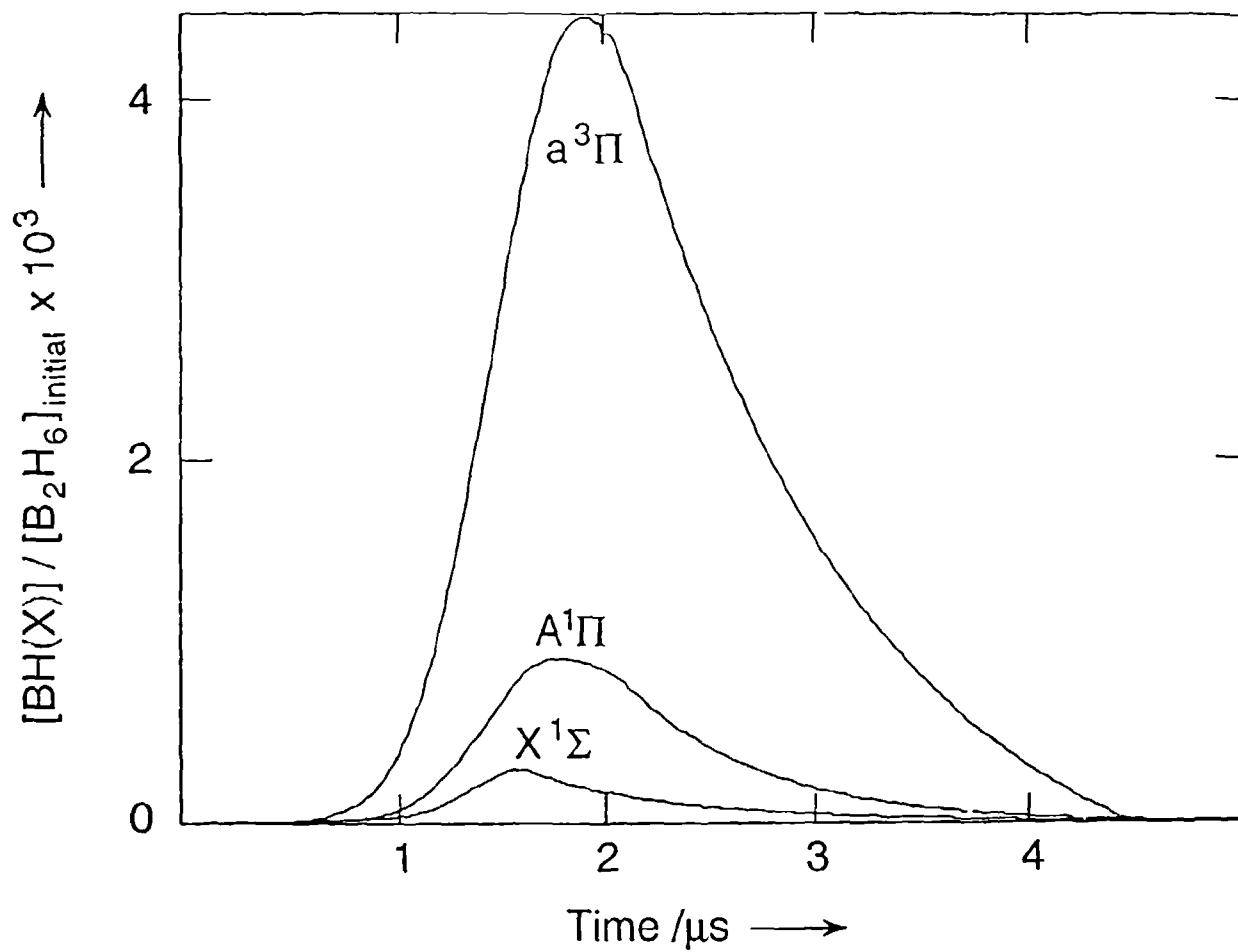


Fig. 7 Calculated BH concentrations in the presence of pump species NF(a) obtained by a kinetics code based on reactions (1)–(3).

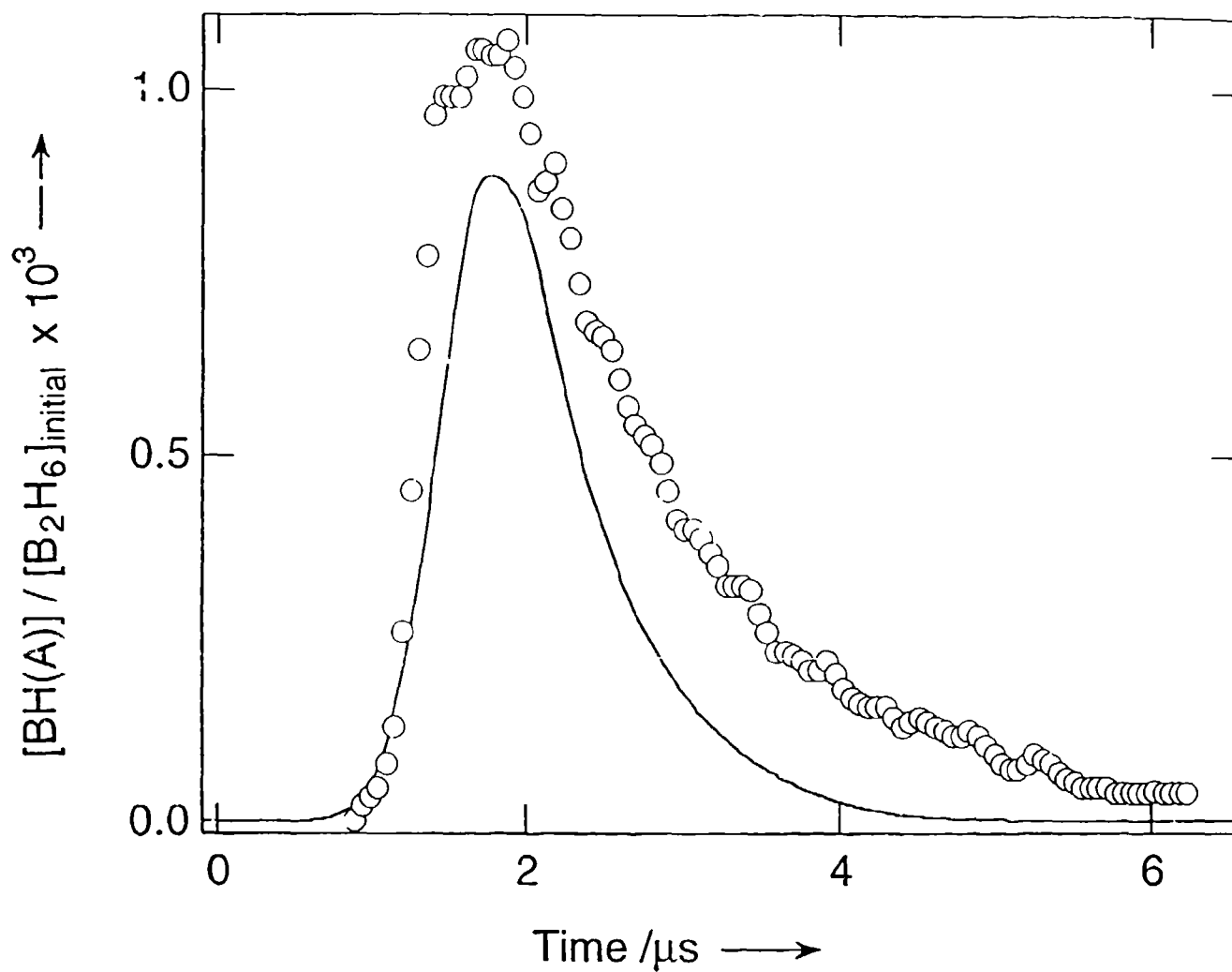


Fig. 8 Comparison of measured (open circles) and calculated (solid line) BH(A) time profiles.

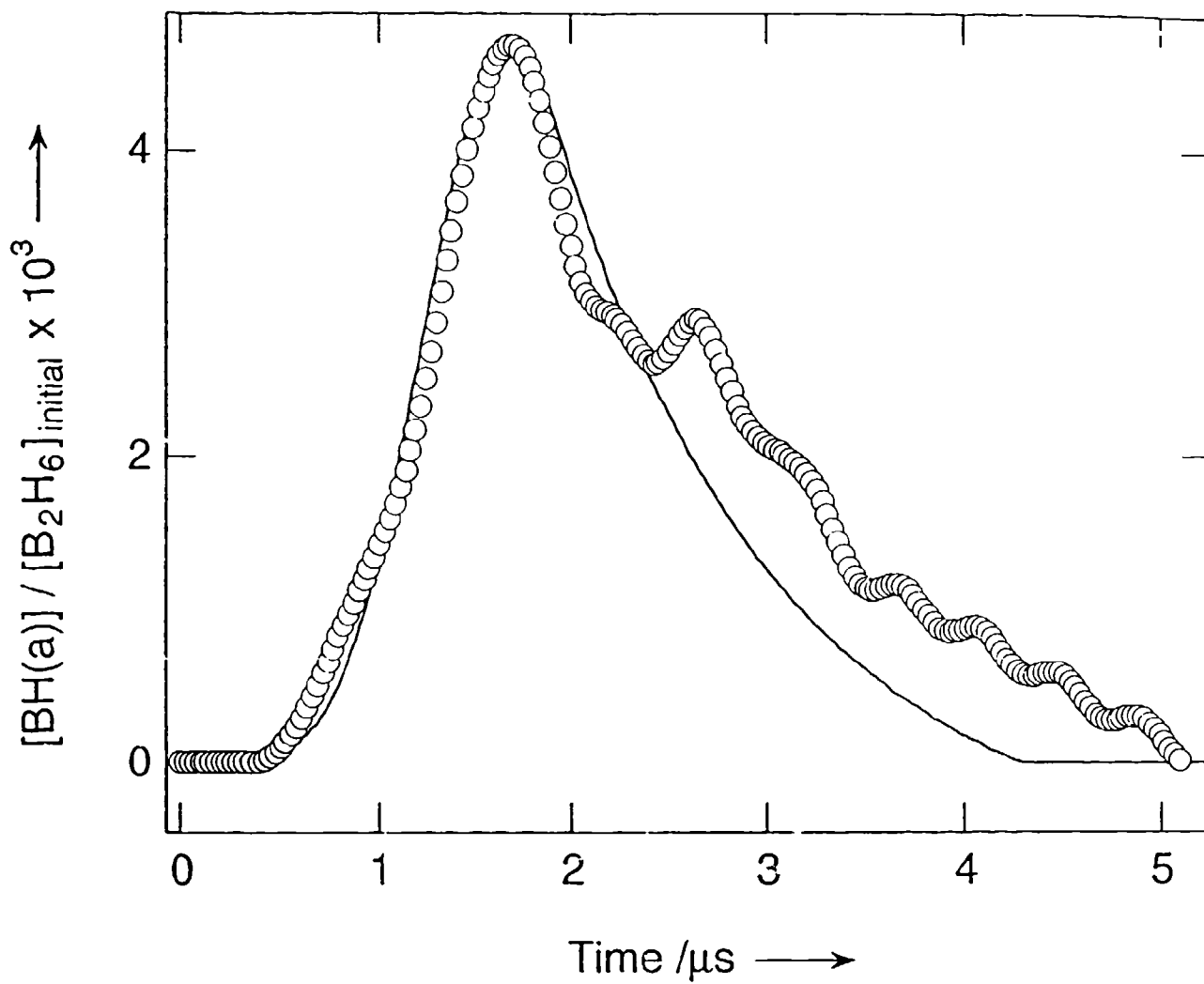


Fig. 9 Comparison of measured (open circles) and calculated (solid line) BH(a) time profiles.

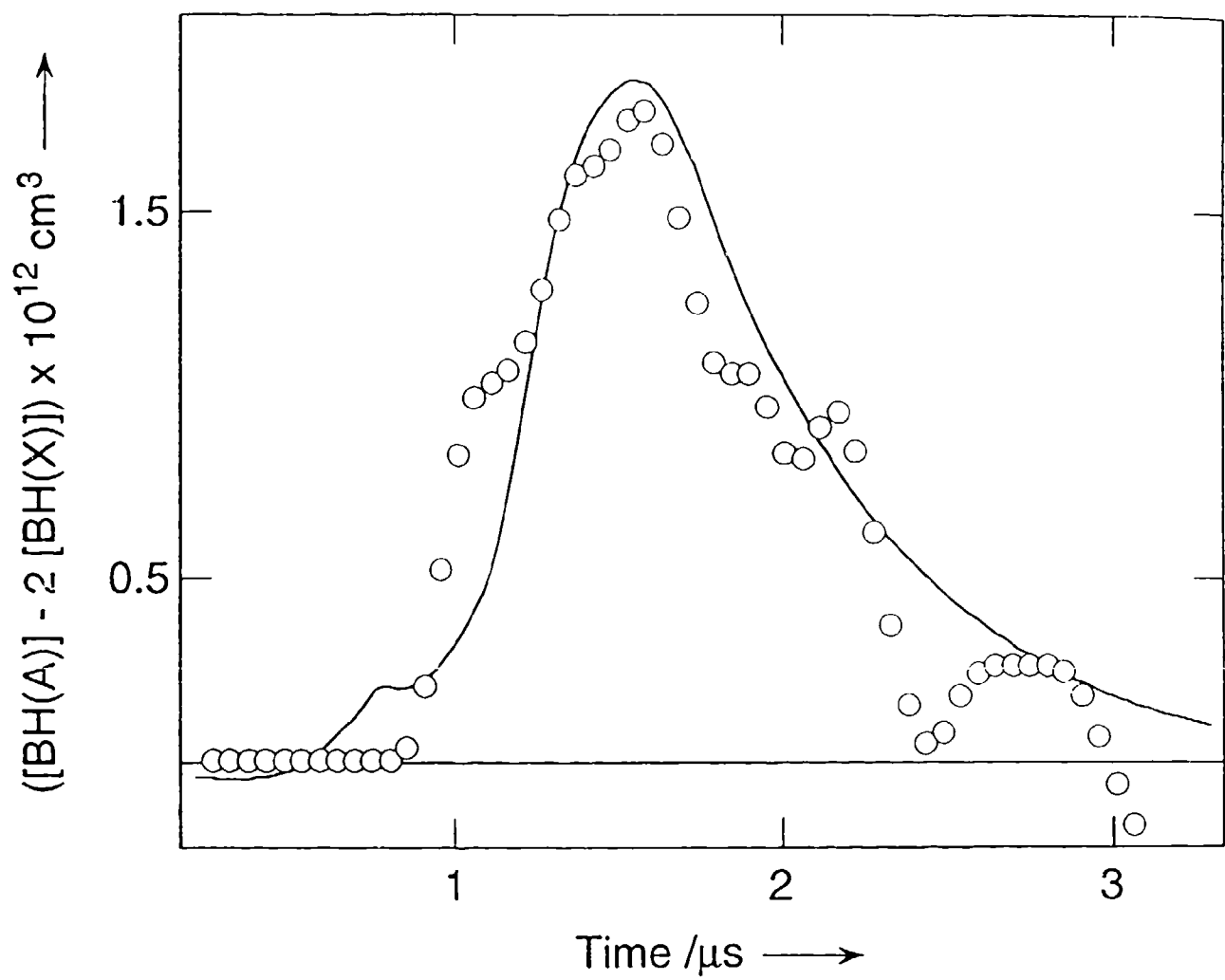


Fig. 10 Comparison of measured¹ (open circles) and calculated (solid line) BH(A - X) inversion densities as a function of time.

Production of IF[B³Π(0⁺)] in the Presence of High NF(a¹Δ) Densities

**E. Boehmer and D.J. Benard
Science Center
Rockwell International Corporation
Thousand Oaks, CA 91360**

and

**S.J. Davis
Physical Sciences, Inc.
Andover, MA 01810**

Abstract

The energy transfer reaction of NF(a¹Δ) with IF(X¹Σ⁺, v["]) was studied at total system pressures of 25 Torr. Metastable NF(a) was generated by quantitative thermally induced FN₃ dissociation, and IF(X, v["]) was produced in the fast reaction of F-atoms with I₂ or CF₃I. The F-atom concentration generated by IR multiphoton dissociation of SF₆ was $2 \pm 1 \times 10^{14}/\text{cm}^3$. Under experimental conditions optimized for maximum IF[B³Π(0⁺)] yield, peak NF(a) density was determined to be $3 \pm 2 \times 10^{15}/\text{cm}^3$. The corresponding peak IF(B) concentration was $2 \pm 1 \times 10^{11}/\text{cm}^3$, and the concentration ratio [IF(B)]/[NF(a)] was independent of the I-atom source used. The emissions of other excited species (NF(b) and I_{1/2}) were strongly coupled and due largely to impurities in the FN₃ flow, which could be removed by a dry ice trap. A vibrational temperature of 1200 ± 100 K for the IF(B) state was determined from its emission spectrum, and the IF(B) kinetic lifetime was calculated from time-resolved fluorescence decay profiles that were also independent of the I-atom source. Reactant gases such as HN₃, FN₃ and vibrationally hot SF₆ did not affect the kinetic lifetime of IF(B); but for SF₆ concentrations $> 5 \times 10^{15}/\text{cm}^3$, IF(X, v["] = 0) removal was observed. Losses of IF(B) due to thermal dissociation and reaction with NF(a) or its byproducts therefore appear to be negligible. The relative ground state populations of IF(X, v["] = 0-2) were measured and were thermal at $T = 2000 \pm 100$ K for both I₂ and CF₃I precursors; IF(X, v["] > 2) was not observed due to experimental limitations. The results support a mechanism involving efficient E-V transfer from NF(a) to IF(X), generating a steady state IF(X, v["] ≥ 10) population independent of the IF source used. This mechanism allows for more than one photon per IF produced (IF recycling) and consequently yields a larger specific energy than the mechanism that is operative at low NF(a) densities. Since large IF(X) concentrations can be generated, the feasibility of a vibrationally assisted IF(X) transfer laser depends principally on management of the IF(X, v["]) distribution under high particle density conditions.

1. Introduction

Due to potential application in chemical laser schemes, resonant energy transfer reactions between a metastable molecule and an emitting species have been an active area of research. The chemical oxygen iodine laser (COIL) is an efficient near-infrared laser based on resonant energy transfer. The required large $O_2(a^1\Delta)$ concentrations are produced in the base catalyzed reaction of Cl_2 with H_2O_2 , followed by energy transfer to lasing species $I_{1/2}$, which subsequently emits light at 1315 nm.¹⁻⁶ Gain and unsaturated lasing in the visible spectral range have also been demonstrated recently for two $NF(a^1\Delta)$ pumped systems.⁷⁻¹⁰ Metastable $NF(a)$ is isoelectronic to $O_2(a)$ and can be generated efficiently in the gas phase by rapid thermally induced quantitative dissociation of FN_3 at concentrations up to $3 \times 10^{16} /cm^3$.^{11,12} These metastable densities are comparable to the $O_2(a)$ concentrations used in COIL devices. As part of a continuing effort in the identification of suitable energy-transfer partners for both $O_2(a)$ and $NF(a)$, several candidate emitters have been investigated intensely. Studies of the collisional and radiative dynamics of the $IF(B)$ state have shown this emitter to be an especially promising visible chemical laser candidate.¹³⁻²⁰

An optically pumped $IF(B \rightarrow X)$ laser has been demonstrated by Davis.²¹⁻²³ The viability of the IF system as a visible wavelength chemically pumped laser candidate has been shown by several studies involving collisional resonant energy transfer between the $IF(X)$ and metastables such as $O_2(a)$, $N_2(A)$, $NF(b)$ and $NF(a)$.²⁴⁻³⁸ Especially interesting are low pressure (0.1–3 Torr) results for $O_2(a)$ and $NF(a)$ as $IF(X)$ pump species since, in these cases, the metastable concentrations can be scaled up to the levels needed for an operational device. The $NF(a)$ densities used in the $IF(X)$ studies to date, however, are much smaller than current generation capabilities.³⁹

Pumping of $IF(X)$ to the B-state by these metastables is attributed to a two-step (energy pooling) mechanism because the electronic excitation energy of either $O_2(a)$ or $NF(a)$ is insufficient for a direct one-step process.^{24,39} However, low pressure studies also demonstrated that when $IF(X)$ is vibrationally excited to levels $v'' \geq 10$, direct one-step collisional excitation can be achieved, as illustrated in Fig. 1.³⁹ The $IF(B)$ yield also improved dramatically when pumped by $O_2(a)$ or $NF(a)$, if $IF(X, v'')$ was quantitatively produced in the fast reaction of F-atoms with molecular iodine.^{24,39}



This reaction efficiently yields nascent IF(X) at high vibrational energy levels ($v'' \geq 10$) and only a negligible fraction of $I_{1/2}$.⁴⁰⁻⁴²

Based on the experimental findings obtained under low pressure conditions, a vibrationally assisted transfer laser concept that relies on resonant energy transfer from NF(a) to vibrationally excited IF(X) has been proposed.³⁹ The first step of the suggested mechanism is the production of hot IF(X, $v'' \geq 10$) by reaction (1). These molecules subsequently collide with metastable NF(a) to form electronically excited IF(B), which reverts to the ground state by radiative decay.³⁹



Inversion in the system is possible because the Franck-Condon factors of the IF(B \rightarrow X) transition⁴³ favor radiation from $v' = 0$ in the B state to vibrationally excited $v'' \sim 5$ energy levels of the ground state that are not significantly populated under thermal conditions.^{44,45}

Previous studies³⁹ have demonstrated linear scaling of the IF(B) yield with NF(a) concentration up to $1 \times 10^{11}/\text{cm}^3$. In this paper we report an investigation of the vibrationally assisted pumping scheme in the presence of much larger transient NF(a) concentrations that were obtained by pulsed CO₂ laser dissociation of FN₃ in the presence of He buffer gas and SF₆ sensitizer. To assess the feasibility of a vibrationally assisted NF/IF transfer laser and the validity of the proposed pump mechanism for high pressure conditions (25 Torr), parameters that relate to the pump rate such as the [IF(B)]/[NF(a)] concentration ratio were measured. Due to the high frequency of collisions in this environment, nonradiative IF(B) decay processes may also successfully compete against reaction (3). These losses include quenching by reagents or by-products, energy pooling with NF(a), and thermal excitation into IF(B, v') states above the predissociation limit.¹⁶ The effect of reactants HN₃, FN₃ and vibrationally hot SF₆ on the IF(B) kinetic lifetime ($\tau_{\text{rad}} \sim 7 \mu\text{s}$)¹⁶⁻¹⁸ was consequently studied by time-resolved pulsed LIF measurements, which also determined the vibrational distribution of the $v'' = 0, 1, 2$ levels of the IF ground state.

The proposed laser concept also hinges on scaling the $\text{IF}(X, v'' \geq 10)$ concentration. Measurements using both vibrationally hot and cold sources of $\text{IF}(X)$ gave insight into the degree of thermalization prior to reaction with $\text{NF}(a)$. Vibrationally hot $\text{IF}(X)$ was obtained using reaction (1), and cold $\text{IF}(X)$ was produced in the fast quantitative reaction of CF_3I with F-atoms.^{46,47}



If the $\text{IF}(X, v'')$ nascent vibrational distribution produced via reaction (1) is sufficiently thermalized prior to reaction with $\text{NF}(a)$, the $\text{IF}(B)$ yield at constant metastable concentration is expected to be independent of the I-atoms source used. Finally, at higher metastable concentrations, the pumping mechanism may change, since the dynamics of $\text{IF}(B)$ formation may be dominated by collisions with $\text{NF}(a)$ and other energetic species, such as $\text{I}_{1/2}$, $\text{NF}(b)$ or vibrationally hot SF_6 , rather than by collisions with the He bath gas. The presence of these energetic species was therefore monitored by their emissions, and the contributions to production of $\text{IF}(B)$ were evaluated.

2. Experimental Section

Hydrogen azide was prepared by the reaction of NaN_3 with excess stearic acid at a temperature of 100–120°C.^{11,12} The azide product was diluted to 5% in He and stored in a stainless steel tank for later use. The FN_3 (~ 3% in He, 3.5 scc/s total flow) was then generated on-line by the reaction of HN_3 with ~ 10% F_2 in He at 25°C and 350 Torr total pressure. The FN_3 flow was either directly expanded across a 100 μm dia. pinhole orifice and subsequently mixed with a continuous flow of SF_6 and other reactants (CF_3I or I_2 , both diluted in He), or first passed through a dry ice-cooled trap to remove impurities. Iodine was introduced by passing metered amounts of He carrier gas through a room temperature I_2 saturator. The mole fraction of I_2 in the effluent was determined from the known vapor pressure curve.⁴⁸ The combined flows were directed via teflon tubing to a windowed stainless steel reaction cell, and all flows were controlled via Tylan electronic mass flow meters. The gas stream was then excited by 10.64 μm radiation from a pulsed CO_2/TEA laser (repetition rate ~ 0.5 Hz), which was focused to a 1 cm^2 cross sectional area at the center of the reaction cell and terminated on a pulse calorimeter. The sidearms of the reactor that conducted the CO_2 laser beam were purged with He, and all gases exited via a sonic orifice to vacuum. The CO_2 laser was operated at constant output energy, and variable attenuators were placed between the laser and reaction cell to adjust the fluence.

The CO₂ laser was used to produce vibrationally excited SF₆ molecules as well as F-atoms by IR multiphoton dissociation.⁴⁹ Vibrationally hot SF₆ contributes to the thermally induced dissociation of FN₃, which is used to generate NF(a). The yield of metastables was monitored by the intensity of NF(a → X) chemiluminescence at 874 nm⁵⁰ that was transmitted through an interference filter and measured by a calibrated silicon photodiode or a GaAs photomultiplier tube (PMT). The transient signals from the detectors were passed through a calibrated wide bandwidth preamplifier and averaged on a digital oscilloscope that was synchronized to the CO₂ laser. Peak NF(a) concentrations were determined by absolute photometry based on knowledge of the A-coefficient,⁵¹ collection geometry and measured filter transmission factors. The total number of F-atoms generated by SF₆ multiphoton dissociation was determined by titration with H₂, or alternately, by titration with I₂. The vibrationally hot HF titration product was observed by its (3-0) overtone emission.⁵²



The F-atoms produced by dissociation of SF₆ also reacted with I₂ according to reaction (1) to yield IF(X) and I-atoms. In the presence of excess I-atoms the following additional processes occur:⁵³⁻⁵⁵



The NF(b) emission at 528 nm,⁵⁰ and the IF(B) emission at 583 nm,⁵⁰ were each filtered by a monochromator and detected using a PMT, as functions of the I₂ concentration. The endpoint of the titration was determined by the onset of strong additional NF(b) emission over the background NF(b) radiation due to a minor (1%) FN₃ dissociation channel.^{11,12} The titration using I₂ yielded results that were in good agreement with the previous titration using H₂.

The reactor conditions were optimized for IF(B) production by varying the total reactor pressure, CO₂ laser fluence, and concentrations of FN₃, SF₆ and I₂. Optimal IF(B) generation was obtained at 3.2 J/cm² laser fluence, and a total system pressure of 25 Torr, using approximately 200-300 mTorr of FN₃, 250 mTorr SF₆ and 10-50 mTorr I₂, with balance He. The peak NF(a) and F-atom concentrations measured by absolute photometry and H₂ titration,

respectively, were $3 \pm 2 \times 10^{15} / \text{cm}^3$ and $2 \pm 1 \times 10^{14} / \text{cm}^3$. These results were limited by the experimental capabilities of our apparatus and should not be considered as the ultimate scaling limits of the chemical system.

2.1 Chemiluminescence

The presence of emitting species in the (490–700 nm) spectral region of interest for IF(B) was monitored with an optical multichannel analyzer (OMA). Alternatively, the IF(B) chemiluminescence was dispersed by a monochromator and then detected by a PMT for monitoring $\Delta v = 1$ and 2 transitions out of $v' = 0$ and 1 at 565, 570, 583 and 589 nm. A typical emission spectrum taken with the OMA is shown in Fig. 2. The dashed line represents the OMA spectral response curve, determined by use of a standard quartz halogen lamp that is traceable to the National Institute of Standards and Technology (Eppley, EV-82). The left edge of the spectrum shows the sharp edge of the NF(b \rightarrow X) emission; with the trap in the FN₃ line, IF(B) and NF(b) are the only significant emitters in the spectral range of 4090–700 nm. Below 520 nm, no signals were observed within the sensitivity limits of the OMA. Consequently, for all subsequent IF(B) measurements, the NF(b) emission was filtered out by a long pass (Oriel 51302) filter. The NF(a \rightarrow X) emission at 874 nm was also isolated by a calibrated narrow band interference filter. The total NF(a) and IF(B) emissions were then measured relative to each other using a single calibrated Si photodiode. The quantum efficiency of the photodiode and the IF(B \rightarrow X) radiative rate were approximately constant over the spectral range of the IF(B) emission.⁴³ Therefore, the IF(B) measurement was independent of the vibrational distribution. The emission signals obtained were corrected for electronic amplification, photodiode spectral response (EG&G, SGD-444) and filter transmission. The peak (optimized) IF(B) concentration obtained by absolute photometry was $2 \pm 1 \times 10^{11} / \text{cm}^3$.

The emission of both NF(b) and I_{1/2} depended strongly on the I₂ and CF₃I concentrations, due to reactions (6) and (7). The excited I_{1/2} atoms were detected by their emission at 1315 nm using an interference filter and a liquid nitrogen cooled intrinsic Ge detector. The I_{1/2} emission intensity was monitored as a function of SF₆ concentration, laser energy and total system pressure, both with and without the cold trap on the FN₃ line. These measurements demonstrated that impurities entrained in the FN₃ flow were responsible for ~75% of the I_{1/2} emission. All subsequent measurements using FN₃ were therefore conducted with the dry ice trap activated.

Intense BH(A \rightarrow X) chemiluminescence centered around ~ 433 nm due to addition of trace amounts of B₂H₆ used to measure the system temperature. As long as only trace amounts of the donor are added, no significant perturbation of the gas temperature or the reaction system occurs. The BH(X) was electronically excited in collisions with NF(a), as described previously,^{9,10} and the relative BH(A \rightarrow X) (v' , v'') = (0, 0) and (1, 1) chemiluminescence was detected with the OMA. Since radiative lifetimes ($A_{\text{BH}} \sim 6/\mu\text{s}$) and Franck-Condon factors (~ 1) for the spectrally resolved $\Delta v = 0$ transitions are essentially identical, the system temperature of 1600 ± 100 K could be derived readily from the intensity ratio with knowledge^{56,57} of the vibrational spacing $\omega_c = 2251.0 \text{ cm}^{-1}$.

2.2 Laser Induced Fluorescence

The IF(X) ground state was monitored by LIF using a high-pressure nitrogen-pumped grating-tuned dye laser that was electronically delayed with respect to the CO₂ laser. The nitrogen laser had a 0.8 ns pulse width and a 1.2 mJ output energy, which was adequate for investigations of the IF(B) lifetime as a function of total system pressure, CO₂ laser energy and reactant concentrations. Coumarin 490 and 520 dyes in methanol were used to achieve tunable output from 490 to 520 nm. The output bandwidth was analyzed via a monochromator and found to be $\lambda \pm 3$ nm (FWHM) and the center wavelength was tunable with an accuracy of ± 1 nm. The relative (averaged) output power of the dye laser was measured with a photodiode for each excitation wavelength.

The dye laser output (probe light) was coupled into the reaction chamber through a quartz window and was propagated perpendicular to both the CO₂ laser path and the axis of optical detection. The beam was focused to a 2 mm dia. spot in the middle of the reaction zone defined by the gas flows and the cross section of the CO₂ laser beam. The probe light was blocked from the PMT detector by a long pass filter, which cut off all radiation at or below the NF(b \rightarrow X) transition. Optimization of the initial alignment was achieved by detection of an intense LIF signal⁵⁸ due to I₂ in the wavelength range 490–520 nm. During dye laser alignment, the CO₂ laser was blocked so that no F-atoms were produced. When the CO₂ laser was unblocked, the LIF signal from I₂ disappeared completely, and the laser induced emission signal from IF was observed on top of the background chemiluminescence. The signal ratio between LIF and chemiluminescence was improved significantly by imaging the volume excited by the dye laser onto a slit mask covering the photosensitive area of the PMT, to selectively reduce the chemiluminescence emitted by the larger reactive volume. Without FN₃ present, the probe laser

was typically delayed 5–70 μs with respect to the CO_2 laser, which assured complete I_2 dissociation and gave insight into changes of the chemical environment with time. However, with FN_3 present in the system, the LIF probe had to be delayed $> 30 \mu\text{s}$ to detect the LIF signal over the chemiluminescence. The LIF signal from $v'' = 0, 1, 2$ to $v' = 3$ was recorded with a digital storage oscilloscope and averaged over typically 32 shots. LIF signals from $v'' > 2$ could not be detected above the random fluctuations in the chemiluminescence signals. The signals obtained were corrected for relative changes in laser energy and Franck-Condon factors⁴³ for the transitions probed, to determine relative $\text{IF}(X, v'')$ concentrations.

3. Results

3.1 Chemiluminescence

The time decay behavior of $\text{IF}(B) v' = 0$ and 1 is shown in Fig. 3. These vibrational states decay at the same rate independent of the I-atom source used. Vibrational temperatures for the $\text{IF}(B)$ state were derived from the $(B \rightarrow X)$ emission spectrum observed with the OMA. A representative chemiluminescence emission spectrum is shown in Fig. 2. Corrections with respect to OMA spectral response and transitions strengths were applied. Values for the transition strengths were taken from Piper and Marinelli.⁴³ The vibrational temperature measured using I_2 as precursor was $1200 \pm 100 \text{ K}$, and substitution of I_2 with CF_3I produced a slightly colder distribution with a characteristic temperature of $1000 \pm 100 \text{ K}$. This result is surprising, since the $\text{IF}(B)$ state is expected to be essentially rotationally and vibrationally thermalized under the experimental conditions used.¹³

After assuring that no other emitters present in the system contaminate the $\text{IF}(B-X)$ spectrum as discussed above, the total IF emission was measured relative to the total $\text{NF}(a)$ emission. Since the $\text{IF}(B)$ concentration in the absence of FN_3 was negligible, implying no significant pump sources other than $\text{NF}(a)$, the steady state relationship

$$k_p [\text{NF}(a)] [\text{IF}(X, v'')] \sim [\text{IF}(B)] \tau_{\text{IF}}^{-1} \quad (9)$$

can be used at the peak of the $\text{IF}(B)$ time profile and combined with the intensity relationships

$$S_{\text{IF}} = C_{\text{FIF}} D_{\text{IF}} G_{\text{IF}} A_{\text{IF}} [\text{IF}(B)] \quad (10)$$

$$S_{\text{NF}} = C_{\text{FNF}} D_{\text{NF}} G_{\text{NF}} A_{\text{NF}} [\text{NF}(a)] \quad (11)$$

to determine the value of k_p . Here C is a common geometric collection factor, τ_{IF} is the net kinetic lifetime of $IF(B)$, $A_{IF} \sim 1.4 \times 10^5 / s^{16-18}$ and $A_{NF} \sim 0.2 / s$.⁵¹ The factors F , D and G are corrections with respect to filter transmission, spectral response of the detector and amplification. Representative relative $IF(B)$ and $NF(a)$ signals after correction for these factors are shown in Fig. 4. Combining equations (9) through (11), where I_{NF} and I_{IF} are the relative photon emission rate yields

$$\left(\frac{I_{IF}}{I_{NF}}\right) = \left(\frac{S_{IF}}{S_{NF}}\right) \left(\frac{F_{NF}}{F_{IF}}\right) \left(\frac{D_{NF}}{D_{IF}}\right) \left(\frac{G_{NF}}{G_{IF}}\right) \left(\frac{A_{NF}}{A_{IF}}\right) \quad (12)$$

$$k_p = \left(\frac{I_{IF}}{I_{NF}}\right) (\tau_{IF} [IF(X, v'' \geq 10)])^{-1}. \quad (13)$$

The measured value (I_{IF}/I_{NF}) was 40 ± 3 . Since the $IF(B)$ concentrations obtained were independent of the I-atom source used, the $IF(X)$ nascent vibrational distribution obtained from reaction (1) may be thermalized prior to reaction with $NF(a)$. In this case, the concentration of $IF(X, v'' \geq 10)$ can be inferred from the vibrational temperature of the ground state and the total $IF(X)$ concentration, measured by the initial yield of F-atoms with excess I_2 or CF_3I present.

3.2 Laser Induced Fluorescence

After experimentally ensuring that the pumped transitions were not saturated, the recorded LIF signals were used to measure the net kinetic $IF(B)$ lifetime, derived from the time decay behavior, as well as the vibrational distribution of the $IF(X)$ ground state, reflected by the corresponding relative amplitudes. The rise time of the signals measured, however, is determined only by the time constant of the amplifier used. The LIF studies were performed as a function of total system pressure, CO_2 laser fluence, and varied concentrations of SF_6 , HN_3 and FN_3 . The results of these measurements were also independent of the I-atom source used.

3.2.1 Decay Kinetics of $IF(B)$

Variations of the total system pressure between 25 and 50 Torr, laser power, and SF_6 concentration had little effect on the time decay behavior of $IF(B)$. In Figs. 5 and 6, representative LIF signals are shown as a function of time after pulsed dye laser excitation for different CO_2 laser fluences and SF_6 concentrations, respectively. Neither HN_3 nor FN_3 was added to the system for these measurements. The measured decay curves can be represented by a

single exponential fit with $\tau = 2 \pm 0.5 \mu\text{s}$. Subsequently, HN_3 and FN_3 were added to the system, and no impact on the kinetic lifetime of $\text{IF}(\text{B})$ could be observed. In Fig. 7 the experimentally obtained signals are represented by open and dark circles, while the single exponential fits are represented by solid lines. Experimental results lead to the reasonable assumption that none of the gases present in the reaction cell has a dominant impact on the $\text{IF}(\text{B})$ kinetic lifetime.

3.2.2 Concentration Scaling of $\text{IF}(\text{X})$

The increase or loss of population in the vibrational $\text{IF}(\text{X})$ states probed by LIF is reflected in the amplitude changes of the LIF signal. While total system pressure (25 and 50 Torr) did not affect the $\text{IF}(\text{X}, \nu'')$ states probed, changes with CO_2 laser fluence (2–4 J/cm²) can be observed as shown in Fig. 5. The CO_2 laser controls the production of F-atoms by IR multiphoton dissociation of SF_6 , and the $\text{IF}(\text{X})$ generation is strongly coupled to this process. A minimum laser energy of 2 J/cm² is necessary to achieve a measurable yield of F-atoms, but above 3 J/cm² the F-atom concentration saturates within the experimental limits of observation. The effect of varied SF_6 concentrations on the amplitude of the LIF signal can be seen in Fig. 6. A minimum SF_6 concentration of at least $2 \times 10^{15} / \text{cm}^3$ is needed to give rise to a significant pool of F-atoms; however, above a SF_6 concentration of $4.5 \times 10^{15} / \text{cm}^3$ the LIF signal amplitude decreases sharply.⁴⁹ This can be attributed to conditions less favorable for multiphoton dissociation, since collisional pooling of SF_6 becomes more important;^{59,60} however, this result does not exclude $\text{IF}(\text{X})$ losses due to reaction with hot SF_6 . Changes in the vibrational distribution due to pumping reactions may also contribute to the amplitude variations of single vibrational energy levels. Amplitude changes of the LIF signal were also observed when HN_3 or FN_3 were added to the system, and the consequences of this observation is discussed below.

3.2.3 Vibrational Temperature of $\text{IF}(\text{X})$

Relative $\text{IF}(\text{X})$ vibrational populations for $\nu'' = 0, 1, 2$ were obtained using both I_2 and CF_3I as the I-atom source. All of the measured relative LIF signals were corrected for both laser intensities and Franck-Condon factors.⁴³ The $\text{IF}(\text{X}, \nu'' = 0, 1, 2)$ populations obtained for CF_3I were thermal and could be well fit to a vibrational temperature of $2000 \pm 100 \text{ K}$, as shown in Fig. 8. Deviations between the calculated and measured data were within $\pm 15\%$ at both $\nu'' = 1$ and 2 when normalized at $\nu'' = 0$. The corresponding LIF signals from $\text{IF}(\text{X})$ obtained when using I_2 as the I-atom source could also be assigned a temperature of $2000 \pm 100 \text{ K}$, although this result is

very likely not an adequate description of the actual vibrational distribution. The measured relative vibrational populations in this case deviated from a Boltzmann curve by + 28 % at $v'' = 1$ and - 39 % at $v'' = 2$. These results are consistent with prior suggestions that the measured vibrational energy levels of the IF ground state are approximately thermalized; however, they do not allow for a conclusive statement about the state of the total IF(X, v'') distribution, since $v'' > 2$ levels could not be probed, and a nonthermal distribution could be present if the IF(X, $v'' \geq 10$) concentration was dominated by a pumping mechanism that was independent of the I-atom source.

4. Discussion

4.1 IF(B) Losses

The vibrational temperature of the IF(B) state $T_{\text{vib}} \sim 1200$ K was colder than the system temperature of 1600 ± 100 K that was measured by using the BH(A - X) emission. This result can possibly be explained by predissociation of the IF(B) state $v' > 8$,¹⁶ which results in vibrational energy loss at elevated temperatures. The measured kinetic decay rate of the IF(B) state ($\Gamma = 4 \times 10^5$ /s) is about a factor three higher than the radiative decay rate measured by Davis,³⁹ and represents the sum over radiative and collisional loss processes according to

$$\Gamma = A_{\text{IF}} + k_{\text{q}} [\text{M}] \quad (14)$$

Using equation (14) yields a collisional loss rate of 2.6×10^5 /s, which includes electronic quenching of IF(B) and losses due to reaction and pumping above the predissociation limit. As a first approximation, a small average bimolecular collisional IF(B) loss rate of $k_{\text{q}} \sim 3 \times 10^{-13}$ cm³/s can be derived, using the total particle density of $[\text{M}] = 8 \times 10^{17}$ /cm³, since individual contributions are not easily traced. A reasonable assumption is that He, N₂ and cold SF₆ contribute very little to the collisional decay,¹³ while the role of other reactants especially vibrationally hot SF₆ is less clear.

4.2 IF(B) Pump Mechanism

The results presented here show the IF(B) yield to be independent of the I-atom source used. In addition, the relative vibrational distributions obtained for $v'' = 0, 1, 2$ were approximately thermalized. Consistent with these results is the assumption that the IF(X) nascent vibrational distribution has thermalized prior to reaction with NF(a). If the relative vibrational

distribution of $v'' = 0, 1, 2$ is an adequate representation of the IF(X) state up to $v'' \sim 20$, a Boltzmann distribution ($T = 2000$ K) can be used to derive the thermal IF(X, $v'' \geq 10$) population, assuming that the total IF(X) concentration is given by the density of F-atoms, as measured by titration. With the vibrational energies given by Marinelli and Piper,⁴³ this procedure yields [IF(X, $v'' \geq 10$)] $\sim 3 \times 10^{12}$ /cm³, and a pump rate constant $k_p = 1 \times 10^{-11}$ cm³/s can then be calculated from equation (13) in Section 3.1 using the relative I_{IF}/I_{NF} emission ratio of ~ 40 and the measured kinetic decay rate for IF(B) of 4×10^5 /s. This result for k_p is a factor of four larger than the value of measured by Davis ($2-3 \times 10^{-12}$ cm³/s) in low density experiments,³⁹ and represents only a lower limit since the total IF concentration is likely to be smaller than the original F-atom concentration, due to reactive loss processes indicated by the effects of SF₆ and FN₃ on the LIF signal amplitudes. The experimental parameter with the largest error in this calculation is the original F-atom concentration of $2 \pm 1 \times 10^{14}$ /cm³, obtained with the two titration methods described above. The combined experimental errors, including variations in vibrational IF(X) temperature and kinetic IF(B) lifetime, however, are still not sufficient to account for the discrepancy in the values for k_p .

The thermal or close to thermal appearance of IF(X) $v'' = 0, 1, 2$ alone does not exclude a non thermal population for $v'' \geq 10$, and the lack of difference between I₂ and CF₃I precursors can be explained by means other than thermalization. Assuming a thermal IF(X) state is not an adequate representation, we used the previously measured IF(X) pump rate of $2-3 \times 10^{-12}$ cm³/s,³⁹ and rearranged equation (13)

$$[\text{IF(X, } v'' \geq 10)] = \left(\frac{I_{\text{IF}}}{I_{\text{NF}}} \right) (\tau_{\text{IF}} k_p)^{-1} \quad (13)$$

to derive the IF(X, $v'' \geq 10$) concentration. A value of 1.2×10^{13} /cm³ is obtained this way, which is a factor of four larger than the thermal concentration of 3×10^{12} /cm³. The interpretation of our experimental results therefore does not strictly require a thermalized IF(X) population, but can be supported by a mechanism that is independent from the I-atom source used. Consistent with this picture is an alternative mechanism based on a fast E-V transfer from NF(a) to IF inferred by Setser.⁵⁵



Under high NF(a) density conditions, vibrational pumping may be followed by efficient electronic excitation in a second collision with NF(a) to yield IF(B), as in reaction (2). Only

under experimental conditions where large particle densities of NF(a) can be maintained and the He buffer gas to metastable ratio is relatively small ($\leq 10^2$), however, is vibrational pumping by NF(a) able to compete with V-T relaxation, resulting in a significant non thermal steady state vibrational distribution of the IF(X) state. If IF is not rapidly removed by other species, then in this case recycling is possible, allowing for more than one photon per IF molecule produced by reactions (1) or (4). Vibrational excitation of the IF(X, $v'' \geq 10$) levels by NF(a) is also consistent with the measured vibrational ground state temperature of $T = 2000 \pm 100$ K, which is 400 K above the system temperature.

These results are very different from those obtained in a low density environment, with a much higher ratio of buffer gas to metastable species ($\geq 10^4$). Under these conditions, the E-V pump rate is not sufficient to compete against fast V-T relaxation; and consequently, enhancements of the IF(B) yield can be achieved only with the original nascent IF(X) distribution obtained in reaction (1). In addition, only one photon per IF molecule is possible, in this case, which has important consequences concerning the specific energy of a laser device.

5. Conclusions

The effect of high NF(a) densities on the IF(B) state and the pump mechanism were investigated. Although a modest decrease in the IF(B) kinetic lifetime was observed, it is not due to NF(a) or its reaction byproducts, and therefore no related scaling problems are anticipated. Measurements of the IF(B)/NF(a) ratio and the relative IF(X) ground state populations for $v'' = 0, 1, 2$ support either a larger pump rate for the reaction of NF(a) with IF(X, $v'' \geq 10$) or a change of mechanism involving a source for vibrationally excited IF that is independent of the I-atom precursor such as fast E-V transfer from NF(a). In the latter case, a steady state concentration of IF(X, $v'' \geq 10$) results, and recycling of the IF emitters may lead to generation of more than one photon per donor molecule. Further experiments are needed to clarify the mechanism under high density conditions by probing these energy levels. An additional concern, still to be addressed, is whether V-T relaxation from the pumped IF(X, $v'' \geq 10$) levels to the lower $v'' \sim 5$ states will degrade the potential for population inversion of the IF(B \rightarrow X, 0-5) laser transition. Since large IF(X) densities can be generated,⁶¹ the feasibility of a vibrationally assisted transfer laser also depends critically on appropriate management of the IF(X) vibrational distribution under high particle density conditions.

References

1. Bachar, J.; Rosenwaks, S. *Appl. Phys. Lett.* **1982**, *41*, 16.
2. Benard, D.J.; McDermott, W.E.; Pchelkin, N.R.; Bousek, R.R. *Appl. Phys. Lett.* **1979**, *34*, 40.
3. McDermott, W.E.; Pchelkin, N.R.; Benard, D.J.; Bousek, R.R. *Appl. Phys. Lett.* **1978**, *32*, 469.
4. Derwent, R.G.; Thrush, B.A. *Chem. Phys. Lett.* **1971**, *9*, 591.
5. Derwent, R.G.; Thrush, B.A. *Trans. Faraday Soc.* **1971**, *67*, 2036.
6. Arnold, S.J.; Finlayson, N.; Ogryzlo, E.A. *J Chem. Phys.* **1966**, *44*, 2529.
7. Benard, D.J.; Boehmer, E. *J. Phys. Chem.* (submitted).
8. Benard, D.J.; Boehmer, E. *Appl. Phys. Lett.* (submitted).
9. Benard, D.J. *Appl. Phys. Lett.* **1993**, *74*, 2900.
10. Benard, D.J.; Winker, B.K. *J. Appl. Phys.* **1991**, *69*, 2805.
11. Benard, D.J.; Winker, B.K.; Seder, T.A.; Cohn, R.H. *J. Phys. Chem.* **1989**, *93*, 4790.
12. Benard, D.J.; Cohn, R.H. *Air Force Astronautics Laboratory Technical Report No. AFAL-TR-87-071* (February, 1988).
13. Wolf, P.J.; Davis, S.J. *J. Chem. Phys.* **1987**, *87*, 3492.
14. Wolf, P.J.; Davis, S.J. *J. Chem. Phys.* **1985**, *83*, 91.
15. Wolf, P.J. Ph.D. *Dissertation*, Air Force Weapons Laboratory **1984**.
16. Davis, S.J.; Hanko, L.; Shea, R.F. *J. Phys. Chem.* **1983**, *78*, 172.
17. Clyne, M.A.A.; McDermid, I.S. *J. Chem. Faraday Trans. 2* **1978**, *74*, 1644.
18. Clyne, M.A.A.; McDermid, I.S. *J. Chem. Faraday Trans. 2* **1977**, *73*, 1094.

19. Clyne, M.A.A.; McDermid, I.S. *J. Chem. Faraday Trans. 2* 1976, 72, 2252.
20. Clyne, M.A.A.; McDermid, I.S. *J. Chem. Faraday Trans. 2* 1975, 72, 2242.
21. Davis, S.J.; Hanco, *J. Chem. Phys.* 1985, 82, 4831.
22. Davis, S.J.; Hanco, *J. Chem. Phys.* 1983, 78, 172.
23. Davis, S.J.; Hanco, L. *Appl. Phys. Lett.* 1980, 37, 692.
24. Davis, S.J.; Woodward, A.M. *J. Phys. Chem.* 1991, 95, 4610 and references therein.
25. Piper, L.G.; Marinelli, W.J. *J. Phys. Chem.* 1989, 93, 4039.
26. Raybone, D.; Watkinson, T.M.; Whitehead, J.C. in *Selectivity in Chemical Reaction*; Whitehead, J.C.; Ed.; NATO ASI Series, Kluwer Academic Press: Dordrecht, 1988.
27. Braynis, H.S.; Raybone, D.; Whitehead, J.C. *J. Chem. Soc. Faraday Trans. 2* 1987, 83, 627.
28. Braynis, H.S.; Raybone, D.; Whitehead, J.C. *J. Chem. Soc. Faraday Trans. 2* 1987, 83, 639.
29. Raybone, D.; Watkinson, T.M.; Whitehead, J.C. *J. Chem. Soc. Faraday Trans. 2* 1987, 83, 767.
30. Raybone, D.; Watkinson, T.M.; Whitehead, J.C. *Chem. Phys. Lett.* 1987, 139, 442.
31. Davis, S.J.; Woodward, A.M. *J. Phys. Chem.* 1987, 91, 3758.
32. Cha, H.; Setser, D.W. *J. Phys. Chem.* 1987, 91, 3758.
33. Pritt, A.T.; Benard, D.J. *J. Chem. Phys.* 1986, 85, 7159.
34. Piper, L.G.; Marinelli, W.J.; Rawlins, W.T.; Green, B.D. *J. Chem. Phys.* 1985, 83, 5602.
35. Pritt, A.T.; Patel, D.; Benard, D.J. *Chem. Phys. Lett.* 1983, 97, 471.
36. Whitefield, P.D.; Shea, R.F.; Davis, S.J. *J. Chem. Phys.* 1983, 78, 6793.

37. Coombe, R.D.; Horn, R.K. *J. Phys. Chem.* **1979**, *83*, 2435.
38. Clyne, M.A.A.; Coxon, J.A.; Townsend, L.W. *J. Chem. Soc. Faraday Trans. 2* **1972**, *68*, 2134.
39. Davis, S.J. private communication.
40. Agrawalla, B.S.; Singh, J.P.; Setser, D.W. *J. Chem. Phys.* **1983**, *79*, 6416.
41. Trickl, T.; Wanner, J. *J. Chem. Phys.* **1983**, *78*, 6091.
42. Appelman, E.H.; Clyne, M.A.A. *J. Chem. Soc. Faraday Trans. 1* **1975**, *71*, 2075.
43. Marinelli, W.J.; Piper, L.G. *J. Quant. Spectrosc. Radiat. Transfer* **1985**, *34*, 321.
44. Girard, B.; Billy, N.; Gouedard, G.; Vigue *J. Chem. Phys.* **1988**, *88*, 2342.
45. Girard, B.; Billy, N.; Gouedard, G.; Vigue *Chem. Phys. Lett.* **1987**, *136*, 1.
46. Collins, A.T.; Trautman, M.; Wanner, J. *J. Chem. Phys.* **1986**, *84*, 3814.
47. Stein, L.; Wanner, J. *J. Chem. Phys.* **1980**, *72*, 1128.
48. Gillespie, L.J.; Fraser, L.H.D. *J. Amer. Chem. Soc.* **1936**, *58*, 2260.
49. Quick, C.R.; Wittig, C. *Chem. Phys. Lett.* **1977**, *48*, 420.
50. Rosen, B. *Spectroscopic Data Relative to Diatomic Molecules* (Pergamon Press, NY) **1970**.
51. Malins, R.J.; Setser, D.W. *J. Phys. Chem.* **1981**, *85*, 1342.
52. Herblin, J.M.; Cohen, N. *Chem. Phys. Lett.* **1973**, *20*, 605.
53. Du, K.Y.; Setser, D.W. *J. Phys. Chem.* **1992**, *96*, 2553.
54. Koffend, J.B.; Weiller, B.H.; Heidner III, R.F. *J. Phys. Chem.* **1992**, *96*, 9315.
55. Herblin, J.M.; Kwok; Spencer, D.J. *J. Appl. Phys.* **1978**, *49*, 3750.

56. Douglass, C.H.; Nelson, H.H.; Rice, J.K. *J. Chem. Phys.* **1989**, *90*, 6940.
57. Luh, W.T.; Stwalley, W.C. *J. Molec. Spectrosc.* **1983**, *102*, 212.
58. Tellinghuisen, J. *J. Chem. Phys.* **1982**, *76*, 4736.
59. Lenzi, M.; Molinari, E.; Piciacchia, G.; Sessa, V.; Terranova, M.L.; *Chem. Phys.* **1990**, *142*, 463.
60. Lenzi, M.; Molinari, E.; Piciacchia, G.; Sessa, V.; Terranova, M.L.; *Chem. Phys.* **1990**, *142*, 473.
61. Helms, C.A.; Hanko, L.; Healey, K.; Hager, G.; Perram, G.P. *J. Appl. Phys.* **1989**, *66*, 6093.

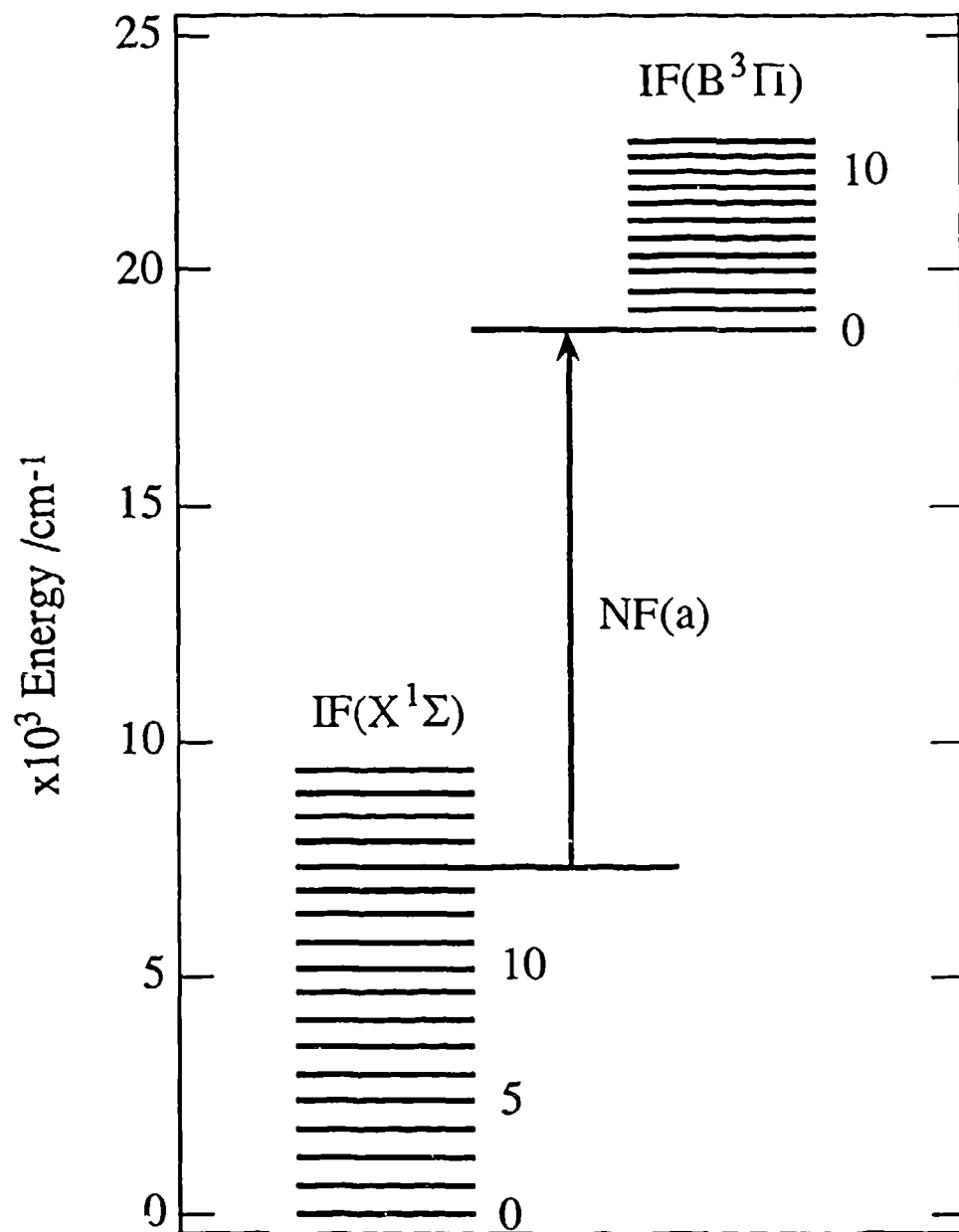


Fig. 1 Schematic energy diagram for IF and a possible NF(a) pumped transition ($X, v'' = 14 \rightarrow B, v' = 0$).

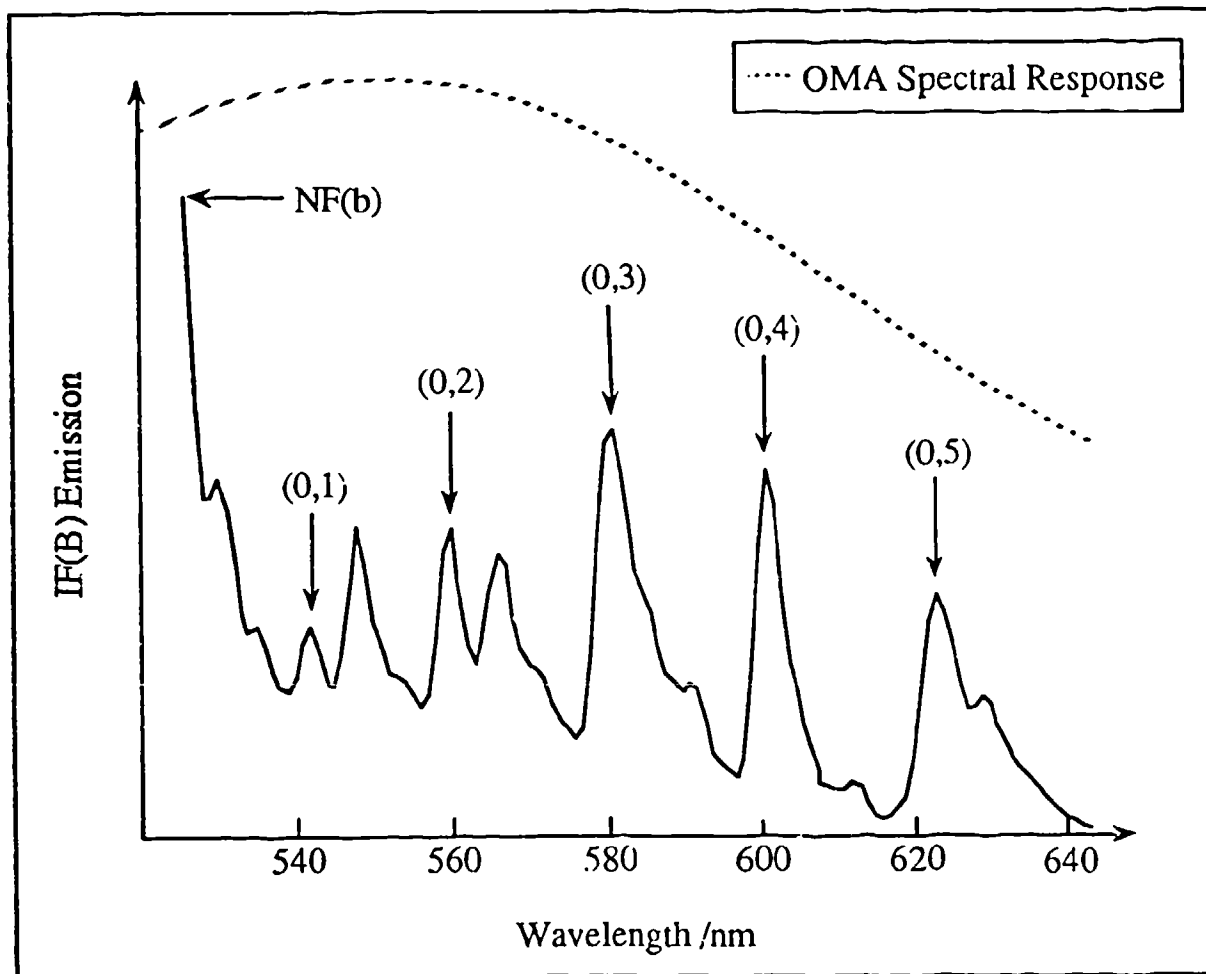


Fig. 2 IF(B) emission spectrum (520 to 640 nm). The dashed line represents the OMA relative spectral response. Transitions from IF(B, $v' = 0$) into IF(X, $v'' = 1, 2, 3, 4, 5$) are indicated by arrows.

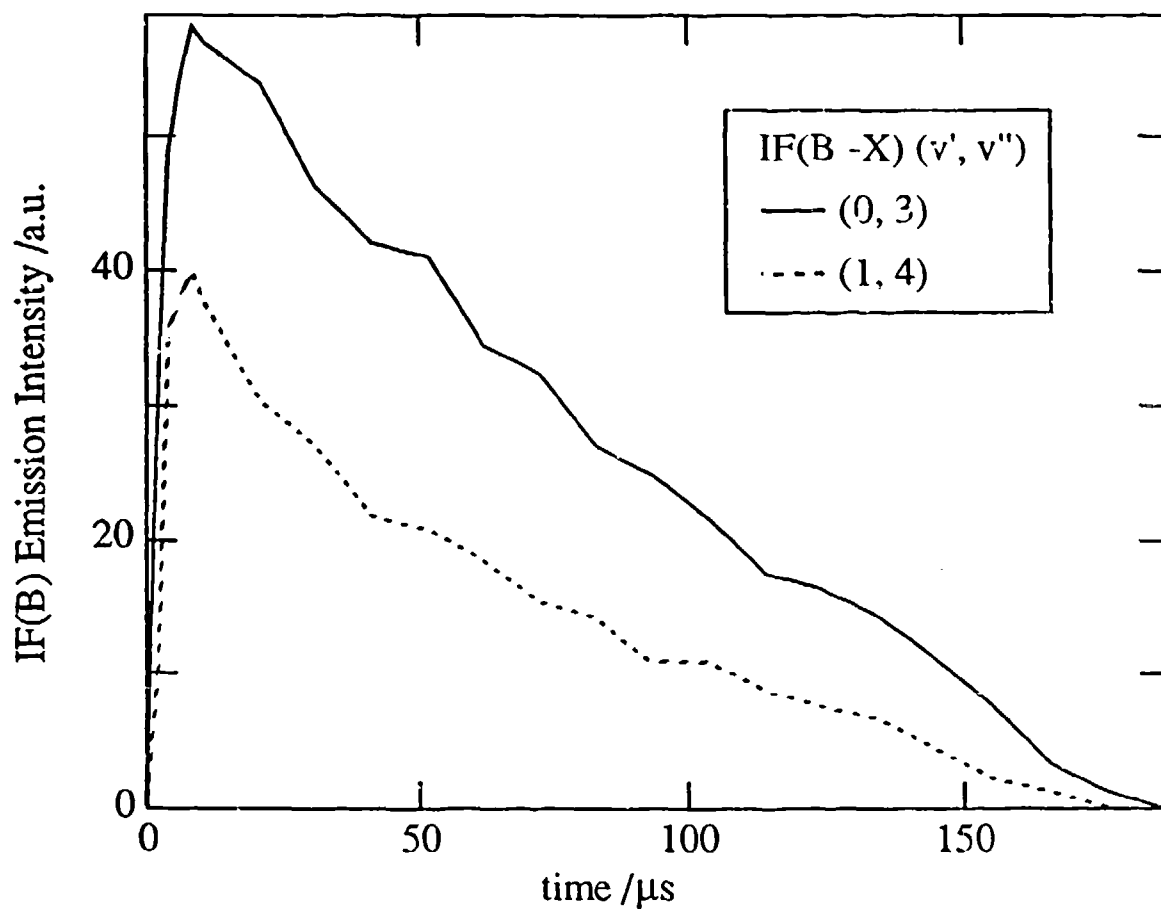


Fig. 3 IF(B) emission signal for IF(B \rightarrow X) (v' , v'') = (0, 3) (solid line) and (1, 4) (dashed line), as a function of time after the CO_2 laser trigger. The signals were not corrected for differences in transition probabilities.

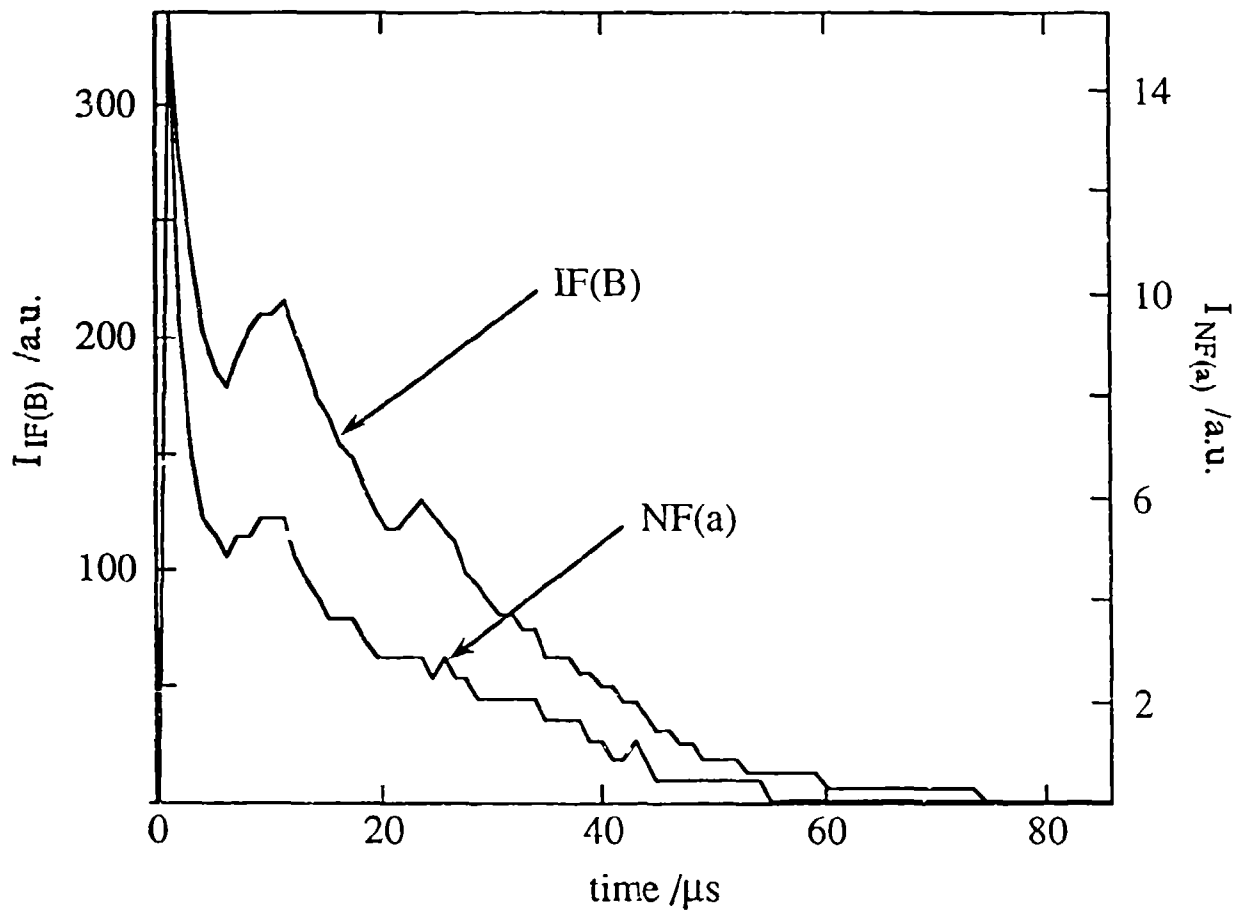


Fig. 4 IF(B) and NF(a) relative emission signals. The signals were corrected for filter transmission, detector spectral response and electronic amplification. Note that the IF(B) relative intensity is shown on the left-hand ordinate; the NF(a) relative emission intensity on the right-hand ordinate.

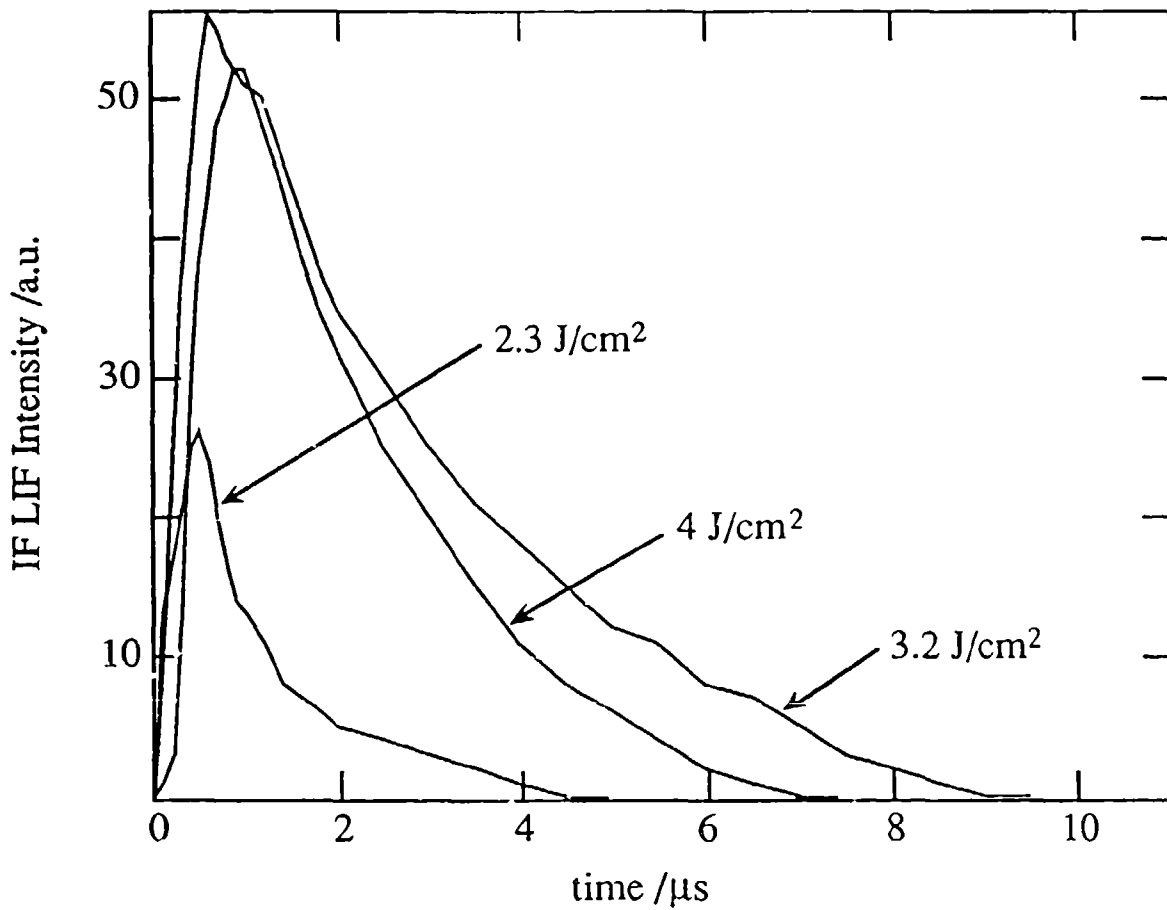


Fig. 5 IF LIF signal as a function of time after the LIF probe pulse for three different CO₂ laser fluences. A minimum laser fluence of 2 J/cm² is required to produce F-atoms by multiphoton dissociation of SF₆.

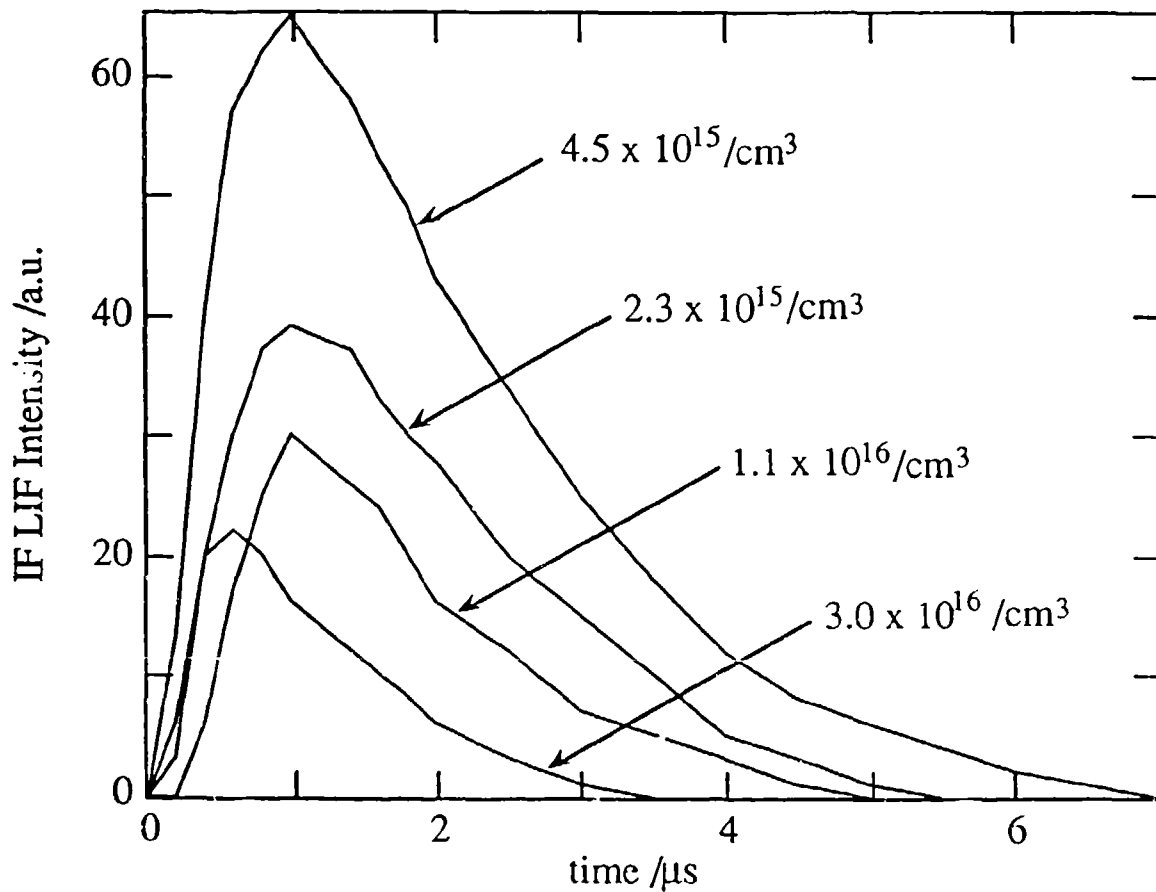


Fig. 6 IF LIF signal as a function of time after the LIF probe pulse at four different SF₆ concentrations. For SF₆ concentrations $> 4 \times 10^{15} / \text{cm}^3$ conditions for SF₆ multiphoton dissociation deteriorate rapidly.

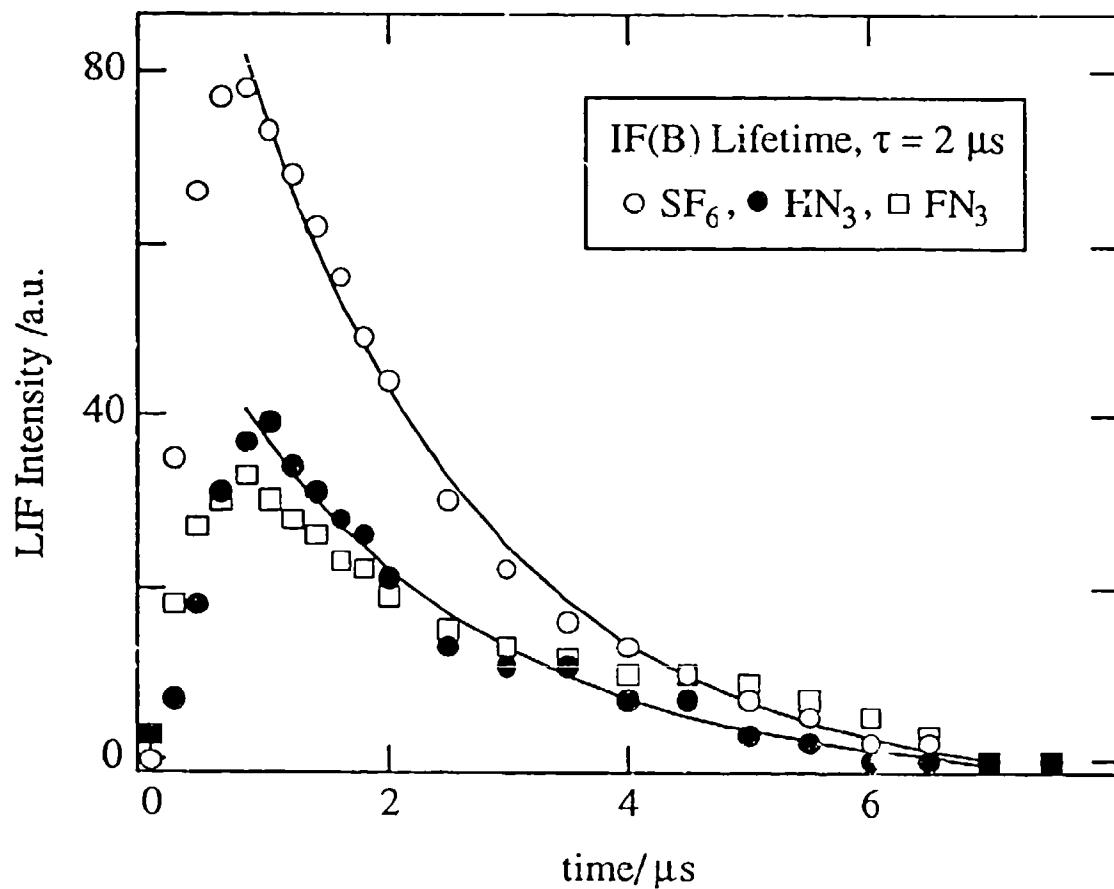


Fig. 7 IF LIF signal as a function of time after the LIF probe in the presence of SF₆ only and with/without HN₃ and FN₃. The solid lines indicate the exponential fit to the experimental decay curve; a lifetime τ of $\sim 2 \mu\text{s}$ was obtained this way.

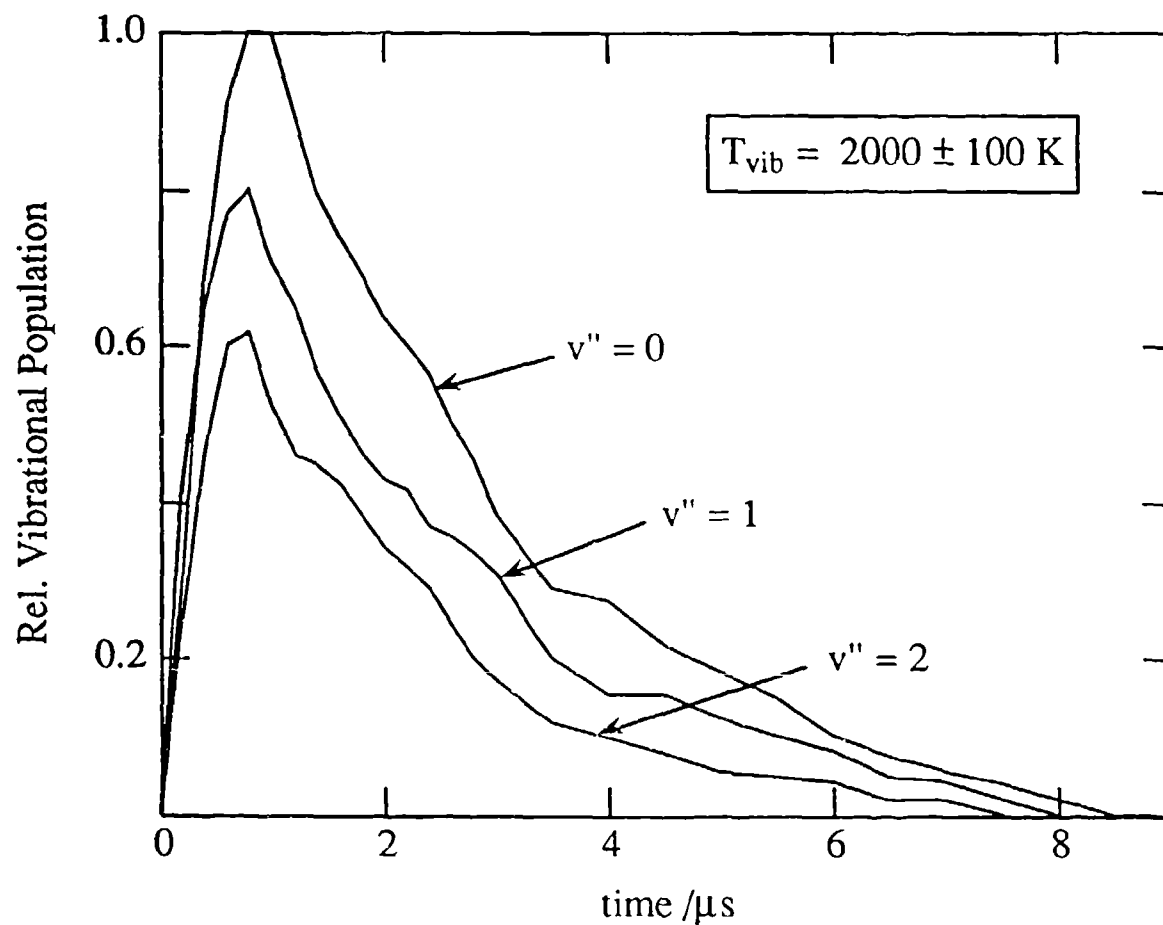


Fig. 8 Relative LIF emissions from $\text{IF}(\text{B}, v' = 3)$ into $\text{IF}(\text{X}, v'' = 0, 1, 2)$ using CF_3I as I-atom source. The signals are corrected for dye laser energy and Franck-Condon factors.